Efficient approximations for the ab initio calculation of nuclear magnetic resonance shielding tensors

Dissertation

zur

Erlangung des Doktorgrades (Dr. rer. nat.)

der

Mathematisch-Naturwissenschaftlichen Fakultät

der

Rheinischen Friedrich-Wilhelms-Universität Bonn

vorgelegt von

Georgi Lazarov Stoychev

aus

Sofia, Bulgarien

Bonn, 2021

Angefertigt mit Genehmigung der Mathematisch-Naturwissenschaftlichen Fakultät der
Rheinischen Friedrich-Wilhelms-Universität Bonn

1. Gutachter: Prof. Dr. Frank Neese

2. Gutachter: Prof. Dr. Stefan Grimme

Tag der Promotion: 14.01.2022

Erscheinungsjahr: 2022

Abstract

Nuclear magnetic resonance (NMR) spectroscopy is an essential analytic technique in chemical, pharmaceutical, and biomedical research and materials sciences. The information that NMR provides about the molecular structure of novel compounds is detailed but indirect, hidden behind the two main quantities that determine the shape of the spectrum: the shielding tensor (observed as a *chemical shift*) and the indirect spin–spin coupling tensor. Thus, computational methods are often used to predict these properties from first principles and correctly interpret complex spectra. The challenge is to develop methods which are both accurate and robust enough to resolve truly complicated structures, and efficient enough to be routinely applicable to large molecular systems. This work aims to facilitate the fast and accurate calculation of NMR shielding tensors in three complementary ways.

First, two popular approaches for speeding up Hartree–Fock (HF) and density functional theory (DFT) calculations, the resolution of the identity (RI) and chain-of-spheres exchange (COSX) approximations, are applied to NMR shielding calculations using gauge-including atomic orbitals (GIAOs). A benchmark study is performed to assess the errors thus introduced in the calculated shieldings, in comparison to the inherent errors due to the level of theory. After selection of appropriate basis sets and integration grids, it is shown that the RI approximation for Coulomb interactions, combined with either the same for exchange interactions (RIJK), or with COSX (RIJCOSX), are both sufficiently accurate. However, for systems with more than 100 electrons and 1000 basis functions, RIJCOSX is more efficient.

Next, NMR shielding calculations with GIAOs are implemented for RI-based second order Møller–Plesset perturbation theory (RI-MP2) and also, for the first time, for double-hybrid DFT (DHDFT). The latter is shown to be substantially more accurate than either MP2 or regular DFT, reproducing NMR chemical shifts within 2 % of the CCSD(T) (coupled clusters with single, double, and perturbative triple excitations) reference values. The accuracy and efficiency of the RI-MP2 approximation is also assessed and it is shown that the implementation is suitable for systems with up to 400 electrons and 2500 basis functions.

Finally, the applicability of MP2 and DHDFT is extended to even larger systems by employing the concepts of local electron correlation within the framework of the domain-based local pair natural orbital (DLPNO) approximation. The formally complete analytic second derivatives of DLPNO-MP2 are derived and implemented for both NMR shieldings and electric dipole polarizabilites. Some numerical stability issues, potentially relevant to other local correlation methods, and their avoidance are discussed. The effect of the DLPNO approximation is assessed for medium-sized systems and it is shown that relative deviations from the RI-MP2 reference result are below 0.5 % for both properties when using the default truncation thresholds. For large systems, the implementation achieves quadratic effective scaling of the computational effort with system size. It is more efficient

than RI-MP2 starting at 280 correlated electrons and is never more than 5–20 times slower than the equivalent HF or hybrid DFT calculation. The largest system treated here at the DLPNO-DHDFT level is the vancomycin molecule with 176 atoms, 542 correlated electrons, and 4700 basis functions.

List of publications

Published parts of this thesis

Parts of this thesis have appeared in the following publications:

1. Stoychev, G. L.; Auer, A. A.; Izsák, R.; Neese, F. Self-Consistent Field Calculation of Nuclear Magnetic Resonance Chemical Shielding Constants Using Gauge-Including Atomic Orbitals and Approximate Two-Electron Integrals. *J. Chem. Theory Comput.* **2018**, *14*, 619–637, DOI:10.1021/acs.jctc.7b01006.

   The implementation for HF and DFT NMR shielding calculations using GIAOs was provided by my co-authors. I made some modifications and optimizations of the code and also performed all reported benchmark calculations and the statistical analysis of the results.

2. Stoychev, G. L.; Auer, A. A.; Neese, F. Efficient and Accurate Prediction of Nuclear Magnetic Resonance Shielding Tensors with Double-Hybrid Density Functional Theory. *J. Chem. Theory Comput.* **2018**, *14*, 4756–4771, DOI:10.1021/acs.jctc.8b00624.

   I performed all derivations, implementation, benchmark calculations, and analysis in this work and was advised by my co-authors.

3. Stoychev, G. L.; Auer, A. A.; Gauss, J.; Neese, F. DLPNO-MP2 Second Derivatives for the Computation of Polarizabilities and NMR Shieldings. *J. Chem. Phys.* **2021**, *154*, 164110, DOI:10.1063/5.0047125.

   I performed all derivations, implementation, benchmark calculations, and analysis in this work and was advised by my co-authors.

Further publications

The publications listed below are not part of this thesis.

1. Stoychev, G. L.; Auer, A. A.; Neese, F. Automatic Generation of Auxiliary Basis Sets. *J. Chem. Theory Comput.* **2017**, *13*, 554–562, DOI:10.1021/acs.jctc.6b01041.

2. Dittmer, A.; Stoychev, G. L.; Maganas, D.; Auer, A. A.; Neese, F. Computation of NMR Shielding Constants for Solids Using an Embedded Cluster Approach with DFT, Double-Hybrid DFT, and MP2. *J. Chem. Theory Comput.* **2020**, *16*, 6950–6967, DOI:10.1021/acs.jctc.0c00067.

3. Auer, A. A.; Tran, V. A.; Sharma, B.; Stoychev, G. L.; Marx, D.; Neese, F. A Case Study of Density Functional Theory and Domain-Based Local Pair Natural Orbital Coupled Cluster for Vibrational Effects on EPR Hyperfine Coupling Constants: Vibrational Perturbation Theory versus Ab Initio Molecular Dynamics. *Mol. Phys.* **2020**, *118*, e1797916, DOI:10.1080/00268976.2020.1797916.

Acknowledgement

First and foremost, I am grateful to Prof. Frank Neese for entrusting me with this project, for giving me space and time to work things out on my own but stepping in when I was stuck, and for being an exemplary supervisor that one can look up to. I would like to thank Prof. Alexander A. Auer for being a motivating mentor and tactful group leader who always has both good advice and silly jokes available.

I thank Frank Wennmohs for the programming know-how and regular discussions, as well as Ute Becker for her help with a myriad of technical issues. I am indebted to Peter Pinski for a thorough introduction into the intricacies of the DLPNO-MP2 method and its derivatives. I have had useful discussions with Giovanni Bistoni, Jürgen Gauß, Benjamin Helmich-Paris, Róbert Izsák, Christoph Riplinger, Kantharuban Sivalingam, and Bernardo de Souza, as well as with Ida-Marie Høyvik and Fred Manby during the 2019 Molecular Quantum Mechanics conference in Heidelberg, to all of whom I am very grateful.

This work was funded by the Max Planck Society and performed at the Max Planck Institute for Chemical Energy Conversion and the Max-Planck-Institut für Kohlenforschung. I appreciate the work of the administrative assistants and secretaries at both institutes, in particular of Gabriele Beckmann.

My heartfelt thanks go to my friends and colleagues who greatly improved my life in Mülheim in various ways: Aleksandra Wandzilak, Anastasios Papadopoulos, Christine Schulz, Corentin Poidevin, Giovanna Bruno, Joanna Kowalska, Jonathon Vandezande, Małgorzata Krasowska, Masaaki Saitow, Marvin Lechner, Miquel Garcia, Romain Berraud-Pache, Van Anh Tran, and Vijay Chilkuri.

I am deeply grateful to my parents, Yasna and Lazar, and my sister Maria for their unfailing care and support. Finally, I sincerely thank my fiancée Steffy for the kindness, love, and patience she gave me during these years.

Contents

Chapter 1

Introduction

1.1 The nuclear magnetic resonance shielding tensor

Nuclear magnetic resonance (NMR) spectroscopy is an essential tool in modern chemistry with a myriad of applications including characterization of novel compounds, measuring reaction kinetics and binding constants, assessing the purity of synthetic products, etc. NMR is very sensitive to changes in the chemical environment of the studied nuclei, however, this structural information is indirect. While advanced experimental techniques, such as two-dimensional NMR spectroscopy, are very powerful in deconvoluting complicated spectra, computational modeling is often necessary in order to interpret the experimental data. The main two observables obtained from NMR spectra are the chemical shift and the indirect nuclear spin–spin coupling both of which can be calculated from first principles for model systems. However, the methods presented in this work are mainly directed at the ab initio computation of chemical shifts.

The chemical shift, δ, is defined as the relative difference of the nuclear magnetic resonance frequency of a sample nucleus, ν_{sample}, with respect to that of a reference nucleus, ν_{ref}, expressed in parts per million (ppm):[1]

$$\delta = \frac{\nu_{\text{sample}} - \nu_{\text{ref}}}{\nu_{\text{ref}}} \tag{1.1}$$

The resonance frequency is proportional to the nuclide's magnetogyric ratio γ and the applied magnetic field B_0:

$$\nu = \frac{\gamma}{2\pi} B_0 \left(1 - \sigma\right) \tag{1.2}$$

This equation defines the shielding constant σ as a dimensionless quantity, usually reported in ppm, which reflects how the magnetic field acting on the nucleus is affected by the induced currents in the surrounding electron density. This dependence on the local electronic environment makes σ and δ sensitive probes for the chemical structure around a given nucleus. In principle, the value of σ depends on the orientation of the molecule in the external magnetic field and therefore both $\boldsymbol{\sigma}$ and $\boldsymbol{\delta}$ are three-dimensional second-rank tensors. However, due to rapid tumbling in the liquid state, only an average isotropic value is observed, which can be calculated from the trace of the tensor:

$$\sigma_{\text{iso}} = \frac{1}{3}(\sigma_{xx} + \sigma_{yy} + \sigma_{zz}) \tag{1.3}$$

The anisotropy of the tensor can also be measured in solid state experiments.

1.2 Ab initio calculation of NMR shielding

The theory behind the computation of NMR parameters from first principles dates back to the 1950s[2] and progress in the field has been the subject of many monographs, reviews, and conference proceedings over the years.[3–15] The following sections point out some of the relevant works, focusing in particular on improvements in the accuracy and/or computational cost of NMR shielding calculations.

Formally, the NMR shielding tensor $\boldsymbol{\sigma}^K$ of nucleus K can be expressed as the second derivative of the energy with respect to the magnetic field $\mathbf{B}$ and the magnetic moment the nucleus, $\mathbf{m}_K$:[13,16]

$$\sigma^K_{\beta\alpha} = \left.\frac{\mathrm{d}^2 E}{\mathrm{d}B_\alpha \mathrm{d}m_{K_\beta}}\right|_{\mathbf{B},\mathbf{m}_K=0}, \qquad \alpha,\beta = x,y,z \tag{1.4}$$

In principle, energy derivatives can be obtained using numerical differentiation techniques, i.e. finite differences. However, such an approach suffers from limited numerical precision, as well a high computational cost due to the large number of energy calculations that must be performed. In addition, it is particularly ill-suited for magnetic properties, as these would require parameterizing the wave function using complex variables, which is not possible in most electronic structure programs. Thus, practical implementations for NMR shielding calculations rely on analytic derivative techniques, which resolve these issues. The downside, however, is that the derivation and implementation of each specific property for each electronic structure method requires significant effort.

1.2.1 The gauge origin problem

An additional complication is the so-called "gauge origin problem",[13,17] which requires special treatment. The external magnetic field is introduced into the Hamiltonian through a vector potential:

$$\mathbf{A}^{\mathrm{e}}(\mathbf{r},\mathbf{B}) = \frac{1}{2}\mathbf{B}\times(\mathbf{r}-\mathbf{R}_O) \tag{1.5}$$

where $\mathbf{r}$ is the electron position and $\mathbf{R}_O$ is the gauge origin, which can be chosen arbitrarily as long as it satisfies the condition

$$\mathbf{B} = \boldsymbol{\nabla}\times\mathbf{A}^{\mathrm{e}}(\mathbf{r},\mathbf{B}) \tag{1.6}$$

In contrast, observable properties of the system, such as the shielding tensor, must be independent of this choice. That is indeed the case for the exact wave function, however, not so for the approximate wave functions used in practice. In fact, not only do the calculated shieldings vary with $\mathbf{R}_O$, the convergence towards the complete basis set (CBS) limit is very slow as the basis set is increased.[16] Several methods have been devised to tackle this problem:

- Individual Gauge for Localized Orbitals (IGLO);[18,19]
- Localized Orbitals/Localized Origins (LORG)[20] and its second order variant SOLO;[21]
- Individual Gauges for Atoms in Molecules (IGAIM);[22]
- Continuous Set of Gauge Transformations (CSGT)[23] and the related Continuous Transformation of the Current Density (CTOCD) variations;[24–26]

- Gauge-Including Atomic Orbitals (GIAOs).[27–31]

Of these, the GIAO approach has been established as the de facto standard, as it formally (and practically) ensures gauge-origin independence of the result, does not require orbital localization (which may fail for delocalized systems), and can be applied to correlated wave function-based methods. Within the GIAO approach a magnetic field dependence is introduced as a phase factor in the definition of the basis functions:

$$\chi_\kappa(\mathbf{B}, \mathbf{r}) = \exp\left[-\mathrm{i}\mathbf{A}^{\mathrm{e}}(\mathbf{R}_K, \mathbf{B}) \cdot \mathbf{r}\right] \varphi_\kappa(\mathbf{r}) \tag{1.7}$$

where φ_κ is a regular Gaussian-type orbital (GTO), centered on atom K and $\mathbf{A}^{\mathrm{e}}_K$ is the local representation of the external field at coordinates $\mathbf{R}_K$, as given by eq. 1.5. In integrals over GIAOs the dependence on $\mathbf{R}_O$ cancels out,[32,33] making the calculated properties gauge origin-independent. Note that derivatives of these integrals with respect to $\mathbf{B}$ (at the zero-field limit) are strictly imaginary. In practice, the imaginary unit is factored out and thus a real representation is sufficient for the perturbed integrals with the minor complication that the resulting matrices are antisymmetric.[16]

1.2.2 Wave function theory

In the field of wave function theory, the Hartree–Fock (HF) method has undoubtedly provided useful insights but it has been shown to predict NMR shieldings rather far from the experimental observations, due to a lack of electron correlation effects. Shielding calculations using correlated wave function-based methods and analytic derivative techniques were pioneered by Gauss, first at the level of second order Møller–Plesset perturbation theory (MP2),[34,35] and subsequently at higher orders of perturbation theory and coupled cluster (CC) theory,[36–41] as well as configuration interaction (CI) up to full CI (FCI).[42] While calculations at high levels of CC theory are only feasible for rather small molecules, they provide accurate reference values, against which to benchmark other computational methods. In this respect, CC with single, double, and perturbative triple excitations (CCSD(T)) has been established as the "gold standard". MP2 has been shown to offer a good balance between cost and accuracy in the calculated NMR shieldings,[34,35,43–47] although it can fail completely for systems with significant static correlation. In these cases a multiconfigurational approach may be more appropriate,[48–50] though single reference CC calculations are usually also successful.[39,41]

A somewhat empirical way to improve MP2 results is to scale the same-spin (SS) and opposite-spin (OS) contributions to the energy by different factors in the so-called spin-component-scaled MP2 (SCS-MP2) approach.[51–53] The related spin-opposite-scaled MP2 (SOS-MP2) method completely neglects the SS contribution and yields similar accuracy with the added benefit of reduced formal scaling of the computational effort with system size from $\mathcal{O}(N^5)$ to $\mathcal{O}(N^4)$, provided a Laplace transform-based implementation is used. Fitting the scaling parameters in SCS-MP2 (or SOS-MP2) to better reproduce CCSD(T) NMR shielding constants is also possible,[54] although this somewhat obscures the physical meaning behind these parameters.

1.2.3 Density functional theory

A rather more popular approach to the calculation of chemical shifts is density functional theory (DFT), which has a significantly lower computational cost.[10,55–57] The proper

treatment of magnetic perturbations in the context DFT is the subject of ongoing discussion.[58–62] Most common density functionals (DFs) do not depend on the external magnetic field, and therefore produce exchange and correlation (XC) energies, which are unphysically constant in the presence of such. While it is possible to introduce an explicit magnetic field dependence,[63] the more widely-accepted approach is current density functional theory (CDFT), pioneered by Vignale and Rasolt,[64,65] who introduced the paramagnetic current density as an independent variable, although this choice is also subject to debate.[66] CDFT is still actively developed and was recently extended to functionals based on the meta-generalized-gradient approximation (meta-GGA).[62,67–70] However, while the current density contributions to NMR shieldings can be substantial,[59,62] CDFT results are not necessarily substantially better than those obtained with standard current-independent DFs.[58,70–72] Therefore, for pragmatic reasons the latter are widely used for the calculation of magnetic properties, with different functionals showing varying degrees of accuracy.[47,73] While there are DFs specifically optimized for NMR shielding calculations,[74,75] some general application meta-GGAs like VS98, and M06-L have been shown to be particularly well-suited for NMR chemical shifts.[76]

According to the "Jacob's ladder" classification, introduced by Perdew,[77] the highest level (fifth rung) DFT methodologies include a non-local correlation energy contribution by taking into account the virtual molecular orbitals (MOs). One possible approach of this type is double-hybrid DFT (DHDFT), whereby an MP2-like term is added to the total energy.[78,79] Combining this with SCS-MP2 and the empirical dispersion correction (denoted D3BJ in its most popular formulation), introduced by Grimme,[80–82] gives the general formulation of dispersion-corrected spin-component-scaled double-hybrid DFT (DSD-DFT), developed by Kozuch and Martin.[83–85] In extensive benchmark studies of themochemistry, kinetics and noncovalent interactions, double-hybrid density functionals (DHDFs) have been clearly shown to outperform lower-rung DFs, with DSD-BLYP and DSD-PBEP86 among the most accurate.[86–89] DSD-DFT functionals also perform better than other common DFs or MP2 in calculations of properties, for which they were not specifically optimized, such as harmonic vibrational frequencies,[84,85] dipole moments,[90] and polarizabilities.[91] This suggests they may be sufficiently "universal" to also produce high quality results for other response properties. Note that, as discussed above, the XC functionals used in DHDFT are independent of the magnetic field. While it may be expected that this deficiency is partly offset by the inclusion of Hartree–Fock (HF) exchange and MP2 correlation, this issue is not examined in the current work. Analytic derivatives for DHDFT have been derived and implemented previously for geometric gradients,[92,93] as well as NMR shieldings,[94] however, without proper treatment of the gauge origin problem.

1.3 Shielding calculations for large systems

A fundamental challenge of computational chemistry is how to apply its methods to ever larger systems. This is also relevant to NMR shielding calculations, as particularly biomolecules and natural products can have hundreds or thousands of atoms, while simulations of condensed phases may require inclusion of many molecules to obtain reliable results. Thus, it is worthwhile to improve the efficiency of computational methods as much as possible, in terms of both formal scaling with system size and overall time and resources required.

One possibility is to exploit the local nature of NMR shielding by dividing the system

into fragments and performing separate calculations for these fragments, accounting in some approximate way for their interaction with the rest of the system.[95–102] Such approaches have been successfully applied to chemical shift calculations of entire proteins. A benefit of methods based on simple electrostatic embedding of the target fragment within the surroundings, such as quantum-mechanics/molecular mechanics (QM/MM)[96,97,99] or ONIOM-like schemes,[100,101,103,104] is that one can in principle apply arbitrary levels of theory for the individual sub-calculations. This implies that any efficiency improvements in the underlying computational method can be carried over to much larger systems, provided the latter lend themselves to such fragmentation. Alternatively, if only a few nuclei in the system are of interest, it is possible to reformulate the methodology to selectively calculate only their shielding constants, thereby dramatically reducing the computation time.[105,106]

Complementary to these techniques is the use of efficient integral evaluation algorithms. As is the case for self-consistent field (SCF) calculations of the energy, the computational effort for NMR property calculations is also dominated by the evaluation of two-electron repulsion integrals. Therefore a number of approaches have been developed to reduce the cost of this step, including prescreening procedures, which reduce the number of integrals to be computed, and approximate calculation of the integrals themselves.[107] Ochsenfeld and coworkers have applied advanced screening techniques in combination with the continuous fast multipole method (CFMM) to SCF-level NMR shielding calculations and demonstrated asymptotic linear scaling with system size.[108,109]

Two other popular approaches are the resolution of the identity (RI) and chain-of-spheres (COS) approximations, which have been applied successfully to energy calculations, as well as first and second order geometric perturbations (gradients and Hessians).[110–114] Both approximations provide significant speedups and only introduce small deviations in the results (e.g. errors in the energy up to $100\,\mu E_\mathrm{h}$/atom).[111,113,115,116] For energy calculations on medium to large systems at the HF and hybrid DFT levels, the COS approximation of the exact exchange (COSX) has been shown to be more efficient than the RI approximation of the latter (RIK), due to the more favorable scaling of the COSX algorithm with system size (formally linear, quadratic in practice, as opposed to $\mathcal{O}(N^4)$ for RIK, albeit with a small prefactor).[116] Conversely, the RI approximation of the Coulomb terms (RIJ) usually provides a better balance of cost vs efficiency than the respective COS approximation (COSJ).[113] While the RI approximation has also been employed for the calculation of NMR shielding constants using GIAOs,[106,117] no such implementation of the COS scheme has been reported prior to the present work, although it is similar to the pseudospectral approach of Friesner et al.[118,119]

As part of this thesis deals with extending the applicability of MP2 to much larger systems, it should be viewed as part of an ongoing effort to reduce the computational cost of MP2 response property calculations. Works in this context are the integral-direct GIAO-MP2 implementation for NMR shieldings of Kollwitz, Häser, and Gauss,[120,121] the derivation of RI-MP2 second derivatives in combination with COSX,[94] and the Laplace-based approaches of Ochsenfeld, Hättig, and their coworkers,[122,123] as well as the local correlation methods discussed in the next section.

1.4 Property calculations with local correlation methods

When it comes to reducing the rather steep formal scaling of correlated wave function-based methods such as CC, local correlation approaches, which exploit the "near-sightedness" of dynamic correlation, have been a great success. The early development of local electron correlation methods is due to Pulay and Sæbø,[124–126] although the initial ideas date further back.[127,128] Thanks to recent advancements in several research groups,[122,129–165] the popularity and applicability of these methods for the calculation of relative energies have grown tremendously. With modern approximations, the "gold standard" CCSD(T) method[166] has become available at a computational cost only a few times higher than that of DFT.[167,168] Considering the massive progress that has been made in this field for the calculation of electronic energies, there are comparatively few works that make use of local correlation approximations to compute molecular properties, such as the dipole polarizability, NMR shielding, etc., which are related to derivatives of the energy. This is, in part, because analytic derivatives of local correlation methods are challenging, due to the complexity of the theories.

This is not to say that nothing has been accomplished on this subject. Werner, Schütz, and coworkers have derived and implemented analytic nuclear gradients for several local correlation methods[169–174] based on projected atomic orbitals (PAOs),[124,125] including MP2, and have also used them to semi-numerically calculate vibrational frequencies.[175–177] Gauss and Werner also presented a pilot implementation for NMR shielding calculations with PAO-based local MP2 (LMP2).[178] The first efficient such implementation, also employing the RI approximation, was later reported by Loibl and Schütz,[179] and also adapted to magnetizabilities.[180] Another study by Werner and coworkers examines the accuracy of PAO-based local correlation methods for polarizability calculations via finite differences,[181] an approach which is difficult to apply to magnetic properties, as it requires an implementation based on complex algebra. Maurer and Ochsenfeld developed an AO-based Laplace-transformed MP2 method for the computation of NMR shieldings, which can asymptotically achieve linear scaling, or even sub-linear if only a few nuclei are of interest.[182] Static and dynamic polarizabilities have also been implemented for MP2 and the approximate coupled cluster method CC2, using both RI and a Laplace-transformation.[123] Frank et al. reported analytic gradients for a local MP2 variant, based on pair natural orbitals (PNOs), although they neglected the PNO relaxation.[183] The complete analytic gradient for an orbital-specific virtual (OSV) local MP2 method was also published recently by Yang and coworkers.[184] We should also mention here the work by Crawford and coworkers in the field of local coupled cluster linear response theory for the calculation of molecular properties, including frequency-dependent polarizabilities and specific optical rotations.[185–188] Work in the Neese group has focused on the domain-based local pair natural orbital (DLPNO) approximation and has resulted in orbital-unrelaxed first derivatives of DLPNO-CCSD, which can be used to calculate, e.g., dipole moments and HFCs.[189,190] Fully orbital-relaxed first derivatives and nuclear gradients were also implemented for the DLPNO-MP2 method,[191–193] and those results highlight the importance of the PNO relaxation contributions, e.g. for electric field gradients.[191]

1.5 Relativistic, rovibrational, and environmental effects

The discussion so far dealt with the accurate and efficient calculation of NMR shieldings of static molecules in the gas phase within the non-relativistic and Born–Oppenheimer approximations. However, NMR experiments are performed at a finite temperature and represent averaged parameters for an ensemble of vibrating and rotating conformers of the target molecule, usually in a liquid or frozen solution. Therefore, a direct comparison between computed and measured chemical shifts is only possible if the relativistic, conformational, rovibrational, and environmental (i.e. solvent/crystal) effects are either negligibly small, or properly accounted for in the calculations.

Relativistic effects in general are only significant if the system contains heavy atoms.[9,194–197] In these cases, both scalar relativistic and spin–orbit coupling contributions can become substantial, resulting, for example, in the observable "heavy atom–light atom" (HALA) and "heavy atom–heavy atom" (HAHA) effects. Both scalar and spin–orbit relativistic corrections can be computed using an appropriate modification to the theory, such as the full four-component Dirac–Fock treatment,[198–200] approximate two-component approaches such as the zeroth-order regular approximation (ZORA)[201,202] or the Douglas–Kroll–Hess (DKH) transformation,[203,204] as well as exact two-component (X2C) methods.[205–207]

Different conformers of the same system can have drastically different NMR shieldings. In addition, chemically equivalent nuclei, such as the three hydrogen atoms of a methyl group, appear as a single signal in the spectrum, while they are non-equivalent in static calculations. Therefore, for flexible molecules, which can exist in multiple conformations at room temperature, it is absolutely essential to correctly average the computed properties over the whole conformer–rotamer ensemble. This can be done via some (manual or automatic) sampling procedure, together with accurate estimates of the Boltzmann weights of individual conformers.[208,209] Alternatively, molecular dynamics (MD) approaches can be used, including ab initio MD (AIMD), to compute a time average of the NMR shieldings.[210] The effects of rovibrational averaging can also be substantial.[211] In many cases, they can be estimated using second order vibrational perturbation theory (VPT2),[43,212] while AIMD simulations are another option.[210]

Finally, the effects of the molecular environment are most noticeable in the solid state or in strongly polar and protic solvents.[213,214] In these cases, it may be necessary to explicitly include the surrounding molecules in the model system (often within an MD simulation) in order to obtain accurate predictions.[215–217] For weakly polar and aprotic solvents, an implicit solvent model is often sufficient.[218]

1.6 Scope of the present work

This thesis encompasses three main projects. The first is a detailed study of the accuracy and efficiency of the RI and COS approximations applied to NMR shielding calculations at the SCF (HF and DFT) level with GIAOs. To put the errors due to these approximations in context, a test set of small molecules is assembled and the comparatively larger errors due to basis set incompleteness and the level of theory are assessed. The findings are presented in Chapter 2.

The second project deals with the derivation and implementation of the RI-MP2 and DHDFT methods for NMR shielding calculations using GIAOs. The accuracy of various

double-hybrid functionals, as well as the other sources of error (RI, basis sets, etc.), are assessed using the same set of molecules, which is why these results are also grouped in Chapter 2.

The third project, discussed in Chapter 3, is the derivation and implementation of analytic second derivatives of DLPNO-MP2, applicable to field-response properties, such as dipole polarizabilities and NMR shieldings. A detailed benchmark study of the accuracy and efficiency of the method is also reported. This is the first implementation of formally complete analytic second derivatives of a PNO-based local correlation method and on the one hand it serves as a stepping stone towards DLPNO-CCSD second derivatives. On the other hand, it allows the application of MP2 and DHDFT, which have been shown to be very accurate for polarizabilities and NMR shieldings,[35,47,91] to even larger systems.

All software implementations related to this thesis are included in the ORCA electronic structure program.[219–221]

Note that the derivations and implementations discussed in this work are not directly applicable to harmonic vibrational frequencies, as the efficient evaluation of the nuclear Hessian requires substantially different algorithms.

In addition, relativistic effects are entirely neglected throughout this thesis. Rovibrational influences are circumvented by comparing between equilibrium values computed using various methods and approximations. However, the techniques discussed here are in principle also applicable within schemes such as VPT2 or AIMD. Finally, the results in this work are computed in vacuum, although implicit solvent models are briefly discussed and once again, inclusion of explicit solvent molecules is also possible with the presented methods.

Chapter 2

Efficient NMR shielding calculations at the SCF, MP2, and double-hybrid DFT levels

2.1 Theory

2.1.1 Notation and general considerations

Throughout this chapter $\mu, \nu, \ldots$ label atomic orbitals (AOs), $i, j, \ldots$ and $a, b, \ldots$ label occupied and virtual molecular orbitals (MOs), respectively, and $p, q, \ldots$ label any MOs.

Where a matrix quantity is defined using the same symbol in both the AO and MO basis sets, for example $F_{\mu\nu}$ and F_{pq}, to distinguish these in matrix notation, the index "AO" is added to the former, i.e. $\mathbf{F}_{\mathrm{AO}}$ and $\mathbf{F}$, respectively. A matrix trace is denoted as $\mathrm{tr}(\mathbf{A}) = \sum_i A_{ii}$.

When expressing derivatives in matrix form the following notation is used:

$$\frac{\partial A}{\partial b_{ij}} = C_{ij} \quad \Leftrightarrow \quad \frac{\partial A}{\partial \mathbf{b}} = \mathbf{C} \tag{2.1}$$

$$A^b_{ij} \equiv \left.\frac{\mathrm{d}A_{ij}}{\mathrm{d}b}\right|_{b=0} = C_{ij} \quad \Leftrightarrow \quad \mathbf{A}^b \equiv \left.\frac{\mathrm{d}\mathbf{A}}{\mathrm{d}b}\right|_{b=0} = \mathbf{C} \tag{2.2}$$

A perturbation index in parenthesis, i.e. $\mathbf{A}^{(b)}$ is used to imply that not the full derivative is taken but, e.g., derivatives of the MO coefficients are excluded. In the following, these symbols are defined at first occurrence. In addition, the following shorthand is used to explicitly denote unperturbed quantities:

$$\mathbf{A}^{(0)} \equiv \mathbf{A}|_{b=0} \tag{2.3}$$

In the case of magnetic properties, special attention must be paid to complex conjugation: the superscripts "$*$", "T", and "$\dagger$" are used to denote the complex conjugate, matrix transpose, and complex transpose of a quantity. Because the independent parameters in the derivations are considered complex quantities, Wirtinger derivatives are used throughout,[222] i.e. for a complex parameter $z = x + \mathrm{i}y$ and a function $f(z, z^*)$:

$$\frac{\mathrm{d}f}{\mathrm{d}z} = \frac{1}{2}\frac{\mathrm{d}f}{\mathrm{d}x} - \frac{\mathrm{i}}{2}\frac{\mathrm{d}f}{\mathrm{d}y} \qquad \frac{\mathrm{d}f}{\mathrm{d}z^*} = \frac{1}{2}\frac{\mathrm{d}f}{\mathrm{d}x} + \frac{\mathrm{i}}{2}\frac{\mathrm{d}f}{\mathrm{d}y} \tag{2.4}$$

In addition to the ordinary product and chain rules, the following equalities hold:

$$\left(\frac{\mathrm{d}f}{\mathrm{d}z}\right)^* = \frac{\mathrm{d}f^*}{\mathrm{d}z^*} \qquad \left(\frac{\mathrm{d}f}{\mathrm{d}z^*}\right)^* = \frac{\mathrm{d}f^*}{\mathrm{d}z} \tag{2.5}$$

In general, z and z^* are viewed as independent parameters until a point where they become fully real ($z = z^*$) or fully imaginary ($z = -z^*$).

Atomic units are used in all equations throughout this work.

2.1.2 NMR shielding at the self-consistent field level

In the following, a brief overview is given of the basic theory underlying the calculation of the NMR shielding tensor using analytic derivative techniques, in particular, at the SCF level. For a more thorough discussion the reader is referred to the lecture by Gauss,[16] as well as the extensive review by Helgaker et al.[13] and references therein.

2.1.2.1 The NMR shielding tensor as a derivative of the energy

As mentioned in Section 1.2, the NMR shielding tensor $\boldsymbol{\sigma}^K$ of nucleus K can be expressed as the second derivative of the energy with respect to the magnetic field $\mathbf{B}$ and the magnetic moment of the nucleus, $\mathbf{m}_K$:

$$\sigma^K_{\beta\alpha} = \left.\frac{\mathrm{d}^2 E}{\mathrm{d}B_\alpha \mathrm{d}m_{K_\beta}}\right|_{\mathbf{B},\mathbf{m}_K=0}, \qquad \alpha,\beta = x,y,z \tag{2.6}$$

The energy E is the expectation value of the Hamiltonian, the one-electron part of which is parametrized to depend explicitly on $\mathbf{B}$ and $\mathbf{m}_K$ in the following manner:[33]

$$\mathrm{h}(\mathbf{r},\mathbf{B},\mathbf{m}) = \frac{1}{2}\boldsymbol{\pi}^2 - \mathrm{V}(\mathbf{r}), \qquad \boldsymbol{\pi} = -\mathrm{i}\boldsymbol{\nabla} + \mathbf{A}(\mathbf{r},\mathbf{B},\mathbf{m}) \tag{2.7}$$

where the vector potential $\mathbf{A}$ is given by

$$\mathbf{A}(\mathbf{r},\mathbf{B},\mathbf{m}) = \frac{1}{2}\mathbf{B}\times(\mathbf{r}-\mathbf{R}_O) + \alpha^2 \sum_K \frac{\mathbf{m}_K \times (\mathbf{r}-\mathbf{R}_K)}{|\mathbf{r}-\mathbf{R}_K|} \tag{2.8}$$

where the first term corresponds to the external field, the second arises due to the nuclear magnetic moments. In the above equations, $\mathbf{r}$ and $\mathbf{R}_K$ are the coordinates of the electron and nucleus K, respectively, α is the fine-structure constant, and $\mathbf{R}_O$ is the arbitrarily chosen gauge origin.

Using a density matrix-based formalism, equation 2.6 can be evaluated as

$$\sigma^K_{\beta\alpha} = \left.\frac{\mathrm{d}^2 E}{\mathrm{d}B_\alpha \mathrm{d}m_{K_\beta}}\right|_{\mathbf{B},\mathbf{m}_K=0} = \sum_{\mu\nu} D_{\mu\nu} \frac{\mathrm{d}^2 h_{\mu\nu}}{\mathrm{d}B_\alpha \mathrm{d}m_{K_\beta}} + \sum_{\mu\nu} \frac{\mathrm{d}D_{\mu\nu}}{\mathrm{d}B_\alpha}\frac{\mathrm{d}h_{\mu\nu}}{\mathrm{d}m_{K_\beta}} \tag{2.9}$$

where $\mathbf{D}$ is the density matrix. Note that for non-variational methods, the proper definitions of the density matrices must be used.[34,37,39,223–227] The first and second terms in eq. 2.6 are referred to as the "diamagnetic" and "paramagnetic" parts of the shielding tensor. To compute the latter, the perturbed or "response" density matrix $\mathbf{D}^{\mathbf{B}}$ is required – its evaluation at the HF level is discussed in the following section. The extension to (hybrid) Kohn–Sham DFT (KS-DFT) is given in Section 2.1.4.

2.1.2.2 Coupled perturbed self-consistent field equations

For SCF methods (HF or DFT), the density matrix is defined as:

$$D_{\mu\nu}^{\mathrm{SCF}} = 2\sum_{i} c_{\mu i}^{*} c_{\nu i} \tag{2.10}$$

We can parametrize the dependence of the MO coefficients on the magnetic field as

$$\mathbf{c}(\mathbf{B}) = \mathbf{c}^{(0)}\mathbf{U}(\mathbf{B}) \tag{2.11}$$

Hence, the perturbed density becomes

$$D_{\mu\nu}^{\mathrm{SCF},\mathbf{B}} = 2\sum_{pi} \left(c_{\mu p}^{*} U_{pi}^{\mathbf{B}*} c_{\nu i} + c_{\mu i}^{*} U_{pi}^{\mathbf{B}} c_{\nu p} \right) \tag{2.12}$$

where the superscript $\mathbf{B}$ denotes a magnetic field derivative (at $\mathbf{B} = 0$).

For any value of the external perturbation, the MO coefficients must fulfill the orthonormality condition $S_{pq} = \delta_{pq}$ and the Brillouin condition $F_{ai} = 0$ where S_{pq} and F_{pq} are elements of the overlap and Fock matrices in the MO basis. The unknown coefficients $\mathbf{U}^{\mathbf{B}}$ are constrained by the derivative of these conditions:

$$\frac{\mathrm{d}}{\mathrm{d}\mathbf{B}} S_{pq} = 0 \qquad\qquad \frac{\mathrm{d}}{\mathrm{d}\mathbf{B}} F_{ai} = 0 \tag{2.13}$$

The former gives:

$$U_{qp}^{\mathbf{B}*} + S_{pq}^{(\mathbf{B})} + U_{pq}^{\mathbf{B}} = 0, \quad \text{with} \quad S_{pq}^{(\mathbf{B})} = \sum_{\mu\nu} c_{\mu p}^{(0)*} S_{\mu\nu}^{\mathbf{B}} c_{\nu q}^{(0)} \tag{2.14}$$

while the latter results in the so-called coupled perturbed self-consistent field (CPSCF) equations:

$$0 = F_{ai}^{\mathbf{B}} = \left(\mathbf{U}^{\mathbf{B}\dagger}\mathbf{F} + \mathbf{F}\mathbf{U}^{\mathbf{B}} + \mathbf{c}^{\dagger}\mathbf{h}_{\mathrm{AO}}^{\mathbf{B}}\mathbf{c} + \mathbf{c}^{\dagger}\mathbf{g}_{\mathrm{AO}}^{\mathbf{B}}\left[\mathbf{D}^{\mathrm{SCF}}\right]\mathbf{c} + \mathbf{g}\left[\mathbf{D}^{\mathrm{SCF},\mathbf{B}}\right] \right)_{ai} \tag{2.15}$$

$$h_{\mu\nu} = \langle \mu | \, \mathrm{h} \, | \nu \rangle \tag{2.16}$$

$$g_{\mu\nu}[\mathbf{D}] = J_{\mu\nu}[\mathbf{D}] - \frac{1}{2} K_{\mu\nu}[\mathbf{D}] = \sum_{\kappa\lambda} D_{\kappa\lambda} \left[(\mu\nu|\kappa\lambda) - \frac{1}{2} (\mu\lambda|\kappa\nu) \right] \tag{2.17}$$

where $(\mu\nu|\kappa\lambda)$ are the two-electron repulsion integrals in Mulliken $(1^*1|2^*2)$ notation and $\mathbf{h}_{\mathrm{AO}}$, $\mathbf{g}_{\mathrm{AO}}\left[\mathbf{D}^{\mathrm{SCF}}\right]$, $\mathbf{J}_{\mathrm{AO}}\left[\mathbf{D}^{\mathrm{SCF}}\right]$, and $\mathbf{K}_{\mathrm{AO}}\left[\mathbf{D}^{\mathrm{SCF}}\right]$ are respectively the one-electron, two-electron, Coulomb and exchange parts of the Fock matrix in AO basis. The same symbols without the "AO" index denote the matrices transformed to the MO basis, e.g. $\mathbf{g}\left[\mathbf{D}^{\mathrm{SCF}}\right] = \mathbf{c}^{\dagger}\mathbf{g}_{\mathrm{AO}}\left[\mathbf{D}^{\mathrm{SCF}}\right]\mathbf{c}$. The two-electron operators are also defined analogously for (pseudo-)density matrices in the MO basis, as determined from context.

We evaluate the terms in eq. 2.15 one by one using eq. 2.14 and assuming canonical orbitals, i.e. $F_{pq} = \delta_{pq}\varepsilon_q$:

$$\left(\mathbf{U}^{\mathbf{B}\dagger}\mathbf{F}\right)_{ai} = U_{ia}^{\mathbf{B}*}\varepsilon_i = \left(-S_{ai}^{(\mathbf{B})} - U_{ai}^{\mathbf{B}}\right)\varepsilon_i \tag{2.18}$$

$$\left(\mathbf{F}\mathbf{U}^{\mathbf{B}}\right)_{ai} = \varepsilon_a U_{ai}^{\mathbf{B}} \tag{2.19}$$

$$\left(\mathbf{c}^{\dagger}\mathbf{h}^{\mathbf{B}}\mathbf{c}\right)_{ai} = \sum_{\mu\nu} c_{\mu a}^{*} c_{\nu i} \frac{\mathrm{d}h_{\mu\nu}}{\mathrm{d}\mathbf{B}} \tag{2.20}$$

$$
\begin{aligned}
g^{\mathbf{B}}_{\mu\nu}\left[\mathbf{D}^{\mathrm{SCF}}\right] &= J^{\mathbf{B}}_{\mu\nu}\left[\mathbf{D}^{\mathrm{SCF}}\right] - \frac{1}{2}K^{\mathbf{B}}_{\mu\nu}\left[\mathbf{D}^{\mathrm{SCF}}\right] \\
&= \sum_{\kappa\lambda} D_{\kappa\lambda}\left[\frac{\mathrm{d}\,(\mu\nu|\kappa\lambda)}{\mathrm{d}\mathbf{B}} - \frac{1}{2}\frac{\mathrm{d}\,(\mu\lambda|\kappa\nu)}{\mathrm{d}\mathbf{B}}\right] && (2.21)\\
g_{ai}\left[\mathbf{D}^{\mathrm{SCF},\mathbf{B}}\right] &= \underbrace{-\sum_{bj}\left[U^{\mathbf{B}*}_{bj}\,(aj|bi) + U^{\mathbf{B}}_{bj}\,(ab|ji)\right]}_{K_{ai}[\mathbf{U}^{\mathbf{B}}]} + \underbrace{\sum_{kj} S^{(\mathbf{B})}_{kj}\,(ak|ji)}_{K_{ai}\left[\mathbf{S}^{(\mathbf{B})}\right]} && (2.22)
\end{aligned}
$$

where we have used eq. 2.14 to express the perturbed density matrix as

$$
D^{\mathrm{SCF},\mathbf{B}}_{\mu\nu} = 2\sum_{ai}\left(c^{*}_{\mu a}U^{\mathbf{B}*}_{ai}c_{\nu i} + c^{*}_{\mu i}U^{\mathbf{B}}_{ai}c_{\nu a}\right) - 2\sum_{ij} c^{*}_{\mu j}S^{(\mathbf{B})}_{ij}c_{\nu i} \tag{2.23}
$$

Note that for magnetic perturbations, all integral derivatives are purely imaginary and so are the perturbed MO coefficients, i.e. $\mathbf{U}^{\mathbf{B}*} = -\mathbf{U}^{\mathbf{B}}$. All perturbed Hermitian matrices such as $\mathbf{D}^{\mathrm{SCF},\mathbf{B}}$ are therefore antisymmetric, which is why the Coulomb contributions in eq. 2.22 drop out. The term denoted $K_{ai}\left[\mathbf{U}^{\mathbf{B}}\right]$ in the same equation is not consistent with the definition of the $\mathbf{K}[\mathbf{D}]$ operator above but we use this notation for convenience.

Collecting all terms in eq. 2.15 containing $\mathbf{U}^{\mathbf{B}}$ in the left-hand side we obtain the final form of the CPSCF equations in the canonical MO basis. These can be formulated in matrix form by combining the indices ai into a single index:

$$
\begin{aligned}
\mathbf{A}\mathbf{U}^{\mathbf{B}} &= -\mathbf{L}^{\mathbf{B}} && (2.24)\\
A_{ai,bj} &= (\varepsilon_a - \varepsilon_i)\,\delta_{ai,bj} + (aj\,|\,bi) - (ab\,|\,ji) && (2.25)\\
L^{\mathbf{B}}_{ai} &= h^{(\mathbf{B})}_{ai} + \sum_{j}\left[2\,(ai|jj)^{(\mathbf{B})} - (aj|ji)^{(\mathbf{B})}\right] - \varepsilon_i S^{(\mathbf{B})}_{ai} + \sum_{jk} S^{(\mathbf{B})}_{kj}\,(ak|ji) && (2.26)\\
h^{(\mathbf{B})}_{pq} &= \sum_{\mu\nu} c^{(0)*}_{\mu p}h^{\mathbf{B}}_{\mu\nu}c^{(0)}_{\nu q} && (2.27)\\
(pq|rs)^{(\mathbf{B})} &= \sum_{\mu\nu\kappa\lambda} c^{(0)*}_{\mu p}c^{(0)}_{\nu q}c^{(0)*}_{\kappa r}c^{(0)}_{\lambda s}\,(\mu\nu|\kappa\lambda)^{\mathbf{B}} && (2.28)
\end{aligned}
$$

The discussion above also applies to KS-DFT, however, some additional terms arise due to the XC functional, which are discussed in Section 2.1.4. Inclusion of implicit solvent effects is discussed in Section 2.1.5.

2.1.2.3 GIAO Integrals

The dependence of the AOs on $\mathbf{B}$ and of the Hamiltonian on both $\mathbf{B}$ and $\mathbf{m}_K$ leads to non-zero derivatives of molecular integrals with respect to these quantities. The exact form of the derivative GIAO integrals was derived in detail by Helgaker and Jørgensen.[33] We summarize the working equations here for completeness:

$$
\begin{aligned}
\left.\frac{\mathrm{d}\,(\mu_M\nu_N\,|\,\kappa_K\lambda_L)}{\mathrm{d}\mathbf{B}}\right|_{\mathbf{B}=0} &= \frac{\mathrm{i}}{2}\,(\mu_M\nu_N|\left[\mathbf{O}_{MN}\mathbf{r}_1 + \mathbf{O}_{KL}\mathbf{r}_2\right]r_{12}^{-1}\,|\kappa_K\lambda_L) && (2.29)\\
\left.\frac{\mathrm{d}S_{\mu\nu}}{\mathrm{d}\mathbf{B}}\right|_{\mathbf{B}=0} &= \frac{\mathrm{i}}{2}\,\langle\mu_M|\,\mathbf{O}_{MN}\mathbf{r}\,|\nu_N\rangle && (2.30)\\
\left.\frac{\mathrm{d}h_{\mu\nu}}{\mathrm{d}\mathbf{B}}\right|_{\mathbf{B}=0} &= \frac{\mathrm{i}}{2}\,\langle\mu_M|\,\mathbf{O}_{MN}\mathbf{r}\mathrm{h}\,|\nu_N\rangle + \frac{1}{2}\,\langle\mu_M|\,\mathbf{L}_N\,|\nu_N\rangle && (2.31)
\end{aligned}
$$

$$\left.\frac{\mathrm{d}h_{\mu\nu}}{\mathrm{d}\mathbf{m}_K}\right|_{\mathbf{m}_K=0} = \alpha^2 \left\langle \mu_M \left| \frac{\mathbf{L}_N}{r_N^3} \right| \nu_N \right\rangle \tag{2.32}$$

$$\left.\frac{\mathrm{d}^2 h_{\mu\nu}}{\mathrm{d}\mathbf{B}\mathrm{d}\mathbf{m}_K}\right|_{\mathbf{B},\mathbf{m}_K=0} = \frac{\alpha^2}{2} \left\langle \mu_M \left| \frac{\mathrm{i}\mathbf{O}_{MN}\mathbf{r}\mathbf{L}_N^{\mathrm{T}} + (\mathbf{r}_M \cdot \mathbf{r}_N)\,\mathbf{1} - \mathbf{r}_M\mathbf{r}_N^{\mathrm{T}}}{r_N^3} \right| \nu_N \right\rangle \tag{2.33}$$

$$\mathbf{L}_N = -\mathrm{i}\mathbf{r}_N \times \boldsymbol{\nabla} \tag{2.34}$$

$$\mathbf{R}_{MN} = \mathbf{R}_M - \mathbf{R}_N = \begin{bmatrix} X_{MN} & Y_{MN} & Z_{MN} \end{bmatrix} \tag{2.35}$$

$$\mathbf{O}_{MN} = \begin{bmatrix} 0 & -Z_{MN} & Y_{MN} \\ Z_{MN} & 0 & -X_{MN} \\ -Y_{MN} & X_{MN} & 0 \end{bmatrix} \tag{2.36}$$

Note that the definition of the matrix $\mathbf{O}$ allows for integral derivatives with respect to the magnetic field to be calculated similarly to geometric derivative integrals, required for analytic gradient calculations. The evaluation of the contributions involving the two-electron integrals (eq. 2.29) can be carried out efficiently using either RI or COS, both of which are discussed in the following sections.

2.1.2.4 Resolution of the identity approximation

In the RI or density fitting approximation, a product of Gaussian-type orbitals (GTOs) is expanded as a linear combination of auxiliary basis functions (denoted $K, L, \dots$). In the present case, the unperturbed Coulomb integrals can be approximated using RI as[228]

$$J_{\mu\nu}^{\mathrm{RI}}\left[\mathbf{D}^{\mathrm{SCF}}\right] = \sum_K d_K\,(\mu\nu|K) \tag{2.37}$$

$$d_K = \sum_L \left(\mathbf{V}^{-1}\right)_{KL} \sum_{\kappa\lambda} D_{\kappa\lambda}^{\mathrm{SCF}}\,(\kappa\lambda|L) \tag{2.38}$$

where the integrals involved are defined as

$$(\mu\nu|K) = \int \varphi_\mu^*(\mathbf{r}_1)\,\varphi_\nu(\mathbf{r_1})\,r_{12}^{-1}\eta_K(\mathbf{r}_2)\,\mathrm{d}\mathbf{r}_1\mathrm{d}\mathbf{r}_2 \tag{2.39}$$

$$V_{KL} = \int \eta_K^*(\mathbf{r}_1)\,r_{12}^{-1}\eta_L(\mathbf{r}_2)\,\mathrm{d}\mathbf{r}_1\mathrm{d}\mathbf{r}_2 \tag{2.40}$$

Several efficient algorithms exist for the evaluation of the Coulomb term, in this work the Split-RI-J algorithm is used.[229] The exchange matrix is evaluated using the expression[110,230]

$$K_{\mu\nu}^{\mathrm{RI}}\left[\mathbf{D}^{\mathrm{SCF}}\right] = 2\sum_{iK} (\mu i|K)\,(\nu i\,|\,\widetilde{K}) \tag{2.41}$$

$$(\mu i|K) = \sum_\lambda c_{\lambda i}\,(\mu\lambda|K) \tag{2.42}$$

$$(\mu i\,|\,\widetilde{K}) = \sum_L \left(\mathbf{V}^{-1}\right)_{KL} (\mu i|L) \tag{2.43}$$

It should be noted that RI does not reduce the formal scaling (only the prefactor) of the evaluation of the exchange term, unlike it does for the Coulomb contribution. The RI metric $\mathbf{V}$ does not need to be explicitly inverted. Instead, eqs. 2.38 and 2.43 are solved using a Cholesky decomposition of $\mathbf{V}$.

In order to apply the RI approximation to the two-electron integrals in the CPSCF equations, several modifications are made. The $\mathbf{K}\left[\mathbf{S}^{(\mathbf{B})}\right]$ term can be assembled from stored four-index MO basis integrals evaluated using RI:

$$K_{ai}^{\mathrm{RI}}\left[\mathbf{S}^{(\mathbf{B})}\right] = \sum_{jk} S_{kj}^{(\mathbf{B})} \left(ak|ji\right)^{\mathrm{RI}} \tag{2.44}$$

$$\left(pq|rs\right)^{\mathrm{RI}} = \sum_{KL} \left(pq|K\right) \left(\mathbf{V}^{-1}\right)_{KL} \left(rs|L\right) \tag{2.45}$$

$$\left(pq|K\right) = \sum_{\mu\nu} c_{\mu p}^{*} c_{\nu q} \left(\mu\nu|K\right) \tag{2.46}$$

Likewise, the $\mathbf{K}\left[\mathbf{U}^{\mathbf{B}}\right]$ term on the left-hand side of the CPSCF equation can be assembled at every iteration from stored integrals:

$$K_{ai}^{\mathrm{RI}}\left[\mathbf{U}^{\mathbf{B}}\right] = \sum_{jb} U_{bj}^{\mathbf{B}} \left[\left(aj|bi\right)^{\mathrm{RI}} - \left(ab|ji\right)^{\mathrm{RI}}\right] \tag{2.47}$$

While it significantly speeds up the calculation (see Section 2.3.10.1), storing the four-index integrals on disk also leads to large disk space requirements. In case these become prohibitive, $\mathbf{K}\left[\mathbf{U}^{\mathbf{B}}\right]$ may instead be computed on-the-fly in each iteration using standard integral-direct techniques. An integral-direct RIK implementation for this term is not discussed here, however it is not expected to be very efficient. Unlike the exchange contribution in the SCF (eq. 2.41), where only the integrals $(\mu i|K)$ are evaluated at every iteration, for eq. 2.47 it is also required to recalculate $(\mu a|K)$, which significantly increases the computational effort.

Somewhat more involved are the $\mathbf{g}^{\mathbf{B}}\left[\mathbf{D}^{\mathrm{SCF}}\right]$ terms, where the three-index perturbed integrals are required:

$$\left(\mu i|K\right)^{(\mathbf{B})} = \sum_{\nu} c_{\nu i}^{(0)} \left(\mu\nu|K\right)^{\mathbf{B}} \tag{2.48}$$

$$\left(\mu\nu|K\right)^{\mathbf{B}} = \left.\frac{\mathrm{d}\left(\mu\nu|K\right)}{\mathrm{d}\mathbf{B}}\right|_{\mathbf{B}=0} = \frac{\mathrm{i}}{2} \left\langle \mu_M \nu_N \right| \mathbf{O}_{MN} \mathbf{r}_1 r_{12}^{-1} \left| K \right\rangle \tag{2.49}$$

$$J_{\mu\nu}^{\mathrm{RI},\mathbf{B}}\left[\mathbf{D}^{\mathrm{SCF}}\right] = \sum_{K} d_K \left(\mu\nu|K\right)^{\mathbf{B}} \tag{2.50}$$

$$K_{\mu\nu}^{\mathrm{RI},\mathbf{B}}\left[\mathbf{D}^{\mathrm{SCF}}\right] = 2 \sum_{iK} \left[\left(\mu i|K\right)^{(\mathbf{B})} \left(\nu i \,|\, \widetilde{K}\right) - \left(\mu i \,|\, \widetilde{K}\right) \left(\nu i|K\right)^{(\mathbf{B})}\right] \tag{2.51}$$

The fitting coefficients d_K are independent of the perturbation because $D_{\kappa\lambda}^{\mathrm{SCF}}$ is symmetric, while $(\kappa\lambda|L)^{\mathbf{B}}$ is antisymmetric in κ and λ and therefore the trace of their product is zero. Note that the auxiliary basis functions are not field-dependent to ensure gauge invariance of the three-index integrals.[117]

2.1.2.5 Chain of spheres approximation

Unlike RI, the COS approximation does lower the formal scaling of the exchange term, for the evaluation of which it is especially well suited. The COS method is a seminumerical technique, in which the integration over $\mathbf{r}_2$ is done numerically as a sum over grid points g, weighted by w_g[113]

$$K_{\mu\nu}^{\mathrm{COS}}\left[\mathbf{D}^{\mathrm{SCF}}\right] = \sum_{g} W_{\mu g} G_{\nu g} \tag{2.52}$$

$$G_{\nu g} = \sum_{\kappa} F_{\kappa g} A^{g}_{\kappa\nu}, \tag{2.53}$$

$$W_{\mu g} = \sqrt{w_g}\varphi_{\mu}(\mathbf{r}_g) \tag{2.54}$$

$$F_{\kappa g} = \sum_{\lambda} D^{\mathrm{SCF}}_{\kappa\lambda} W_{\lambda g} \tag{2.55}$$

$$A^{g}_{\kappa\nu} = \int \varphi_{\kappa}(\mathbf{r})\, \varphi_{\nu}(\mathbf{r})\, |\mathbf{r} - \mathbf{r}_g|^{-1}\, \mathrm{d}\mathbf{r} \tag{2.56}$$

The numerical error can be reduced by employing the so-called "overlap-fitting" procedure,[231] whereby the following expression is used instead of eq. 2.52:

$$K^{\mathrm{COS}}_{\mu\nu}\left[\mathbf{D}\right] = \sum_{g} Q_{\mu g} G_{\nu g} \tag{2.57}$$

where the matrix $\mathbf{Q}$ is defined as

$$\mathbf{Q} = \mathbf{S}_{\mathrm{AO}} \left(\mathbf{W}\mathbf{W}^{\mathrm{T}}\right)^{-1} \mathbf{W} \tag{2.58}$$

where $\mathbf{S}_{\mathrm{AO}}$ is the analytic overlap matrix in the AO basis.

The Coulomb term can also be approximated (COSJ):

$$J^{\mathrm{COS}}_{\mu\nu}\left[\mathbf{D}^{\mathrm{SCF}}\right] = \sum_{\kappa\lambda} D_{\kappa\lambda}\, (\mu\nu\,|\,\kappa\lambda) = \sum_{g} W_{\mu g} W_{\nu g} I_g \tag{2.59}$$

$$I_g = \sum_{\kappa\lambda} D^{\mathrm{SCF}}_{\kappa\lambda} A^{g}_{\kappa\lambda} \tag{2.60}$$

While the evaluation of eq. 2.59 can be implemented very efficiently, a large number of grid points is required to achieve sufficient accuracy, making this approach inferior to the RIJ approximation (eq. 2.37),[113] and hence it is not employed in this work (for the unperturbed integrals).

The $\mathbf{K}\left[\mathbf{U}^{\mathbf{B}}\right]$ and $\mathbf{K}\left[\mathbf{S}^{(\mathbf{B})}\right]$ terms require no special attention – they are evaluated using equations 2.53–2.58 by replacing $\mathbf{D}^{\mathrm{SCF}}$ with the appropriate effective density matrix, i.e. the first or second term of eq. 2.23, respectively, transformed to the AO basis. Note that special care must be taken when evaluating 2.55 because the perturbed density is antisymmetric.

The GIAO terms are also evaluated in the AO-basis. We first split the derivative integrals into two parts in order to make use of permutational symmetry:

$$\begin{aligned}
&(\mu_M \lambda_L|\, \mathbf{O}_{ML} \mathbf{r}_1 r_{12}^{-1}\, |\kappa_K \nu_N) + (\mu_M \lambda_L|\, \mathbf{O}_{KN} \mathbf{r}_2 r_{12}^{-1}\, |\kappa_K \nu_N) \\
&\quad = \left(\overline{\mu\lambda}\middle|\kappa\nu\right)^{\mathbf{B}} + (\mu\lambda|\overline{\kappa\nu})^{\mathbf{B}} \\
&\quad = \left(\overline{\mu\lambda}\middle|\kappa\nu\right)^{\mathbf{B}} - (\overline{\nu\kappa}|\lambda\mu)^{\mathbf{B}}
\end{aligned} \tag{2.61}$$

A bar over the AO labels signifies that a derivative is taken only of those basis functions. Exploiting also the symmetry of the density matrix, we obtain for $\mathbf{K}^{\mathbf{B}}\left[\mathbf{D}^{\mathrm{SCF}}\right]$:

$$K^{\mathbf{B}}_{\mu\nu}\left[\mathbf{D}^{\mathrm{SCF}}\right] = \sum_{\kappa\lambda} D^{\mathrm{SCF}}_{\kappa\lambda} \left(\overline{\mu\lambda}\middle|\kappa\nu\right)^{\mathbf{B}} - \sum_{\kappa\lambda} D^{\mathrm{SCF}}_{\kappa\lambda} (\overline{\nu\kappa}|\lambda\mu)^{\mathbf{B}} = \widetilde{K}^{\mathbf{B}}_{\mu\nu} - \widetilde{K}^{\mathbf{B}}_{\nu\mu} \tag{2.62}$$

where the last equality defines $\widetilde{\mathbf{K}}^{\mathbf{B}}$. It is useful to look at the perturbation along one coordinate:

$$\widetilde{K}^{B_x}_{\mu\nu} = \frac{\mathrm{i}}{2} \sum_{\kappa\lambda} D^{\mathrm{SCF}}_{\kappa\lambda} \left[Y_{ML}\, (\mu_M \lambda_L|\, z_1 r_{12}^{-1}\, |\kappa_K \nu_N) - Z_{ML}\, (\mu_M \lambda_L|\, y_1 r_{12}^{-1}\, |\kappa_K \nu_N)\right]$$

$$\overset{\text{COS}}{\approx} \frac{\mathrm{i}}{2} \sum_{\kappa\lambda} D^{\text{SCF}}_{\kappa\lambda} \sum_{g} w_g \varphi_\mu(\mathbf{r}_g)\, \varphi_\nu(\mathbf{r}_g)\, A^g_{\kappa\nu} \left[Y_M z_g - Y_L z_g - Z_M y_g + Z_L y_g\right]$$
$$= \frac{\mathrm{i}}{2} \sum_{g} \left[\overline{W}^x_{\mu g} G_{\nu g} + W_{\mu g} \overline{G}^x_{\nu g}\right] \tag{2.63}$$

and finally, introducing overlap-fitting:

$$\widetilde{K}^{\text{COS},B_x}_{\mu\nu} = \frac{\mathrm{i}}{2} \sum_{g} \left[\overline{Q}^x_{\mu g} G_{\nu g} + Q_{\mu g} \overline{G}^x_{\nu g}\right] \tag{2.64}$$

where the barred quantities are defined as

$$\overline{W}^x_{\mu g} = \sqrt{w_g} \varphi_\mu\left(\mathbf{r}_g\right) \left[Y_M z_g - Z_M y_g\right] \tag{2.65}$$
$$\overline{G}^x_{\nu g} = \sum_{\kappa} \overline{F}^x_{\kappa g} A^g_{\kappa\nu} \tag{2.66}$$
$$\overline{F}^x_{\kappa g} = \sum_{\lambda} D^{\text{SCF}}_{\kappa\lambda} W_{\lambda g} \left[Z_L y_g - Y_L z_g\right] \tag{2.67}$$
$$\overline{Q}^x_{\mu g} = Q_{\mu g} \left[Y_M z_g - Z_M y_g\right] \tag{2.68}$$

$\mathbf{K}^{\mathbf{B}}\left[\mathbf{D}^{\text{SCF}}\right]$ is therefore approximated as

$$\mathbf{K}^{\text{COS},\mathbf{B}}\left[\mathbf{D}^{\text{SCF}}\right] = \widetilde{\mathbf{K}}^{\text{COS},\mathbf{B}} - \widetilde{\mathbf{K}}^{\text{COS},\mathbf{B},\text{T}} \tag{2.69}$$

The perturbed Coulomb term can also be approximated using COS:

$$J^{\text{COS},B_x}_{\mu\nu}\left[\mathbf{D}^{\text{SCF}}\right] = \sum_{\kappa\lambda} D^{\text{SCF}}_{\kappa\lambda} \left(\overline{\mu\nu}|\kappa\lambda\right)^{B_x} = \frac{\mathrm{i}}{2} \sum_{g} W_{\mu g} W_{\nu g} \left[Y_{ML} z_g - Z_{ML} y_g\right] I_g \tag{2.70}$$

The $\left(\mu\nu\middle|\overline{\kappa\lambda}\right)^{\mathbf{B}}$ term vanishes because it is antisymmetric in κ and λ while the density is symmetric, so the trace of their product is zero.

2.1.3 Analytic derivatives of RI-MP2 and RI-DHDFT

The theory of MP2-level NMR shielding calculations is well known[34,35,120] and adaptations to SCS-,[54] local,[122,178] and RI-accelerated local MP2[179] have been developed and implemented. The extension to DHDFT is rather simple and in general presents fewer difficulties than geometric DHDFT derivatives.[92,94] In this section, a derivation of RI-MP2 analytic second derivatives for NMR shieldings is presented, in the context of DSD-DFT for the sake of generality.

2.1.3.1 Lagrangian formulation

The general DSD-DFT energy expression is[83–85]

$$E^{\text{DSD-DFT}} = \underbrace{E_{\text{T}} + E_{\text{J}} + E_{\text{ne}} + c_{\text{X}} E^{\text{HF}}_{\text{X}} + \left(1 - c_{\text{X}}\right) E^{\text{DFT}}_{\text{X}} + c_{\text{C}} E^{\text{DFT}}_{\text{C}} + s_6 E_{\text{D}}}_{E^{\text{SCF}}}$$
$$+ \underbrace{c_{\text{O}} E^{\text{MP2}}_{\text{O}} + c_{\text{S}} E^{\text{MP2}}_{\text{S}}}_{E^{\text{MP2}}} \tag{2.71}$$

where the terms are, respectively, the kinetic energy, the electron–electron and electron–nuclear Coulomb energies, exact (HF) exchange, exchange and correlation DF contributions, empirical dispersion correction, and opposite-spin and same-spin MP2 correlation energies. Depending on the values of the coefficients in eq. 2.71, one may also obtain e.g. "pure" dispersion-corrected DFT ($c_\mathrm{X} = c_\mathrm{O} = c_\mathrm{S} = 0$), pure HF ($c_\mathrm{X} = 1$, $c_\mathrm{O} = c_\mathrm{S} = c_\mathrm{C} = s_6 = 0$), pure MP2 ($c_\mathrm{X} = c_\mathrm{O} = c_\mathrm{S} = 1$, $c_\mathrm{C} = s_6 = 0$), as well as simpler DHDFs like B2PLYP ($c_\mathrm{O} = c_\mathrm{S} = 1 - c_\mathrm{C}$, $s_6 = 0$). These coefficients are assumed to be included in the definitions of E^SCF and E^MP2. The DSD-DFT shielding tensor may also be split into SCF and MP2 contributions:

$$\boldsymbol{\sigma}_A^\text{DSD-DFT} = \boldsymbol{\sigma}_A^\mathrm{SCF} + \boldsymbol{\sigma}_A^\mathrm{MP2} \tag{2.72}$$

Note that the empirical dispersion correction only depends on the nuclear coordinates and therefore does not contribute to the shielding tensor. The SCF contribution $\boldsymbol{\sigma}_A^\mathrm{SCF}$ is calculated as described in Section 2.1.2 with the only difference that the DFT correlation terms (discussed in Section 2.1.4) are scaled by c_C.

Because the usual RI-MP2 energy expression is not variational, it is convenient to use the following Lagrangian formulation:

$$\mathcal{L} = E^\mathrm{SCF} + E_2^\mathrm{RI} + C_\mathrm{Bri} + C_\mathrm{MOO} + C_\mathrm{CV} \tag{2.73}$$

where E_2^RI is the Hylleraas functional,[232] in the generator state matrix formulation,[233,234] C_Bri is the Brillouin condition, C_MOO is the MO orthonormality constraint, and C_CV is the core–valence separation condition in the case of the frozen-core approximation. These terms will be described in detail below. The Hylleraas functional:

$$E_2^\mathrm{RI} = \sum_{i \geq j} \mathrm{tr}\Big(\mathbf{K}^{ji} \widetilde{\mathbf{T}}^{ij} + \mathbf{K}^{ji*} \widetilde{\mathbf{T}}^{ij*}\Big) + \mathrm{tr}\big(\mathbf{D}' \mathbf{F}^\mathrm{T}\big) \tag{2.74}$$

depends on the spin-adapted excitation amplitudes $T_{ab}^{ij} = T_{ba}^{ji}$ and introduces the contravariant amplitudes $\widetilde{T}_{ab}^{ij}$ defined as

$$\widetilde{T}_{ab}^{ij} = 2\,(1 + \delta_{ij})^{-1} \left[(c_\mathrm{S} + c_\mathrm{O})\, T_{ab}^{ij} - c_\mathrm{S} T_{ba}^{ij}\right] \tag{2.75}$$

where δ_{ij} is the Kronecker delta symbol. Eq. 2.75 is obtained as in refs. 233 and 234, employing in addition the SCS-MP2 ansatz.[51] The orbital-unrelaxed MP2 difference density matrix $\mathbf{D}'$, contracted with the Fock matrix $\mathbf{F}$, only has occupied–occupied and virtual–virtual blocks given by

$$D'_{ij} = -\sum_k (1 + \delta_{jk})\, \mathrm{tr}\Big(\widetilde{\mathbf{T}}^{kj*} \mathbf{T}^{ik}\Big) \tag{2.76}$$

$$D'_{ab} = \sum_{i \geq j} \Big(\widetilde{\mathbf{T}}^{ji*} \mathbf{T}^{ij} + \widetilde{\mathbf{T}}^{ij*} \mathbf{T}^{ji}\Big)_{ab} \tag{2.77}$$

Finally, the two electron repulsion integrals in the RI-MP2[235,236] approximation are defined as

$$K_{ab}^{ij} = \sum_{KL} (ia|K) \left(\mathbf{V}^{-1}\right)_{KL} (L|jb) \tag{2.78}$$

with $V_{KL} = (K|L)$ being the auxiliary basis Coulomb metric.

Turning to the constraints in eq. 2.73,

$$C_{\mathrm{Bri}} = \frac{1}{2}\sum_{ia}\left(z_{ai}F_{ai} + z^*_{ai}F^*_{ai}\right) = \mathrm{tr}\left(\mathbf{z}^{\mathrm{T}}\mathbf{F}\right) \tag{2.79}$$

$$C_{\mathrm{CV}} = \frac{1}{2}\sum_{i}^{\text{valence}}\sum_{m}^{\text{core}}\left(\bar{z}_{im}F_{im} + \bar{z}^*_{im}F^*_{im}\right) = \mathrm{tr}\left(\bar{\mathbf{z}}^{\mathrm{T}}\mathbf{F}\right) \tag{2.80}$$

$$C_{\mathrm{MOO}} = \sum_{pq} x_{pq}\left(S_{pq} - \delta_{pq}\right) = \mathrm{tr}(\mathbf{x}\left(\mathbf{S} - \mathbf{I}\right)) \tag{2.81}$$

where z_{ai}, x_{pq}, $\bar{z}_{im}$, and their complex conjugates are the undetermined Lagrange multipliers, which can be arranged in Hermitian matrices $\mathbf{z}$, $\mathbf{x}$, and $\bar{\mathbf{z}}$, defined in the respective blocks with

$$z_{ia} \equiv z^*_{ai} \tag{2.82}$$

$$\bar{z}_{mi} \equiv \bar{z}^*_{im} \tag{2.83}$$

$$x_{qp} \equiv x^*_{pq}, \quad q < p \tag{2.84}$$

The arbitrary factors of $\frac{1}{2}$ in C_{Bri} and C_{CV} are added for consistency with derivations for nuclear gradients where the complex conjugates z^*_{ai} and $\bar{z}^*_{im}$ are not necessary. Note that special care needs to be taken regarding complex conjugation, as the magnetic perturbation leads to imaginary matrix elements.

2.1.3.2 First derivatives

The derivative of the Lagrangian in eq. 2.73 with respect to the nuclear magnetic moment component $m_{K\beta}$ is

$$\begin{aligned}\frac{\mathrm{d}\mathcal{L}}{\mathrm{d}m_{K\beta}} &= \frac{\partial\mathcal{L}}{\partial m_{K\beta}} + \mathrm{tr}\left(\frac{\partial\mathcal{L}}{\partial\mathbf{U}}\frac{\partial\mathbf{U}^{\mathrm{T}}}{\partial m_{K\beta}} + \frac{\partial\mathcal{L}}{\partial\mathbf{U}^{\dagger}}\frac{\partial\mathbf{U}^{*}}{\partial m_{K\beta}}\right) + \sum_{i\geq j}\mathrm{tr}\left(\frac{\partial\mathcal{L}}{\partial\mathbf{T}^{ij}}\frac{\partial\mathbf{T}^{ij,\mathrm{T}}}{\partial m_{K\beta}} + \frac{\partial\mathcal{L}}{\partial\mathbf{T}^{ij,\dagger}}\frac{\partial\mathbf{T}^{ij,*}}{\partial m_{K\beta}}\right) \\ &\quad + \mathrm{tr}\left(\frac{\partial\mathcal{L}}{\partial\mathbf{x}}\frac{\partial\mathbf{x}^{\mathrm{T}}}{\partial m_{K\beta}} + \frac{\partial\mathcal{L}}{\partial\mathbf{z}}\frac{\partial\mathbf{z}^{\mathrm{T}}}{\partial m_{K\beta}} + \frac{\partial\mathcal{L}}{\partial\bar{\mathbf{z}}}\frac{\partial\bar{\mathbf{z}}^{\mathrm{T}}}{\partial m_{K\beta}}\right) \\ &= \frac{\partial\mathcal{L}}{\partial m_{K\beta}} = \sum_{\mu\nu}\left(D^{\mathrm{SCF}}_{\mu\nu} + D_{\mu\nu}\right)h^{m_{K\beta}}_{\mu\nu}\end{aligned} \tag{2.85}$$

where the orbital-relaxed difference density matrix $D_{\mu\nu}$ is defined as:[223,225,237]

$$\mathbf{D} = \mathbf{c}^*\left(\mathbf{D}' + \frac{1}{2}\mathbf{z} + \frac{1}{2}\bar{\mathbf{z}}\right)\mathbf{c}^{\mathrm{T}} \tag{2.86}$$

The second equality in eq. 2.85 holds when the Lagrangian is made stationary with respect to variation in all parameters, i.e. the conditions $\partial\mathcal{L}/\partial\mathbf{U} = \partial\mathcal{L}/\partial\mathbf{T}^{ij} = \partial\mathcal{L}/\partial\mathbf{x} = \partial\mathcal{L}/\partial\mathbf{z} = \partial\mathcal{L}/\partial\bar{\mathbf{z}} = 0$ (and their complex conjugates) are fulfilled. These conditions also provide the necessary expressions for $\mathbf{T}^{ij}$, $\mathbf{z}$ and $\bar{\mathbf{z}}$ which we will derive below.

Taking first the amplitude stationarity conditions, it can easily be shown using eq. 2.75 that

$$\frac{\partial\mathcal{L}}{\partial T^{ij}_{ab}} = 2\left(1+\delta_{ij}\right)^{-1}\left[\left(c_{\mathrm{S}} + c_{\mathrm{O}}\right)\frac{\partial\mathcal{L}}{\partial\widetilde{T}^{ij}_{ab}} - c_{\mathrm{S}}\frac{\partial\mathcal{L}}{\partial\widetilde{T}^{ij}_{ba}}\right] \tag{2.87}$$

Therefore, instead of the conditions $^{\partial\mathcal{L}}/_{\partial\mathbf{T}^{ij}} = 0$ we will use $^{\partial\mathcal{L}}/_{\partial\widetilde{\mathbf{T}}^{ij}} = 0$, because the latter are more concise:

$$0 \equiv \frac{\partial\mathcal{L}}{\partial\widetilde{T}^{ij*}_{ab}} = K^{ij*}_{ab} + \sum_c \left(T^{ij}_{ac}F_{bc} + F_{ac}T^{ij}_{cb}\right) - \sum_k \left(F_{kj}T^{ik}_{ab} + F_{ki}T^{kj}_{ab}\right) \equiv R^{ij}_{ab} \tag{2.88}$$

$$0 \equiv \frac{\partial\mathcal{L}}{\partial\widetilde{T}^{ij}_{ab}} = R^{ij*}_{ab} \tag{2.89}$$

eq. 2.89 comes from the properties of Wirtinger derivatives (see Section 2.1.1) and the fact that the Lagrangian is real. At the stationary point $R^{ij}_{ab} = 0$ and if we substitute it back into the Hylleraas functional we can recognize the expression for the RI-MP2 correlation energy.

$$E_2^{\mathrm{RI}} = \sum_{i\geq j}\sum_{ab}\left(K^{ij}_{ab}\widetilde{T}^{ij}_{ab} + \widetilde{T}^{ij*}_{ab}R^{ij}_{ab}\right) \tag{2.90}$$

If the Fock matrix is expanded in terms of canonical orbitals in eq. 2.88, i.e. $F_{pq} = \varepsilon_p\delta_{pq}$ we obtain the familiar closed-form expression for the amplitudes:

$$T^{ij}_{ab} = K^{ij*}_{ab}\left(\varepsilon_i + \varepsilon_j - \varepsilon_a - \varepsilon_b\right)^{-1} \tag{2.91}$$

Next, we derive the orbital rotation stationarity conditions:

$$0 \equiv \frac{\partial\mathcal{L}}{\partial\mathbf{U}} = \underbrace{\frac{\partial E^{\mathrm{SCF}}}{\partial\mathbf{U}}}_{0} + \frac{\partial}{\partial\mathbf{U}}\sum_{i\geq j}\mathrm{tr}\left(\mathbf{K}^{ji}\widetilde{\mathbf{T}}^{ij} + \mathbf{K}^{ji*}\widetilde{\mathbf{T}}^{ij*}\right) + \frac{\partial}{\partial\mathbf{U}}\mathrm{tr}\left(\mathbf{D}\mathbf{F}^{\mathrm{T}}_{\mathrm{AO}}\right) + \frac{\partial C_{\mathrm{MOO}}}{\partial\mathbf{U}} \tag{2.92}$$

where $\mathbf{F}_{\mathrm{AO}}$ is the AO-basis Fock matrix $F_{\mu\nu}$. The first term is zero because the SCF energy is already variational. Proceeding with the other terms:

$$\frac{\partial}{\partial U_{pq}}\sum_{i\geq j}\mathrm{tr}\left(\mathbf{K}^{ji}\widetilde{\mathbf{T}}^{ij} + \mathbf{K}^{ji*}\widetilde{\mathbf{T}}^{ij*}\right) = \sum_{Kbj}\left[\delta_{qb}\left(jp^{(0)}\middle|K\right)\Gamma^K_{jq} + \delta_{qj}\left(bp^{(0)}\middle|K\right)\Gamma^{K*}_{qb}\right] \tag{2.93}$$

$$\begin{aligned}\frac{\partial}{\partial U_{pq}}\mathrm{tr}\left(\mathbf{D}\mathbf{F}^{\mathrm{T}}_{\mathrm{AO}}\right) = &\left[\mathbf{c}^{(0),\mathrm{T}}\mathbf{F}^*_{\mathrm{AO}}\mathbf{c}^*\left(\mathbf{D}' + \frac{1}{2}\mathbf{z} + \frac{1}{2}\bar{\mathbf{z}}\right)\right]_{pq} \\ &+ 2\delta_{qi}\left(\mathbf{c}^{(0),\mathrm{T}}\mathbf{g}^*_{\mathrm{AO}}[\mathbf{D}]\mathbf{c}^*\right)_{pq}\end{aligned} \tag{2.94}$$

$$\frac{\partial C_{\mathrm{MOO}}}{\partial U_{pq}} = \left(\mathbf{c}^{(0),\mathrm{T}}\mathbf{S}^*_{\mathrm{AO}}\mathbf{c}^*\mathbf{x}\right)_{pq} \tag{2.95}$$

where $\mathbf{S}_{\mathrm{AO}}$ is the AO-basis overlap matrix $S_{\mu\nu}$, $\mathbf{g}^*[\mathbf{D}]$ is the complex conjugate of the two-electron repulsion operator defined in eq. 2.17 over the MP2 difference density $\mathbf{D}$, and the three-index two-particle density Γ^K_{ia} is defined as:[92,237]

$$\Gamma^K_{ia} = \sum_{jbL}\left(1+\delta_{ij}\right)\widetilde{T}^{ij}_{ab}\left(jb|L\right)\left(\mathbf{V}^{-1}\right)_{LK} \tag{2.96}$$

$$\left(qp^{(0)}\middle|K\right) = \sum_{\mu\nu} c^*_{\mu q}c^{(0)}_{\nu p}\left(\mu\nu|K\right) \tag{2.97}$$

The contributions coming from the XC functional in the case of DHDFT are given in Section 2.1.4 and drop out in the case of pure MP2. Note two peculiarities in eqs. 2.93–2.95: first, some of the MO coefficient matrices no longer depend on the external perturbation (i.e., we have $\mathbf{c}^{(0)}$ instead of $\mathbf{c}$) for subsequent derivatives, and second, eq. 2.92 (as well as

its complex conjugate) depends on the Lagrange multipliers $\mathbf{x}$. Therefore, we construct the linear combination:

$$\begin{aligned} 0 \equiv \frac{\partial \mathcal{L}}{\partial U_{pq}} - \frac{\partial \mathcal{L}}{\partial U^*_{qp}} = \sum_{Kbj} \big[& \delta_{qb} \left(jp^{(0)} \middle| K \right) \Gamma^K_{jq} + \delta_{qj} \left(bp^{(0)} \middle| K \right) \Gamma^{K*}_{qb} \\ & - \delta_{pb} \left(q^{(0)} j \middle| K \right) \Gamma^{K*}_{jp} - \delta_{pj} \left(q^{(0)} b \middle| K \right) \Gamma^K_{pb} \big] \\ & + \left[\mathbf{c}^{(0),\mathrm{T}} \mathbf{F}^*_{\mathrm{AO}} \mathbf{c}^* \left(\mathbf{D}' + \frac{1}{2}\mathbf{z} + \frac{1}{2}\bar{\mathbf{z}} \right) - \left(\mathbf{D}' + \frac{1}{2}\mathbf{z} + \frac{1}{2}\bar{\mathbf{z}} \right) \mathbf{c}^{\mathrm{T}} \mathbf{F}^*_{\mathrm{AO}} \mathbf{c}^{(0)*} \right]_{pq} \\ & + 2\delta_{qi} \left(\mathbf{c}^{(0),\mathrm{T}} \mathbf{g}^*_{\mathrm{AO}}[\mathbf{D}] \mathbf{c}^* \right)_{pq} - 2\delta_{pi} \left(\mathbf{c}^{\mathrm{T}} \mathbf{g}^*_{\mathrm{AO}}[\mathbf{D}] \mathbf{c}^{(0)*} \right)_{pq} \\ & + \left(\mathbf{c}^{(0),\mathrm{T}} \mathbf{S}^*_{\mathrm{AO}} \mathbf{c}^* \mathbf{x} \right)_{pq} - \left(\mathbf{x}^\dagger \mathbf{c}^{\mathrm{T}} \mathbf{S}^*_{\mathrm{AO}} \mathbf{c}^{(0)*} \right)_{pq} \end{aligned} \tag{2.98}$$

At $\mathbf{U} = \mathbf{I}$ the last two terms cancel out and the virtual–virtual, core–core, and valence–valence blocks are trivially zero. The core–valence block gives the equations for $\bar{z}_{im}$ (referred to as "Z-CV equations" below):[179,237,238]

$$0 \equiv \left[\frac{\partial \mathcal{L}}{\partial U_{im}} - \frac{\partial \mathcal{L}}{\partial U^*_{mi}} \right] \Bigg|_{\mathbf{U}=\mathbf{I}} = \frac{1}{2} \sum_j F_{ji} \bar{z}_{jm} - \frac{1}{2} \sum_n F_{mn} \bar{z}_{in} - \sum_{Kb} (mb|K) \, \Gamma^K_{ib} \tag{2.99}$$

which yield a closed-form solution for canonical orbitals:

$$\bar{z}_{im} = 2 \left(\varepsilon_i - \varepsilon_m \right)^{-1} \sum_{Kb} (mb|K) \, \Gamma^K_{ib} \tag{2.100}$$

The occupied–virtual block of eq. 2.98 gives the equations for z_{ai},

$$\begin{aligned} 0 \equiv \left[\frac{\partial \mathcal{L}}{\partial U_{ai}} - \frac{\partial \mathcal{L}}{\partial U^*_{ia}} \right] \Bigg|_{\mathbf{U}=\mathbf{I}} = & \frac{1}{2} \sum_b F_{ba} z_{bi} - \frac{1}{2} \sum_j z_{aj} F_{ij} + 2 g^*_{ai}[\mathbf{D}] \\ & + \sum_{Kb} (ba|K) \, \Gamma^{K*}_{ib} - \sum_{Kj} (ij|K) \, \Gamma^{K*}_{ja} \end{aligned} \tag{2.101}$$

which take the following form, assuming canonical orbitals, and must be solved iteratively:

$$\left(\varepsilon_a - \varepsilon_i \right) z_{ai} + 2 g^*_{ai}[\mathbf{z}] = X_{ai} \tag{2.102}$$

$$X_{ai} = 2 \sum_{Kj} (ij|K) \, \Gamma^{K*}_{ja} - 2 \sum_{Kb} (ba|K) \, \Gamma^{K*}_{ib} - 4 g^*_{ai} \left[\mathbf{D}' + \frac{1}{2} \bar{\mathbf{z}} \right] \tag{2.103}$$

These are equivalent to Handy and Schäfer's "z-vector equations",[239] which here arise naturally from the Lagrangian formulation and are referred to as "Z-CPSCF equations". The two-electron Fock response term may be approximated using the RIJK,[111] RIJONX, or RIJCOSX[113] approaches, of which the latter is the most efficient for large systems, due to its more favorable scaling behavior.[93,116]

Note that evaluation of the Lagrange multipliers for the orthonormality condition x_{pq} is not necessary for the first derivative, eq. 2.85, because the basis functions do not depend on the nuclear magnetic moment. Nevertheless, x_{pq} are needed for the evaluation of the second derivative as shown in the next section. Defining for convenience:

$$\mathcal{L}_{\text{-MOO}} = \mathcal{L} - C_{\text{MOO}} \tag{2.104}$$

we get the following equations for x_{pq}:

$$x_{pq} = -\left.\frac{\partial \mathcal{L}_{\text{-MOO}}}{\partial U_{pq}}\right|_{\mathbf{U}=\mathbf{I}} \tag{2.105}$$

$$x_{pq} = -\left.\frac{\partial \mathcal{L}_{\text{-MOO}}}{\partial U^*_{qp}}\right|_{\mathbf{U}=\mathbf{I}} \tag{2.106}$$

These solutions are identical, provided that eq. 2.98 is fulfilled.

2.1.3.3 Second derivatives

The second derivative of the RI-MP2 Lagrangian with respect to the nuclear magnetic moment component $m_{K\beta}$ and the external magnetic field component B_α, is equal to the derivative of eq. 2.85:

$$\frac{\mathrm{d}^2\mathcal{L}}{\mathrm{d}B_\alpha \mathrm{d}m_{K\beta}} = \sum_{\mu\nu} \left(D^{\text{SCF}}_{\mu\nu} + D_{\mu\nu}\right) h^{m_{K\beta},B_\alpha}_{\mu\nu} + \sum_{\mu\nu} \left(D^{\text{SCF},B_\alpha}_{\mu\nu} + D^{B_\alpha}_{\mu\nu}\right) h^{m_{K\beta}}_{\mu\nu} \tag{2.107}$$

where the SCF response density matrix $D^{\text{SCF},B_\alpha}_{\mu\nu}$ is defined in eq. 2.12. The RI-MP2 response difference density is defined as the derivative of eq. 2.86:

$$\mathbf{D}^{\mathbf{B}} = \mathbf{c}^* \left(\mathbf{D}'^{\mathbf{B}} + \frac{1}{2}\mathbf{z}^{\mathbf{B}} + \frac{1}{2}\bar{\mathbf{z}}^{\mathbf{B}}\right) \mathbf{c}^{\mathrm{T}} + \mathbf{c}^{\mathbf{B}*} \left(\mathbf{D}' + \frac{1}{2}\mathbf{z} + \frac{1}{2}\bar{\mathbf{z}}\right) \mathbf{c}^{\mathrm{T}} + \mathbf{c}^* \left(\mathbf{D}' + \frac{1}{2}\mathbf{z} + \frac{1}{2}\bar{\mathbf{z}}\right) \mathbf{c}^{\mathbf{B},\mathrm{T}} \tag{2.108}$$

where

$$D'^{\mathbf{B}}_{ij} = \sum_k (1+\delta_{jk}) \left(\mathrm{tr}\left(\widetilde{\mathbf{T}}^{kj*\mathbf{B}} \mathbf{T}^{ik}\right) + \mathrm{tr}\left(\widetilde{\mathbf{T}}^{kj*} \mathbf{T}^{ik,\mathbf{B}}\right)\right) \tag{2.109}$$

$$D'^{\mathbf{B}}_{ab} = \sum_{i\geq j} \left(\widetilde{\mathbf{T}}^{ji*\mathbf{B}} \mathbf{T}^{ij} + \widetilde{\mathbf{T}}^{ij*\mathbf{B}} \mathbf{T}^{ji} + \widetilde{\mathbf{T}}^{ji*} \mathbf{T}^{ij,\mathbf{B}} + \widetilde{\mathbf{T}}^{ij*} \mathbf{T}^{ji,\mathbf{B}}\right)_{ab} \tag{2.110}$$

The perturbed parameters $\mathbf{c}^{\mathbf{B}}$, $\mathbf{T}^{ij,\mathbf{B}}$, $\mathbf{z}^{\mathbf{B}}$, and $\bar{\mathbf{z}}^{\mathbf{B}}$ are obtained from magnetic field derivatives of the Lagrangian stationarity conditions, which we present below. Analogous equations are derived in refs. 34, 35, 120, and 179

The coefficients $U^{\mathbf{B}}_{ai}$ are computed as solutions to the CPSCF equations,[240] 2.24, which come about from the condition $C^{\mathbf{B}}_{\text{Bri}} = 0$. The $U^{\mathbf{B}}_{ij}$ and $U^{\mathbf{B}}_{ab}$ blocks are also required and are only constrained by the perturbed orthonormality condition $C^{\mathbf{B}}_{\text{MOO}} = 0$, eq. 2.14. Thus, they can be chosen in different ways, the most common being

$$U^{\mathbf{B}}_{ij} = -\frac{1}{2} S^{(\mathbf{B})}_{ij} \tag{2.111}$$

$$U^{\mathbf{B}}_{ab} = -\frac{1}{2} S^{(\mathbf{B})}_{ab} \tag{2.112}$$

However, a computationally more efficient alternative choice of $U^{\mathbf{B}}_{ij}$, resulting in perturbed canonical orbitals,[39,120,241] is presented in Section 2.1.3.4.

The magnetic field derivative of the amplitude stationarity conditions, eq. 2.88, gives the equations for $\mathbf{T}^{ij,\mathbf{B}}$, which take the following form, assuming canonical orbitals:

$$T^{ij,\mathbf{B}}_{ab} = (\varepsilon_i + \varepsilon_j - \varepsilon_a - \varepsilon_b)^{-1} \left[K^{ij*\mathbf{B}}_{ab} + \sum_c \left(T^{ij}_{ac} F^{\mathbf{B}}_{bc} + F^{\mathbf{B}}_{ac} T^{ij}_{cb}\right) - \sum_k \left(F^{\mathbf{B}}_{kj} T^{ik}_{ab} + F^{\mathbf{B}}_{ki} T^{kj}_{ab}\right)\right] \tag{2.113}$$

where the perturbed exchange integrals in the RI approximation are

$$K_{ab}^{ij,\mathbf{B}} = \sum_{KL} \left[(ia|K)^{\mathbf{B}} \left(\mathbf{V}^{-1}\right)_{KL} (L|jb) + (ia|K) \left(\mathbf{V}^{-1}\right)_{KL} (L|jb)^{\mathbf{B}} \right] \tag{2.114}$$

$$(pq|K)^{\mathbf{B}} = \sum_{\mu\nu} \left[c_{\mu p}^{*} c_{\nu q} (\mu\nu|K)^{\mathbf{B}} + \left(c_{\mu p}^{*} c_{\nu q}^{\mathbf{B}} + c_{\mu p}^{\mathbf{B}*} c_{\nu q} \right) (\mu\nu|K) \right] \tag{2.115}$$

Note once again that the auxiliary basis functions are independent of the magnetic field. As pointed out by Loibl et al.,[117,179] using GIAO-type fitting functions instead would violate gauge invariance, because the explicit dependence on the gauge origin would not cancel out in the perturbed three index integrals.

The derivatives of the MO rotation stationarity conditions can be expressed as follows, using eqs. 2.14, and 2.105:

$$\begin{aligned} 0 \equiv \left. \frac{\mathrm{d}\partial\mathcal{L}}{\mathrm{d}\mathbf{B}\partial\mathbf{U}} \right|_{\mathbf{B}=0} &= \left. \frac{\mathrm{d}\partial\mathcal{L}_{\text{-MOO}}}{\mathrm{d}\mathbf{B}\partial\mathbf{U}} \right|_{\mathbf{B}=0} + \left(\mathbf{S}^{(\mathbf{B})*} + \mathbf{U}^{\mathbf{B}*} \right) \mathbf{x} + \mathbf{x}^{\mathbf{B}} \\ &= \left. \frac{\mathrm{d}\partial\mathcal{L}_{\text{-MOO}}}{\mathrm{d}\mathbf{B}\partial\mathbf{U}} \right|_{\mathbf{B}=0} + \mathbf{U}^{\mathbf{B},\mathrm{T}} \left. \frac{\mathrm{d}\partial\mathcal{L}_{\text{-MOO}}}{\mathrm{d}\mathbf{B}\partial\mathbf{U}} \right|_{\mathbf{U}=\mathbf{I}} + \mathbf{x}^{\mathbf{B}} \end{aligned} \tag{2.116}$$

and likewise for the complex conjugate. The second term reintroduces the MO response which is "missing" in eqs. 2.93–2.94. We then take the linear combination in which $\mathbf{x}^{\mathbf{B}}$ cancels out:

$$\begin{aligned} 0 \equiv \frac{\mathrm{d}\partial\mathcal{L}}{\mathrm{d}\mathbf{B}\partial U_{pq}} - \frac{\mathrm{d}\partial\mathcal{L}}{\mathrm{d}\mathbf{B}\partial U_{qp}^{*}} = \frac{\mathrm{d}}{\mathrm{d}\mathbf{B}} \Bigg\{ & \sum_{Kbj} \left[\delta_{qb} (jp|K) \Gamma_{jq}^{K} + \delta_{qj} (bp|K) \Gamma_{qb}^{K*} \right. \\ & \left. - \delta_{pb} (qj|K) \Gamma_{jp}^{K*} - \delta_{pj} (qb|K) \Gamma_{pb}^{K} \right] \\ & + \left[\mathbf{F}^{*} \left(\mathbf{D}' + \frac{1}{2}\mathbf{z} + \frac{1}{2}\bar{\mathbf{z}} \right) - \left(\mathbf{D}' + \frac{1}{2}\mathbf{z} + \frac{1}{2}\bar{\mathbf{z}} \right) \mathbf{F}^{*} \right]_{pq} \\ & + 2\delta_{qi} g_{pq}^{*}[\mathbf{D}] - 2\delta_{pi} g_{pq}^{*}[\mathbf{D}] \Bigg\} \end{aligned} \tag{2.117}$$

We note in passing that after solving eq. 2.117, eq. 2.116 can be solved for the perturbed Lagrange multipliers $\mathbf{x}^{\mathbf{B}}$, which are, however, not needed to calculate the NMR shielding tensor. The virtual–virtual, core–core, and valence–valence blocks of eq. 2.117 are zero. The core–valence block gives the perturbed Z-CV equations which give a closed-form solution for $\bar{z}_{im}^{\mathbf{B}}$ in the case of canonical orbitals:

$$\bar{z}_{im}^{\mathbf{B}} = (\varepsilon_i - \varepsilon_m)^{-1} \left[2 \sum_{Kb} \left((mb|K)^{\mathbf{B}} \Gamma_{ib}^{K} + (mb|K) \Gamma_{ib}^{K,\mathbf{B}} \right) - \sum_{j} F_{ji}^{\mathbf{B}} \bar{z}_{jm} + \sum_{n} F_{mn}^{\mathbf{B}} \bar{z}_{in} \right] \tag{2.118}$$

The occupied–virtual block gives the equations for $z_{ai}^{\mathbf{B}}$,

$$\left(\varepsilon_a - \varepsilon_i \right) z_{ai}^{\mathbf{B}} + 2 g_{ai}^{*}\left[\mathbf{z}^{\mathbf{B}}\right] = \overline{X}_{ai}^{\mathbf{B}} \tag{2.119}$$

$$\begin{aligned} \overline{X}_{ai}^{\mathbf{B}} = & 2 \sum_{Kj} \left[(ij|K)^{\mathbf{B}} \Gamma_{ja}^{K*} + (ij|K) \Gamma_{ja}^{K*\mathbf{B}} \right] \\ & - 2 \sum_{Kb} \left[(ba|K)^{\mathbf{B}} \Gamma_{ib}^{K*} + (ba|K) \Gamma_{ib}^{K*\mathbf{B}} \right] \end{aligned}$$

$$- \sum_b F^{\mathbf{B}}_{ba} z_{bi} + \sum_j z_{aj} F^{\mathbf{B}}_{ij} - 4 \left(g^*_{ai} \left[\mathbf{D}' + \frac{1}{2}\bar{\mathbf{z}} + \frac{1}{2}\mathbf{z}^{(0)} \right] \right)^{\mathbf{B}} \tag{2.120}$$

where the derivative of two-electron Fock response operator (for an arbitrary MO matrix $\mathbf{Q}$) is

$$(\mathbf{g}^*[\mathbf{Q}])^{\mathbf{B}}_{ai} = g^{(\mathbf{B})*}_{ai}[\mathbf{Q}] + g^*_{ai}\left[\mathbf{Q}^{\mathbf{B}} + \mathbf{U}^{\mathbf{B}*}\mathbf{Q} + \mathbf{Q}\mathbf{U}^{\mathbf{B},\mathrm{T}}\right] + \left(\mathbf{g}^*[\mathbf{Q}]\mathbf{U}^{\mathbf{B}*} + \mathbf{U}^{\mathbf{B},\mathrm{T}}\mathbf{g}^*[\mathbf{Q}]\right)_{ai} \tag{2.121}$$

and the derivative of the three-index density is

$$\Gamma^{K,\mathbf{B}}_{ia} = \sum_{jbL} (1+\delta_{ij}) \left[\widetilde{T}^{ij,\mathbf{B}}_{ab} (jb|L) + \widetilde{T}^{ij}_{ab} (jb|L)^{\mathbf{B}} \right] \left(\mathbf{V}^{-1}\right)_{LK} \tag{2.122}$$

2.1.3.4 Perturbed canonical orbitals

Due to the last two terms in eq. 2.113, the calculation of the MP2 response density becomes a formally $O(N^6)$ scaling step. In addition, if the amplitudes are calculated in multiple batches, such that T^{ij}_{ab} are only available for i within the batch, the last term in eq. 2.113 requires amplitudes outside the batch. This was noted by Kollwitz and Gauss in their direct GIAO-MP2 implementation,[120] who suggested the use of perturbed canonical orbitals,[39,238,241] i.e. choosing $U^{\mathbf{B}}_{ij}$ coefficients such that the internal block of $\mathbf{F}^{\mathbf{B}}$ vanishes:

$$\begin{aligned} 0 \equiv F^{\mathbf{B}}_{ij} &= U^{\mathbf{B}}_{ij}\varepsilon_i - U^{\mathbf{B}}_{ji}\varepsilon_j + F^{(\mathbf{B})}_{ij} \\ &= U^{\mathbf{B}}_{ij}\varepsilon_i - \left(U^{\mathbf{B}}_{ij} + S^{(\mathbf{B})}_{ij}\right)\varepsilon_j + F^{(\mathbf{B})}_{ij} \end{aligned} \tag{2.123}$$

$$U^{\mathbf{B}}_{ij} = \frac{F^{(\mathbf{B})}_{ij} - S^{(\mathbf{B})}_{ij}\varepsilon_j}{\varepsilon_j - \varepsilon_i} \tag{2.124}$$

Thus the internal Fock matrix contribution to $\mathbf{T}^{ij,\mathbf{B}}$ vanishes and the formal scaling is reduced to $O(N^5)$. A complication arises when (near-)degenerate orbitals i and j are present which would make the denominator of eq. 2.124 (near-)zero. In these cases $U^{\mathbf{B}}_{ij}$ are chosen according to eq. 2.111 and the corresponding contributions to the perturbed amplitudes are calculated. Hence, only those amplitudes $\mathbf{T}^{kj}$ ($\mathbf{T}^{ik}$) are required for which $\varepsilon_k \approx \varepsilon_i$ ($\varepsilon_k \approx \varepsilon_j$), or, after assigning $U^{\mathbf{B}}_{ij}$, those for which $\left|F^{\mathbf{B}}_{ki}\right|$ ($\left|F^{\mathbf{B}}_{kj}\right|$) is greater than some threshold, e.g. 10^{-5}. In our implementation these amplitudes are either precalculated and stored on disk or reevaluated on the fly. The latter option leads to significant computational overhead and should only be used in the unlikely case (for feasible system sizes) of insufficient disk space.

2.1.4 Exchange–correlation functional terms

For brevity in the previous sections, we have focused on the HF and MP2 methods because the treatment of (hybrid) KS-DFT and DHDFT is analogous, with some additional details. In this section, we examine the terms that arise due to the XC functional. The DFT XC energy contribution is

$$E^{\mathrm{DFT}}_{\mathrm{XC}} = \int f_{\mathrm{XC}}[\rho(\mathbf{r}), \gamma(\mathbf{r})] \mathrm{d}\mathbf{r} \tag{2.125}$$

where we have assumed that f_{XC} is a GGA functional which depends, in the closed-shell case, on the electronic density ρ and its gradient invariant γ expressed using the SCF density matrix $\mathbf{D}^{\mathrm{SCF}}$ as

$$\rho_{\mathrm{SCF}} = \sum_{\mu\nu} D^{\mathrm{SCF}}_{\mu\nu} \Omega_{\mu\nu} \tag{2.126}$$

$$\Omega_{\mu\nu} = \chi^*_\mu \chi_\nu \tag{2.127}$$

$$\gamma_{\mathrm{SCF}} = \left|\boldsymbol{\nabla}\rho_{\mathrm{SCF}}\right|^2 \tag{2.128}$$

$$\boldsymbol{\nabla}\rho_{\mathrm{SCF}} = \sum_{\mu\nu} D^{\mathrm{SCF}}_{\mu\nu} \boldsymbol{\nabla}\Omega_{\mu\nu} \tag{2.129}$$

The Fock matrix therefore also contains an XC potential term:[242]

$$F_{\mu\nu} \leftarrow V^{\mathrm{XC}}_{\mu\nu} = \langle\mu|\, \mathrm{V}_{\mathrm{XC}} \,|\nu\rangle = \int \left[\frac{\partial f_{\mathrm{XC}}}{\partial\rho}\Omega_{\mu\nu} + 2\frac{\partial f_{\mathrm{XC}}}{\partial\gamma}\boldsymbol{\nabla}\rho_{\mathrm{SCF}}\boldsymbol{\nabla}\Omega_{\mu\nu}\right] \mathrm{d}\mathbf{r} \tag{2.130}$$

In addition, the two-electron operator is redefined as:

$$g_{\mu\nu}[\mathbf{D}] = J_{\mu\nu}[\mathbf{D}] - \frac{c_{\mathrm{X}}}{2} K_{\mu\nu}[\mathbf{D}] \tag{2.131}$$

Thus, for hybrid DFT all exact exchange contributions to the CPSCF equations (i.e. $\mathbf{K}^{\mathbf{B}}\left[\mathbf{D}^{\mathrm{SCF}}\right]$, $\mathbf{K}\left[\mathbf{U}^{\mathbf{B}}\right]$, and $\mathbf{K}\left[\mathbf{S}^{(\mathbf{B})}\right]$) have to be scaled by $0 < c_{\mathrm{X}} \leq 1$, which is the amount of exact exchange that should be included for the given functional. For "pure" functionals $c_{\mathrm{X}} = 0$ and these terms do not need to be calculated, resulting in a closed-form expression for the CPSCF equations. The same applies to the respective contributions in DHDFT. Note that the DFT exchange and correlation scaling coefficients, $(1 - c_{\mathrm{X}})$ and c_{C}, respectively (cf. eq. 2.71), are implicitly included in the definition of f_{XC}.

$\mathbf{V}^{\mathrm{XC}}$ depends on the MO coefficients through $\mathbf{D}^{\mathrm{SCF}}$ and therefore minimizing the DHDFT Lagrangian with respect to orbital rotations gives rise to an additional Fock response term in the Z-CPSCF equations eq. 2.101:

$$0 \equiv \left[\frac{\partial\mathcal{L}}{\partial U_{ai}} - \frac{\partial\mathcal{L}}{\partial U^*_{ia}}\right]\Bigg|_{\mathbf{U}=\mathbf{I}} \leftarrow 2\mathcal{R}^{\mathrm{XC}}_{ai}[\mathbf{D}] \tag{2.132}$$

where

$$\begin{aligned}\mathcal{R}^{\mathrm{XC}}_{ai}[\mathbf{D}] = \sum_{\mu\nu} c_{\mu a} c^*_{\nu i} \int \Bigg\{ &\left[\frac{\partial^2 f_{\mathrm{XC}}}{\partial\rho^2}\left[\mathbf{D}^{\mathrm{SCF}}\right] + 2\frac{\partial^2 f_{\mathrm{XC}}}{\partial\rho\partial\gamma}\left[\mathbf{D}^{\mathrm{SCF}}\right]\right]\rho_{\mathbf{D}}\Omega_{\mu\nu} \\ &+ \left[\frac{\partial^2 f_{\mathrm{XC}}}{\partial\gamma\partial\rho}[\mathbf{P}] + 2\frac{\partial^2 f_{\mathrm{XC}}}{\partial\gamma^2}\left[\mathbf{D}^{\mathrm{SCF}}\right]\right]\gamma_{\mathrm{SCF}}\boldsymbol{\nabla}\rho_{\mathbf{D}}\boldsymbol{\nabla}\Omega_{\mu\nu}\Bigg\}\mathrm{d}\mathbf{r}\end{aligned} \tag{2.133}$$

with $\rho_{\mathbf{D}} = \sum_{\mu\nu} D_{\mu\nu}\Omega_{\mu\nu}$.

As discussed in the Introduction, most common XC functionals do not have an explicit dependence on the external magnetic field. However, when using GIAOs, the electronic density and its gradient depend on the magnetic field through both $\mathbf{D}^{\mathrm{SCF}}$ and the basis functions:

$$\Omega^{\mathbf{B}}_{\mu\nu} = \frac{\mathrm{i}}{2}\left(\mathbf{R}_{MN} \times \mathbf{r}\right)\Omega^{(0)}_{\mu\nu} = -\Omega^{\mathbf{B}}_{\nu\mu} \tag{2.134}$$

$$(\boldsymbol{\nabla}\Omega_{\mu\nu})^{\mathbf{B}} = \frac{\mathrm{i}}{2}\left(\mathbf{R}_{MN}\times\mathbf{r}\right)\left(\Omega^{(0)}_{\mu\nu} + \boldsymbol{\nabla}\Omega^{(0)}_{\mu\nu}\right) = -\left(\boldsymbol{\nabla}\Omega_{\nu\mu}\right)^{\mathbf{B}} \tag{2.135}$$

where $\mathbf{R}_{MN}$ is the distance vector between the centers of AOs μ and ν. Due to the anti-symmetry of the perturbed quantities, the full derivatives of the density and its gradient vanish:

$$\rho^{\mathbf{B}}_{\mathrm{SCF}} = \sum_{\mu\nu} D^{\mathrm{SCF},\mathbf{B}}_{\mu\nu}\Omega_{\mu\nu} + \sum_{\mu\nu} D^{\mathrm{SCF}}_{\mu\nu}\Omega^{\mathbf{B}}_{\mu\nu} = 0 \tag{2.136}$$

$$\left(\boldsymbol{\nabla}\rho_{\mathrm{SCF}}\right)^{\mathbf{B}} = \sum_{\mu\nu} D^{\mathrm{SCF},\mathbf{B}}_{\mu\nu}\boldsymbol{\nabla}\Omega_{\mu\nu} + \sum_{\mu\nu} D^{\mathrm{SCF}}_{\mu\nu}\left(\boldsymbol{\nabla}\Omega_{\mu\nu}\right)^{\mathbf{B}} = 0 \tag{2.137}$$

$$\gamma^{\mathbf{B}}_{\mathrm{SCF}} = 2\boldsymbol{\nabla}\rho_{\mathrm{SCF}}\left(\boldsymbol{\nabla}\rho_{\mathrm{SCF}}\right)^{\mathbf{B}} = 0 \tag{2.138}$$

Hence, using the notation of Section 2.1.2.3, the XC contribution to the perturbed Fock matrix is:

$$\begin{aligned} F^{\mathbf{B}}_{\mu\nu} \leftarrow V^{\mathrm{XC},\mathbf{B}}_{\mu\nu} &= \frac{\mathrm{i}}{2}\left\langle\mu_M\right|\mathbf{O}_{MN}\mathbf{r}\mathrm{V}_{\mathrm{XC}}\left|\nu_N\right\rangle \\ &= \int\left[\frac{\partial f_{\mathrm{XC}}}{\partial\rho}\Omega^{\mathbf{B}}_{\mu\nu} + 2\frac{\partial f_{\mathrm{XC}}}{\partial\gamma}\boldsymbol{\nabla}\rho_{\mathrm{SCF}}\left(\boldsymbol{\nabla}\Omega_{\mu\nu}\right)^{\mathbf{B}}\right]\mathrm{d}\mathbf{r} \end{aligned} \tag{2.139}$$

Finally, the contributions to the perturbed Z-CPSCF equations are:

$$0 \equiv \left[\frac{\mathrm{d}\partial\mathcal{L}}{\mathrm{d}\mathbf{B}\partial U_{ai}} - \frac{\mathrm{d}\partial\mathcal{L}}{\mathrm{d}\mathbf{B}\partial U^{*}_{ia}}\right]\Bigg|_{\mathbf{B}=0} \leftarrow 2\Big(\mathbf{U}^{\mathbf{B},\mathrm{T}}\boldsymbol{\mathcal{R}}^{\mathrm{XC}}[\mathbf{D}] + \boldsymbol{\mathcal{R}}^{\mathrm{XC}}[\mathbf{D}]\mathbf{U}^{\mathbf{B}*} + \boldsymbol{\mathcal{R}}^{\mathrm{XC}(\mathbf{B})}[\mathbf{D}]\Big)_{ai} \tag{2.140}$$

where

$$\begin{aligned} \mathcal{R}^{\mathrm{XC}(\mathbf{B})}_{ai}[\mathbf{D}] = \sum_{\mu\nu} c_{\mu a}c^{*}_{\nu i}\int\Bigg\{&\left[\frac{\partial^2 f_{\mathrm{XC}}}{\partial\rho^2}\left[\mathbf{D}^{\mathrm{SCF}}\right] + 2\frac{\partial^2 f_{\mathrm{XC}}}{\partial\rho\partial\gamma}\left[\mathbf{D}^{\mathrm{SCF}}\right]\right]\rho_{\mathbf{D}}\Omega^{\mathbf{B}}_{\mu\nu} \\ &+ \left[\frac{\partial^2 f_{\mathrm{XC}}}{\partial\gamma\partial\rho}[\mathbf{P}] + 2\frac{\partial^2 f_{\mathrm{XC}}}{\partial\gamma^2}\left[\mathbf{D}^{\mathrm{SCF}}\right]\right]\gamma_{\mathrm{SCF}}\boldsymbol{\nabla}\rho_{\mathbf{D}}\left(\boldsymbol{\nabla}\Omega_{\mu\nu}\right)^{\mathbf{B}}\Bigg\}\mathrm{d}\mathbf{r} \end{aligned} \tag{2.141}$$

Note that, unlike for electric or geometric perturbations,[92] terms which include third derivatives of the XC functional vanish.

A complication arises for meta-GGA functionals that depend on the kinetic energy density τ, which in the closed-shell case can be expressed as:

$$\tau = \frac{1}{2}\sum_{\mu\nu} D^{\mathrm{SCF}}_{\mu\nu}\boldsymbol{\nabla}\chi^{*}_{\mu}\cdot\boldsymbol{\nabla}\chi_{\nu} \tag{2.142}$$

This quantity is known to not be gauge-invariant, even if GIAOs are used (as defined above), unless modified appropriately.[67,68,243] Two such modifications are proposed in the literature: one by Maximoff and Scuseria (τ_{MS}),[68] and one by Dobson (τ_{D}),[244] and have also been compared in the context of NMR shielding.[62,72] In particular, the following term is relevant:

$$\begin{aligned} \left(\boldsymbol{\nabla}\chi^{*}_{\mu}\cdot\boldsymbol{\nabla}\chi_{\nu}\right)^{B_\alpha} = &\frac{i}{2}\left(\mathbf{R}_{MN}\times\mathbf{r}\right)_{\alpha}\boldsymbol{\nabla}\varphi^{*}_{\mu}\cdot\boldsymbol{\nabla}\varphi_{\nu} \\ &+ \frac{i}{2}\varphi^{*}_{\mu}\left(\mathbf{B}\times\mathbf{R}_{MO}\right)^{B_\alpha}\cdot\boldsymbol{\nabla}\varphi_{\nu} - \frac{i}{2}\boldsymbol{\nabla}\varphi^{*}_{\mu}\cdot\left(\mathbf{B}\times\mathbf{R}_{NO}\right)^{B_\alpha}\varphi_{\nu} \end{aligned}$$

It is the last two terms that violate the gauge-invariance. In all calculations discussed here, these terms are simply neglected. This ad-hoc gauge-invariant approach, while not justified theoretically, has been shown to produce results that are no worse, and in some cases even better, than the τ_{MS} and τ_{D} ansätze, when compared to CCSD(T) reference data.[72] In addition, it does not introduce unphysical components in the shielding tensor, as is the case for τ_{MS}, and it does not require iterative solution of the CPSCF equations for pure DFT, as is the case for τ_{D}. All of these approaches were implemented in ORCA subsequent to the publication of ref. 72 but are not discussed further in this thesis.

2.1.5 Implicit solvent terms

If an implicit solvation model is used, such as the conductor-like polarizable continuum model (CPCM) implemented in ORCA,[245,246] the Fock matrix is corrected with an additional term:

$$F_{\mu\nu} \leftarrow V^{\mathrm{sol}}_{\mu\nu} = \langle\mu|\,\mathrm{V}_{\mathrm{sol}}\,|\nu\rangle = \int \left(v^{\mathrm{sol}}_{\mathrm{nuc}} + v^{\mathrm{sol}}_{\mathrm{el}}\left[\mathbf{D}^{\mathrm{SCF}}\right]\right)\Omega_{\mu\nu}\mathrm{d}\mathbf{r} \tag{2.143}$$

$$v^{\mathrm{sol}}_{\mathrm{nuc}} = -f_\varepsilon \sum_{st}\left(\mathbf{A}^{-1}\right)_{st} |\,\mathbf{r}-\mathbf{r}_s\,|^{-1} \sum_K \frac{Z_K}{|\,\mathbf{R}_K-\mathbf{r}_t\,|} \tag{2.144}$$

$$v^{\mathrm{sol}}_{\mathrm{el}}\left[\mathbf{D}^{\mathrm{SCF}}\right] = f_\varepsilon \sum_{st}\left(\mathbf{A}^{-1}\right)_{st} |\,\mathbf{r}-\mathbf{r}_s\,|^{-1} \int \frac{\rho_{\mathrm{SCF}}(\mathbf{r}')}{|\,\mathbf{r}'-\mathbf{r}_t\,|}\mathrm{d}\mathbf{r}' \tag{2.145}$$

where Z_K is the charge of nucleus K and $\mathbf{R}_K$ is its position; the indices s and t denote surface elements; f_ε is a function, which depends on the dielectric constant of the solvent; and the matrix $\mathbf{A}$ (defined as $\mathbf{S}$ in ref. 245) depends on the areas and relative positions of the surface elements. Both the nuclear and the electronic terms, $v^{\mathrm{sol}}_{\mathrm{nuc}}$ and $v^{\mathrm{sol}}_{\mathrm{el}}$ respectively, contribute to the CPSCF equations, due to the GIAO response:

$$\begin{aligned} F^{\mathbf{B}}_{\mu\nu} \leftarrow V^{\mathrm{sol},\mathbf{B}}_{\mu\nu} &= \frac{\mathrm{i}}{2}\,\langle\mu_M\,|\,\mathbf{O}_{MN}\mathbf{r}\mathrm{V}_{\mathrm{sol}}\,|\,\nu_N\rangle \\ &= \int \left(v^{\mathrm{sol}}_{\mathrm{nuc}} + v^{\mathrm{sol}}_{\mathrm{el}}\left[\mathbf{D}^{\mathrm{SCF}}\right]\right)\Omega^{\mathbf{B}}_{\mu\nu}\mathrm{d}\mathbf{r} \end{aligned} \tag{2.146}$$

Only $v^{\mathrm{sol}}_{\mathrm{el}}$ contributes to the Fock response in the Z-CPSCF equations:

$$0 \equiv \left[\frac{\partial\mathcal{L}}{\partial U_{ai}} - \frac{\partial\mathcal{L}}{\partial U^*_{ia}}\right]\Bigg|_{\mathbf{U}=\mathbf{I}} \leftarrow 2\mathcal{R}^{\mathrm{sol}}_{ai}[\mathbf{D}] \tag{2.147}$$

$$\mathcal{R}^{\mathrm{sol}}_{ai}[\mathbf{D}] = \sum_{\mu\nu} c_{\mu a}c^*_{\nu i}\int v^{\mathrm{sol}}_{\mathrm{el}}[\mathbf{D}]\Omega_{\mu\nu}\mathrm{d}\mathbf{r} \tag{2.148}$$

where $v^{\mathrm{sol}}_{\mathrm{el}}[\mathbf{D}]$ (for any matrix $\mathbf{D}$) is defined as in eq. 2.145 with $\rho_{\mathbf{D}}$ substituted for ρ_{SCF}. Finally, the contributions to the perturbed Z-CPSCF equations are:

$$0 \equiv \left[\frac{\mathrm{d}\partial\mathcal{L}}{\mathrm{d}\mathbf{B}\partial U_{ai}} - \frac{\mathrm{d}\partial\mathcal{L}}{\mathrm{d}\mathbf{B}\partial U^*_{ia}}\right]\Bigg|_{\mathbf{B}=0} \leftarrow 2\Big(\mathbf{U}^{\mathbf{B},\mathrm{T}}\boldsymbol{\mathcal{R}}^{\mathrm{sol}}[\mathbf{D}] + \boldsymbol{\mathcal{R}}^{\mathrm{sol}}[\mathbf{D}]\mathbf{U}^{\mathbf{B}*} + \boldsymbol{\mathcal{R}}^{\mathrm{sol}(\mathbf{B})}[\mathbf{D}]\Big)_{ai} \tag{2.149}$$

where

$$\mathcal{R}^{\mathrm{sol}(\mathbf{B})}_{ai}[\mathbf{D}] = \sum_{\mu\nu} c_{\mu a}c^*_{\nu i}\int v^{\mathrm{sol}}_{\mathrm{el}}[\mathbf{D}]\Omega^{\mathbf{B}}_{\mu\nu}\mathrm{d}\mathbf{r} \tag{2.150}$$

Note that the solvent potential is self-consistently optimized with the SCF electron density, rather than the full MP2 density. This approach, often denoted "PTE", is not only more convenient to derive and implement, but is actually the theoretically consistent choice for second order perturbation theory, according to an analysis by Ángyán.[247]

2.2 Implementation of the RI-MP2 response density calculation

In ORCA the relaxed RI-MP2 difference density $\mathbf{D}$ is evaluated as discussed in ref. 92. The algorithm is similar to that of Weigend and Häser,[237] with some notable differences. For detailed descriptions of these implementations, the reader is referred to those publications. Here we briefly summarize the main steps:

1. The integrals $(ip|K)$ are calculated and stored on disk.
2. The occupied MOs are split into batches according to available memory.
3. In each batch of i, integrals are read and amplitudes $\mathbf{T}^{ij}$ and $\widetilde{\mathbf{T}}^{ij}$ are calculated (eqs. 2.91 and 2.75).
4. Contributions to $\mathbf{D}'$ (eqs. 2.76–2.77), $\mathbf{\Gamma}^K$ (eq. 2.96), and $\mathbf{X}$ (eq. 2.103) are accumulated.
5. After the main loop, the two-electron response operator $\mathbf{g}^*[\mathbf{D}']$ (eq. 2.17) is constructed and added to $\mathbf{X}$.
6. The Z-CPSCF equations (eq. 2.102) are solved and the relaxed density matrix $\mathbf{D}$ is stored on disk.

The expressions for the magnetic field-perturbed quantities $\mathbf{D}'^{\mathbf{B}}$, $\mathbf{\Gamma}^{K,\mathbf{B}}$, $\mathbf{T}^{ij,\mathbf{B}}$ (first term), and $\overline{\mathbf{X}}^{\mathbf{B}}$ (first four terms) – eqs. 2.109, 2.110, 2.122, 2.113, and 2.120, respectively – are analogous to the respective unperturbed quantities $\mathbf{D}'$, $\mathbf{\Gamma}^i$, $\mathbf{T}^{ij}$, and $\mathbf{X}$ – eqs. 2.76, 2.77, 2.96, 2.91, and 2.103, respectively – except that the former contain six times as many contributions (recalling that the magnetic field has three components). Therefore, the algorithm to calculate these terms is also analogous to that for first DHDFT and RI-MP2 derivatives, discussed above and in refs. 92 and 237, with six times as many operations (seven times as many in case the unperturbed quantity needs to be recalculated as well – this is the case for $\mathbf{T}^{ij}$ and $\mathbf{\Gamma}^K$) and four times higher memory requirements (including the unperturbed quantities), leading to an expected increase of the computation cost by a factor of up to 20–30. Both unperturbed and perturbed three index integrals, $(ip|K)$ and $(ip|K)^{\mathbf{B}}$, are precalculated and stored on disk. The similarities and differences between the algorithms for the calculation of $\mathbf{D}$ and $\mathbf{D}^{\mathbf{B}}$ can be seen in Scheme 2.1.

The last two terms in eq. 2.113 require special treatment, which is discussed in Section 2.1.3.4. As explained there, it is usually more efficient to store the unperturbed amplitudes on disk. Another potential bottleneck are the contributions to $D'^{\mathbf{B}}_{kj}$ (eq. 2.109) where all $\mathbf{T}^{ij}$ and $\mathbf{T}^{ij,\mathbf{B}}$ are required for a given i. One approach, which is used for the equivalent contributions to D'_{kj} is to keep these amplitudes in memory. However, due to the higher memory requirements, more batches would be needed, resulting in additional overhead. Alternatively, the amplitudes for the batch can be stored on disk and processed in a second loop over i. This also produces overhead in the form of disk input/output

Scheme 2.1: Algorithms for the calculation of $\mathbf{D}$ (left) and $\mathbf{D}^{\mathbf{B}}$ (right), aligned to highlight the analogous steps. Frozen-core and XC contributions are omitted for simplicity.

Make and store all $(ip|K)$

for batch $I \in$ {occupied} **do**
  for $i \in I$ **do**
    for $j \in$ {occupied} **do**
      Make $\mathbf{T}^{ij}$ (and $\widetilde{\mathbf{T}}^{ij}$).
      if $j \leq i$ **then**
        $\mathbf{T}^{ij}$ contribs. to E^{MP2} and $\mathbf{D}'$
      end if
      $\mathbf{T}^{ij}$ contribs. to Γ^{K}_{ia}
    end for (j)
    for $j \in$ {occupied} **do**
      for $k \leq j$ **do**
        $\mathbf{T}^{ik}$ contribs. to $\mathbf{D}'$
      end for (k)
    end for (j)
    3-internal $\mathbf{\Gamma}^{K}$ contribs. to $\mathbf{X}$
  end for (i)
  3-external $\mathbf{\Gamma}^{K}$ contribs. to $\mathbf{X}$
end for (I)
Fock response contribs. to $\mathbf{X}$
Solve Z-CPSCF equations and complete $\mathbf{D}$

Make and store all $(ip|K)$ and $(ip|K)^{\mathbf{B}}$
Map $L(i \to k)$ where $F_{ki} > F_{\mathrm{Cut}}$
Read $\mathbf{D}$ and all $U^{\mathbf{B}}_{ai}$. Complete $\mathbf{U}^{\mathbf{B}}$ and $\mathbf{F}^{\mathbf{B}}$
for batch $I \in$ {occupied} **do**
  for $i \in I$ **do**
    for $j \in$ {occupied} **do**
      Make $\mathbf{T}^{ij}$ (and $\widetilde{\mathbf{T}}^{ij}$).
      $\mathbf{K}^{ij*}$, $\mathbf{K}^{ij*\mathbf{B}}$, and $\mathbf{T}^{ij}$ contribs. to $\mathbf{T}^{ij,\mathbf{B}}$
      for $k \in L(i \to k)$ **do**
        Make/read $\mathbf{T}^{kj}$
        $\mathbf{T}^{kj}$ contrib. to $\mathbf{T}^{ij,\mathbf{B}}$
      end for(k)
      for $k \in L(j \to k)$ **do**
        Make/read $\mathbf{T}^{ik}$
        $\mathbf{T}^{ik}$ contrib. to $\mathbf{T}^{ij,\mathbf{B}}$
      end for(k)
      Complete $\mathbf{T}^{ij,\mathbf{B}}$ (and $\widetilde{\mathbf{T}}^{ij,\mathbf{B}}$).
      if $j \leq i$ **then**
        $\mathbf{T}^{ij}$ and $\mathbf{T}^{ij,\mathbf{B}}$ contribs. to $\mathbf{D}'^{\mathbf{B}}$
      end if
      $\mathbf{T}^{ij}$ and $\mathbf{T}^{ij,\mathbf{B}}$ contribs. to Γ^{K}_{ia} and $\Gamma^{K,\mathbf{B}}_{ia}$
    end for (j)
    for $j \in$ {occupied} **do**
      for $k \leq j$ **do**
        $\mathbf{T}^{ik}$, $\mathbf{T}^{ij}$, $\mathbf{T}^{ik,\mathbf{B}}$, and $\mathbf{T}^{ij,\mathbf{B}}$ contribs. to $\mathbf{D}'^{\mathbf{B}}$
      end for (k)
    end for (j)
    3-internal $\mathbf{\Gamma}^{K}$ and $\mathbf{\Gamma}^{K,\mathbf{B}}$ contribs. to $\overline{\mathbf{X}}^{\mathbf{B}}$
  end for (i)
  3-external $\mathbf{\Gamma}^{K}$ and $\mathbf{\Gamma}^{K,\mathbf{B}}$ contribs. to $\overline{\mathbf{X}}^{\mathbf{B}}$
end for (I)
Fock response contribs. to $\overline{\mathbf{X}}^{\mathbf{B}}$
Solve perturbed Z-CPSCF equations and complete $\mathbf{D}^{\mathbf{B}}$

(I/O) and recalculation of the contravariant amplitudes $\widetilde{\mathbf{T}}^{ij}$ and $\widetilde{\mathbf{T}}^{ij,\mathbf{B}}$ and is therefore only necessary when memory is a limiting factor.

As is the case for $\mathbf{X}$,[92] the three external index contributions to $\overline{\mathbf{X}}^{\mathbf{B}}$ (second and third terms in eq. 2.120) are evaluated by partially transforming $\mathbf{\Gamma}^{K}$ and $\mathbf{\Gamma}^{K,\mathbf{B}}$ to the AO basis,

$$\Gamma^{K}_{i\mu} = \sum_{b} c_{\mu b} \Gamma^{K}_{ib} \tag{2.151}$$

$$\Gamma^{K,\mathbf{B}}_{i\mu} = \sum_{b} \left[c^{\mathbf{B}}_{\mu b} \Gamma^{K}_{ib} + c_{\mu b} \Gamma^{K,\mathbf{B}}_{ib} \right] \tag{2.152}$$

and contracting them with AO-basis three index integrals, generated on the fly:

$$\overline{X}^{\mathbf{B}}_{ai} \leftarrow -2 \sum_{\nu} c^{\mathbf{B}}_{\nu a} \sum_{K\mu} (\mu\nu|K)\, \Gamma^{K*}_{i\mu} - 2 \sum_{\nu} c_{\nu a} \sum_{K\mu} \left[(\mu\nu|K)^{\mathbf{B}}\, \Gamma^{K*}_{i\mu} + (\mu\nu|K)\, \Gamma^{K*\mathbf{B}}_{i\mu} \right] \tag{2.153}$$

As in the DHDFT gradient implementation in ORCA,[92] but unlike the original algorithm by Weigend and Häser,[237] Γ^{K}_{ia} and $\Gamma^{K,\mathbf{B}}_{ia}$ for the whole batch are kept in memory, although in principle it is also possible to store them on disk to reduce memory demands at the cost of a higher I/O overhead.

A final point to consider is the evaluation of two-electron Fock response terms in eqs. 2.102 and 2.119, as well as those in the perturbed Fock matrix $\mathbf{F}^{\mathbf{B}}$. The latter were discussed at length in Section 2.1.2 and that discussion largely applies also to the GIAO integrals $\mathbf{g}^{(\mathbf{B})*}[\mathbf{D}]$. Theoretically it is most consistent to apply to these terms the same approximation (e.g. RIJK or RIJCOSX) that was used in the SCF procedure. However, the RI approximation to the exchange integrals offers no computational advantage when the latter are to be contracted with a density matrix defined in the entire MO space. Therefore, in our implementation the LHS terms are treated with the RIJONX approximation, which allows for better prescreening. An alternative is to store the required $(aj|bi)$ and $(ab|ji)$ integrals on disk, rather than recalculate them at each CPSCF iteration. This is most efficiently done via an RI transformation during the first run through the RI-MP2 program, where the integrals $(ia|K)$ and $(ij|K)$ are already available, although $(ab|K)$ are normally not. Note, however, that the RI-MP2 auxiliary basis set (denoted AuxC) is used, rather than the one used for the SCF (denoted AuxJ). In Section 2.3.10.2 we compare the efficiency of these two approaches.

2.3 Results and discussion

2.3.1 Test set

While multiple authors have performed benchmark studies on the calculation of NMR properties and have proposed different test sets of molecules,[47,73,76] we chose to compile a new test set with the following requirements in mind: *(i)* it should include magnetically active nuclei of several different (and chemically important) elements; *(ii)* for each element, a broad range of shielding values should be covered; *(iii)* the size and number of molecules should still allow for quick optimization of computational parameters; and *(iv)* experimental gas-phase absolute shielding constants should ideally be available for most, if not all, nuclei. We propose the following set of 15 molecules: C_4H_4O (furan), CF_4, CH_3COCH_3, CH_4, CO, F_2, OF_2, H_2O, HF, N_2, N_2O, NH_3, PF_3, PH_3, and PN. The test set includes a total of 34 chemically inequivalent shielding constants – 8 for ^{1}H, 7 for ^{13}C, 5 for

^{15}N, 6 for ^{17}O, 5 for ^{19}F, and 3 for ^{31}P – which span most of the range of possible shielding values for each element. High-quality GIAO-CCSD(T) calculations, including zero-point vibrational corrections have previously been performed for all of these molecules.[43–46,73] In addition, experimental data for absolute gas-phase shielding constants are available for 29 of the 34 shielding constants (all except C and H in C_4H_4O and H in CH_3COCH_3) (see Table 2.1 for references).

Note that the experimental value quoted for the ^{1}H shielding of PH_3 in the initial publication of these results (ref. 261)) was 27.89 ppm, taken from ref. 262. This value was not actually used in the benchmark calculations, as comparisons were made with respect to the CCSD(T) values and the empirical equilibrium estimates, for those nuclei for which a vibrational correction was available. However, it is likely the experimental shielding of 27.89 ppm is erroneous as it disagrees significantly form the CCSD(T) result and is more than 1 ppm away from the value of 29.24 ppm quoted in ref. 248. ref. 262 also quotes the ^{1}H shielding in NH_3 as 32.10 ppm, which also appears to be in error.

2.3.2 Computational details

Software. Molecular geometries were optimized at the CCSD(T)/cc-pVTZ level[263–265] using the program CFOUR.[266] The latter was also used to perform canonical GIAO-MP2[34,35] and GIAO-CCSD(T)[37,39] calculations for reference (see Table 2.1 and Sections 2.3.3 and 2.3.5). All other calculations were performed with a development version of ORCA 4.[219–221] Figures in this work were predominantly generated using Matplotlib,[267] and depictions of molecules – using Avogadro.[268]

Electronic structure methods. NMR shielding tensors were calculated with various methods to compare the accuracy of the latter (vs reference data) and to put other errors (due to basis sets, etc.) in perspective. In addition to HF, MP2 was used, as well as two spin-component-scaled variants: Grimme's original SCS-MP2[51] and Fink's S2-MP2 parametrization.[52] Several well-established DFT functionals were included at various rungs of "Jacob's Ladder": GGA (BLYP,[269,270] PBE,[271] B97-D3,[80] KT2,[74] and KT3[75]), global hybrid GGA (B3LYP[272] and PBE0[273]), meta-GGA (TPSS,[274] M06-L,[275] and r^{2}SCAN[276]), hybrid meta-GGA (TPSSh,[277] M06,[278] and M06-2X[278]), range-separated hybrid with and without non-local correlation (ωB97X-V[279] and ωB97X-D3BJ[280]), and double hybrid (B2PLYP,[78] B2GP-PLYP,[281] DSD-BLYP,[85] DSD-PBEP86,[85] and ωB97X-2[282]). For functionals that are not implemented natively in ORCA, the interface to LibXC was used.[283]

Note that there are multiple slightly different parametrizations of DSD-PBEP86, some of which were unfortunately introduced with the same names.[83–85,89] We denote with "DSD-PBEP86" the 2013 version parametrized together with the D3BJ dispersion correction (the latter does not contribute to calculated shielding) and the version parametrized without an empirical dispersion correction – with "NoDSD-PBEP86".[85] Where applicable, we use the prefixes "ae-" and "fc-" to signify all-electron and frozen-core calculations (with the same functional parameters). A more recent work re-parametrized the DSD-PBEP86 functional over the whole GMTKN55 dataset, introducing "revDSD-PBEP86" (here we use the D3BJ version) and the partially re-optimized "revωB97X-2".[89] The same article includes different versions with and without core correlation for some functionals, but here we use the same parameters. For clarity, the actual parameters for all DHDFs used in this work are listed in Table C.15.

Table 2.1: Benchmark set and gas phase shielding constants (ppm), calculated at the CCSD(T)/pcSseg-4 level in this work, compared to two previously published theoretical estimates T1 and T2, including vibrational corrections (VC), and to experimental gas phase data. Empirical equilibrium shielding constants are calculated by subtracting the VC from the experimental results.

	Molecule	CCSD(T)	T1 Eq.[a]	T2 Eq.	T1 VC[b]	T2 VC	Exp.	Emp. Eq.	Exp. Ref.
^{1}H	PH_3	29.46					29.24		248
	HF	28.82	28.83		−0.33		28.64	28.97[b]	249, 250
	H_2O	30.65	30.65	30.87[em]	−0.52	−0.54[jm]	30.05	30.57[b]	249
	NH_3	31.44	31.44		−0.61		30.68	31.29[b]	249
	CH_4	31.39	31.30		−0.63		30.80	31.43[b]	249, 251
	$(CH_3)_2CO$	29.53		29.64[em]		−0.64[jm]			
	furan (at C2/5)	24.03		24.15[em]		−0.45[jm]			
	furan (at C3/4)	25.02		25.14[em]		−0.42[jm]			
^{13}C	$(CH_3)_2\underline{C}O$	−10.84		−10.0[c]		−0.8[h]	−13.2	−12.4[h]	252, 253
	CO	2.56	2.24	3.0[c]	−0.18	−1.0[h]	0.9	1.9[h]	253
	CF_4	65.96		65.3[c]		−1.4[h]	64.4	65.8[h]	252, 253
	furan (C2/5)	47.36		48.9[em]		−3.6[jm]			
	furan (C3/4)	81.67		83.0[em]		−3.4[jm]			
	$(\underline{C}H_3)_2CO$	162.88		163.1[c]		−3.3[h]	157.9	161.2[h]	252, 253
	CH_4	199.39	198.93	198.8[c]	−3.7	−2.6[h]	195.0	197.6[h]	252, 253
^{15}N	PN	−344.71	−343.97		−5.3		−349	−343.7[b]	254
	N_2	−61.16	−60.43	−59.8[d]	−4.3	−3.3[i]	−61.6	−58.3[i]	255
	N$\underline{N}$O	11.74	12.56	12.8[d]	−3.9	−3.1[i]	11.3	14.4[i]	255
	$\underline{N}$NO	106.22	106.45	107.6[d]	−8.4	−6.8[i]	99.5	106.3[i]	255
	NH_3	270.40	270.66	270.7[d]	−8.7	−6.8[i]	264.5	271.3[i]	255
^{17}O	OF_2	−446.32	−447.09	−439.8[e]	−44.3	−34.0[j]	−493.6	−459.6[j]	256
	$(CH_3)_2CO$	−297.91		−301.6[e]		−3.8[j]	−309.1	−305.3[j]	256
	CO	−55.42	−55.05	−56.3[e]	−5.8	−3.8[j]	−62.7	−58.9[j]	256
	furan	64.82		64.7[e]		−11.6[j]	50.3	61.9[j]	256
	NNO	198.77	199.02	198.2[e]	−12.9	−8.2[j]	181.0	189.2[j]	256
	H_2O	337.63	338.01	338.2[e]	−14.2	−9.6[j]	323.5	333.1[j]	256
^{19}F	F_2	−192.76		−191.3[f]		−23.6[k]	−233.2	−209.6[k]	253, 257
	OF_2	−24.28	−23.95	−22.6[f]	−25.0	−23.7[k]	−59.7	−36.0[k]	253, 258, 259
	PF_3	231.81					230.8		253, 257
	CF_4	267.58		266.8[f]		−7.3[k]	258.6	265.9[k]	253, 257
	HF	419.91	420.31	418.9[f]	−11.8	−8.6[k]	409.6	418.2[k]	253
^{31}P	PN	51.61	50.59	53.4[g]	−6.9	−4.4[l]	53.0	57.4[l]	254
	PF_3	224.80		230.1[g]		−2.3[l]	222.7	225.0[l]	260
	PH_3	604.51		607.1[g]		−9.5[l]	594.5	604.0[l]	260

[a] Geometry: CCSD(T)/cc-pVTZ; NMR shielding: CCSD(T)/extrapolated aug-cc-pCV[TQ]Z.[73]
[b] ZPV corrections: B3LYP/aug-cc-pCVTZ.[73]
[c] Geometry: CCSD(T)/cc-pVTZ; NMR shielding: CCSD(T)/13s9p4d3f.[43]
[d] Geometry: CCSD(T)/cc-pVQZ; NMR shielding: CCSD(T)/13s9p4d3f.[46]
[e] Geometry: CCSD(T)/cc-pVTZ; NMR shielding: CCSD(T)/pz3d2f.[45]
[f] Geometry: CCSD(T)/cc-pVTZ; NMR shielding: CCSD(T)/13s9p4d3f.[44]
[g] Geometry: CCSD(T)/cc-pVQZ; NMR shielding: CCSD(T)/15s12p4d3f2g.[46]
[h] ZPV corrections: MP2/cc-pVTZ (force field) + MP2/qz2p (NMR shielding).[43]
[i] ZPV corrections: CCSD(T)/cc-pVTZ (force field) + CCSD(T)/qz2p (NMR shielding).[46]
[j] ZPV and thermal corrections: MP2/cc-pVTZ (force field) + MP2/qz2p (NMR shielding).[45]
[k] ZPV and thermal corrections: MP2/cc-pVTZ (force field) + MP2/qz2p (NMR shielding).[44]
[l] ZPV corrections: CCSD(T)/cc-pVTZ (force field) + CCSD(T)/qz3d1f (NMR shielding).[46]
[m] Previously unpublished value.

Basis sets. Despite the use of GIAOs, basis set convergence of calculated shielding constants towards the complete basis set (CBS) limit can be fairly slow.[13,284] Therefore, it is important when assessing the performance of different methods to make an effort to reduce the basis set error. For this study, the pcSseg-n (n =0–4) family of basis sets was chosen (further denoted pSn for the sake of brevity),[284] a segmented contracted version of the pcS-n basis sets.[285] Both basis set families were optimized for DFT-level NMR calculations but the latter have also been shown to converge rapidly towards the CBS limit at the MP2-level.[47,286] The pcSseg-4 basis set is very close to this limit, with a residual basis set error estimated at $\sim 0.2\,\%$ in the original publication,[284] which is within the margin of error in the experimental data and also significantly smaller than e.g. the size of the vibrational corrections. In Table 2.1 our CCSD(T)/pcSseg-4 results are compared to the extrapolated aug-cc-pCV[TQ]Z data by Teale et al.[73] The differences are on the order of 0.01–0.1 ppm for H and less than 1 ppm for heavier nuclei, which translates to a relative deviation of $\sim 0.5\,\%$. It should be noted that Teale et al. used an extrapolation scheme fitted for total energies and this choice has been criticized by Jensen et al. who suggest a lower exponent for the extrapolation (1.05 rather than 1.63) based on comparison with accurate calculations in a multiwavelet basis.[287] The latter also estimated that the B3LYP/pcSseg-4 shielding constants for hydrogen and for second row elements are accurate to ~ 0.01 ppm and ~ 0.1 ppm, respectively. A comparison of the HF/pcSseg-4 shielding constants in our test set to the data of Teale et al. and Jensen et al. (see Table C.17) also suggests that the pcSseg-4 basis set is a better estimate of the CBS limit than the aug-cc-pCV[TQ]Z extrapolation. However, the pcSseg-4 basis set is too large for routine applications and it is also worth pointing out that when calculating chemical shifts, one can often rely on error cancellation and achieve accurate results with much more modest basis sets. Hence, the smaller pcSseg-2 and pcSseg-3 basis sets were used for most of this study. The additional basis set incompleteness error thus introduced is evaluated in Section 2.3.4. It has been shown that for larger systems the computational effort can be further reduced, with minimal loss of accuracy, by using smaller basis sets for atoms far from the nuclei of interest.[286] However, because the molecules in our test set are small and all their shielding constants are to be calculated, no such scheme was used.

Various auxiliary basis sets are used for the RI approximation and their efficiency and accuracy are studied in detail in Sections 2.3.5, 2.3.7, and 2.3.8. For RIJ and RIJK the "universal" basis sets by Weigend are compared, labeled def2-J and def2-JK, respectively.[115,288] The latter is larger and while it was optimized to fit exchange integrals it also leads to smaller errors in the Coulomb contributions, as was noted in the original publication. Results are also presented for an auxiliary basis set, generated by the AutoAux procedure implemented in ORCA, which creates a large, uncontracted fitting basis, suitable for all types of two-electron integrals, albeit not as economical as the optimized auxiliary basis sets.[289] Auxiliary basis sets used for the RI-MP2 approximation (abbreviated as "AuxC basis sets") are usually specific to the fitted orbital basis set (OBS). The chosen pS2, pS3, and pS4 OBSs are of triple-, quadruple-, and quintuple-zeta quality, respectively, and contain tight functions to better describe the core region. Regrettably, no auxiliary basis sets have been specifically optimized for these OBSs. Hence, we have chosen the AuxC basis sets, here denoted cw$n$C ($n = 3, 4, 5$),[290] optimized for Peterson's cc-pwCVXZ (X = T, Q, 5) basis sets,[291] which also contain additional tight functions. Alternatively, we employ the AutoAux scheme to generate large fitting basis sets for each OBS.

Numerical precision. In order to reduce numerical noise, tight convergence thresholds were used for the iterative SCF and CPSCF solutions, and a dense DFT grid (g7, $\varepsilon = 5.67$ – see below, ORCA keyword "`grid7`") was employed for the evaluation of DFT functionals (unless otherwise noted). Thus, the isotropic shielding constants are calculated with a precision of at least 4 significant figures.

The grids used for the COS approximation are constructed from spherical atom-centered grids and their accuracy is controlled by two main parameters: (1) ε, which determines the number of radial "shells" n_r according to the formula $n_r = \max[13, 15\varepsilon + 5r - 40]$, where r is the row in the periodic table for a given element (cf. eq. 14 in ref. 292); (2) gn ($n = 1$–7), which signifies the Lebedev angular grids used (26–590 points, respectively, see Table S1 for details). The pruning algorithm of Gill et al. is applied,[293] whereby an atom is partitioned into five regions and a denser angular grid is used for radial shells in the valence region than in the core and outermost regions (see Table C.16). In addition, the atomic size adjustment and the M3 mapping, proposed by Treutler and Ahlrichs (eqs. 13 and 18 in ref. 294), are employed.

Error measurement. We use several statistical measures of the deviation of the shieldings, σ or chemical shifts, δ, calculated according to a given protocol (method, basis, etc.) with respect to a given reference (e.g. CCSD(T) data). The mean error (ME), mean absolute error (MAE), mean relative error (MRE), mean absolute relative error (MARE), maximum errors and relative errors (MaxAE and MaxARE, respectively), and standard deviation of the (relative) errors (SDE and SDRE) are defined as:

$$
\begin{aligned}
\Delta\sigma_i &= \sigma_i - \sigma_i^{\text{ref}} & \tilde{\Delta}\sigma_i &= \frac{\sigma_i - \sigma_i^{\text{ref}}}{\left|\sigma_i^{\text{ref}}\right|} \\
\text{ME}_\sigma &= \frac{1}{N}\sum_{i=1}^{N} \Delta\sigma_i & \text{MRE}_\sigma &= \frac{1}{N}\sum_{i=1}^{N} \tilde{\Delta}\sigma_i \\
\text{MAE}_\sigma &= \frac{1}{N}\sum_{i=1}^{N} |\Delta\sigma_i| & \text{MARE}_\sigma &= \frac{1}{N}\sum_{i=1}^{N} \left|\tilde{\Delta}\sigma_i\right| \\
\text{MaxAE}_\sigma &= \max_i \left[\, |\Delta\sigma_i| \,\right] & \text{MaxARE}_\sigma &= \max_i \left[\, \left|\tilde{\Delta}\sigma_i\right| \,\right] \\
\text{SDE}_\sigma &= \sqrt{\frac{1}{N}\sum_{i=1}^{N} (\Delta\sigma_i)^2 - (\text{ME}_\sigma)^2} \\
\text{SDRE}_\sigma &= \sqrt{\frac{1}{N}\sum_{i=1}^{N} \left(\tilde{\Delta}\sigma_i\right)^2 - (\text{MRE}_\sigma)^2}
\end{aligned}
\tag{2.154}
$$

The same quantities (with an index δ) are defined analogously for the chemical shifts, which are given by $\delta_i = \sigma_{\text{std}} - \sigma_i$, where σ_{std} is the shielding of the given nucleus in a "standard" compound, calculated at the same level of theory. We use CH_4 as a standard for ^{13}C and ^{1}H, NH_3 for ^{15}N, H_2O for ^{17}O, HF for ^{19}F, and PH_3 for ^{31}P.

In the box-and-whiskers plots used throughout the rest of this work boxes show the interquartile range (IQRE or IQRRE), i.e. the range of errors (or relative errors), excluding the top and bottom 25 %; whiskers show the minimum and maximum errors (MinE and MaxE) or relative errors (MinRE and MaxRE); and lines show the median errors (MedE)

or relative errors (MedRE) and the ME or MRE. The Range of (relative) errors (RanE or RanRE), defined as the difference between the minimum and maximum, is also discussed. Note that wherever relative errors are calculated, those data with small reference values (less than 10 ppm for shieldings and 1 ppm for chemical shifts) were excluded from the analysis because they disproportionately skew the results. The excluded nuclei are listed in the figure captions.

Because systematic deviations in the absolute shielding may partially cancel out in practical applications, it is more pragmatic to look at errors in the chemical shifts. On the other hand, the orders of magnitude of both shieldings and shifts vary significantly for different nuclides, so some form of scaling is necessary in order to combine all benchmark data into a single convenient statistic. The mean absolute relative error in the chemical shifts (MARE_δ) is one such possible measure. However, in addition to the need to eliminate data with small reference values, as mentioned above, the MARE_δ is inevitably biased by the choice of standard nucleus. Therefore, we also introduce the following measure, denoted as "mean relative range of errors" (MRRE):

$$\mathrm{MRRE}_\sigma = \frac{1}{N_{\mathrm{elem}}} \sum_{A}^{\mathrm{elem}} \frac{\max_{i\in A}\left[\Delta\sigma_i\right] - \min_{i\in A}\left[\Delta\sigma_i\right]}{\max_{i\in A}\left[\sigma_i^{\mathrm{ref}}\right] - \min_{i\in A}\left[\sigma_i^{\mathrm{ref}}\right]} \tag{2.155}$$

The full range of shielding errors for a given nuclide gives an the upper bound for the chemical shift error. The range of shieldings for the respective element (in our carefully selected test set) is close to the experimentally observed range and thus provides an appropriate scaling factor, giving a "relative range" of errors. The average of these relative ranges over all elements is the MRRE.

In the following Section 2.3.3 we will assess the accuracy of HF, RI-MP2, and (DH)DFT NMR shielding calculations that is inherent to the methods themselves, by comparing to the reference data in Table 2.1. In subsequent sections we will examine errors due to basis set incompleteness in the orbital (Section 2.3.4) and AuxC (Section 2.3.5) basis sets, the frozen core approximation (Section 2.3.6), and two-electron integral approximations in the Fock matrix (Sections 2.3.7 and 2.3.8).

2.3.3 Method accuracy

In this section we evaluate the deviations, inherent to the methods used, in the calculated shieldings from the CCSD(T) data presented in Table 2.1. The latter are very close to the empirical equilibrium data, so similar conclusions can be drawn from either reference. Therefore, only the CCSD(T) reference is discussed here and a comparison to the empirical equilibrium data is given in Appendix C. While HF and DFT methods are computationally inexpensive, they are not particularly accurate or precise for the calculation of magnetic properties in comparison to correlated wave function-based approaches such as CCSD(T), and in the case of DFT, results may vary significantly between functionals. The performance of these methods has been discussed extensively,[43–47,62,73] but for consistency they are also compared here. A direct comparison with previously published results, e.g., those of Teale et al.,[73] is difficult because of the different sets of molecules. Nevertheless, similar trends can be observed in our study, as shown below. The chemical shielding constants for all nuclei in the test set were calculated using the methods listed in Section 2.3.2, with the pcSseg-4 basis set (and the cc-pwCV5Z/C AuxC set, where applicable), which is assumed to be sufficiently close to the CBS limit. No approximations were employed for the two-electron integrals. It is important to note that no vibrational

or thermal corrections were applied. These, however are not expected to significantly improve the agreement with experiment at this level of theory and indeed for DFT, would likely worsen it.[73] It is useful to separately discuss mean field (SCF) methods and those including second order perturbation theory (PT2) contributions, i.e. (SCS-)MP2 and DHDFT, due to the rather large differences in both cost and accuracy between the two categories.

2.3.3.1 SCF methods

The errors in the shieldings for different groups of nuclides are shown in Figure 2.1, where the mean field methods are grouped in the top subplot. The data for ^{15}N, ^{17}O, ^{19}F, and ^{31}P nuclei are analyzed together because they span similar ranges of shielding values. From the figure, it is apparent that the errors are very widely distributed. In addition, DFT tends to underestimate the shielding constants with the exception of ^{1}H (and possibly M06-L for other nuclides). In relative chemical shifts this bias would cancel out only partially due to the large variance in the errors.

As expected, the missing electron correlation in HF leads to rather poor results, despite the fairly small mean error. On the other hand, comparing BLYP, PBE, and TPSS with their hybrid counterparts shows that the inclusion of exact exchange eliminates some outliers and leads to overall narrower error distributions. Especially interesting is the performance of the M06 group of functionals, of which M06-L is indeed quite accurate for our test set, confirming the conclusions of Zhao and Truhlar.[76] However, M06 and M06-2X show by far the poorest performance in our test set, worse even than HF (except for hydrogen). There is no mention of this discrepancy in ref. 76, indeed the hybrid functionals in the M06 family are not discussed at all. In any case, this result simply confirms that a DFT functional, which is accurate for a certain property, e.g. the energy, is not necessarily also good for others. The r^{2}SCAN functional stands out as particularly accurate, especially for ^{13}C shieldings. Note, however, that the good performance of meta-GGA functionals (M06-L in particular) may be somewhat fortuitous, due to the ad-hoc treatment of τ (see Section 2.1.4), as suggested in ref. 72.

The effect of error cancellation when calculating chemical shifts – which are the experimentally measured quantities – can be seen in Figure 2.2, which shows the relative errors in the shifts for all nuclei. There is still a significant systematic deviation for some methods, indicating that the shielding for the standard nucleus happened to carry a rather extreme (either small or large) error. Thus, we turn to the MRRE$_\sigma$ measure, shown in Figure 2.3, which does not carry this bias. A numerical comparison of the MRRE$_\sigma$ and MARE$_\delta$ is also presented in Table 2.2. While the ranking of methods changes slightly, depending on the statistical criterion, some trends seem consistent:

- HF, M06-2X, and M06 perform rather poorly.
- Hybrid functionals are somewhat more accurate than their pure counterparts.
- KT2, KT3, TPSS, TPSSh, and M06-L are more robust than BLYP, B3LYP, PBE, and PBE0.
- The VV10 non-local correlation contribution does not significantly affect the ωB97X results.
- The most accurate mean-field methods employed here have a MARE$_\delta$ of 4–6 % and MRRE$_\sigma$ of 5–7 %.

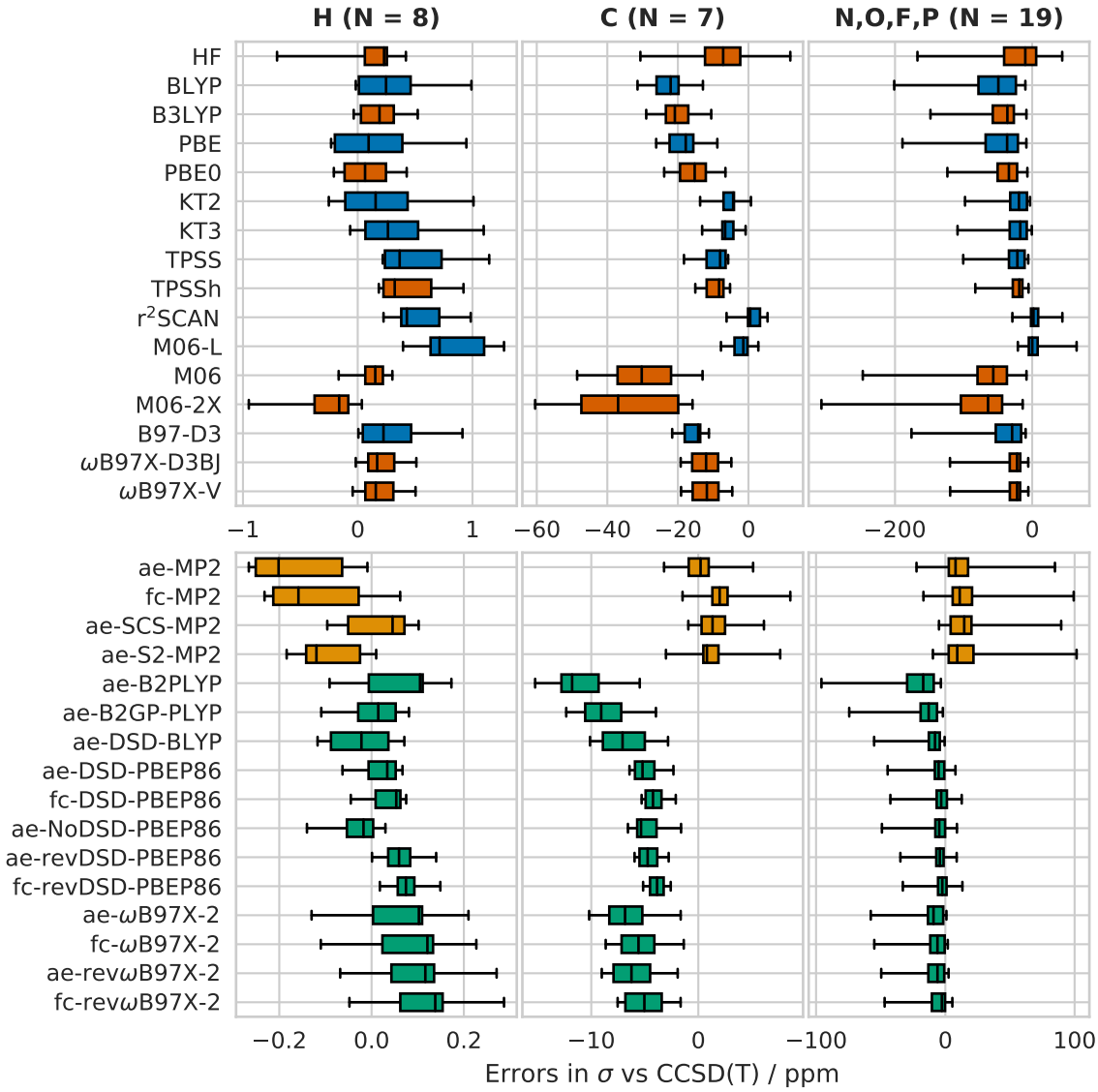

Figure 2.1: Deviations of isotropic shielding constants (ppm) for groups of nuclei, calculated using different methods and the pcSseg-4 basis set, from CCSD(T) results. The number of nuclei in each group is given in parentheses. Boxes show the IQRE_σ, whiskers show the MinE_σ and MaxE_σ, and lines show the MedE_σ. Pure functionals are shown in blue, hybrids and HF in orange, MP2 variants in yellow, and DHDFs in green. Note the different scales used for the abscissa.

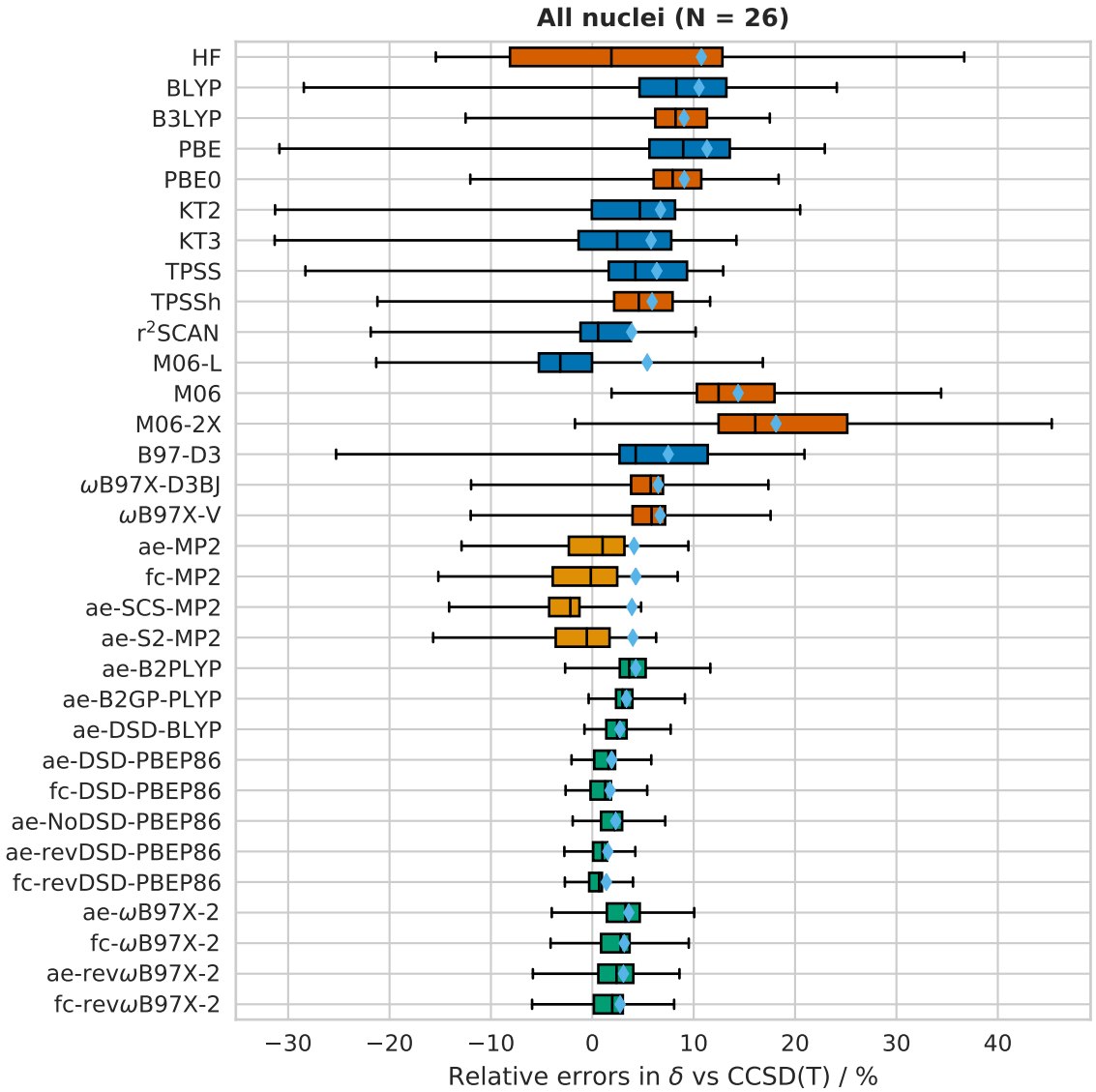

Figure 2.2: Relative deviations of chemical shifts (%), calculated using different methods and the pcSseg-4 basis set, from CCSD(T) results. The number of data points is given in parentheses. Excluded: $N\underline{H}_3$ and $\underline{H}_2O$. Boxes show the $IQRRE_\delta$, whiskers show the $MinRE_\delta$ and $MaxRE_\delta$, lines show the $MedRE_\delta$, and diamonds show the $MARE_\delta$. Pure functionals are shown in blue, hybrids and HF in orange, MP2 variants in yellow, and DHDFs in green.

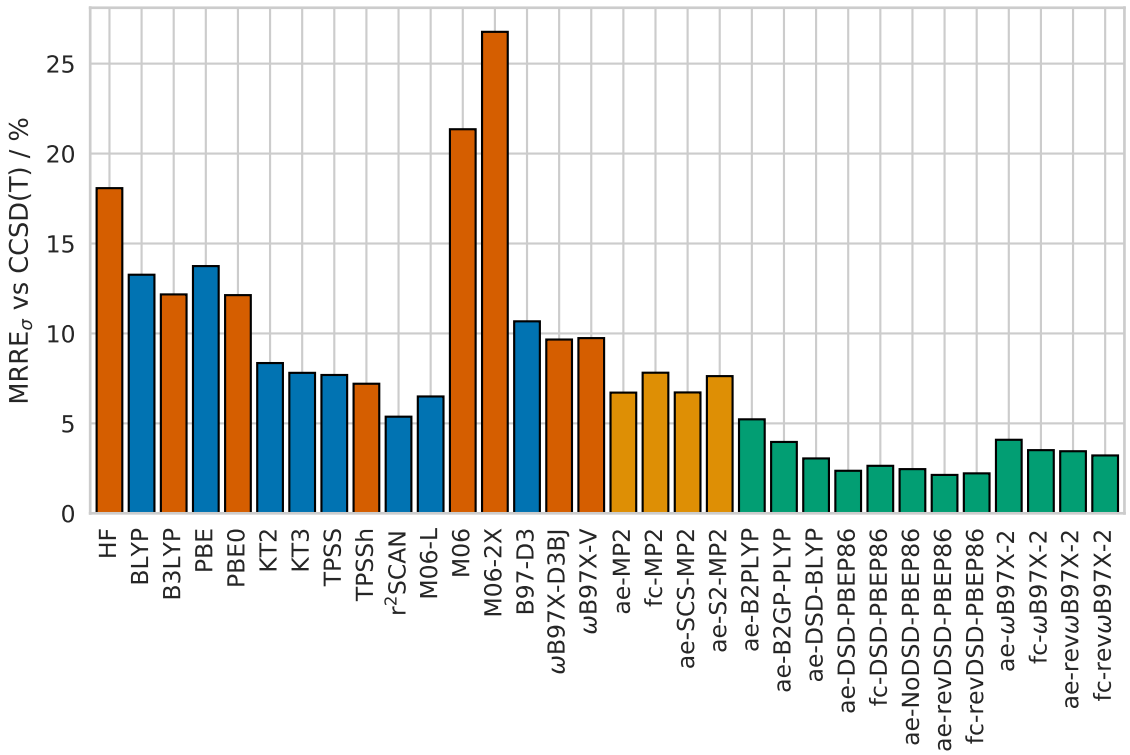

Figure 2.3: Mean relative range of shielding errors (MRRE_σ, see eq. 2.155) in percent, calculated using different methods and the pcSseg-4 basis set, from CCSD(T) results. Pure functionals are shown in blue, hybrids and HF in orange, MP2 variants in yellow, and DHDFs in green.

- The r^{2}SCAN functional performs remarkably well with $\mathrm{MARE}_\delta = 4\,\%$.

Thus, while HF and DFT can be invaluable and efficient tools for the estimation of NMR shielding constants, they are far from quantitatively accurate. Any errors introduced by further approximations – including smaller basis sets, RI, etc. – should therefore be viewed in comparison to the errors inherent in the methods.

2.3.3.2 PT2 methods

The data for MP2 variants and DHDFs are also shown in Figures 2.1 (shielding error distributions), 2.2 (relative chemical shift error distributions), 2.3 (MRRE_σ), and Table 2.2 (shielding error ranges, MRRE_σ, and MARE_δ). While the effect of the frozen-core approximation will be examined separately in Section 2.3.6, we include both all-electron and frozen-core alternatives of MP2 and DHDFT here, in order to account for possible error compensation and because some DHDFs were in fact parametrized for use with frozen core electrons.

MP2 shows a significant improvement over HF and is mostly better than DFT – the systematic deviation is consistently small for all elements and the error distributions are narrower, except for N and P shieldings where r^{2}SCAN, M06-L, TPSSh, and the KT functionals perform better. Note the particularly good performance of MP2 for carbon shieldings, which has been discussed before.[43,47] The frozen core approximation introduces a small systematic deviation, which is fortuitous for proton shieldings, but overall fc-MP2 is slightly less accurate than the all-electron approach. SCS-MP2 improves the results for ^{1}H shieldings but does not appear significantly better for the other nuclides, while

Table 2.2: Summary of shielding errors vs CCSD(T) data for different methods. The full range of errors for different nuclides is given in ppm. The MARE_δ (see eq. 2.154) and MRRE_σ, (see eq. 2.155) are given in percent.

Method	MARE_δ	MRRE_σ	H	C	N	O	F	P
HF	10.76	18.08	1.12	42.5	159.0	33.9	49.4	192.7
BLYP	10.53	13.26	1.01	18.5	69.5	189.1	77.5	50.2
B3LYP	9.05	12.17	0.56	18.4	93.0	137.2	59.3	79.7
PBE	11.32	13.74	1.18	17.3	66.5	179.8	73.0	69.9
PBE0	9.08	12.13	0.64	17.4	94.2	112.8	48.1	101.6
KT2	6.73	8.35	1.26	14.4	30.5	90.6	38.6	18.9
KT3	5.80	7.81	1.16	12.3	28.8	108.2	39.8	1.5
TPSS	6.36	7.69	0.93	12.5	36.9	94.4	34.7	21.9
TPSSh	5.90	7.20	0.74	9.8	49.4	76.8	24.1	37.6
r^2SCAN	3.88	5.37	0.76	11.6	6.6	72.9	24.0	11.9
M06-L	5.42	6.50	0.88	10.6	22.4	75.7	30.3	21.1
M06	14.39	21.35	0.47	35.5	175.3	202.1	99.2	190.2
M06-2X	18.12	26.77	0.99	44.6	243.3	201.9	94.7	250.6
B97-D3	7.49	10.67	0.91	10.4	46.5	164.1	72.7	35.9
ωB97X-D3BJ	6.50	9.66	0.53	14.3	79.3	73.8	26.5	96.0
ωB97X-V	6.69	9.74	0.55	14.5	79.7	73.4	25.9	97.2
ae-MP2	4.12	6.71	0.26	8.3	79.3	45.9	15.5	63.9
fc-MP2	4.29	7.82	0.29	10.1	93.4	47.4	17.4	77.8
ae-SCS-MP2	3.90	6.72	0.20	7.1	86.9	31.2	18.9	72.4
ae-S2-MP2	4.00	7.63	0.19	10.7	96.6	40.8	16.0	80.4
ae-B2PLYP	4.29	5.23	0.26	9.8	21.7	91.3	28.9	18.0
ae-B2GP-PLYP	3.37	3.97	0.19	8.4	14.1	71.6	18.1	15.9
ae-DSD-BLYP	2.73	3.05	0.19	7.3	8.7	54.2	9.3	13.6
ae-DSD-PBEP86	1.91	2.36	0.13	4.1	12.4	44.4	7.8	8.5
fc-DSD-PBEP86	1.76	2.64	0.17	5.0	13.7	49.2	7.1	8.5
ae-NoDSD-PBEP86	2.31	2.46	0.12	3.2	15.9	44.5	6.4	12.8
ae-revDSD-PBEP86	1.53	2.13	0.14	3.2	12.4	34.7	6.6	10.5
fc-revDSD-PBEP86	1.39	2.22	0.13	2.6	15.6	34.0	5.3	14.4
ae-ωB97X-2	3.60	4.09	0.34	8.6	9.4	58.5	15.3	24.2
fc-ωB97X-2	3.15	3.51	0.34	7.3	6.9	56.8	13.4	13.8
ae-revωB97X-2	3.07	3.45	0.34	7.1	6.2	52.1	13.7	15.8
fc-revωB97X-2	2.74	3.22	0.34	5.9	7.9	50.5	13.4	11.4

the S2-MP2 variant is overall no better than standard MP2. Maurer and Ochsenfeld have shown that the accuracy of SCS-MP2 for shieldings can be substantially improved by optimizing the c_{SS} and c_{OS} coefficients.[54] However, the vastly different optimal values for each combination of basis set and target element, makes it impossible to attach any physical interpretation to these parameters, essentially turning SCS-MP2 into a rather expensive semi-empirical method.

Transitioning into DHDFT, it is interesting to compare B3LYP, MP2, and B2PLYP: the former two show systematic deviations in the calculated shieldings with opposite signs, while the latter is somewhere in between. While this is not surprising, one can suppose that optimizing the c_{C} parameter can further reduce the systematic error in B2PLYP shieldings. The resulting functional would be analogous to B2K-PLYP and B2T-PLYP,[295] optimized for kinetics and thermochemistry, respectively. At the very least, an analysis similar to that performed in the optimization of the B2GP-PLYP functional,[281] could provide insight into the dependence of the calculated shieldings on the parameters c_{C} and c_{X} (as well as c_{OS} and c_{SS}). Such an analysis is outside the scope of the current work, however, B2GP-PLYP and the more flexible DSD-BLYP do represent incremental quantitative improvements over B2PLYP. This suggests that the more flexible training sets used for the parametrization resulted in more accurate methods, even for properties not included in the training data, as was observed for vibrational frequencies.[85]

Next, we note the outstanding performance of the DSD-PBEP86 functional: it produces the narrowest error distributions of all methods tested here and while there is a

significant systematic deviation in the carbon shieldings, this is expected to cancel out in relative chemical shifts. Indeed both the $MARE_\delta$ and $MRRE_\sigma$ measures are lowest for the DSD-PBEP86 variants (1.4–1.9 % and 2.1–2.6 %, respectively). The revised parametrization (revDSD-PBEP86) slightly improves the results with marginally narrower error distributions and decreased systematic error (except for ^{1}H). On the other hand, the NoDSD-PBEP86 version, parametrized without a dispersion correction and with 10 % more same-spin MP2 correlation, is notably worse. Even though the semi-empirical dispersion term does not contribute to the shielding, including its parameters in the optimization produces a more flexible functional form, which allows for better accuracy in the target quantity, and apparently also in NMR shieldings. The frozen-core approximation has a smaller influence on DHDFT than on MP2, due to the smaller proportion of PT2 correlation. For the DSD-PBEP86 variants it leads to a lower $MARE_\delta$ (by about 0.15 %) but a higher $MRRE_\sigma$ (by 0.1–0.2 %), which makes it difficult to decide for or against it based on these data alone.

Finally, the range-separated DHDF ωB97X-2 is a marked improvement over the related ωB97X-D3BJ, although it does not outperform DSD-PBEP86. Its reparametrized version is also somewhat more accurate, as is the case for the other DHDFs, and in this case the frozen-core approximation appears to be advantageous, regardless of the statistical measure employed. A minor exception is the small systematic deviation in ^{1}H shieldings, which should cancel out for chemical shifts.

In summary, the most accurate conventional functionals explored here – r^{2}SCAN, M06-L, KT3, and TPSSh – result in $MARE_\delta$ of 3.9, 5.4, 5.8, and 5.9 % and $MRRE_\sigma$ of 5.4, 6.5, 7.8, and 7.2 %, respectively. MP2 and SCS-MP2 are an improvement (except perhaps over r^{2}SCAN) with a $MARE_\delta$ of 3.9 and 4.1 %, respectively, and $MRRE_\sigma = 6.7$ % for both. B2PLYP is not particularly better with $MARE_\delta = 4.3$ % and $MRRE_\sigma = 5.2$ %. However, the best DHDF tested, revDSD-PBEP86, shows remarkable accuracy with $MARE_\delta = 1.5$ % and $MRRE_\sigma = 2.1$ %, which enables, for example, the confident assignment of carbon shifts only a few ppm apart.

2.3.4 Basis Set Error

After a critical assessment of the errors due to the method, we turn our attention to the choice of basis set, which is usually the second largest source of error. The pcSseg-4 basis set allows for results very close to the CBS limit, however it is probably too large for routine applications. Hence, the smaller pcSseg-2 and pcSseg-3 basis sets were used for the rest of this study. An estimate of the error introduced by this choice is made by comparing the shielding constants obtained with pcSseg-2, respectively with pcSseg-3, to the ones obtained with pcSseg-4. This gives a lower bound of the basis set error because there is still some degree of incompleteness in the pcSseg-4 basis set (as discussed in Section 2.3.2). In addition, a slower convergence can be expected for correlated wave function-based methods, than for mean-field approaches. Likewise, DHDFs should exhibit a stronger dependence on the basis set size than other DFs, as is the case for energies.[86] Note that basis set names are abbreviated to pSn (n =2–4) in the figures. Calculations in this section were performed with no approximation for the two-electron part of the Fock matrix, while the RI-MP2 approximation was used together with the cc-pwCVQZ/C and cc-pwCV5Z/C AuxC basis sets for the pcSseg-2 and pcSseg-3 OBSs, respectively, which introduces only negligible additional errors as shown in Section 2.3.5.

The deviations of shielding constants for groups of nuclei are presented in Figure 2.4

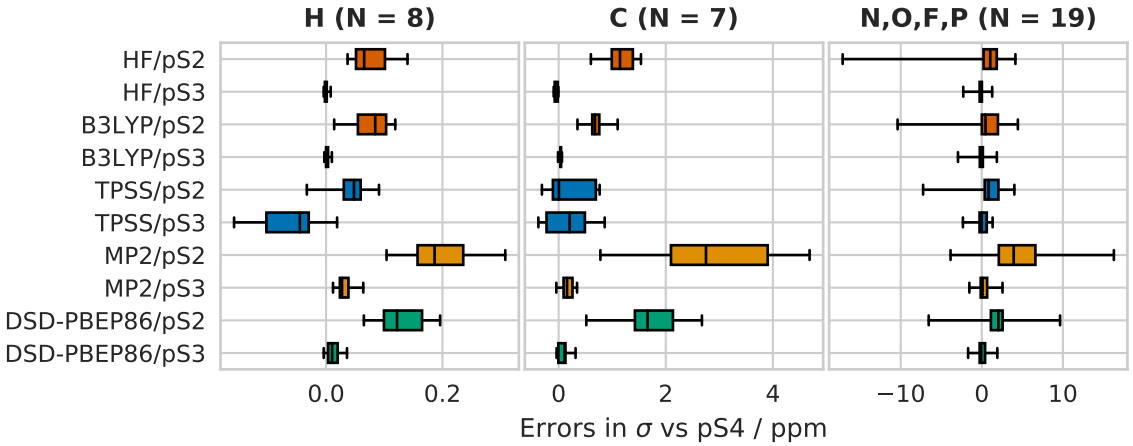

Figure 2.4: Deviations of shielding constants (ppm) for groups of nuclei, calculated using different methods and basis sets, from pS4 results for the same method. The number of nuclei in each group is given in parentheses. Boxes show the IQRE_σ, whiskers show the MinE_σ and MaxE_σ, and lines show the MedE_σ.

for a representative set of methods – HF, B3LYP, TPSS, ae-MP2, and ae-DSD-PBEP86. While there is some variation between the SCF-level results, pcSseg-2 predictably leads to larger errors than pcSseg-3, with MARE_σ values vs pcSseg-4 of 0.8–1.4 % and 0.2–0.4 %, respectively, which is in good agreement with Jensen's original results.[284] Therefore, the basis set incompleteness error is more than an order of magnitude smaller than the method error and insignificant in comparison. On the other hand, the basis set errors for MP2/pS2 are more than twice as large as for HF/pS2 and fall within the same order of magnitude as the method error, which is due also to the superior accuracy of MP2. As expected, the basis set errors for DSD-PBEP86 are between those for HF/B3LYP and MP2 and also within the same order of magnitude as the method error.

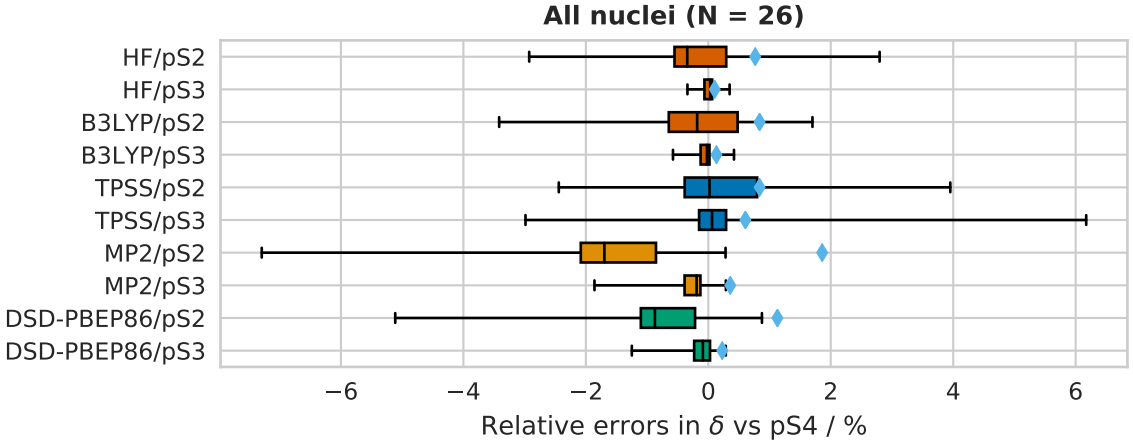

Figure 2.5: Relative deviations of chemical shifts (%), calculated using different methods and basis sets, from pS4 results for the same method. The number of data points is given in parentheses. Excluded: $\underline{\mathrm{N}}\mathrm{H}_3$ and $\underline{\mathrm{H}}_2\mathrm{O}$. Boxes show the IQRRE_δ, whiskers show the MinRE_δ and MaxRE_δ, lines show the MedRE_δ, and diamonds show the MARE_δ.

Because of the significant systematic deviations in the shieldings, it can be expected that the basis set incompleteness errors for chemical shifts will be smaller. The latter are shown in Figure 2.5. Apparently, the systematic errors do cancel out for the SCF methods but not entirely for the perturbative approaches. Therefore it cannot be

claimed that either MP2 or DSD-PBEP86 chemical shifts are sufficiently converged at the triple-zeta (pS2) level. However, due to fortuitous error compensation, the deviations for both approaches with respect to the CCSD(T)/pS4 reference are actually smaller for pS2 than for pS3 with MARE_δ of 3.70, 1.41, 4.00, and 1.84 % for MP2/pS2/cw4C, DSD-PBEP86/pS2/cw4C, MP2/pS3/cw5C, and DSD-PBEP86/pS3/cw5C, respectively. This error cancellation has been noted before – e.g. in refs. 296, 43, and 47 – and while it is not necessarily reliable, it provides some justification for the use of the smaller pS2 basis set. Note, however, that because SCS-MP2 already underestimates the chemical shifts at the pS4 level, a reduction of the basis set size to pS2 leads to an increase in the total error versus CCSD(T)/pS4 with $\mathrm{MARE}_\delta = 5.2\,\%$.

These results suggest that any further errors in SCF-level calculations (e.g. as introduced by the RIJK/RIJCOSX approximations) should be below 1 %, preferably by at least an order of magnitude, especially for the more accurate perturbative approaches. This would ensure that they are insignificant compared to the other errors associated with the calculation (due to the method, the basis set, vibrational corrections, etc.).

2.3.5 RI-MP2 auxiliary basis sets

In order to reliably evaluate the accuracy of DHDFT NMR shielding calculations, we selected suitable AuxC basis sets to make sure that the errors due to the RI-MP2 approximation are negligible. For our benchmarking purposes we have decided on a very conservative threshold of 0.01 and 0.1 % for the MARE_σ and MaxARE_σ, respectively. In routine applications less stringent thresholds and therefore smaller AuxC basis sets may be sufficient. In this section we show that the AuxC choices in Sections 2.3.3 and 2.3.4 are justified, and discuss more efficient alternatives.

As explained in Section 2.3.2, we use the cc-pwCVXZ/C (X = T, Q, 5) AuxC basis sets (denoted cw$n$C, n =3–5), as well as large even-tempered fitting basis sets, generated with the AutoAux scheme. As well as the default settings for the latter, denoted AA, we generate a near-complete AuxC basis (using the ORCA keywords `AutoAuxSize=3` and `AutoAuxLMax=true`), denoted AA3l, which encompasses the full product space of the atomic OBS.[a] This allows us to validate the correctness of our implementation at the limit of very large AuxC basis sets by comparing our RI-MP2 NMR shielding results to canonical MP2 values.

The results of the comparison are presented in Figure 2.6. The first thing to note is that for very large AuxC sets, the errors are vanishingly small, i.e. the RI-MP2 shielding constants converge to the canonical MP2 values. Second, the pS2/cw3C and pS3/cw4C combinations result in errors slightly above our chosen thresholds (MARE_σ of 0.03 and 0.02 % and MaxARE_σ of 0.17 and 0.13 %, respectively). As mentioned above, these errors are quite acceptable for most applications, especially when compared to the other sources of error (method, OBS, etc.). However, in order to accurately estimate these other errors, we have chosen the pS2/cw4C, pS3/cw5C, and pS4/cw5C combinations as default for the rest of this study. It is also worth noting that although not parametrized for shielding calculations, the AutoAux scheme produces sufficiently accurate AuxC basis sets for the purpose, albeit around 1.5 times larger than the cw$n$C sets of similar quality.

[a] Note that the pcSseg-4 basis set contains functions with an angular momentum of $l = 5$ so fitting its full product space in principle requires auxiliary basis functions up to $l = 10$, while the maximum allowed in ORCA is $l = 7$.

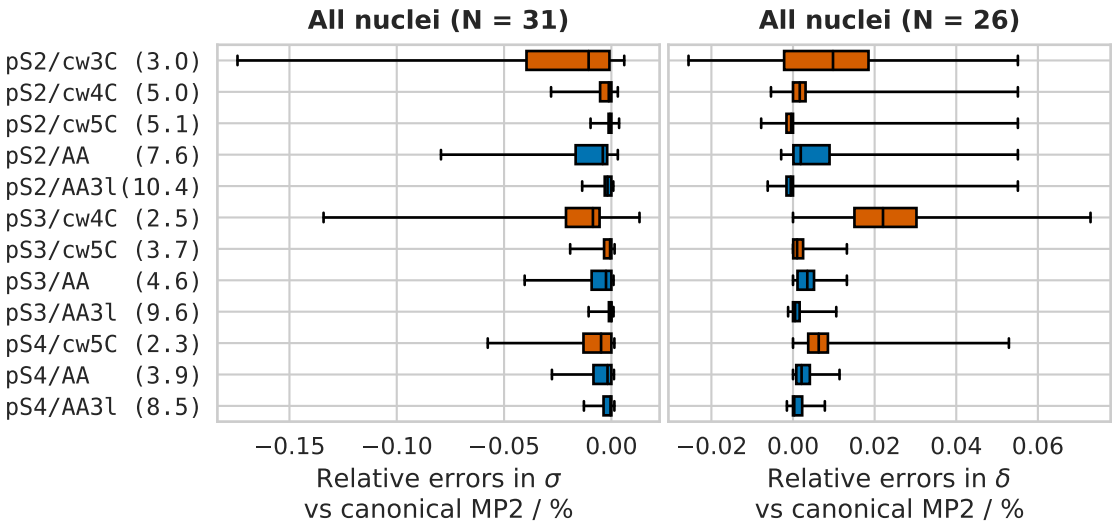

Figure 2.6: Relative deviations (%) of shielding constants (left) and chemical shifts (right), calculated at the RI-MP2 level using different OBS/AuxC combinations, from canonical MP2 results with the same OBS. Excluded, left: $\underline{C}O$, $CH_3\underline{C}OCH_3$, and $\underline{F}_2O$; right: $N\underline{H}_3$ and $\underline{H}_2O$. The average AuxC/OBS size ratios are given in parentheses. Boxes show the IQRRE, whiskers show the MinRE and MaxRE, and lines show the MedRE.

2.3.6 Frozen core approximation

The usual justification for using the frozen-core (FC) approximation is that the core electron contribution to the correlation energy does not change significantly during chemical bonding and therefore cancels out in the calculation of relative energies (between systems of the same chemical composition). However, this argumentation does not necessary apply to calculated NMR properties for several reasons. First, the shielding tensor is inherently sensitive to changes in the electron density near the nucleus. Second, in the calculation of chemical shifts the reference system can, and often does, have completely different chemical structure from the studied system and may therefore exhibit very different core correlation effects. While the FC approximation is employed for shielding calculations in the local RI-MP2 implementation of Loibl and Schütz,[179] little justification is given for its use. In this section we attempt to gauge the size of the errors introduced by the FC approximation. It is important to note that our test set does not include heavy nuclei or other systems for which core correlation is known to be important. Hence, the FC errors reported here are likely underestimated and should only be used as a guideline.

Figure 2.7 shows the FC error in the shieldings for MP2 and DSD-PBEP86. Note that in this plot the nuclei are grouped by rows in the periodic table to highlight the larger errors for heavier elements. In addition, hydrogen only has valence electrons, hence for ^{1}H shielding the FC error is due to the influence of the core electrons from neighboring atoms. Naturally, the deviations are smaller for DSD-PBEP86 because of the overall scaling of the MP2 contribution, hence we will only discuss the MP2 results. One important observation is that all FC errors are positive, i.e. the shieldings are always overestimated in the FC approximation. Such a systematic deviation would cancel out in chemical shifts, which is a point in favor of the approximation. However, note also the wide range of errors: depending on the chosen reference, the expected error cancellation might be very different. There is also a clear basis set dependence of the FC error. This is due to the inability of the smaller basis sets, especially pS2, to adequately describe the core region. The pS4 values should therefore be considered the mosts representative.

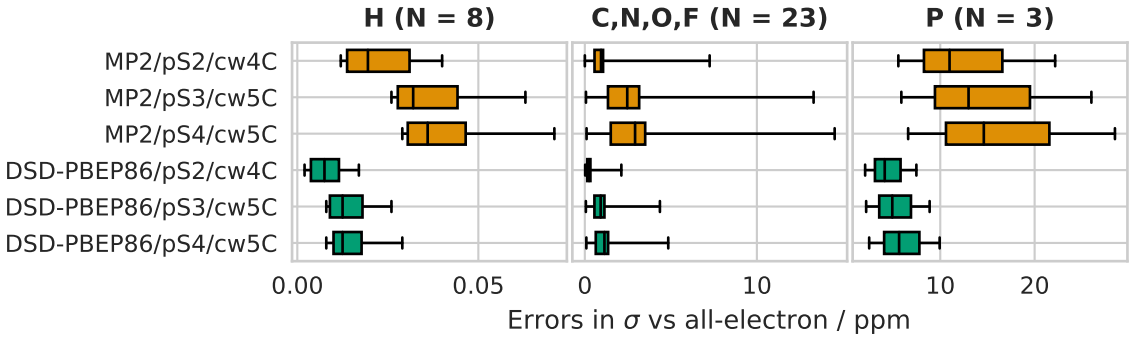

Figure 2.7: Deviations of shielding constants (ppm) for groups of nuclei, calculated with the frozen-core approximation, from all-electron results for the same method. The number of nuclei in each group is given in parentheses. Boxes show the IQRE_σ, whiskers show the MinE_σ and MaxE_σ, and lines show the MedE_σ.

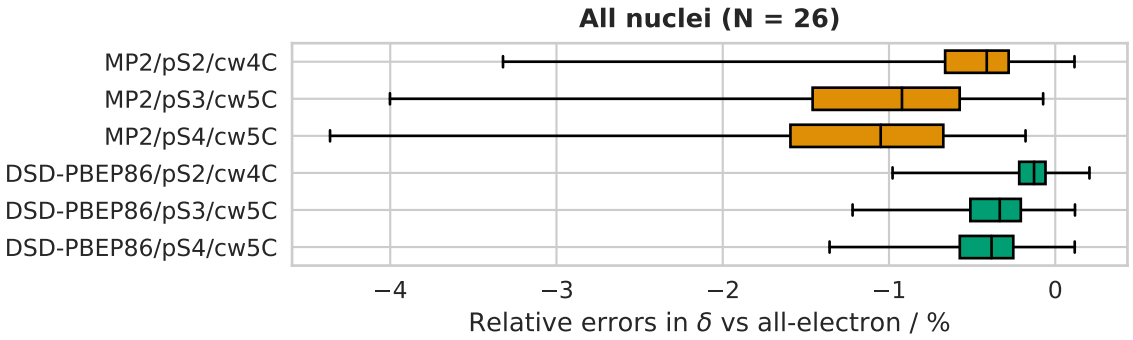

Figure 2.8: Relative deviations of chemical shifts (%), calculated with the frozen-core approximation, from all-electron results for the same method. The number of data points is given in parentheses. Excluded: $\mathrm{N\underline{H}_3}$ and $\mathrm{\underline{H}_2O}$. Boxes show the IQRRE_δ, whiskers show the MinRE_δ and MaxRE_δ, and lines show the MedRE_δ.

Table 2.3: Analysis of the frozen core (FC) errors in the shielding constants and chemical shifts of ^{31}P in PN. All values, except in the last two columns, are in ppm.

	HF	ae-MP2	fc-MP2	ae-MP2 − HF	fc-MP2 − HF	Δ_{FC}	$\frac{\Delta_{\mathrm{FC}}}{\text{ae-MP2}}$/%	$\frac{\Delta_{\mathrm{FC}}}{\text{ae-MP2}-\text{HF}}$/%
$\sigma(\mathrm{\underline{P}H_3})$	584	609	616	26	32	7	1	26
$\sigma(\mathrm{\underline{P}N})$	-110	107	135	217	246	28	27	13
$\delta(\mathrm{\underline{P}N})$	694	502	480	-192	-213	-22	-4	11

The chemical shift data in Figure 2.8 show that in fact the systematic deviations do not cancel out, at least using the chosen references. This is perhaps best understood by an example: the largest frozen core error in our test set – 28 ppm – is for the phosphorus shielding in PN, which is 27 % of the total shielding constant and 13 % of the MP2 contribution (see Table 2.3). The FC error for the reference nucleus in PH_3 is only 7 ppm (26 % of the MP2 contribution). Therefore the final absolute error in the chemical shift is 22 ppm, which is only 4 % of the total shift value but 11 % of the MP2 contribution. While an error of 4 % might be considered acceptable in some cases, it is of the same order of magnitude as the method error, thereby increasing the deviation with respect to CCSD(T)/pS4 from 9 to 13 %. Moreover, it is apparent that one cannot rely on error cancellation in the chemical shifts, as the absolute FC error is not much smaller and the relative error decreases only because the denominator is larger for the shifts than for the shieldings (694 vs 107 ppm).

While this is the most extreme example in our test set, similar observations can be made for most of the other nuclei. Therefore, we conclude that use of the FC approximation is not justified for NMR chemical shift calculations, as the resultant errors – $\mathrm{MARE}_\delta = 1.268$ and 0.457 % for MP2 and DSD-PBEP86, respectively – are of the same order of magnitude as the inherent accuracies of the methods. A final point to make is that while the FC errors are smaller for lighter elements, so are the computational savings gained by the approximation. Conversely, calculations on heavier nuclei could benefit more from freezing the core electrons, but the errors thus introduced would also be greater.

2.3.7 RIJK or RIJCOSX approximations

As outlined in Section 2.1.2, the RI and COS approximations can be applied to two-electron integrals at several different stages of the calculation: the Coulomb ($\mathbf{J}[\mathbf{D}]$) and exchange ($\mathbf{K}[\mathbf{D}]$) parts of the Fock matrix, and to the $\mathbf{J}^{\mathbf{B}}[\mathbf{D}]$, $\mathbf{K}^{\mathbf{B}}[\mathbf{D}]$, and $\mathbf{g}\left[\mathbf{D}^{\mathbf{B}}\right]$ contributions to the CPSCF equations, the latter of which is split into an occupied-virtual $\mathbf{K}\left[\mathbf{U}^{\mathbf{B}}\right]$ block on the left-hand side, which is evaluated at every iteration and an occupied-occupied block $\mathbf{K}\left[\mathbf{S}^{(\mathbf{B})}\right]$ on the right-hand side, which is only evaluated once, as are the $\mathbf{J}^{\mathbf{B}}[\mathbf{D}]$ and $\mathbf{K}^{\mathbf{B}}[\mathbf{D}]$ terms. The error in the NMR shielding constants, caused by fitting each of these contributions by means of the RI or COS approximations is analyzed in this section.

For the perturbed integrals over GIAOs, $\mathbf{g}^{\mathbf{B}}[\mathbf{D}]$, all combinations of RI and COS for the Coulomb and exchange parts, as well as exact evaluation, have been implemented. For the regular two-electron integrals only the exact, RIJK, RIJONX (RI for Coulomb and analytic exchange) and RIJCOSX approaches are available.

2.3.7.1 RI

The errors in the calculated shielding constants, introduced by the RI approximation are presented in Figure 2.9. Not surprisingly, errors in the shielding constants are smaller with the def2-JK fitting basis than with def2-J for the $\mathbf{J}[\mathbf{D}]$ contribution. For $\mathbf{J}^{\mathbf{B}}[\mathbf{D}]$, however, at first glance def2-J seems to performs about as well as def2-JK. In fact, the larger MaxRE_σ for def2-JK is due to a negligible error of 0.033 ppm for $\underline{\mathrm{F}}_2\mathrm{O}$, which has a small reference value of ≈ 22 ppm. Overall, errors with def2-JK are smaller than with def2-J. The former are two orders of magnitude smaller than the basis set errors discussed in Section 2.3.4 and therefore perfectly acceptable. Hence, def2-JK basis set is

preferred over def2-J and is used in the following calculations. AutoAux results in smaller errors than def2-JK but it is also significantly larger: the average ratio of auxiliary to orbital basis functions is 5.1 for AutoAux and 2.0 for def2-JK. For this reason, it is only recommended when a no suitable optimized auxiliary basis set is available.

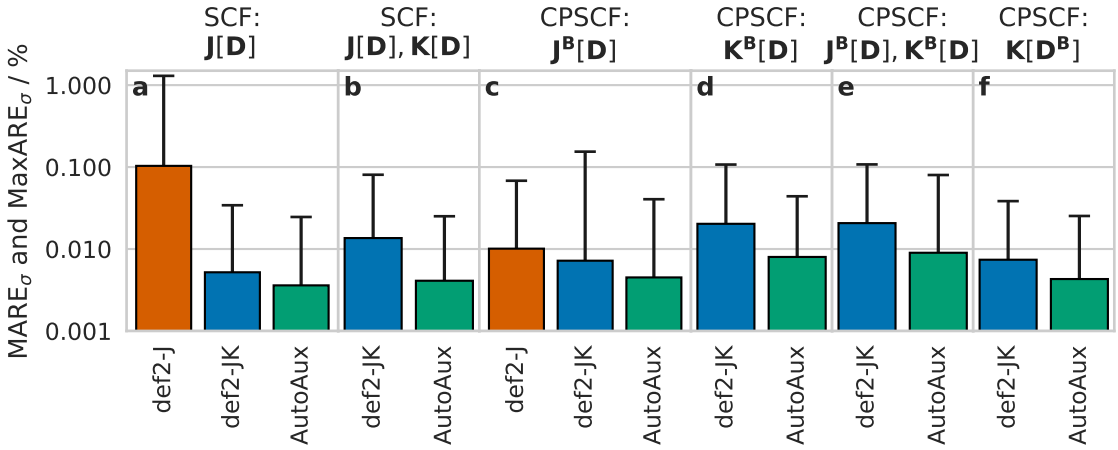

Figure 2.9: Mean absolute relative errors (boxes) and maximal absolute relative errors (whiskers) in the HF/pcSseg-2 shielding constants due to applying the RI approximation to different two-electron integrals: a) only the $\mathbf{J}[\mathbf{D}]$ term in the SCF (eq. 2.37); b) both the $\mathbf{J}[\mathbf{D}]$ and $\mathbf{K}[\mathbf{D}]$ terms in the SCF (eqs. 2.37 and 2.41); c) only the $\mathbf{J}^{\mathbf{B}}[\mathbf{D}]$ term in the CPSCF (eq. 2.50); d) only the $\mathbf{K}^{\mathbf{B}}[\mathbf{D}]$ term in the CPSCF (eq. 2.51); e) both the $\mathbf{J}^{\mathbf{B}}[\mathbf{D}]$ and $\mathbf{K}^{\mathbf{B}}[\mathbf{D}]$ terms in the CPSCF (eqs. 2.50 and 2.51); f) only the $\mathbf{K}[\mathbf{D}^{\mathbf{B}}]$ term in the CPSCF (eqs. 2.44 and 2.47). Note the logarithmic scale.

It is important to point out that the def2-JK fitting basis set was not designed to fit integrals with external indices, yet at least in combination with the orbital basis sets used here it only introduces small errors even when fitting $(ab|ji)$ and $(aj|bi)$. This implies that it contains both tight enough exponents in the core region and polarization functions with high enough angular momentum to fit the pcSseg-2 basis set (E.g. pcSseg-2 has up to f-functions for carbon, while def2-JK and pcSseg-3 extend up to g-functions).

Applying the RI approximation to both Coulomb and exchange contributions results in somewhat larger errors than fitting Coulomb alone, but nevertheless in the same order of magnitude. A detailed analysis shows that the errors coming from the different contributions are linearly additive. This makes it easy to predict the accumulation of errors from approximating different integrals. Note however that the errors may have different signs, so they partially cancel out.

Overall, the accuracy of the RIJK approximation in conjunction with the pcSseg-2 and def2-JK basis sets is more than sufficient, i.e. errors are more than an order of magnitude below the basis set incompleteness error.

2.3.7.2 COS

The COS approximation allows for practically arbitrary accuracy if a sufficiently tight grid is used, with the angular grid having the largest impact. Hence, in order to study the effect of the latter, the radial accuracy parameter ε was set to 5.0, which is high enough to eliminate the additional error. The optimal value of ε is discussed further below.

The errors in the calculated shielding constants, introduced by the COS approximation with different angular grids are presented in Figure 2.10. The first conclusion one can

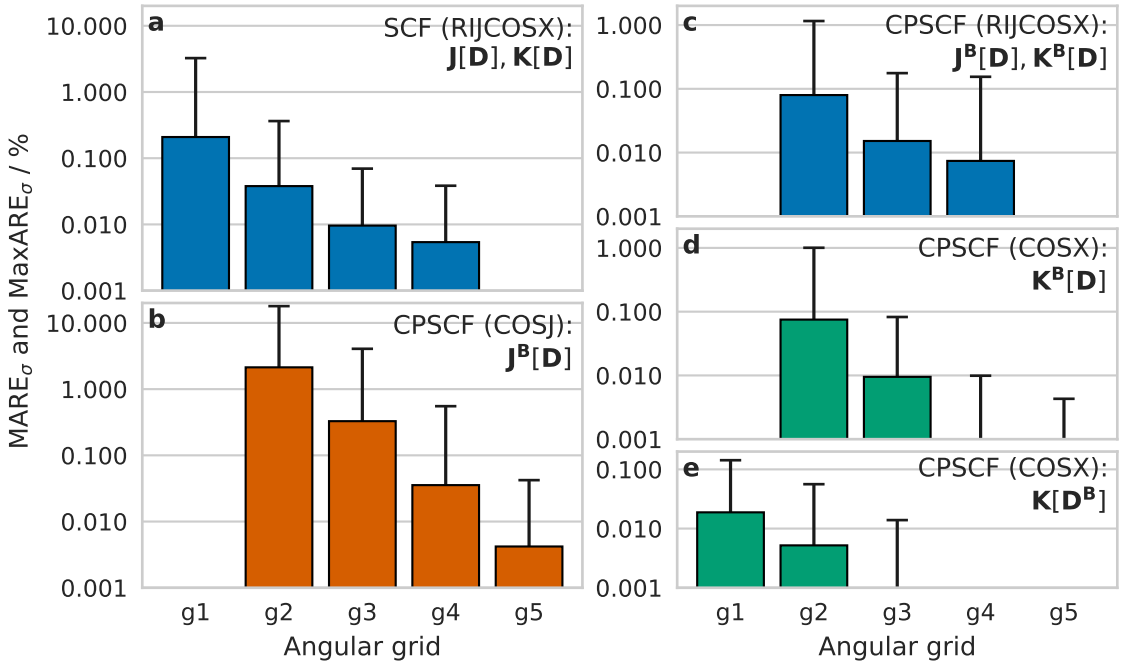

Figure 2.10: Mean absolute relative errors (boxes) and maximal absolute relative errors (whiskers) in the HF/pcSseg-2 shielding constants due to applying the following approximations, with angular grids g1–g5, to different two-electron integrals: a) RI for the $\mathbf{J}[\mathbf{D}]$ term and COS for the $\mathbf{K}[\mathbf{D}]$ term in the SCF (eqs. 2.37 and 2.57); b) COS for the $\mathbf{J}^{\mathbf{B}}[\mathbf{D}]$ term in the CPSCF (eq. 2.70); c) RI for the $\mathbf{J}^{\mathbf{B}}[\mathbf{D}]$ term and COS for the $\mathbf{K}^{\mathbf{B}}[\mathbf{D}]$ term in the CPSCF (eqs. 2.50 and 2.69); d) COS for the $\mathbf{K}^{\mathbf{B}}[\mathbf{D}]$ term in the CPSCF (eq. 2.69); e) COS for the $\mathbf{K}\left[\mathbf{D}^{\mathbf{B}}\right]$ term in the CPSCF (eq. 2.57). The radial integration accuracy was set to $\varepsilon = 5.0$. The def2-JK basis set was used for the RIJ parts. Note the logarithmic scale.

reach from these results is that the COSJ approximation of $\mathbf{J}^{\mathbf{B}}[\mathbf{D}]$ is only acceptably accurate for very dense grids, starting around g4. Preliminary estimates of the efficiency showed that with grids of this size, the COSJ approximation is no longer competitive with the RIJ algorithm. This was noted for the SCF Coulomb integrals in the original publication.[113] Hence, use of COSJ for the GIAO integrals is also discouraged. However, one advantage of COS over RI is the possibility to reach arbitrary precision, albeit with huge grids. While this work was in progress, the analytic integrals over GIAOs in ORCA were not sufficiently optimized, so calculations employing the COSJX approximation with the largest possible grid (g7) took a fraction of the time and produced numerically identical results.

On the other hand, using COSX for either of $\mathbf{K}[\mathbf{D}]$ and $\mathbf{K}^{\mathbf{B}}[\mathbf{D}]$, one finds that g3 is sufficiently tight to reach an accuracy comparable with RIJK. This is much larger than the default grids used for energies and gradients, but can still be preferable over RIK for large systems (see timings in Section 2.3.10.1). The $\mathbf{K}\left[\mathbf{D}^{\mathbf{B}}\right]$ contributions to the CPSCF equations are much less demanding: g1 provides accuracy, comparable to that of the other contributions.

Combining the RIJ and COSX approximation, the linear additivity of the errors is once again apparent: with a dense enough grid the RIJCOSX error is virtually identical to the RIJ error. Note than the def2-JK basis set was also used for RIJCOSX, as it was determined to be more accurate.

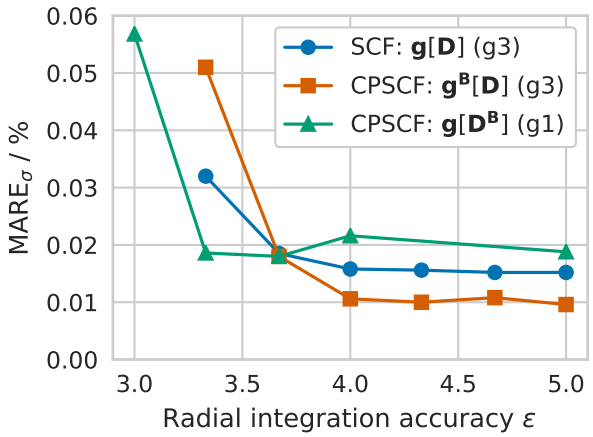

Figure 2.11: Convergence of the mean absolute relative error (vs exact evaluation) in the HF/pcSseg-2 shielding constants, due to applying the RIJCOSX approximation to different two-electron integrals, with the increase of the radial integration accuracy parameter ε. "gn" denotes the angular grid used.

Having selected the optimal angular grids for each contribution, it is appropriate to determine the smallest possible value for the radial integration accuracy parameter ε. Figure 2.11 shows the convergence of the error with the increase of ε for the grids selected above. For both terms fitted with the g3 angular grid a value of 4.0 is sufficient and for g1 the error is already converged at a radial accuracy of 3.3.

In summary, while the COSJ approximation is not recommended, because of the high requirements for grid size, the RIJCOSX approximation is shown to be of comparable accuracy to RIJK, provided that appropriate grids are used. The optimal grid settings are g3 with $\varepsilon = 4.01$ for the $\mathbf{K}[\mathbf{D}]$ and $\mathbf{K}^{\mathbf{B}}[\mathbf{D}]$ terms and g1 with $\varepsilon = 3.34$ for $\mathbf{K}\left[\mathbf{D}^{\mathbf{B}}\right]$.

2.3.7.3 Effect of basis set size and application to DFT

An increase in the RI-error is to be expected if a basis set with higher angular momentum functions is fitted with the same auxiliary basis set. Indeed, as shown in Table 2.4, errors for the pcSseg-3 basis set are slightly larger but still within the imposed limits. Conversely, the COSX errors tend to be smaller for the larger basis set. This is fortunate because it implies they are consistently smaller than the basis set incompleteness error.

Table 2.4: Basis set dependence of the errors in the HF shielding constants due to applying the RI and COS approximations to different integrals. ME_σ, SDE_σ, MAE_σ, and MaxE_σ are given in ppm and MRE_σ, SDRE_σ, MARE_σ, and MaxRE_σ are given in percent (see eq 2.154).

Approximation	Basis	ME_σ	SDE_σ	MAE_σ	MaxE_σ	MRE_σ	SDRE_σ	MARE_σ	MaxRE_σ
SCF: Approximate $\mathbf{J}[\mathbf{D}]$									
RIJ/def2-JK	pcSseg-2	0.002	0.027	0.010	−0.113	0.003	0.008	0.005	0.029
RIJ/def2-JK	pcSseg-3	0.008	0.034	0.017	0.138	0.009	0.017	0.011	0.079
SCF: Approximate $\mathbf{J}[\mathbf{D}]$ and $\mathbf{K}[\mathbf{D}]$									
RIJCOSX/g2[a,b]	pcSseg-2	0.013	0.055	0.035	0.179	0.029	0.075	0.038	0.326
RIJCOSX/g2[a,b]	pcSseg-3	0.004	0.030	0.017	0.109	0.003	0.020	0.013	−0.084
RIJCOSX/g3[a,b]	pcSseg-2	0.002	0.026	0.012	−0.110	0.004	0.016	0.010	0.060
RIJCOSX/g3[a,b]	pcSseg-3	0.009	0.035	0.018	0.134	0.010	0.022	0.013	0.113
RIJK/def2-JK	pcSseg-2	0.013	0.025	0.016	0.102	0.012	0.019	0.014	0.067
RIJK/def2-JK	pcSseg-3	0.022	0.035	0.025	0.146	0.020	0.027	0.022	0.102
CPSCF: Approximate $\mathbf{J}^{\mathbf{B}}[\mathbf{D}]$									
RIJ/def2-JK	pcSseg-2	−0.005	0.016	0.007	−0.075	−0.005	0.025	0.007	−0.147
RIJ/def2-JK	pcSseg-3	−0.005	0.014	0.007	−0.053	−0.005	0.027	0.007	−0.157
CPSCF: Approximate $\mathbf{K}^{\mathbf{B}}[\mathbf{D}]$									
COSX/g2[a]	pcSseg-2	−0.100	0.499	0.149	−2.842	−0.049	0.185	0.075	−0.930
COSX/g2[a]	pcSseg-3	−0.021	0.214	0.062	−1.171	−0.005	0.044	0.021	−0.201
COSX/g3[a]	pcSseg-2	0.002	0.021	0.010	−0.082	−0.001	0.018	0.010	−0.073
COSX/g3[a]	pcSseg-3	0.001	0.007	0.004	0.026	−0.001	0.008	0.004	−0.038
RIK/def2-JK	pcSseg-2	−0.010	0.030	0.022	−0.091	−0.011	0.029	0.020	−0.087
RIK/def2-JK	pcSseg-3	−0.012	0.036	0.025	−0.113	−0.013	0.034	0.023	0.103
CPSCF: Approximate $\mathbf{J}^{\mathbf{B}}[\mathbf{D}]$ and $\mathbf{K}^{\mathbf{B}}[\mathbf{D}]$									
RIJCOSX/g2[a,b]	pcSseg-2	−0.105	0.511	0.152	−2.918	−0.054	0.206	0.080	−1.077
RIJCOSX/g2[a,b]	pcSseg-3	−0.026	0.223	0.067	−1.225	−0.011	0.055	0.027	−0.210
RIJCOSX/g3[a,b]	pcSseg-2	−0.003	0.033	0.016	−0.157	−0.006	0.033	0.015	−0.161
RIJCOSX/g3[a,b]	pcSseg-3	−0.004	0.014	0.008	−0.042	−0.006	0.029	0.010	−0.167
RIJK/def2-JK	pcSseg-2	−0.015	0.035	0.025	−0.129	−0.016	0.026	0.021	−0.087
RIJK/def2-JK	pcSseg-3	−0.017	0.041	0.028	−0.158	−0.018	0.028	0.023	−0.096
CPSCF: Approximate $\mathbf{K}[\mathbf{D}^{\mathbf{B}}]$									
COSX/g1[a]	pcSseg-2	0.008	0.041	0.022	0.212	0.006	0.034	0.019	0.124
COSX/g1[a]	pcSseg-3	−0.000	0.010	0.007	0.033	0.003	0.007	0.005	0.024
RIK/def2-JK	pcSseg-2	−0.002	0.006	0.005	−0.014	−0.003	0.011	0.007	0.031
RIK/def2-JK	pcSseg-3	−0.003	0.010	0.007	−0.042	−0.003	0.012	0.008	0.039

[a] The radial integration accuracy was set to $\varepsilon = 5.0$.
[b] The def2-JK basis set was used for the RIJ part.

All calculations so far were performed at the HF level for simplicity. A comparison with DFT results employing the B3LYP and TPSS functionals is given in Table 2.5. A significant difference is that the RIK and COSX errors are lower for DFT compared to HF, by a factor of 4–5 in the MAE_σ and MaxE_σ values. Assuming the apparent linear additivity of error, discussed in the previous sections, this can be rationalized by the fact that in hybrid DFT the HF exchange contributions, and any errors introduced therein, get scaled by a factor c_X smaller than unity (0.2 in the case of B3LYP). On the other

hand, the fact that the RI errors due to the $\mathbf{J}^{\mathbf{B}}[\mathbf{D}]$ term are also smaller for DFT, is simply a statistical artifact. A close examination reveals that the difference in absolute errors is due to a single large error in the HF chemical shielding value for phosphorus in PH_3, while the difference in relative errors is due to the smaller HF reference value for fluorine in F_2O. Approximating both Coulomb- and exchange-type contributions results in total errors for DFT which are still somewhat lower than for HF. This effect, along with the conclusions from the previous paragraph means that for hybrid DFT calculations with the pcSseg-3 basis set it might be feasible to use somewhat smaller COSX grids (e.g. g2 instead of g3).

Table 2.5: Method dependence of the errors in the shielding constants due to applying the RI and COS approximations to different integrals. All calculations employ the pcSseg-2 basis set. ME_σ, SDE_σ, MAE_σ, and $MaxE_\sigma$ are given in ppm and MRE_σ, $SDRE_\sigma$, $MARE_\sigma$, and $MaxRE_\sigma$ are given in percent (see eq 2.154).

Approximation	Method	ME_σ	SDE_σ	MAE_σ	$MaxE_\sigma$	MRE_σ	$SDRE_\sigma$	$MARE_\sigma$	$MaxRE_\sigma$
SCF: Approximate $\mathbf{J}[\mathbf{D}]$									
RIJ/def2-JK	HF	0.002	0.027	0.010	−0.113	0.003	0.008	0.005	0.029
RIJ/def2-JK	B3LYP	0.003	0.019	0.008	0.101	0.003	0.010	0.006	0.044
RIJ/def2-JK	TPSS	0.003	0.019	0.008	0.086	0.002	0.012	0.007	−0.048
SCF: Approximate $\mathbf{J}[\mathbf{D}]$ and $\mathbf{K}[\mathbf{D}]$									
RIJCOSX/g2[a,b]	HF	0.013	0.055	0.035	0.179	0.029	0.075	0.038	0.326
RIJCOSX/g2[a,b]	B3LYP	0.005	0.017	0.010	0.066	0.010	0.029	0.012	0.168
RIJCOSX/g3[a,b]	HF	0.002	0.026	0.012	−0.110	0.004	0.016	0.010	0.060
RIJCOSX/g3[a,b]	B3LYP	0.003	0.019	0.009	0.097	0.004	0.015	0.008	0.075
RIJK/def2-JK	HF	0.013	0.025	0.016	0.102	0.012	0.019	0.014	0.067
RIJK/def2-JK	B3LYP	0.006	0.019	0.009	0.101	0.007	0.014	0.007	0.081
CPSCF: Approximate $\mathbf{J}^{\mathbf{B}}[\mathbf{D}]$									
RIJ/def2-JK	HF	−0.005	0.016	0.007	−0.075	−0.005	0.025	0.007	−0.147
RIJ/def2-JK	B3LYP	−0.003	0.010	0.005	−0.035	−0.002	0.008	0.004	−0.037
RIJ/def2-JK	TPSS	−0.003	0.010	0.005	−0.037	−0.002	0.008	0.004	−0.041
CPSCF: Approximate $\mathbf{K}^{\mathbf{B}}[\mathbf{D}]$									
COSX/g2[a]	HF	−0.100	0.499	0.149	−2.842	−0.049	0.185	0.075	−0.930
COSX/g2[a]	B3LYP	−0.021	0.111	0.034	−0.626	−0.005	0.028	0.015	−0.111
COSX/g3[a]	HF	0.002	0.021	0.010	−0.082	−0.001	0.018	0.010	−0.073
COSX/g3[a]	B3LYP	0.000	0.004	0.002	−0.017	−0.001	0.006	0.003	−0.031
RIK/def2-JK	HF	−0.010	0.030	0.022	−0.091	−0.011	0.029	0.020	−0.087
RIK/def2-JK	B3LYP	−0.002	0.006	0.004	−0.018	−0.003	0.006	0.004	−0.022
CPSCF: Approximate $\mathbf{J}^{\mathbf{B}}[\mathbf{D}]$ and $\mathbf{K}^{\mathbf{B}}[\mathbf{D}]$									
RIJCOSX/g2[a,b]	HF	−0.105	0.511	0.152	−2.918	−0.054	0.206	0.080	−1.077
RIJCOSX/g2[a,b]	B3LYP	−0.024	0.114	0.036	−0.647	−0.006	0.031	0.016	−0.115
RIJCOSX/g3[a,b]	HF	−0.003	0.033	0.016	−0.157	−0.006	0.033	0.015	−0.161
RIJCOSX/g3[a,b]	B3LYP	−0.002	0.012	0.006	−0.038	−0.002	0.011	0.005	−0.044
RIJK/def2-JK	HF	−0.015	0.035	0.025	−0.129	−0.016	0.026	0.021	−0.087
RIJK/def2-JK	B3LYP	−0.005	0.013	0.007	−0.053	−0.005	0.009	0.006	−0.036
CPSCF: Approximate $\mathbf{K}[\mathbf{D}^{\mathbf{B}}]$									
COSX/g1[a]	HF	0.008	0.041	0.022	0.212	0.006	0.034	0.019	0.124
COSX/g1[a]	B3LYP	0.002	0.010	0.005	0.054	0.000	0.010	0.005	−0.044
RIK/def2-JK	HF	−0.002	0.006	0.005	−0.014	−0.003	0.011	0.007	0.031
RIK/def2-JK	B3LYP	−0.001	0.001	0.001	−0.005	−0.001	0.003	0.001	−0.013

[a] The radial integration accuracy was set to $\varepsilon = 5.0$.
[b] The def2-JK basis set was used for the RIJ part.

2.3.7.4 Approximating all terms (RIJK vs RIJCOSX)

After evaluating the errors coming from approximating each term, in the following we compare the accuracy of the RIJK and RIJCOSX approximations in a more realistic scenario, where the same approximation is used throughout the calculation. The selected settings are summarized in Table 2.6. Two grid combinations have been defined, labeled small (S) and large (L). Option L represents the grid settings accurate enough for HF/pcSseg-2 calculations as discussed above, while option S employs looser grids and is expected to be applicable for hybrid DFT calculations, where the COSX errors are smaller. In ORCA 4, the two grid combinations can quickly be requested using the simple input commands "`gridx6 nofinalgridx`" and "`gridx8 nofinalgridx`",[a] respectively. The def2-JK auxiliary basis set is used throughout for both RIJK and RIJCOSX. As noted previously, the RI-based transformation of $(aj|bi)$ and $(ab|ji)$ needed for $\mathbf{K}\left[\mathbf{U}^{\mathbf{B}}\right]$ can introduce a storage bottleneck, hence this term can instead be calculated in an AO-direct fashion using exact 4-index integrals at each CPSCF iteration. This procedure is denoted "RIJK*". For pure DFT functionals, only the Coulomb term is approximated using RI and the def2-JK auxiliary basis set – this is denoted "RIJ".

Table 2.6: Recommended combinations of approximations for the different two-electron terms, given in the form "COS/[angular grid]/[radial integration accuracy]" or "RI/[auxiliary basis set]"

	Term	RIJCOSX-S	RIJCOSX-L	RIJK	RIJK*
SCF	$\mathbf{J}[\mathbf{D}]$	RI/def2-JK	RI/def2-JK	RI/def2-JK	RI/def2-JK
	$\mathbf{K}[\mathbf{D}]$	COS/g2/$\varepsilon = 4.01$	COS/g3/$\varepsilon = 4.01$	RI/def2-JK	RI/def2-JK
CPSCF	$\mathbf{J}^{\mathbf{B}}[\mathbf{D}]$	RI/def2-JK	RI/def2-JK	RI/def2-JK	RI/def2-JK
	$\mathbf{K}^{\mathbf{B}}[\mathbf{D}]$	COS/g2/$\varepsilon = 4.01$	COS/g3/$\varepsilon = 4.01$	RI/def2-JK	RI/def2-JK
	$\mathbf{K}\left[\mathbf{S}^{(\mathbf{B})}\right]$	COS/g1/$\varepsilon = 3.34$	COS/g1/$\varepsilon = 3.34$	RI/def2-JK	RI/def2-JK
	$\mathbf{K}\left[\mathbf{U}^{\mathbf{B}}\right]$	COS/g1/$\varepsilon = 3.34$	COS/g1/$\varepsilon = 3.34$	RI/def2-JK	Exact

The distributions of shielding errors and relative errors in chemical shifts, calculated using these approximations, are shown in Figures 2.12 and 2.13, respectively. These data should be viewed in comparison to the basis set incompleteness errors presented in Figures 2.4 and 2.5, summarized as a MARE_δ of 0.8 % and 0.1 % for pcSseg-2 and pcSseg-3, respectively. Overall, the RIJK approximation with the def2-JK auxiliary basis set is robust, resulting in consistently small errors with $\mathrm{MARE}_\delta \approx 0.01$–$0.03$ %, which is an order of magnitude less than the basis set error. For HF, RIJCOSX-L is roughly as accurate as RIJK, while RIJCOSX-S is not recommended with a MARE_δ of 0.16 and 0.08 % for pcSseg-2 and pcSseg-3, respectively. For hybrid DFT, largely due to the exact exchange scaling factor, RIJCOSX-S already produces errors well below the basis set error at $\mathrm{MARE}_\delta \approx 0.04$ % for both basis sets.

2.3.8 RI-MP2 combined with approximate Fock matrix formation

In this section we apply the RIJK and RIJCOSX approximations to the two-electron Fock matrix terms in MP2 and DHDFT and assess the additional errors thus introduced.

[a] The given keywords actually correspond to $\varepsilon = 3.67$ for g1, instead of 3.34 but this difference is largely immaterial.

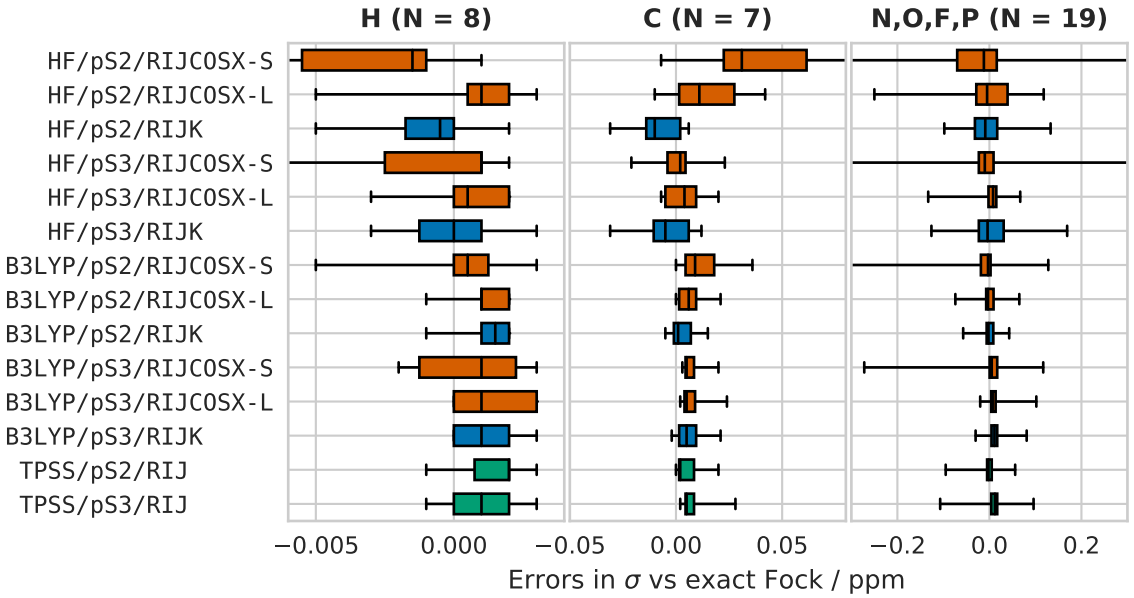

Figure 2.12: Deviations of shielding constants (ppm) for groups of nuclei, calculated using different methods, basis sets, and two-electron integral approximations, from results for the same method and basis without the approximations. The number of nuclei in each group is given in parentheses. Boxes show the IQRE_σ, whiskers show the MinE_σ and MaxE_σ, and lines show the MedE_σ. Note that some whiskers extend beyond the axis limits.

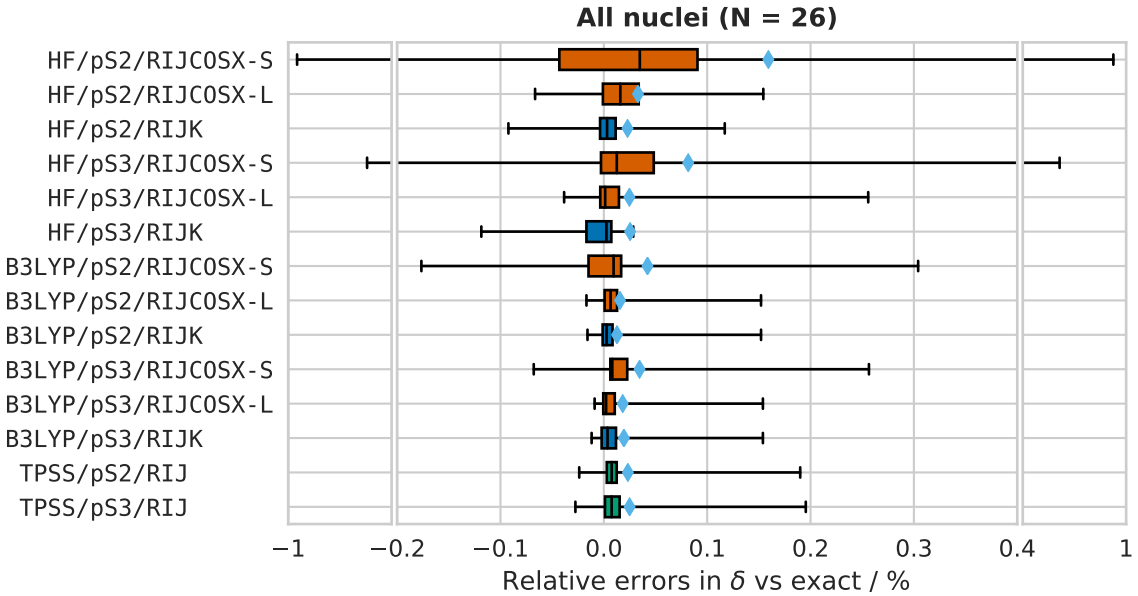

Figure 2.13: Relative deviations of chemical shifts (%), calculated using different methods, basis sets, and two-electron integral approximations, from results for the same method and basis without the approximations. The number of data points is given in parentheses. Excluded: $\mathrm{NH_3}$ and $\mathrm{H_2O}$. Boxes show the IQRRE_δ, whiskers show the MinRE_δ and MaxRE_δ, lines show the MedRE_δ, and diamonds show the MARE_δ. Note the broken x-axis: the limits on both sides of the gap are the same but the scale is different.

Ideally, the latter should be at least an order of magnitude below the method and basis set errors. Here we extend the definitions from Table 2.6 such that the grid used for the CPSCF RHS is also used for the Fock response terms in the RHS of the Z-CPSCF equations, while the grid used for the CPSCF LHS is also used for the LHS of the Z-CPSCF equations. In order to minimize additional errors due to the RI-MP2 approximation, the cc-pwCVQZ/C and cc-pwCV5Z/C AuxC basis sets were used for pcSseg-2 and pcSseg-3, respectively.

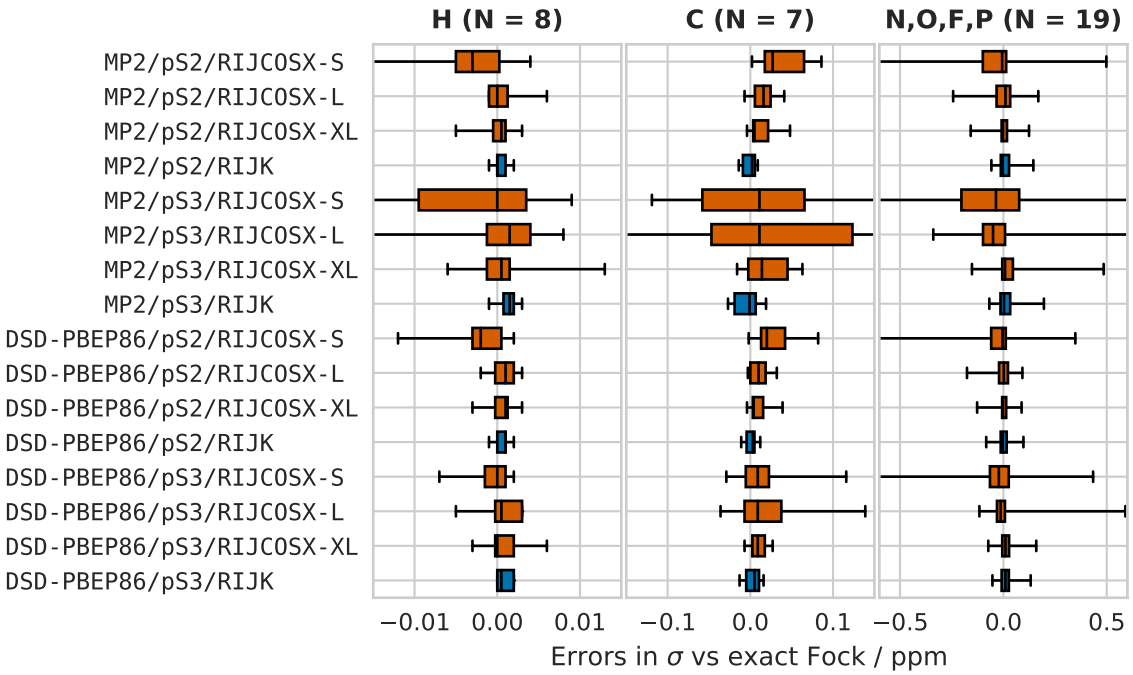

Figure 2.14: Deviations of shielding constants (ppm) for groups of nuclei, calculated using the RIJK and RIJCOSX approximations for the two-electron Fock matrix contributions, from results using exact two-electron integrals for these terms. The number of nuclei in each group is given in parentheses. Boxes show the IQRE_σ, whiskers show the MinE_σ and MaxE_σ, and lines show the MedE_σ. Note that some whiskers extend beyond the axis limits.

The shielding errors are shown in Figure 2.14. The first thing to notice is that the RIJK errors are very small, which confirms that the def2-JK basis set is large enough to be used with pS2 and pS3. On the other hand, RIJCOSX-S errors are an order of magnitude larger. RIJCOSX-L errors are smaller with pS2 but not with pS3, which is unexpected, as we had previously observed that the COSX errors (with a given grid setting) decrease with increasing basis set size (see Section 2.3.7.3). Additional testing revealed that a large part to the error is due to the smaller grid used in the Z-CPSCF equations LHSs. Therefore, we propose a third set of grid parameters, denoted RIJCOSX-XL, whereby $g3/\varepsilon = 4.0$ is used for the CPSCF and Z-CPSCF equations RHSs, as in RIJCOSX-L, and $g2/\varepsilon = 4.0$ is used for the LHSs. Using these settings, the RIJCOSX errors are roughly of the same magnitude as the RIJK errors. It should be stressed however, that for pS2 the RIJCOSX-S errors are already an order of magnitude below the basis set error and for pS3 the RIJCOSX-L errors are several times smaller then the basis set error, albeit not a whole order of magnitude. Therefore, the RIJCOSX-L settings should be quite sufficient for regular applications and the RIJCOSX-XL settings need only be used when very precise results are required.

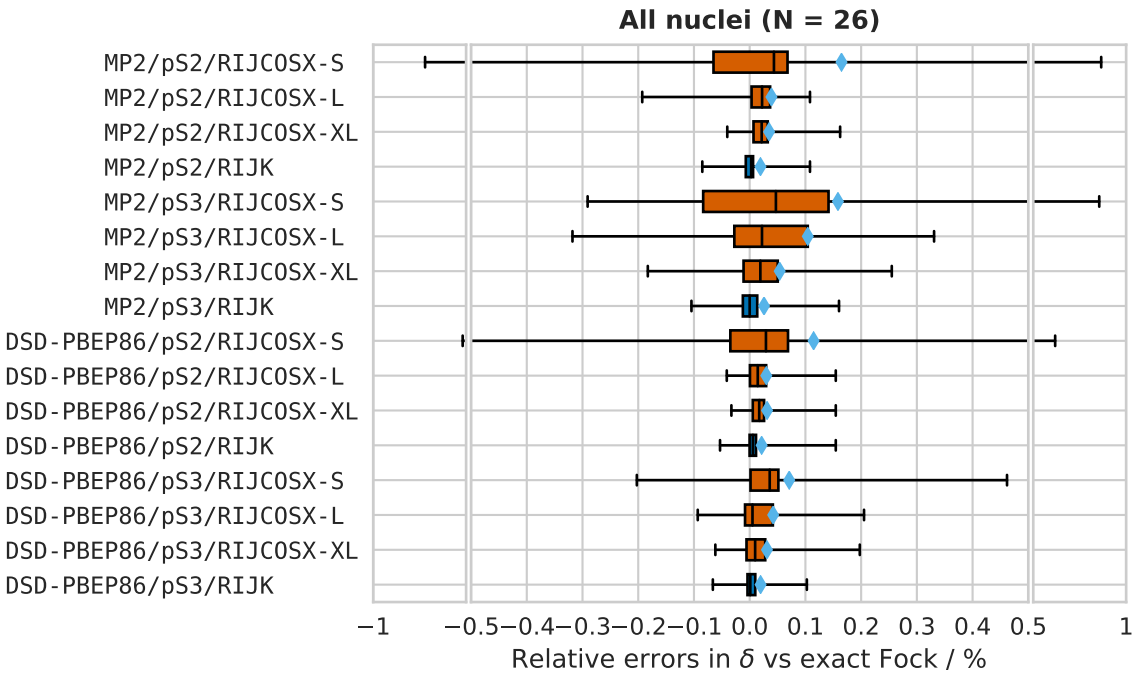

Figure 2.15: Relative deviations of chemical shifts (%), calculated using the RIJK and RIJCOSX approximations for the two-electron Fock matrix contributions, from results using exact two-electron integrals for these terms. The number of data points is given in parentheses. Excluded: $N\underline{H}_3$ and $\underline{H}_2O$. Boxes show the $IQRRE_\delta$, whiskers show the $MinRE_\delta$ and $MaxRE_\delta$, lines show the $MedRE_\delta$, and diamonds show the $MARE_\delta$. Note the broken x-axis: the limits on both sides of the gap are the same but the scale is different.

Because the shielding errors are rather unsystematic, they do not cancel out in chemical shifts (Figure 2.15). Hence, the conclusion above applies here as well: RIJCOSX-S may be used with the pS2 basis set, as the resultant errors are far below the basis set error ($MARE_\delta = 0.17$ and 0.12 % for MP2 and DSD-PBEP86, respectively), while RIJCOSX-L is more robust overall with $MARE_\delta$ of 0.04, 0.03, 0.10 and 0.04 % for MP2/pS2/cw4C, DSD-PBEP86/pS2/cw4C, MP2/pS3/cw5C, and DSD-PBEP86/pS3/cw5C, respectively. RIJK results in negligible errors ($MARE_\delta < 0.03$ % in all cases) and is therefore the preferred approximation for smaller systems, while RIJCOSX should be used for larger calculations due to its more favorable scaling behavior.

2.3.9 Combined effect of all error sources

The magnitude of errors, coming from different sources, in the calculated chemical shifts can be easily compared in Table 2.7. Largest are the deviations of different methods from the CCSD(T)/pS4 reference, discussed in Section 2.3.3. Close to the CBS limit the ranking of the chosen methods is (from highest to lowest accuracy): DSD-PBEP86, MP2, TPSS, B3LYP, and HF.

When the RI-MP2 and RIJCOSX errors are compared to those from the method and basis set, pS2/cw3C, pS3/cw4C, and RIJCOSX-L can be seen as a good balance of cost and accuracy. Although not discussed above, the effect of the DF integration grid was also studied: while the default grid for energy calculations (grid 2) may be somewhat unreliable for chemical shifts, the values obtained with grids 3 and 4 are an order of magnitude more accurate, hence these grid settings are recommended.

Finally, the last two rows of Table 2.7 show the total error versus CCSD(T)/pS4, when

Table 2.7: $MARE_\delta$ (%) due to different sources of error (excluding H shifts in H_2O and NH_3).

Source of error	Basis[a]	HF	B3LYP	TPSS	MP2	DSD-PBEP86
Method[b]	pS4	10.762	9.048	6.362	4.118	1.914
Frozen core[c]	pS4				1.268	0.457
Basis set[d]	pS2	0.766	0.836	0.838	1.860	1.129
	pS3	0.105	0.133	0.606	0.359	0.228
RIJK[e]	pS2	0.023	0.013	0.023[g]	0.019	0.022
	pS3	0.025	0.019	0.025[g]	0.026	0.020
RIJCOSX-S[ef]	pS2	0.159	0.042		0.165	0.115
	pS3	0.082	0.035		0.158	0.071
RIJCOSX-L[ef]	pS2	0.033	0.016		0.039	0.030
	pS3	0.025	0.018		0.104	0.042
RIJCOSX-XL[ef]	pS2				0.035	0.031
	pS3				0.054	0.031
RI-MP2	pS2/cw3C				0.016[h]	0.009[i]
	pS2/cw4C				0.005[h]	0.004[i]
	pS3/cw4C				0.025[h]	0.011[i]
	pS3/cw5C				0.002[h]	0.001[i]
	pS4/cw5C				0.009[h]	
DFT grid 1[j]	pS2			0.275		0.086
DFT grid 2[j]	pS2			0.218		0.076
DFT grid 3[j]	pS2			0.034		0.010
DFT grid 4[j]	pS2			0.028		0.002
DFT grid 5[j]	pS2			0.012		0.001
DFT grid 6[j]	pS2			0.009		0.001
Total[bk]	pS2/cw3C	11.055	9.123	6.271	3.695	1.420
Total[bk]	pS3/cw4C	10.832	9.048	6.075	4.064	1.863

[a] The pS2/cw4C, pS3/cw5C, and pS4/cw5C OBS/AuxC combinations were used for the RI-MP2 approximation (where applicable), except where explicitly specified. [b] Vs CCSD(T)/pS4. [c] Vs all-electron calculations with the same basis set. [d] Vs pS4. [e] Using the def2-JK AuxJ basis, vs the same method/basis with no approximation in the two-electron Fock contributions. [f] See Table 2.6 and Section 2.3.8 for grid settings used. [g] No exact exchange – RI used only for Coulomb terms. [h] Vs canonical MP2 results obtained using CFOUR. [i] Vs AA3l near-complete AuxC basis. [j] Vs grid 7. Grids 1–7 employ 50-, 110-, 194-, 302-, 434-, 590-, and 770-point Lebedev angular grids and radial integration parameters of 4.34, 4.34, 4.34, 4.67, 5.01, 5.34, and 5.67, respectively. Default pruning settings in ORCA were used. [k] All-electron calculations using RIJCOSX-L (just RIJ for TPSS) and DFT grid 4.

all the relevant approximations (RIJCOSX, RI-MP2, smaller basis sets and DFT grid, but not FC) have been applied. As noted in Section 2.3.4, some methods benefit from error compensation when a smaller basis set is used, while others suffer from an accumulation of errors. Even so, the final ranking of the given methods does not change in this case.

2.3.10 Comparison of efficiency

2.3.10.1 SCF methods

In previous sections we discussed the accuracy of the RIJK and RIJCOSX approximations and settled on recommended auxiliary basis set and grid settings. In the following we compare the computational efficiency of both approaches for the calculation of shielding constants of larger systems at the HF level (the conclusions should also be applicable to hybrid DFT). The systems selected are benzene, coronene, and a "tweezer" host-guest complex (see Figure 2.16). The latter was investigated by Brown et al. in a proof-of-concept paper on the advantages of combining solid-state NMR experiments with quantum-chemical calculations.[297] Coronene and the tweezer complex were also used as test cases by Loibl, Manby and Schütz for their local GIAO-HF and GIAO-MP2 implementations.[117,179] Because of the different approximations employed, as well as the different basis sets used, no direct comparison is attempted here. The benzene molecule was optimized at the RIJK-B3LYP-D3BJ/def2-TZVP/def2-JK level and the structures of the other two systems were optimized at the RI-BP86-D3BJ/def2-SVP/def2-J level. The final MO coefficients from the optimization were used as a guess for subsequent calculations. Wall-clock times for different parts of the calculation are shown in Figure 2.16 along with the number of electrons N_{el}, basis functions N_{bas}, and auxiliary basis functions N_{aux} for each example. The recommended grid settings and basis sets were used (see Table 2.6).

The efficiency of the RIJCOSX and RIJK approximations for SCF calculations has been compared previously,[116] and as expected, especially with the large grids employed here, the RIJCOSX approximation is only faster for the largest system. With the chosen settings, the COSX approximation to $\mathbf{K}^{\mathbf{B}}[\mathbf{D}]$ takes roughly the same amount of time as the RIJ approximation to $\mathbf{J}^{\mathbf{B}}[\mathbf{D}]$. However, the poor scaling of the RIK method already shows for the coronene molecule and for the tweezer system it is a significant bottleneck.

The solution of the CPSCF equations using RIJCOSX is much less time consuming than the SCF iterations, mostly because a small grid is used for the repeated evaluation of $\mathbf{K}\left[\mathbf{U}^{\mathbf{B}}\right]$. If the two-electron integrals are evaluated exactly in an integral-direct fashion (case "RIJK*" in Figure 2.16), the CPSCF dominates the computation time. Pre-calculating the integrals (case "RIJK") drastically reduces the time spent on CPSCF iterations for the smaller systems, even considering the time required for the calculation and storage of the necessary integrals. However, disk space becomes a bottleneck for large systems: the calculation on the tweezer could not be performed because the available 400 GB of scratch space were insufficient.

The additional computational effort required due to the inclusion of exact (HF) exchange can be estimated by comparing to timings for a "pure" DFT functional such as TPSS (see Table 2.8 below). In that case, not only are the $\mathbf{K}^{\mathbf{B}}[\mathbf{D}]$ and $\mathbf{K}\left[\mathbf{D}^{\mathbf{B}}\right]$ terms omitted from the CPSCF equations, but the iterative solution of the latter is skipped entirely. Considering also that "pure" functionals are only slightly less accurate than their hybrid counterparts (as shown in Section 2.3.3), it seems reasonable to only include exact exchange if the SCF solution is required for further treatment within correlated methods.

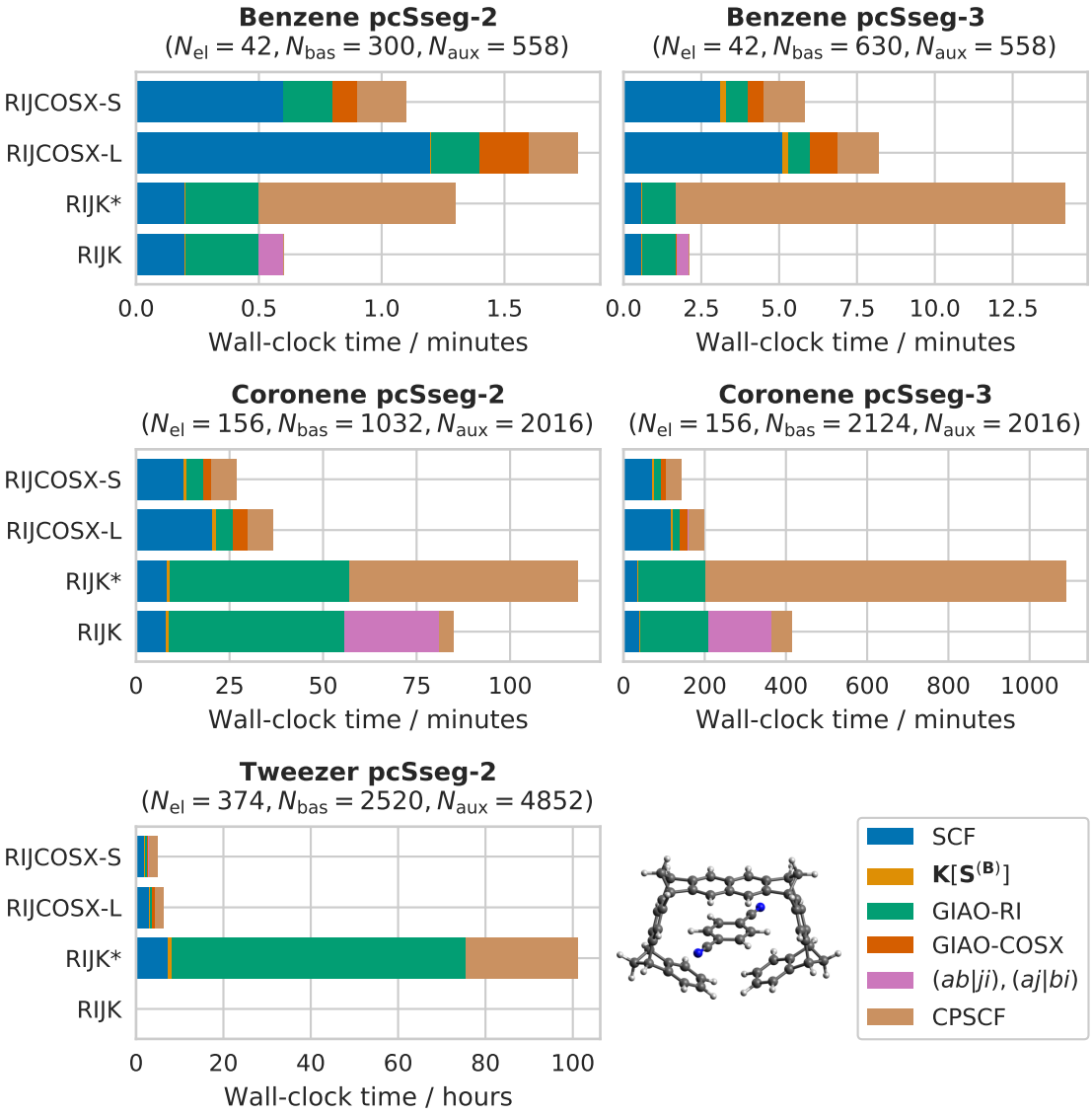

Figure 2.16: Wall-clock time for different parts of the calculation (adding up to over 99 % of the total time): SCF iterations, RI- and COSX-contributions to $\mathbf{g}^{\mathbf{B}}[\mathbf{D}]$ ("GIAO-RI" and "GIAO-COSX", respectively), RIK/COSX evaluation of the $\mathbf{K}\left[\mathbf{S}^{(\mathbf{B})}\right]$ term, pre-computation of the $(ab|ji)$ and $(aj|bi)$ integrals in the RIJK case, and convergence of the CPSCF equations to 1×10^{-6}. See Table 2.6 for the settings used. Calculations were performed for benzene, coronene, and the "tweezer" complex (depicted in the figure). All calculations ran on 8 CPU cores with 2 GB memory per core.

In summary the RIJK approximation is especially efficient for smaller systems with large basis sets. For systems over 100 electrons and 1000 basis functions, the RIJCOSX approach is recommended. It is worth noting that using the looser grid (RIJCOSX-S) only provides significant speedups for the smallest calculations (where RIJK is even faster) and considering the larger errors involved, it is advisable to use a denser grid (RIJCOSX-L).

2.3.10.2 RI-MP2 and DHDFT

In Section 2.3.3 we have shown the superior accuracy of DHDFs (DSD-PBEP86 in particular) for the computation of NMR chemical shifts, compared to SCF-level methods and MP2. However, it must be stressed that, although applicable to much larger systems than coupled cluster theory would be feasible for, these calculations are significantly more time-consuming than the hybrid DFT equivalents, and even more so than pure DFT shielding calculations, where even the iterative solution of the CPSCF equations is not needed. Therefore, in this section we evaluate the performance of our implementation for larger systems. The (all-electron) DSD-PBEP86/pS2/cw3C level of theory was used throughout this section.

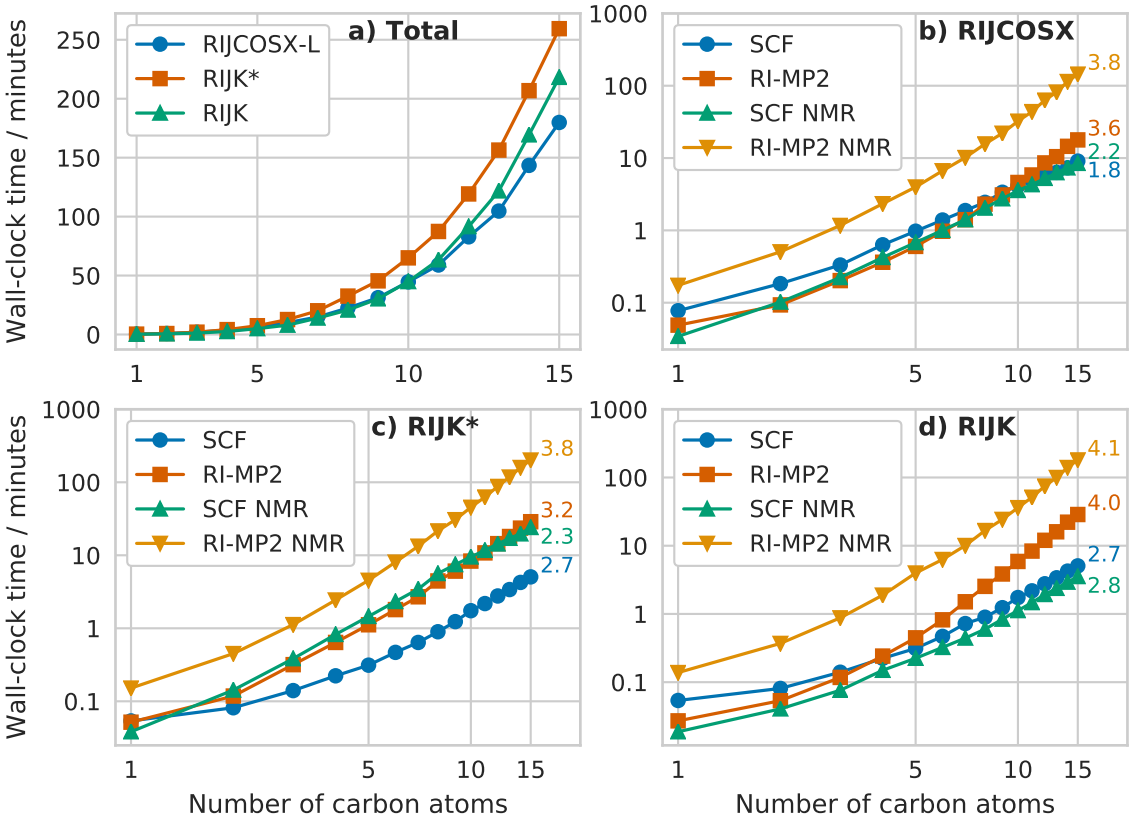

Figure 2.17: Wall-clock computation times for DSD-PBEP86/pS2/cw3C NMR shielding calculations on linear alkane chains ($C_nH_{(2n+2)}$) using different approximations for the Fock matrix contributions (as defined in Table 2.6). (a) Total computation times. (b-d) Timings for separate calculation parts using each of the approximations; the numbers on the right denote the effective scaling exponent determined from the last five points in each series. The calculations were performed on 8 Intel Xeon E7-8837 2.67 GHz cores with 8 GB RAM per core.

The computational effort is dominated by the evaluation of the MP2 response density $\mathbf{D^B}$ (a detailed breakdown of contributions to the total computation time is given in

Appendix C). The latter formally scales as $\mathcal{O}(N^5)$ with system size and can be up to 20–30 times more expensive than the evaluation of $\mathbf{D}$, as discussed in Section 2.2. However, the approximation used for the two-electron integrals, originating from the Fock operator, also has an effect on the timing. Figure 2.17 shows the total computation times for DSD-PBEP86 NMR shielding calculations on idealized linear alkane chains ($H(CH_2)_nH$). Here we compare the "RIJCOSX-L", "RIJK", and "RIJK*" approaches, as defined in Section 2.3.7.4. The effective scaling with system size is determined as the slope of a linear fit (on a log–log scale) of the last five points in each series. The RIJK option is fastest up to about $C_{10}H_{22}$, beyond which the RIJCOSX-L approach is more efficient. RIJK* is slightly faster than RIJCOSX-L for the two smallest systems but for $C_{15}H_{32}$ it already takes about 44 % more time. For the larger systems, the RIJK computation times are between those of the other two options. However, this result depends on the speed of disk I/O operations (a RAID 0 hard disk configuration was used in this case). Therefore it can be concluded that for very small systems the choice of approximation is largely immaterial, while for larger systems of about 100 electrons or more the RIJCOSX-L approximation is recommended.

A further illustration is given in Table 2.8 for several "real world" systems: the benzene, caffeine, coronene, and penicillin G molecules and the "tweezer" host–guest complex discussed in Section 2.3.10.1.[a] The latter is the largest system studied in this section with 374 electrons and 2520 basis functions. Note that, to reduce memory requirements, the perturbed amplitudes for each batch were stored on disk, as discussed in Section 2.2. For comparison, TPSS/pS2 calculations were also performed on these systems. Table 2.8 provides separate timings for different calculation parts: the SCF solution, assembly of the CPSCF RHS, solution of the CPSCF equations, and calculation of the MP2 relaxed density and response density matrices. Note that for TPSS only the first two steps are necessary. The final lines of the table allow for a quick comparison of the total computation time required for NMR shielding calculations with a pure DF (TPSS), a hybrid DF (here taken as the SCF part of DSD-PBEP86), and a DHDF (DSD-PBEP86). Due to the efficiency of the RIJCOSX approximation, hybrid DFT calculations are consistently only a few times more expensive than pure DFT ones. However, the cost of DHDFT quickly grows to more than an order of magnitude above hybrid DFT, with the largest calculation taking 6 days to complete and requiring 1 TB of disk space. It is clear that in order to apply DHDFT to much larger systems, a local correlation approximation is needed.

[a] For benzene, $R_{CC} = 1.3908\,\text{Å}$ and $R_{CH} = 1.0828\,\text{Å}$. Cartesian coordinates for the other systems are provided in Appendix E.

Table 2.8: System size indicators and wall-clock computation times (in minutes) for some medium-sized systems. Grid 4 was used for XC functional integration. The calculations were performed on 8 Intel Xeon E5-2687 v4 3.0 GHz cores with 8 GB RAM per core.

	Benzene	Caffeine	Coronene	Penicillin	Tweezer
Atoms	12	24	36	41	92
Electrons	42	102	156	176	374
Basis functions (pS2)	300	644	1032	1087	2520
AuxC functions (cw3C)	846	1854	3024	3158	7296
AuxJ functions (def2-JK)	558	1242	2016	2114	4852
Grid points (COSX-L)	23218	47803	74108	78287	172573
TPSS					
SCF (RI)	0.1	0.6	1.4	1.7	10.7
RHS (RI)	0.1	0.7	2.3	1.6	13.5
DSD-PBEP86/RIJCOSX-L					
SCF (RIJCOSX)	0.4	2.8	9.2	7.6	63.1
RHS (RIJCOSX)	0.2	1.3	4.3	3.7	32.2
CPSCF (RIJCOSX)	0.1	1.0	3.0	4.3	48.0
RI-MP2: $\mathbf{D}$	0.3	2.9	14.0	18.4	668.0
RI-MP2: $\mathbf{D}^{\mathbf{B}}$	1.7	19.0	108.7	144.4	7831.2
DSD-PBEP86/RIJK(RITrafo)					
SCF (RIJK)	0.2	1.4	5.5	6.0	
RHS (RIJK)	0.1	0.7	2.6	3.2	
CPSCF (RITrafo)	0.0	0.1	0.9	1.6	
RI-MP2: $\mathbf{D}$	0.2	3.5	27.9	39.5	
RI-MP2: $\mathbf{D}^{\mathbf{B}}$	1.5	21.1	133.8	185.6	
Comparison					
Total TPSS	0.3	1.3	3.8	3.4	25.4
Total PBEP86/RIJCOSX-L	0.7	5.1	16.5	15.6	143.4
Total DSD-PBEP86/RIJCOSX-L	2.7	27.0	139.2	178.3	8642.7
Total PBEP86/RIJK(RITrafo)[a]	0.3	4.1	26.2	35.4	
Total DSD-PBEP86/RIJK(RITrafo)	2.0	26.9	170.8	236.0	

[a] Including the RI transformation and storage of $(ia|jb)$ and $(ij|ab)$ integrals.

Chapter 3

Computation of polarizabilities and NMR shieldings with domain-based local pair natural orbital MP2

3.1 Theory

The focus of this thesis is the computation of NMR shielding tensors and therefore the goal of the following section is the derivation of analytic second derivatives of DLPNO-MP2 in that context. However, with small generalizations, it is possible to simultaneously derive other second order properties such as the electric dipole polarizability. Similar to the shielding tensor for nucleus K, $\boldsymbol{\sigma}^K$, the polarizability tensor $\boldsymbol{\alpha}$ can also be obtained as a second derivative of the energy:[298]

$$\sigma^K_{\beta\alpha} = \frac{\mathrm{d}^2 E}{\mathrm{d}B^{\mathrm{ext}}_\alpha \mathrm{d}m^K_\beta} = \sum_{\mu\nu}\left[D_{\mu\nu}\frac{\mathrm{d}^2 h_{\mu\nu}}{\mathrm{d}B^{\mathrm{ext}}_\alpha \mathrm{d}m^K_\beta} + \frac{\mathrm{d}D_{\mu\nu}}{\mathrm{d}B^{\mathrm{ext}}_\alpha}\frac{\mathrm{d}h_{\mu\nu}}{\mathrm{d}m^K_\beta}\right] \tag{3.1}$$

$$\alpha_{\alpha\beta} = -\frac{\mathrm{d}^2 E}{\mathrm{d}F^{\mathrm{ext}}_\alpha \mathrm{d}F^{\mathrm{ext}}_\beta} = -\sum_{\mu\nu}\frac{\mathrm{d}D_{\mu\nu}}{\mathrm{d}F^{\mathrm{ext}}_\alpha}\frac{\mathrm{d}h_{\mu\nu}}{\mathrm{d}F^{\mathrm{ext}}_\beta} \tag{3.2}$$

where, as in the previous chapter, E, $\mathbf{D}$, and $\mathbf{h}$ are the method-specific energy expression, density matrix, and one-electron part of the Fock matrix, respectively; α and β denote arbitrary Cartesian directions; $\mathbf{F}^{\mathrm{ext}}$, $\mathbf{B}^{\mathrm{ext}}$ (the superscript "ext" is used in this chapter for consistency between the two fields), and $\mathbf{m}^K$ are the external electric and magnetic fields and the nuclear magnetic moment of K, respectively. Note that the expressions in eqs. 3.1 and 3.2 are not symmetric with respect to the perturbation and thus not the only possible expressions for these properties. Notice also that $\mathbf{h}$ only contains terms that are linear in $\mathbf{F}^{\mathrm{ext}}$:

$$\mathrm{h}\left(\mathbf{r}, \mathbf{F}^{\mathrm{ext}}\right) = \frac{1}{2}\boldsymbol{\nabla}^2 - \mathrm{V}(\mathbf{r}) - \mathbf{F}^{\mathrm{ext}} \cdot \boldsymbol{\mu} \tag{3.3}$$

$$\boldsymbol{\mu} = -\mathbf{r} + \sum_K^{\mathrm{nuc}} Z_K \mathbf{R}_K \tag{3.4}$$

$$\frac{\mathrm{d}h_{\mu\nu}}{\mathrm{d}F^{\mathrm{ext}}_\alpha} = -\langle\mu|\, r_\alpha \,|\nu\rangle \tag{3.5}$$

$$\frac{\mathrm{d}^2 h_{\mu\nu}}{\mathrm{d}F^{\mathrm{ext}}_\alpha \mathrm{d}F^{\mathrm{ext}}_\beta} = 0 \tag{3.6}$$

where $\mathbf{r}$ is the electronic coordinate with respect to the global origin and Z_K and $\mathbf{R}_K$ are the charge and position of nucleus K. In the following discussion, $\boldsymbol{\lambda}$ will denote a generic multi-dimensional perturbation (like $\mathbf{F}^{\text{ext}}$ or $\mathbf{B}^{\text{ext}}$).

As the derivations below are already rather complicated, they are limited to pure MP2. However, the extension to DHDFT and the extra terms required are identical to those discussed in Chapter 2 (see Section 2.1.4). Similarly, the inclusion of an implicit solvent model is analogous to the RI-MP2 case (see Section 2.1.5).

3.1.1 Notation

Due to the many basis transformations and domain truncations involved in local correlation methods, mathematical notation can quickly become cumbersome, imprecise, or both. Here we try to give a brief explanation of the symbols used in the present derivations. Table 3.1 lists the symbols used to denote different sets of orbitals. Note that virtual orbitals belonging to a specific orbital or pair domain, are usually denoted with corresponding lower indices, e.g. $\tilde{\mu}_i$ or $\tilde{a}_{ij}$. However, the occupied orbital indices are often obvious from context, or are added as upper indices of a matrix, e.g. $F^i_{\tilde{\mu}}$ or $T^{ij}_{\tilde{a}\tilde{b}}$, and thus the repetition is avoided to simplify the notation.

Be aware that despite the similar notation, the symbols $K^{ij}_{\tilde{a}\tilde{b}}$, $T^{ij}_{\tilde{a}\tilde{b}}$, $F^{ij}_{\tilde{a}\tilde{b}}$, and $S^{ij}_{\tilde{a}\tilde{b}}$ have rather different meanings: the first denotes the two-electron repulsion integral $(i\tilde{a}_{ij} \,|\, j\tilde{b}_{ij})$, the second parametrizes excitations from orbitals i and j into PNOs $\tilde{a}$ and $\tilde{b}$, while the last two are simply the Fock and overlap matrix elements in the PNO basis of pair ij.

The conventions introduced in Section 2.1.1 also apply here. Note that, while consistency with Chapter 2 is preserved as much as possible, some symbols are redefined in this chapter.

Table 3.1: Notation

Indices	Basis set
i, j, k, l	(localized) occupied orbitals, or valence orbitals in particular
m, n	(localized) core orbitals
a, b, c, d	canonical virtual orbitals
p, q, r, s	occupied or virtual molecular orbitals
μ, ν, η	atomic orbitals (AOs)
$\tilde{\mu}', \tilde{\nu}', \tilde{\eta}'$	normalized redundant projected atomic orbitals (PAOs)
$\tilde{\mu}, \tilde{\nu}, \tilde{\eta}$	orbital/pair domain of orthonormal pseudo-canonical non-redundant projected atomic orbitals (NPAOs)
$\tilde{a}, \tilde{b}, \tilde{c}, \tilde{d}$	pair natural orbitals (PNOs)
$\tilde{a}', \tilde{b}', \tilde{c}', \tilde{d}'$	discarded/"complementary" pair natural orbitals (CPNOs)
$\tilde{a}'', \tilde{b}'', \tilde{c}'', \tilde{d}''$	union of PNOs and CPNOs

3.1.2 The domain-based local pair natural orbital MP2 method

Here we provide a brief review of the closed-shell (spin-restricted) DLPNO-MP2 method, which has been described in significant detail elsewhere.[144,193] The following steps are taken to obtain the DLPNO-MP2 energy:

1. The SCF equations are solved, giving the HF energy, E_{HF}, and canonical molecular orbitals (CMOs).

2. The occupied orbitals are localized according to the Foster–Boys (FB) criterion, as modified by Boys (referred to below as FB localization).[299,300] Core and valence orbitals are localized separately.

3. PAOs $\tilde{\mu}'_{\mathrm{u}}$ ("u" stands for unnormalized) are obtained as

$$|\tilde{\mu}'_{\mathrm{u}}\rangle = \left(1 - \sum_i |i\rangle \langle i|\right) |\mu\rangle \equiv \sum_\nu \widetilde{P}^{\mathrm{u}}_{\nu\tilde{\mu}'_{\mathrm{u}}} |\nu\rangle \tag{3.7}$$

   and then normalized using the factor $N_{\tilde{\mu}'} = \langle\tilde{\mu}'_{\mathrm{u}}|\tilde{\mu}'_{\mathrm{u}}\rangle^{-\frac{1}{2}}$:

$$|\tilde{\mu}'\rangle = N_{\tilde{\mu}'} |\tilde{\mu}'_{\mathrm{u}}\rangle \equiv \sum_\nu \widetilde{P}_{\nu\tilde{\mu}'} |\nu\rangle \tag{3.8}$$

4. For each occupied orbital, a correlation domain of PAOs is selected, based on the differential overlap criterion

$$\mathrm{DOI}_{i\tilde{\mu}'} = \sqrt{\left\langle |\, i\,|^2 \middle| |\,\tilde{\mu}'\,|^2 \right\rangle} > T_{\mathrm{CutDOPre}} \tag{3.9}$$

   with the default value of the parameter $T_{\mathrm{CutDOPre}} = 0.03$. These domains are then extended to all PAOs coming from the included atoms.

5. Non-redundant orthonormal PAOs (NPAOs) are constructed by diagonalizing the overlap matrix of each PAO domain, discarding eigenvectors with eigenvalues below T_{S} (10^{-8} by default) and normalizing the rest. These are then transformed into pseudo-canonical NPAOs $\{\tilde{\mu}\}$ by diagonalizing the NPAO Fock matrix.

6. Strongly correlated electron pairs are determined using a three-step procedure. A pair ij is kept if the differential overlap between the two orbitals, DOI_{ij}, is greater than $T_{\mathrm{CutDOij}} = 10^{-5}$ and the semi-canonical pair energy estimate, eq. 3.10, using the collinear dipole approximation to the exchange integrals (i.e. $M^{ij,\mathrm{col}}_{\tilde{\mu}\tilde{\nu}}$ from eq. 3.12 instead of $M^{ij}_{\tilde{\mu}\tilde{\nu}}$),[301] is greater than $T_{\mathrm{CutPre}} = 10^{-6}$. The energy contribution from the screened-out pairs, ΔE_{Pre}, is estimated using the more accurate dipole approximation to the exchange integrals,[136] eq. 3.11.

$$\varepsilon^{\mathrm{dip}}_{ij} = -4 \sum_{\tilde{\mu}\tilde{\nu}} \frac{M^{ij}_{\tilde{\mu}\tilde{\nu}} M^{ij*}_{\tilde{\mu}\tilde{\nu}}}{F^i_{\tilde{\mu}} + F^j_{\tilde{\nu}} - F_{ii} - F_{jj}} \tag{3.10}$$

$$M^{ij}_{\tilde{\mu}\tilde{\nu}} = \frac{\mathbf{r}_{i\tilde{\mu}}\mathbf{r}_{j\tilde{\nu}}}{|\mathbf{R}_{ij}|^3} - 3\frac{(\mathbf{r}_{i\tilde{\mu}}\mathbf{R}_{ij})\,(\mathbf{r}_{j\tilde{\nu}}\mathbf{R}_{ij})}{|\mathbf{R}_{ij}|^5} \tag{3.11}$$

$$M^{ij,\mathrm{col}}_{\tilde{\mu}\tilde{\nu}} = 4\frac{\mathbf{r}_{i\tilde{\mu}}\mathbf{r}_{j\tilde{\nu}}}{|\mathbf{R}_{ij}|^3} \tag{3.12}$$

$$\mathbf{R}_{ij} = \mathbf{r}_{ii} - \mathbf{r}_{jj} \tag{3.13}$$

$$\mathbf{r}_{i\tilde{\mu}} = \langle i|\,\mathbf{r}\,|\tilde{\mu}_i\rangle \tag{3.14}$$

   $F^i_{\tilde{\mu}}$ and $F^j_{\tilde{\nu}}$ are NPAO orbital energies in the domain of orbitals i and j, respectively, while F_{ii} and F_{jj} are elements of the Fock matrix in the localized MO (LMO) basis.

7. The correlation domains are reconstructed as in step 4 but with a tighter threshold $T_{\mathrm{CutDO}} = 0.01$. Pair domains are then made as the union of orbital domains. The pair domain PAOs are later orthonormalized as in step 5.

8. PNOs are constructed by diagonalizing the semi-canonical pair density $\breve{\mathbf{D}}^{ij}$ in the basis of NPAOs for the given orbital pair:

$$\breve{D}^{ij}_{\tilde{\mu}\tilde{\nu}} = \sum_{\tilde{\eta}} \left[\widetilde{\breve{T}}^{ij*}_{\tilde{\mu}\tilde{\eta}} \breve{T}^{ij}_{\tilde{\nu}\tilde{\eta}} + \widetilde{\breve{T}}^{ij*}_{\tilde{\eta}\tilde{\mu}} \breve{T}^{ij}_{\tilde{\eta}\tilde{\nu}} \right] \tag{3.15}$$

$$\breve{T}^{ij}_{\tilde{\mu}\tilde{\nu}} = -\frac{(\tilde{\mu}_{ij} i|\tilde{\nu}_{ij} j)}{F^{ij}_{\tilde{\mu}} + F^{ij}_{\tilde{\nu}} - F_{ii} - F_{jj}} \tag{3.16}$$

$$\widetilde{\breve{T}}^{ij}_{\tilde{\mu}\tilde{\nu}} = \frac{1}{1+\delta_{ij}} \left(4\breve{T}^{ij}_{\tilde{\mu}\tilde{\nu}} - 2\breve{T}^{ij}_{\tilde{\nu}\tilde{\mu}} \right) \tag{3.17}$$

where $F^{ij}_{\tilde{\mu}}$ and $F^{ij}_{\tilde{\nu}}$ are NPAO orbital energies in the ij pair domain and δ_{ij} is the Kronecker delta. PNOs with an occupation number greater than $T_{\mathrm{CutPNO}} = 10^{-8}$ are kept, while the rest form the "complementary" PNO (CPNO) basis referred to below. A tighter threshold, $T_{\mathrm{CutPNO}} \times T_{\mathrm{ScalePNOCore}} = 10^{-10}$, is used for pairs which include core orbitals.[302] The PAO to PNO transformation matrices are stored on disk. A correction to the energy, ΔE_{PNO}, is computed as the difference between the semi-canonical correlation energy, calculated in the NPAO and PNO basis sets.

9. The full amplitude equations $\partial E_2^{\mathrm{DLPNO}} / \partial \widetilde{T}^{ij*}_{\tilde{a}\tilde{b}} = 0$ (see Section 3.1.3 for definitions) are solved iteratively in the PNO basis and the final DLPNO-MP2 energy is calculated:

$$E_{\mathrm{DLPNO\text{-}MP2}} = E_{\mathrm{HF}} + E_2^{\mathrm{DLPNO}} + \Delta E_{\mathrm{PNO}} + \Delta E_{\mathrm{Pre}} \tag{3.18}$$

The following sections list the steps necessary to compute analytic derivatives, based on the DLPNO-MP2 energy.

3.1.3 DLPNO-MP2 Lagrangian

Because the DLPNO-MP2 energy expression is non-variational, a Lagrangian formulation is used for analytic derivatives,[226] which is slightly different from the one used previously:[191,192]

$$\begin{aligned} \mathcal{L} = {} & E_{\mathrm{HF}} + E_2^{\mathrm{DLPNO}} + \Delta E_{\mathrm{PNO}} + \Delta E_{\mathrm{Pre}} \\ & + C_{\mathrm{Bri}} + C_{\mathrm{Loc}} + C_{\mathrm{CV}} + C_{\mathrm{SC}} + C_{\mathrm{PNO}} \\ & + C_{\mathrm{MOO}} + C_{\mathrm{PNOO}} + C_{\mathrm{NPAOO}} \end{aligned} \tag{3.19}$$

The first four terms are the energy contributions, the next five are the Brillouin, localization, core–valence, semicanonical, and PNO Lagrangian constraints, and the last three are orthonormality conditions for the MOs, PNOs and NPAOs. The various terms will be explained in the present section. E_{HF} is the HF energy expression:

$$E_{\mathrm{HF}} = 2\sum_i h_{ii} + \sum_{ij} \left[2\,(ii|jj) - (ij|ji) \right] \tag{3.20}$$

with two-electron integrals in the Mulliken $(1^*1|2^*2)$ notation. E_2^{DLPNO} is the PNO-basis Hylleraas functional in the spin-adapted form:[234]

$$E_2^{\mathrm{DLPNO}} = \sum_{i \geq j} \sum_{\tilde{a}\tilde{b}} \left[K^{ij}_{\tilde{a}\tilde{b}} \widetilde{T}^{ij}_{\tilde{a}\tilde{b}} + K^{ij*}_{\tilde{a}\tilde{b}} \widetilde{T}^{ij*}_{\tilde{a}\tilde{b}} + D^{ij}_{\tilde{a}\tilde{b}} F^{ij}_{\tilde{a}\tilde{b}} \right] - \sum_{ij} D_{ij} F_{ij} \tag{3.21}$$

$$D^{ij}_{\tilde{a}\tilde{b}} = \sum_{\tilde{c}} \left[\widetilde{T}^{ij*}_{\tilde{a}\tilde{c}} T^{ij}_{\tilde{b}\tilde{c}} + \widetilde{T}^{ij*}_{\tilde{c}\tilde{a}} T^{ij}_{\tilde{c}\tilde{b}} \right] \tag{3.22}$$

$$D_{ij} = \sum_{k} (1 + \delta_{jk}) \sum_{\tilde{a}\tilde{b}\tilde{c}\tilde{d}} S^{ik,kj*}_{\tilde{a}\tilde{b}} \widetilde{T}^{kj*}_{\tilde{b}\tilde{c}} S^{kj,ik}_{\tilde{c}\tilde{d}} T^{ik}_{\tilde{d}\tilde{a}} \tag{3.23}$$

$$K^{ij}_{\tilde{a}\tilde{b}} = \left(i\tilde{a}_{ij} \middle| j\tilde{b}_{ij} \right) \tag{3.24}$$

$$S^{ij,kl}_{\tilde{a}\tilde{b}} = \left\langle \tilde{a}_{ij} \middle| \tilde{b}_{kl} \right\rangle \tag{3.25}$$

$$\widetilde{T}^{ij}_{\tilde{a}\tilde{b}} = \frac{1}{1 + \delta_{ij}} \left(4T^{ij}_{\tilde{a}\tilde{b}} - 2T^{ij}_{\tilde{b}\tilde{a}} \right) \tag{3.26}$$

ΔE_{PNO} is an estimate for the error due to the PNO truncation, calculated as the difference between the correlation energy computed from the semicanonical amplitudes in the full NPAO basis and in the truncated PNO basis:

$$\Delta E_{\mathrm{PNO}} = \frac{1}{2} \sum_{i \geq j} \left[\sum_{\tilde{a}''\tilde{b}''} \left(K^{ij}_{\tilde{a}''\tilde{b}''} \widetilde{\overline{T}}^{ij}_{\tilde{a}''\tilde{b}''} + K^{ij*}_{\tilde{a}''\tilde{b}''} \widetilde{\overline{T}}^{ij*}_{\tilde{a}''\tilde{b}''} \right) - \sum_{\tilde{a}\tilde{b}} \left(K^{ij}_{\tilde{a}\tilde{b}} \widetilde{\overline{T}}^{ij}_{\tilde{a}\tilde{b}} + K^{ij*}_{\tilde{a}\tilde{b}} \widetilde{\overline{T}}^{ij*}_{\tilde{a}\tilde{b}} \right) \right] \tag{3.27}$$

The energy contribution of the screened-out pairs takes the form of an approximate Hylleraas functional:

$$\begin{aligned} \Delta E_{\mathrm{Pre}} = 4 \sum_{i>j} 1_{\mathrm{S}}(ij) \sum_{\tilde{\mu}\tilde{\nu}} \Big[& M^{ij}_{\tilde{\mu}\tilde{\nu}} t^{ij}_{\tilde{\mu}\tilde{\nu}} + M^{ij*}_{\tilde{\mu}\tilde{\nu}} t^{ij*}_{\tilde{\mu}\tilde{\nu}} - (F_{ii} + F_{jj}) t^{ij*}_{\tilde{\mu}\tilde{\nu}} t^{ij}_{\tilde{\mu}\tilde{\nu}} \\ & + \sum_{\tilde{\eta}} \left(F^{i}_{\tilde{\mu}\tilde{\nu}} t^{ij*}_{\tilde{\mu}\tilde{\eta}} t^{ij}_{\tilde{\nu}\tilde{\eta}} + F^{j}_{\tilde{\mu}\tilde{\nu}} t^{ij*}_{\tilde{\eta}\tilde{\mu}} t^{ij}_{\tilde{\eta}\tilde{\nu}} \right) \Big] \end{aligned} \tag{3.28}$$

where $1_{\mathrm{S}}(ij) = 1$ if pair ij was screened out, 0 otherwise. The dipole approximation to the exchange integrals is given in eq. 3.11. The Brillouin condition is formulated as

$$C_{\mathrm{Bri}} = \frac{1}{2} \sum_{ai} \left(z_{ai} F_{ai} + z^*_{ai} F^*_{ai} \right) \tag{3.29}$$

where z_{ai} is the required Lagrange parameter. Introducing a magnetic field means that all quantities throughout the formalism are necessarily complex. Therefore, for any Lagrangian condition, it is necessary to constrain both its real and imaginary part or, equivalently, the condition and its complex conjugate. We favor the latter approach here, which also leads to complex Lagrange multipliers and their conjugates as separate optimization parameters, which can be arranged in Hermitian matrices, e.g. $z_{ia} \equiv z^*_{ai}$. For infinitesimal perturbations, the final working equations in the first order of the perturbation are always fully real (e.g. for electric fields) or fully imaginary (e.g. for magnetic fields), and are therefore over-parametrized. Thus, linear combinations are formed to obtain separate equations for the real and imaginary components of the Lagrange multipliers, of which one provides the required solution, and the other trivially gives zero. The factors of one half in eq. 3.29 as well as eqs. 3.32, 3.34, 3.39, and 3.43 (see below) are introduced for consistency with the definitions of the Lagrange multipliers in ref. 192. We also note in passing that eq. 3.19 is formulated such that all terms are real.

In the present derivation, the molecular orbital (MO) response to perturbations is parametrized as:[303]

$$\mathbf{c}(\boldsymbol{\lambda}) = \mathbf{c}^{(0)} \mathbf{U}(\boldsymbol{\lambda}), \quad \mathbf{U}(0) = \mathbf{I} \tag{3.30}$$

where $\mathbf{c}$ denotes the LMO coefficients. In contrast to the exponential parametrization used in refs. 191 and 192, $\mathbf{U}$ is not constrained to be unitary but is instead constrained by the MO orthonormality condition

$$C_{\mathrm{MOO}} = \sum_{pq} x_{pq} \left(S_{pq} - \delta_{pq}\right) \tag{3.31}$$

which is fulfilled by the CMO coefficients and the unperturbed LMO coefficients $\mathbf{c}^{(0)}$. Here, x_{pq} are the associated Lagrange multipliers. The term C_{Loc} enforces the FB localization condition separately on the core and valence orbitals and introduces the required Lagrange multipliers l_{ij}:

$$C_{\mathrm{Loc}} = \frac{1}{2} \sum_{i<j}^{\mathrm{valence}} \left(l_{ij} s_{ij} + l_{ij}^* s_{ij}^*\right) + \frac{1}{2} \sum_{m<n}^{\mathrm{core}} \left(l_{mn} s_{mn} + l_{mn}^* s_{mn}^*\right) \tag{3.32}$$

$$s_{ij} = \left(\mathbf{r}_{ii} - \mathbf{r}_{jj}\right) \mathbf{r}_{ij} = -s_{ji}^* \tag{3.33}$$

The final MO constraint is the core-valence separation condition with an associated Lagrange parameter $\bar{z}_{im}$:

$$C_{\mathrm{CV}} = \frac{1}{2} \sum_{i}^{\mathrm{valence}} \sum_{m}^{\mathrm{core}} \left(\bar{z}_{im} F_{im} + \bar{z}_{im}^* F_{im}^*\right) \tag{3.34}$$

Recall that the core and valence orbitals are localized separately because different PNO truncation thresholds are used for pairs which include core orbitals.[302] Therefore, the core-valence separation condition is necessary even if all electrons are included in the correlation treatment. On the other hand, the localization condition for core orbitals is not needed if the latter are not localized, which is the case in the frozen-core approximation.

We denote the PNOs by $\tilde{a}, \tilde{b}, \tilde{c}, \tilde{d}$, the CPNOs by $\tilde{a}', \tilde{b}', \tilde{c}', \tilde{d}'$ and the union of the two spaces with $\tilde{a}'', \tilde{b}'', \tilde{c}'', \tilde{d}''$. The transformation matrices from redundant PAOs to each of these sets (for orbital pair ij) are denoted by $d^{ij}_{\tilde{\mu}'\tilde{a}}$, $d'^{ij}_{\tilde{\mu}'\tilde{a}'}$, and $d''^{ij}_{\tilde{\mu}'\tilde{a}''}$, respectively. The PNOs and CPNOs combined span the same space as the NPAOs. In the presence of a perturbation, we allow the PNOs to relax within the entire PNO+CPNO space. Rotations within each domain are thus parametrized as

$$\mathbf{d}''^{ij}(\boldsymbol{\lambda}) = \mathbf{d}''^{ij(0)} \boldsymbol{\theta}^{ij}(\boldsymbol{\lambda}), \quad \boldsymbol{\theta}^{ij}(0) = \mathbf{I} \tag{3.35}$$

Analogously to $\mathbf{U}$, the matrices $\boldsymbol{\theta}^{ij}$ are not necessarily unitary but rather are constrained by the PNO (and CPNO) orthonormality condition:

$$C_{\mathrm{PNOO}} = \sum_{i \geq j} \sum_{\tilde{a}''\tilde{b}''} x^{ij}_{\tilde{a}''\tilde{b}''} \left(S^{ij}_{\tilde{a}''\tilde{b}''} - \delta_{\tilde{a}''\tilde{b}''}\right) \quad \text{with} \quad \mathbf{S}^{ij} \equiv \mathbf{S}^{ij,ij} \tag{3.36}$$

Note that below, $\mathbf{S}^{ij}$ is expanded as

$$\mathbf{S}^{ij} = \boldsymbol{\theta}^{ij\dagger} \boldsymbol{\mathcal{S}}^{ij} \boldsymbol{\theta}^{ij} = \boldsymbol{\theta}^{ij\dagger} \mathbf{d}''^{ij(0)\dagger} \widetilde{\mathbf{S}} \mathbf{d}''^{ij(0)} \boldsymbol{\theta}^{ij} \tag{3.37}$$

$$\widetilde{S}_{\tilde{\mu}'\tilde{\nu}'} = \langle \tilde{\mu}' | \tilde{\nu}' \rangle \tag{3.38}$$

where $\boldsymbol{\mathcal{S}}^{ij}$ is the PAO overlap matrix transformed to the unperturbed PNO+CPNO basis. A further PNO constraint ensures that the semi-canonical pair densities $\breve{\mathbf{D}}^{ij}$ remain block-diagonal:

$$C_{\mathrm{PNO}} = \frac{1}{2} \sum_{i \geq j} \sum_{\tilde{a}\tilde{b}'} \left(v^{ij}_{\tilde{a}\tilde{b}'} \breve{D}^{ij}_{\tilde{a}\tilde{b}'} + v^{ij*}_{\tilde{a}\tilde{b}'} \breve{D}^{ij*}_{\tilde{a}\tilde{b}'}\right) \tag{3.39}$$

where $v^{ij}_{\tilde{a}\tilde{b}'}$ are unknown Lagrange multipliers. An orthonormality condition also applies to the orbital domain NPAOs used for the prescreening correction, parametrized as

$$\boldsymbol{\pi}^i(\boldsymbol{\lambda}) = \boldsymbol{\pi}^{i(0)}\boldsymbol{\theta}^i(\boldsymbol{\lambda}), \quad \boldsymbol{\theta}^i(0) = \mathbf{I} \tag{3.40}$$

$$C_{\mathrm{NPAOO}} = \sum_i \sum_{\tilde{\mu}\tilde{\nu}} x^i_{\tilde{\mu}\tilde{\nu}} \left(S^i_{\tilde{\mu}\tilde{\nu}} - \delta_{\tilde{\mu}\tilde{\nu}}\right) \tag{3.41}$$

where $\pi^i_{\tilde{\mu}'\tilde{\nu}}$ are the transformation matrices from redundant to non-redundant orbital domain PAOs, $\mathbf{S}^i$ is the overlap matrix in the latter basis, and $x^i_{\tilde{\mu}\tilde{\nu}}$ are the necessary Lagrange multipliers. Finally, the semi-canonical amplitudes are parametrized as

$$\breve{\mathbf{T}}^{ij} = \boldsymbol{\theta}^{ij\dagger}\widehat{\mathbf{T}}^{ij}\boldsymbol{\theta}^{ij*} \tag{3.42}$$

and the semi-canonical residual conditions C_{SC} are included in the Lagrangian:

$$C_{\mathrm{SC}} = \frac{1}{2}\sum_{i\geq j}\sum_{\tilde{a}''\tilde{b}''}\left(w^{ij}_{\tilde{a}''\tilde{b}''}\breve{R}^{ij}_{\tilde{a}''\tilde{b}''} + w^{ij*}_{\tilde{a}''\tilde{b}''}\breve{R}^{ij*}_{\tilde{a}''\tilde{b}''}\right) \tag{3.43}$$

where $w^{ij}_{\tilde{a}''\tilde{b}''}$ are Lagrange multipliers and the semi-canonical residuals $\breve{R}^{ij}_{\tilde{a}''\tilde{b}''}$ are defined as

$$\breve{R}^{ij}_{\tilde{a}''\tilde{b}''} = K^{ij*}_{\tilde{a}''\tilde{b}''} + \sum_{\tilde{c}''}\left(\breve{T}^{ij}_{\tilde{a}''\tilde{c}''}F^{ij}_{\tilde{b}''\tilde{c}''} + F^{ij}_{\tilde{a}''\tilde{c}''}\breve{T}^{ij}_{\tilde{c}''\tilde{b}''}\right) - \breve{T}^{ij}_{\tilde{a}''\tilde{b}''}\left(F_{ii} + F_{jj}\right) \tag{3.44}$$

The optimization parameters in the present DLPNO-MP2 Lagrangian are thus: U_{pq}, $T^{ij}_{\tilde{a}\tilde{b}}$, $\widehat{T}^{ij}_{\tilde{a}''\tilde{b}''}$, $\theta^{ij}_{\tilde{a}''\tilde{b}''}$, $\theta^i_{\tilde{\mu}\tilde{\nu}}$, $t^{ij}_{\tilde{\mu}\tilde{\nu}}$, z_{ai}, $\bar{z}_{im}$, l_{ij}, x_{pq}, $v^{ij}_{\tilde{a}\tilde{b}'}$, $x^{ij}_{\tilde{a}''\tilde{b}''}$, $x^i_{\tilde{\mu}\tilde{\nu}}$, $w^{ij}_{\tilde{a}''\tilde{b}''}$ and their complex conjugates.

3.1.4 Equations for first derivatives

The derivative of the DLPNO-MP2 energy with respect to the first external perturbation $\boldsymbol{\kappa}$ (in this work either an electric field or nuclear magnetic moment, on which only the one-electron part of the Hamiltonian depends) is equal to the respective partial derivative of the Lagrangian

$$\frac{\mathrm{d}E_{\text{DLPNO-MP2}}}{\mathrm{d}\boldsymbol{\kappa}} = \frac{\partial\mathcal{L}}{\partial\boldsymbol{\kappa}} = \sum_{\mu\nu}\left(D^{\mathrm{SCF}}_{\mu\nu} + D_{\mu\nu}\right)h^{\boldsymbol{\kappa}}_{\mu\nu} \tag{3.45}$$

if and only if the Lagrangian is made stationary with respect to all parameters. The equations for the necessary stationarity conditions will be presented in this section. Despite the slightly different formulation of the Lagrangian, the final working equations are completely equivalent to those derived in ref. 192. Note that eq. 3.45 is only valid if the basis functions do not depend on the perturbation $\boldsymbol{\kappa}$. Therein, $\mathbf{D}^{\mathrm{SCF}}$ is the SCF density matrix:

$$D^{\mathrm{SCF}}_{\mu\nu} = 2\sum_i c^*_{\mu i}c_{\nu i} \tag{3.46}$$

while $\mathbf{D}$ is the orbital-relaxed DLPNO-MP2 difference density matrix:

$$\mathbf{D} = \mathbf{D}' + \frac{1}{2}\mathbf{c}^*\left(\mathbf{z} + \bar{\mathbf{z}}\right)\mathbf{c}^{\mathrm{T}} \tag{3.47}$$

where, as stated above, only the occupied-virtual and virtual-occupied blocks of $\mathbf{z}$ are non-zero with $z_{ia} \equiv z^*_{ai}$. Analogously, $\bar{\mathbf{z}}$ only has non-zero core-valence blocks with $\bar{z}_{mi} \equiv \bar{z}^*_{im}$. $\mathbf{D}'$ is the "PNO-relaxed" difference density matrix:

$$\mathbf{D}' = \widetilde{\mathbf{P}}^* \mathbf{D}'^{\mathrm{v}} \widetilde{\mathbf{P}}^{\mathrm{T}} - \mathbf{c}^* \mathbf{D}'^{\mathrm{o}} \mathbf{c}^{\mathrm{T}} \tag{3.48}$$

$$D'^{\mathrm{o}}_{ij} = D_{ij} + \frac{1}{2} \sum_{k \geq l} \delta_{ij} \left(\delta_{ik} + \delta_{il}\right) \mathrm{tr}\left(\mathbf{w}^{kl} \breve{\mathbf{T}}^{lk} + \mathbf{w}^{kl*} \breve{\mathbf{T}}^{lk*}\right) + D^{\mathrm{o(Pre)}}_{ij} \tag{3.49}$$

$$D'^{\mathrm{v}}_{\tilde{\mu}'\tilde{\nu}'} = \sum_{i \geq j} D'^{ij}_{\tilde{\mu}'\tilde{\nu}'} + D^{\mathrm{v(Pre)}}_{\tilde{\mu}'\tilde{\nu}'} \tag{3.50}$$

$$\mathbf{D}'^{ij} = \mathbf{d}^{ij*} \mathbf{D}^{ij} \mathbf{d}^{ij,\mathrm{T}} + \frac{1}{2} \mathbf{d}''^{ij*} \left(\mathbf{w}^{ij} \breve{\mathbf{T}}^{ji} + \mathbf{w}^{ij,\mathrm{T}} \breve{\mathbf{T}}^{ij} + \breve{\mathbf{T}}^{ji*} \mathbf{w}^{ij*} + \breve{\mathbf{T}}^{ij*} \mathbf{w}^{ij\dagger}\right) \mathbf{d}''^{ij,\mathrm{T}} \tag{3.51}$$

The prescreening contributions are defined as:

$$D^{\mathrm{o(Pre)}}_{ij} = 4\delta_{ij} \sum_k 1_{\mathrm{S}}(ik) \, \mathrm{tr}\left(\mathbf{t}^{ik*} \mathbf{t}^{ki}\right) \tag{3.52}$$

$$\mathbf{D}^{\mathrm{v(Pre)}} = 4 \sum_{ij} 1_{\mathrm{S}}(ij) \boldsymbol{\pi}^{i*} \mathbf{t}^{ij*} \mathbf{t}^{ji} \boldsymbol{\pi}^{i,\mathrm{T}} \tag{3.53}$$

The values of the required variables are obtained by solving the stationarity conditions equations (and their complex conjugates):

$$\begin{aligned} 0 \equiv \frac{\partial \mathcal{L}}{\partial T^{ij}_{\tilde{a}\tilde{b}}} = \frac{\partial \mathcal{L}}{\partial w^{ij}_{\tilde{a}''\tilde{b}''}} = \frac{\partial \mathcal{L}}{\partial v^{ij}_{\tilde{a}\tilde{b}'}} = \frac{\partial \mathcal{L}}{\partial z_{ai}} = \frac{\partial \mathcal{L}}{\partial \bar{z}_{im}} = \frac{\partial \mathcal{L}}{\partial l_{ij}} = \frac{\partial \mathcal{L}}{\partial t^{ij}_{\tilde{\mu}\tilde{\nu}}} \\ = \frac{\partial \mathcal{L}}{\partial x^{ij}_{\tilde{a}''\tilde{b}''}} = \frac{\partial \mathcal{L}}{\partial x^{i}_{\tilde{\mu}\tilde{\nu}}} = \frac{\partial \mathcal{L}}{\partial x_{pq}} = \frac{\partial \mathcal{L}}{\partial \widehat{T}^{ij}_{\tilde{a}''\tilde{b}''}} = \frac{\partial \mathcal{L}}{\partial \theta^{ij}_{\tilde{a}''\tilde{b}''}} = \frac{\partial \mathcal{L}}{\partial \theta^{i}_{\tilde{\mu}\tilde{\nu}}} = \frac{\partial \mathcal{L}}{\partial U_{pq}} \end{aligned} \tag{3.54}$$

The first ten are already fulfilled at the end of the DLPNO-MP2 energy calculation. The PNO amplitudes are obtained by iteratively solving the amplitude equations:

$$\begin{aligned} 0 \equiv \frac{\partial \mathcal{L}}{\partial \widetilde{T}^{ij*}_{\tilde{a}\tilde{b}}} = \frac{\partial E^{\mathrm{DLPNO}}_2}{\partial \widetilde{T}^{ij*}_{\tilde{a}\tilde{b}}} = K^{ij*}_{\tilde{a}\tilde{b}} + \sum_{\tilde{c}} \left(T^{ij}_{\tilde{a}\tilde{c}} F^{ij}_{\tilde{b}\tilde{c}} + F^{ij}_{\tilde{a}\tilde{c}} T^{ij}_{\tilde{c}\tilde{b}}\right) \\ - \sum_{k\tilde{c}\tilde{d}} \left(F_{kj} S^{ij,ik}_{\tilde{a}\tilde{c}} T^{ik}_{\tilde{c}\tilde{d}} S^{ik,ij*}_{\tilde{d}\tilde{b}} + F_{ki} S^{ij,kj}_{\tilde{a}\tilde{c}} T^{kj}_{\tilde{c}\tilde{d}} S^{kj,ij*}_{\tilde{d}\tilde{b}}\right) \end{aligned} \tag{3.55}$$

Note that the equations obtained from the derivative with respect to the contravariant amplitudes, $\partial\mathcal{L}/\partial\widetilde{\mathbf{T}}^{ij}$, are equivalent to a linear combination of $\partial\mathcal{L}/\partial\mathbf{T}^{ij}$ and $\partial\mathcal{L}/\partial\mathbf{T}^{ji}$ but produce a more convenient expression (as was shown for RI-MP2 in Section 2.1.3.2). As explained in refs. 130 and 144, terms in the sum over k in eq. 3.55 are skipped if the corresponding element of the Fock matrix has an absolute value below a threshold $F_{\mathrm{Cut}} = 10^{-5}$.

The semi-canonical amplitude stationarity conditions take the form:

$$\begin{aligned} 0 \equiv \frac{\partial \mathcal{L}}{\partial \widehat{\mathbf{T}}^{ij}} = \boldsymbol{\theta}^{ij*} \Bigg[\frac{1}{1+\delta_{ij}} \left(2\mathbf{K}^{ij} - \mathbf{K}^{ji} - 2\mathbf{N}^{ij}\mathbf{K}^{ij}\mathbf{N}^{ij} + \mathbf{N}^{ij}\mathbf{K}^{ji}\mathbf{N}^{ij}\right) \\ + \frac{1}{2} \left(\mathbf{v}^{ij,\mathrm{T}} \widetilde{\breve{\mathbf{T}}}^{ij*} + \widetilde{\breve{\mathbf{T}}}^{ij*} \mathbf{v}^{ij} + \mathbf{F}^{ij*} \mathbf{w}^{ij} + \mathbf{w}^{ij} \mathbf{F}^{ij} - \mathbf{w}^{ij} \left(F_{jj} + F_{ii}\right)\right) \Bigg] \boldsymbol{\theta}^{ij\dagger} \end{aligned} \tag{3.56}$$

$$0 \equiv \frac{\partial \mathcal{L}}{\partial \widehat{\mathbf{T}}^{ij*}} = \left(\frac{\partial \mathcal{L}}{\partial \widehat{\mathbf{T}}^{ij}}\right)^* \tag{3.57}$$

The matrix $N^{ij}_{\tilde{a}''\tilde{b}''} = \sum_{\tilde{c}} \delta_{\tilde{c}\tilde{a}''}\delta_{\tilde{c}\tilde{b}''}$ is introduced to "select" the truncated PNO basis. eq. 3.56 can be transformed to the pseudo-canonical NPAO basis using the unitary matrix $S^{ij(0)}_{\tilde{a}''\tilde{\mu}}$ and solved for $\mathbf{w}^{ij}$ at $\boldsymbol{\lambda} = 0$ (i.e. $\boldsymbol{\theta}^{ij} = \mathbf{I}$):

$$\begin{aligned}\left(F^{ij}_{\tilde{\mu}} + F^{ij}_{\tilde{\nu}} - F_{jj} - F_{ii}\right) w^{ij}_{\tilde{\mu}\tilde{\nu}} = -\sum_{\tilde{a}''\tilde{b}''} S^{ij(0)}_{\tilde{a}''\tilde{\mu}} \Bigg[&\frac{1 - \delta_{\tilde{a}\tilde{a}''}\delta_{\tilde{b}\tilde{b}''}}{1 + \delta_{ij}} \left(4\mathbf{K}^{ij} - 2\mathbf{K}^{ji}\right) \\ &+ \left(\mathbf{v}^{ij,\mathrm{T}} \widetilde{\breve{\mathbf{T}}}^{ij*} + \widetilde{\breve{\mathbf{T}}}^{ij*} \mathbf{v}^{ij}\right) \Bigg]_{\tilde{a}''\tilde{b}''} S^{ij(0)}_{\tilde{b}''\tilde{\nu}}\end{aligned} \tag{3.58}$$

with

$$w^{ij}_{\tilde{\mu}\tilde{\nu}} = \sum_{\tilde{a}''\tilde{b}''} S^{ij(0)}_{\tilde{a}''\tilde{\mu}} w^{ij}_{\tilde{a}''\tilde{b}''} S^{ij(0)}_{\tilde{b}''\tilde{\nu}} \tag{3.59}$$

Equations for $\mathbf{v}^{ij}$ are obtained from the Lagrangian stationarity conditions with respect to $\theta^{ij}_{ab'}$:

$$\begin{aligned}\sum_{\tilde{c}} v^{ij}_{\tilde{c}\tilde{b}'} \breve{D}^{ij}_{\tilde{c}\tilde{a}} - \sum_{\tilde{c}'} \breve{D}^{ij}_{\tilde{b}'\tilde{c}'} v^{ij}_{\tilde{a}\tilde{c}'} = &2 \frac{\partial E_2^{\mathrm{DLPNO}}}{\partial \theta^{ij}_{\tilde{b}'\tilde{a}}}\Bigg|_{\boldsymbol{\lambda}=0} \\ &- \sum_{\tilde{c}} \left[K^{ji}_{\tilde{b}'\tilde{c}} \widetilde{\widehat{T}}^{ij}_{\tilde{c}\tilde{a}} + K^{ij}_{\tilde{b}'\tilde{c}} \widetilde{\widehat{T}}^{ij}_{\tilde{a}\tilde{c}} + K^{ij*}_{\tilde{a}\tilde{c}} \widetilde{\widehat{T}}^{ij*}_{\tilde{b}'\tilde{c}} + K^{ij*}_{\tilde{c}\tilde{a}} \widetilde{\widehat{T}}^{ij*}_{\tilde{c}\tilde{b}'} \right]\end{aligned} \tag{3.60}$$

These can be solved in the PNO+CPNO basis, which diagonalizes $\breve{\mathbf{D}}^{ij}$. A detailed derivation, as well as expressions for $\mathbf{x}^{ij}$ is given in Appendix D. The remaining Lagrange multipliers $\mathbf{z}$, $\bar{\mathbf{z}}$, and $\mathbf{x}$ are determined from the MO rotation stationarity conditions. As expected, the Lagrangian is invariant to rotations among virtual orbitals, but occupied–virtual and occupied–occupied (core–core or valence–valence) rotations lead to the so-called z-vector coupled perturbed self-consistent field (Z-CPSCF)[239] and z-vector coupled perturbed localization (Z-CPL)[169] equations for $\mathbf{z}$ and $\mathbf{l}$, respectively, while rotations between core and valence orbitals result in the z-vector core–valence (Z-CV) equations for $\bar{\mathbf{z}}$. For rotations within a block of localized orbitals (either core or valence), we obtain the Z-CPL equations:

$$R^{\mathrm{loc}}_{ij}[\mathbf{l}] - \left(R^{\mathrm{loc}}_{ji}[\mathbf{l}]\right)^* = -L_{ij} \tag{3.61}$$

$$\begin{aligned}L_{ij} = &2\sum_k D'^{\mathrm{o}}_{ik} F_{jk} - 2\sum_k F_{ki} D'^{\mathrm{o}}_{kj} \\ &+ \sum_{K\tilde{\mu}'} \Gamma^{K*}_{j\tilde{\mu}'} (K|i\tilde{\mu}') - \sum_{K\tilde{\mu}'} \Gamma^{K}_{i\tilde{\mu}'} (j\tilde{\mu}'|K) + L^{\mathrm{Pre}}_{ij}\end{aligned} \tag{3.62}$$

where i, j, k are all within the same (core or valence) block. The localization response operator is defined as follows (note the change in sign and indexing compared to ref. 192):

$$R^{\mathrm{loc}}_{pi}[\mathbf{l}] = \sum_k \Big[l_{ki} r_{kp} (r_{kk} - r_{ii}) - r_{ip} (r_{ki} l_{ki} + r^*_{ki} l^*_{ki}) \Big] \quad \text{with} \quad \mathbf{l}^\dagger = -\mathbf{l} \tag{3.63}$$

$\Gamma^K_{i\tilde{\mu}'}$ is the two-body density matrix:

$$\Gamma^K_{i\tilde{\mu}'} = \sum_j (1 + \delta_{ij})\, G^{i(ij)}_{K\tilde{\mu}'} \tag{3.64}$$

$$G^{i(ij)}_{K\tilde{\mu}'} = \sum_{L\tilde{a}''\tilde{b}''} d''^{ij}_{\tilde{\mu}'\tilde{a}''} g^{ij}_{\tilde{a}''\tilde{b}''} \left(j\tilde{b}''\middle|L\right) \left(\mathbf{V}^{-1}\right)_{LK} \quad \text{with} \quad V_{KL} = (K|L) \tag{3.65}$$

$$g^{ij}_{\tilde{a}''\tilde{b}''} = \delta_{\tilde{a}''\tilde{a}}\delta_{\tilde{b}''\tilde{b}} \left(2\widetilde{T}^{ij}_{\tilde{a}\tilde{b}} - \widetilde{\overline{T}}^{ij}_{\tilde{a}\tilde{b}}\right) + \widetilde{\overline{T}}^{ij}_{\tilde{a}''\tilde{b}''} + w^{ij*}_{\tilde{a}''\tilde{b}''} \tag{3.66}$$

L^{Pre}_{ij} contains contributions from the approximate exchange integrals in the prescreening correction:

$$L^{\mathrm{Pre}}_{ij} = \sum_x \left[\sum_{\tilde{\mu}'} \left(r^{x*}_{i\tilde{\mu}'} y^{\alpha,x*}_{j\tilde{\mu}'} - r^{x}_{j\tilde{\mu}'} y^{\alpha,x}_{i\tilde{\mu}'}\right) + \frac{1}{2} r^{x*}_{ij} \left(y^{\beta,x}_{j} + y^{\beta,x*}_{j} - y^{\beta,x}_{i} - y^{\beta,x*}_{i}\right)\right] \tag{3.67}$$

where

$$y^{\alpha,x}_{i\tilde{\mu}'} = 8 \sum_j 1_{\mathrm{S}}(ij) \sum_{\tilde{\nu}\tilde{\eta}} \pi^{i}_{\tilde{\mu}'\tilde{\nu}} t^{ij}_{\tilde{\nu}\tilde{\eta}} \left[\frac{r^{x}_{j\tilde{\eta}}}{|\mathbf{R}_{ij}|^3} - 3\frac{R^{x}_{ij}\left(\mathbf{r}_{j\tilde{\eta}}\mathbf{R}_{ij}\right)}{|\mathbf{R}_{ij}|^5}\right] \tag{3.68}$$

$$\begin{aligned} y^{\beta,x}_{i} = \sum_j 1_{\mathrm{S}}(ij) \sum_{\tilde{\mu}\tilde{\nu}} t^{ij}_{\tilde{\mu}\tilde{\nu}} \Bigg[& \left(48\frac{\mathbf{r}_{i\tilde{\mu}}\mathbf{r}_{j\tilde{\nu}}}{|\mathbf{R}_{ij}|^5} - 240\frac{\left(\mathbf{r}_{i\tilde{\mu}}\mathbf{R}_{ij}\right)\left(\mathbf{r}_{j\tilde{\nu}}\mathbf{R}_{ij}\right)}{|\mathbf{R}_{ij}|^7}\right) R^{x}_{ji} \\ & - 48\frac{r^{x}_{i\tilde{\mu}}\left(\mathbf{r}_{j\tilde{\nu}}\mathbf{R}_{ij}\right) + r^{x}_{j\tilde{\nu}}\left(\mathbf{r}_{i\tilde{\mu}}\mathbf{R}_{ij}\right)}{|\mathbf{R}_{ij}|^5}\Bigg] \end{aligned} \tag{3.69}$$

The Z-CPL eqs. 3.61 must be solved iteratively. The stationarity condition w.r.t. rotations between core and valence MOs gives the Z-CV equations:

$$\sum_k \bar{z}_{mk} F_{jk} - \sum_n F_{nm} \bar{z}_{nj} = L^{\mathrm{CV}}_{mj} \tag{3.70}$$

$$L^{\mathrm{CV}}_{mj} = \sum_{K\tilde{\mu}'} \Gamma^{K*}_{j\tilde{\mu}'} (K|m\tilde{\mu}') - \sum_{K\tilde{\mu}'} \Gamma^{K}_{m\tilde{\mu}'} (j\tilde{\mu}'|K) + R^{\mathrm{loc}}_{mj}[\mathbf{l}] - \left(R^{\mathrm{loc}}_{jm}[\mathbf{l}]\right)^* + L^{\mathrm{Pre}}_{mj} \tag{3.71}$$

These are solved in the CMO basis. Note that in frozen-core calculations the terms involving $\Gamma^{K}_{m\tilde{\mu}'}$, $y^{\alpha,x}_{m\tilde{\mu}'}$, and $y^{\beta,x}_{m}$ drop out.

Finally, the Z-CPSCF equations are obtained from the occupied-virtual block of eq. D.22:

$$\sum_b z_{ib} F_{ab} - \sum_j F_{ji} z_{ja} + 2g_{ai}[\mathbf{z}] = L_{ia} \tag{3.72}$$

with the two-electron operator defined as:

$$g_{ai}[\mathbf{z}] \equiv \sum_{pq} z_{pq} \left(ai \,||\, pq\right) = \sum_{jb} \left[z_{jb} \left(ai \,||\, jb\right) + z^*_{jb} \left(ai \,||\, bj\right)\right] \tag{3.73}$$

$$\left(rs \,||\, pq\right) = (rs|pq) - \frac{1}{2}(rq|ps) \tag{3.74}$$

and likewise for matrices in the AO basis. The right-hand side of eq. 3.72 contains several terms:

$$L_{ia} = Y^{\alpha}_{ia} + \sum_{\tilde{\mu}'} \left[S^*_{i\mu} N_{\tilde{\mu}'} Y^{\beta}_{a\tilde{\mu}'} + S_{a\mu} N_{\tilde{\mu}'} Y^{\beta*}_{i\tilde{\mu}'} - S^*_{i\mu} N_{\tilde{\mu}'} Y^{\gamma}_{\tilde{\mu}'} S_{a\tilde{\mu}'}\right] \tag{3.75}$$

Note that the sum in eq. 3.75 assumes a one-to-one correspondence between PAOs and their parent AOs and that $S_{a\tilde{\mu}'} = S_{a\mu}$. The intermediates $\mathbf{Y}^{\alpha}$, $\mathbf{Y}^{\beta}$, and $\mathbf{Y}^{\gamma}$ are defined as follows:

$$Y^{\alpha}_{ia} = -\sum_{K\tilde{\mu}'} \Gamma^{K}_{i\tilde{\mu}'} (a\tilde{\mu}'|K) - 4g_{ai}\left[\mathbf{D}' + \frac{1}{2}\mathbf{c}^*\bar{\mathbf{z}}\mathbf{c}^{\mathrm{T}}\right] - \left(R^{\mathrm{loc}}_{ai}[\mathbf{l}]\right)^*$$

$$- \sum_{x\tilde{\mu}'} r^x_{a\tilde{\mu}'} y^{\alpha,x}_{i\tilde{\mu}'} - \frac{1}{2} \sum_x r^x_{ai} \left(y^{\beta,x}_i + y^{\beta,x*}_i \right) \tag{3.76}$$

$$Y^{\beta}_{p\tilde{\mu}'} = \sum_{Ki} \Gamma^{K*}_{i\tilde{\mu}'} (K|ip) + 2 \sum_{\tilde{\nu}'} D'^{\mathrm{rv}}_{\tilde{\mu}'\tilde{\nu}'} F_{p\tilde{\nu}'} + \sum_{\tilde{\nu}'} Y^{\delta}_{\tilde{\mu}'\tilde{\nu}'} S_{p\tilde{\nu}'} + \sum_{xi} r^x_{pi} y^{\alpha,x*}_{i\tilde{\mu}'} \tag{3.77}$$

$$\begin{aligned} Y^{\gamma}_{\tilde{\mu}'} = {} & \frac{1}{2} \sum_{Ki} \Gamma^{K}_{i\tilde{\mu}'} (i\tilde{\mu}'|K) + \sum_{\tilde{\nu}'} D'^{\mathrm{rv}}_{\tilde{\mu}'\tilde{\nu}'} F_{\tilde{\mu}'\tilde{\nu}'} + \frac{1}{2} \sum_{\tilde{\nu}'} Y^{\delta}_{\tilde{\mu}'\tilde{\nu}'} S_{\tilde{\mu}'\tilde{\nu}'} + \frac{1}{2} \sum_{xi} y^{\alpha,x}_{i\tilde{\mu}'} r^x_{i\tilde{\mu}'} \\ & + \text{complex conjugate} \end{aligned} \tag{3.78}$$

$$Y^{\delta}_{\tilde{\mu}'\tilde{\nu}'} = \sum_{i \geq j} \left(\xi^{ij}_{\tilde{\mu}'\tilde{\nu}'} + \xi^{ij*}_{\tilde{\nu}'\tilde{\mu}'} - 2 \sum_{\tilde{a}} d''^{ij*}_{\tilde{\mu}'\tilde{a}} \tau^{ij}_{\tilde{a}\tilde{\nu}'} \right) - y^{\delta}_{\tilde{\mu}'\tilde{\nu}'} - y^{\delta*}_{\tilde{\nu}'\tilde{\mu}'} \tag{3.79}$$

$$\begin{aligned} \xi^{ij}_{\tilde{\mu}'\tilde{\nu}'} &= \left(\mathbf{d}''^{ij*} \mathbf{x}^{ij} \mathbf{d}''^{ij,\mathrm{T}} \right)_{\tilde{\mu}'\tilde{\nu}'} \\ &= \sum_{\tilde{b}''\tilde{\lambda}'} d''^{ij*}_{\tilde{\mu}'\tilde{b}''} d''^{ij}_{\tilde{\lambda}'\tilde{b}''} \left[-\frac{1}{2} \sum_K \left(G^{i(ij)}_{K\tilde{\nu}'} \left(i\tilde{\lambda}' \middle| K \right) + G^{j(ij)}_{K\tilde{\nu}'} \left(j\tilde{\lambda}' \middle| K \right) \right) \right. \\ &\quad \left. - \sum_{\tilde{\kappa}'} F_{\tilde{\kappa}'\tilde{\lambda}'} D'^{\mathrm{rv}}_{\tilde{\kappa}'\tilde{\nu}'} + \sum_{\tilde{\kappa}'\tilde{a}} S_{\tilde{\kappa}'\tilde{\lambda}'} \tau^{ij*}_{\tilde{a}\tilde{\kappa}'} d^{ij}_{\tilde{\nu}'\tilde{a}} \right] \end{aligned} \tag{3.80}$$

$$\begin{aligned} \tau^{ij}_{\tilde{a}\tilde{\kappa}'} = \sum_k \Big[& F_{kj} \left(\widetilde{\mathbf{T}}^{ij*} \mathbf{S}^{ij,ki} \mathbf{T}^{ki} + \widetilde{\mathbf{T}}^{ji*} \mathbf{S}^{ij,ki} \mathbf{T}^{ik} \right) \mathbf{d}^{ki,\mathrm{T}} \\ & + F_{ki} \left(\widetilde{\mathbf{T}}^{ij*} \mathbf{S}^{ij,jk} \mathbf{T}^{jk} + \widetilde{\mathbf{T}}^{ji*} \mathbf{S}^{ij,jk} \mathbf{T}^{kj} \right) \mathbf{d}^{jk,\mathrm{T}} \Big]_{\tilde{a}\tilde{\kappa}'} \end{aligned} \tag{3.81}$$

$$\mathbf{y}^{\delta} = - \sum_i \boldsymbol{\pi}^{i*} \mathbf{x}^i \boldsymbol{\pi}^{i,\mathrm{T}} = 4 \sum_{ij} 1_{\mathrm{S}}(ij) \boldsymbol{\pi}^{i*} \left(\mathbf{M}^{ij} + \mathbf{F}^{i*} \mathbf{t}^{ij*} \right) \mathbf{t}^{ji} \boldsymbol{\pi}^{i,\mathrm{T}} \tag{3.82}$$

As discussed in Appendix D, $\mathbf{x}^{ij}$ is already Hermitian if eqs. 3.58 and 3.60 are fulfilled, so the first two terms in eq. 3.79 are actually equivalent. The same applies to the multipliers $\mathbf{x}^i$, which are obtained analogously by solving $\partial\mathcal{L}/\partial\boldsymbol{\theta}^i = \partial\mathcal{L}/\partial\boldsymbol{\theta}^{i\dagger} = 0$. We note that the first term in eq. 3.82 is missing from eq. 56 of ref. 192, which appears to be an error in the publication as the term was in fact implemented in the DLPNO-MP2 gradient code. This is the final major step of the DLPNO-MP2 density calculation, after which $\mathbf{D}$ can be completed.

3.1.5 Equations for second derivatives

The second derivative of the DLPNO-MP2 energy with respect to perturbations $\boldsymbol{\kappa}$ and $\boldsymbol{\lambda}$, the latter being an electric or magnetic field in this work, is equal to the derivative of eq. 3.45:

$$\frac{\mathrm{d}^2 E_{\text{DLPNO-MP2}}}{\mathrm{d}\boldsymbol{\lambda}\mathrm{d}\boldsymbol{\kappa}} = \frac{\mathrm{d}}{\mathrm{d}\boldsymbol{\lambda}} \frac{\partial\mathcal{L}}{\partial\boldsymbol{\kappa}} = \sum_{\mu\nu} \left(D^{\mathrm{SCF}}_{\mu\nu} + D_{\mu\nu} \right) h^{\boldsymbol{\kappa},\boldsymbol{\lambda}}_{\mu\nu} + \sum_{\mu\nu} \left(D^{\mathrm{SCF},\boldsymbol{\lambda}}_{\mu\nu} + D^{\boldsymbol{\lambda}}_{\mu\nu} \right) h^{\boldsymbol{\kappa}}_{\mu\nu} \tag{3.83}$$

Apart from the second derivative integrals $\mathbf{h}^{\boldsymbol{\kappa},\boldsymbol{\lambda}}$ (which are zero for the polarizability, i.e. when $\boldsymbol{\kappa} = \boldsymbol{\lambda} = \mathbf{F}^{\mathrm{ext}}$), evaluating this expression requires derivatives of the Lagrange parameters and unknown multipliers w.r.t. $\boldsymbol{\lambda}$, which are obtained by taking derivatives of the constraints and stationarity conditions discussed in the previous section. Note that all $\boldsymbol{\lambda}$-derivatives in this section are real for electric perturbations and imaginary for magnetic

ones. The SCF response density $\mathbf{D}^{\mathrm{SCF},\boldsymbol{\lambda}}$ requires the MO response coefficients $\mathbf{U}^{\boldsymbol{\lambda}}$:

$$\begin{aligned} D_{\mu\nu}^{\mathrm{SCF},\boldsymbol{\lambda}} &= 2\sum_{pi}\left(c_{\mu p}^{*}U_{pi}^{\boldsymbol{\lambda}*}c_{\nu i} + c_{\mu i}^{*}U_{pi}^{\boldsymbol{\lambda}}c_{\nu p}\right) \\ &= 2\sum_{ai}\left(c_{\mu a}^{*}U_{ai}^{\boldsymbol{\lambda}*}c_{\nu i} + c_{\mu i}^{*}U_{ai}^{\boldsymbol{\lambda}}c_{\nu a}\right) - 2\sum_{ij}c_{\mu j}^{*}S_{ij}^{(\boldsymbol{\lambda})}c_{\nu i} \end{aligned} \tag{3.84}$$

where in the second line we have used the perturbed MO orthonormality constraint:

$$U_{pq}^{\boldsymbol{\lambda}} + U_{qp}^{\boldsymbol{\lambda}*} + S_{pq}^{(\boldsymbol{\lambda})} = 0 \quad \text{with} \quad S_{pq}^{(\boldsymbol{\lambda})} = \sum_{\mu\nu} c_{\mu p}^{(0)*} S_{\mu\nu}^{\boldsymbol{\lambda}} c_{\nu q}^{(0)} \tag{3.85}$$

We note in passing that the AOs depend on the external magnetic field when GIAOs are used, but not on the external electric field, thus $S_{\mu\nu}^{\mathbf{F}^{\mathrm{ext}}} = 0$. $U_{ai}^{\boldsymbol{\lambda}}$ are obtained from the perturbed Brillouin condition, which in conjunction with eq. 3.85 gives the CPSCF equations:[303]

$$\begin{aligned} \sum_{b} F_{ab}U_{bi}^{\boldsymbol{\lambda}} - \sum_{j} U_{aj}^{\boldsymbol{\lambda}}F_{ji} + 2\sum_{bj}\left[U_{bj}^{\boldsymbol{\lambda}*}\left(ai\,||\,bj\right) + U_{bj}^{\boldsymbol{\lambda}}\left(ai\,||\,jb\right)\right] \\ = \sum_{j} S_{aj}^{(\boldsymbol{\lambda})}F_{ji} - F_{ai}^{(\boldsymbol{\lambda})} + 2\sum_{kj} S_{jk}^{(\boldsymbol{\lambda})}\left(ai\,||\,kj\right) \end{aligned} \tag{3.86}$$

where $\mathbf{F}^{(\boldsymbol{\lambda})}$ excludes derivatives of the MO coefficients. In the electric (magnetic) field case the right-hand side is real (imaginary) and therefore so are $U_{ai}^{\boldsymbol{\lambda}}$. The equations are solved in the CMO basis as usual, and the solution is transformed to the LMO basis. The remaining blocks of $\mathbf{U}^{\boldsymbol{\lambda}}$, which are needed below, are obtained from the perturbed localization, core–valence separation, and MO orthonormality constraints as follows. The core-valence block is obtained from the condition $F_{im}^{\boldsymbol{\lambda}} = 0$ (in conjunction with eq. 3.85):

$$\sum_{j} F_{ij}U_{jm}^{\boldsymbol{\lambda}} - \sum_{n} U_{in}^{\boldsymbol{\lambda}}F_{nm} = \sum_{n} S_{in}^{(\boldsymbol{\lambda})}F_{nm} - F_{im}^{(\boldsymbol{\lambda})} - g_{im}\left[\mathbf{D}^{\mathrm{SCF},\boldsymbol{\lambda}}\right] \tag{3.87}$$

which can be solved in the CMO basis. The valence-valence block of $\mathbf{U}^{\boldsymbol{\lambda}}$ is obtained from the perturbed localization condition $s_{ij}^{\boldsymbol{\lambda}} = 0$, which gives the CPL equations:[169]

$$\sum_{k<l} U_{kl}^{\boldsymbol{\lambda}}A_{kl,ij}^{\mathrm{loc},\pm} = -B_{ij}^{\boldsymbol{\lambda},\pm} \tag{3.88}$$

$$\begin{aligned} B_{ij}^{\boldsymbol{\lambda},\pm} &= s_{ij}^{(\boldsymbol{\lambda})} - \sum_{k<l} S_{lk}^{(\boldsymbol{\lambda})}\left(\frac{\mathrm{d}s_{ij}}{\mathrm{d}U_{lk}} \pm \frac{\mathrm{d}s_{ji}}{\mathrm{d}U_{lk}}\right) \\ &\quad + \sum_{pk}\left(\delta_{pm} + \delta_{pa}\right)U_{pk}^{\boldsymbol{\lambda}}\left(\frac{\mathrm{d}s_{ij}}{\mathrm{d}U_{pk}} \pm \frac{\mathrm{d}s_{ji}}{\mathrm{d}U_{pk}}\right) \end{aligned} \tag{3.89}$$

where the plus/minus signs are used in the magnetic/electric field case, respectively, and

$$A_{pq,rs}^{\mathrm{loc},\pm} = \frac{\mathrm{d}s_{rs}}{\mathrm{d}U_{pq}} + \frac{\mathrm{d}s_{sr}}{\mathrm{d}U_{qp}} \pm \frac{\mathrm{d}s_{sr}}{\mathrm{d}U_{pq}} \pm \frac{\mathrm{d}s_{rs}}{\mathrm{d}U_{qp}} \tag{3.90}$$

$$\frac{\mathrm{d}s_{rs}}{\mathrm{d}U_{pq}} = r_{rs}(r_{rp}\delta_{qr} - r_{sp}\delta_{qs}) + \delta_{qs}r_{rp}(r_{rr} - r_{ss}) \tag{3.91}$$

$\mathbf{s}^{(\boldsymbol{\lambda})}$ excludes derivatives of the MO coefficients and is only non-zero in the GIAO case, where it contains the perturbed dipole integrals:

$$r^{B_\alpha}_{\mu\nu,\beta} = \frac{\mathrm{i}}{2} \langle\mu| \left(\mathbf{R}_{MN} \times \mathbf{r}\right)_\alpha r_\beta |\nu\rangle \tag{3.92}$$

which can be calculated as linear combinations of quadrupole integrals. If all electrons are included in the MP2 treatment, an analogous set of CPL equations must be solved for the core-core block, which can be obtained from eq. 3.88 by substituting core for valence indices and vice versa. In the frozen-core approximation, the core-core block of $\mathbf{U}^{\boldsymbol{\lambda}}$ is only constrained by eq. 3.85, which can be solved as

$$U^{\boldsymbol{\lambda}}_{mn} = U^{\boldsymbol{\lambda}*}_{nm} = -\frac{1}{2} S^{(\boldsymbol{\lambda})}_{mn} \tag{3.93}$$

The same solution is used for the virtual-virtual block of $\mathbf{U}^{\boldsymbol{\lambda}}$. Note that the left-hand side of CPL equations in the electric field case is equivalent to that of the Z-CPL eqs. 3.61, which can be written as

$$\sum_{k<l} l_{kl} A^{\mathrm{loc},-}_{ij,kl} = -L_{ij} \tag{3.94}$$

and $A^{\mathrm{loc},\pm}_{ij,kl} = A^{\mathrm{loc},\pm}_{kl,ij}$ if $s_{ij} = 0$. Therefore, the same solver can be used for both equations (with some modifications for magnetic perturbations).

The expression for the DLPNO-MP2 response difference density $\mathbf{D}^{\boldsymbol{\lambda}}$ is obtained by straightforward differentiation of eqs. 3.47–3.53 and requires the perturbed Lagrange parameters $\mathbf{U}^{\boldsymbol{\lambda}}$, $\mathbf{z}^{\boldsymbol{\lambda}}$, $\bar{\mathbf{z}}^{\boldsymbol{\lambda}}$, $\mathbf{T}^{ij,\boldsymbol{\lambda}}$, $\widehat{\mathbf{T}}^{ij,\boldsymbol{\lambda}}$, $\mathbf{w}^{ij,\boldsymbol{\lambda}}$, $\boldsymbol{\theta}^{ij,\boldsymbol{\lambda}}$, $\mathbf{t}^{ij,\boldsymbol{\lambda}}$, and $\boldsymbol{\theta}^{i,\boldsymbol{\lambda}}$. The PAO coefficients $\widetilde{\mathbf{P}}$ also depend on the perturbation through $\mathbf{U}$:

$$\widetilde{P}^{\boldsymbol{\lambda}}_{\nu\tilde{\mu}'} = \widetilde{P}^{\mathrm{u},\boldsymbol{\lambda}}_{\nu\tilde{\mu}'_\mathrm{u}} N_{\tilde{\mu}'} + \widetilde{P}^{\mathrm{u}}_{\nu\tilde{\mu}'_\mathrm{u}} N^{\boldsymbol{\lambda}}_{\tilde{\mu}'} \tag{3.95}$$

$$\widetilde{P}^{\mathrm{u},\boldsymbol{\lambda}}_{\nu\tilde{\mu}'_\mathrm{u}} = -\frac{1}{2} \sum_\eta \left(P^{\boldsymbol{\lambda}}_{\nu\eta} S_{\eta\mu} + P_{\nu\eta} S^{\boldsymbol{\lambda}}_{\eta\mu}\right) \tag{3.96}$$

$$N^{\boldsymbol{\lambda}}_{\tilde{\mu}'} = -\frac{1}{2} N^3_{\tilde{\mu}'} S^{\boldsymbol{\lambda}}_{\tilde{\mu}'_\mathrm{u}\tilde{\mu}'_\mathrm{u}} \tag{3.97}$$

For magnetic perturbations $N^{\boldsymbol{\lambda}}_{\tilde{\mu}'} = 0$. The perturbed (C)PNO orthonormality condition gives a relationship analogous to eq. 3.85

$$\theta^{ij,\boldsymbol{\lambda}}_{\tilde{a}''\tilde{b}''} + \theta^{ij,\boldsymbol{\lambda}*}_{\tilde{b}''\tilde{a}''} + \mathcal{S}^{ij,\boldsymbol{\lambda}}_{\tilde{a}''\tilde{b}''} = 0 \quad \text{with} \quad \mathcal{S}^{ij,\boldsymbol{\lambda}}_{\tilde{a}''\tilde{b}''} = \sum_{\tilde{\mu}'\tilde{\nu}'} d''^{ij(0)*}_{\tilde{\mu}'\tilde{a}''} \widetilde{S}^{\boldsymbol{\lambda}}_{\tilde{\mu}'\tilde{\nu}'} d''^{ij(0)}_{\tilde{\nu}'\tilde{b}''} \tag{3.98}$$

Note that the perturbed PAO overlap $\widetilde{S}^{\boldsymbol{\lambda}}_{\tilde{\mu}'\tilde{\nu}'}$ includes the PAO response, eq. 3.95, and is non-zero even for electric perturbations, unlike the perturbed AO overlap. We use eq. 3.98 to remove the dependence on $\boldsymbol{\theta}^{ij,\boldsymbol{\lambda}}$ in the perturbed SC residual equations:

$$\begin{aligned}\left(F_{ii} + F_{jj}\right) \widehat{\mathbf{T}}^{ij,\boldsymbol{\lambda}} - \widehat{\mathbf{T}}^{ij,\boldsymbol{\lambda}} \boldsymbol{\mathcal{F}}^{ij*} - \boldsymbol{\mathcal{F}}^{ij} \widehat{\mathbf{T}}^{ij,\boldsymbol{\lambda}} &= \boldsymbol{\mathcal{K}}^{ij,\boldsymbol{\lambda}*} - \widehat{\mathbf{T}}^{ij} \left(F^{\boldsymbol{\lambda}}_{ii} + F^{\boldsymbol{\lambda}}_{jj}\right) \\ &+ \widehat{\mathbf{T}}^{ij} \left(\boldsymbol{\mathcal{F}}^{ij,\boldsymbol{\lambda}*} - \boldsymbol{\mathcal{S}}^{ij,\boldsymbol{\lambda}*} \boldsymbol{\mathcal{F}}^{ij*}\right) + \left(\boldsymbol{\mathcal{F}}^{ij,\boldsymbol{\lambda}} - \boldsymbol{\mathcal{F}}^{ij} \boldsymbol{\mathcal{S}}^{ij,\boldsymbol{\lambda}}\right) \widehat{\mathbf{T}}^{ij}\end{aligned} \tag{3.99}$$

where

$$\mathcal{K}^{ij,\boldsymbol{\lambda}}_{\tilde{a}''\tilde{b}''} = \sum_{\tilde{\mu}'\tilde{\nu}'} d''^{ij(0)}_{\tilde{\mu}'\tilde{a}''} K^{ij,\boldsymbol{\lambda}}_{\tilde{\mu}'\tilde{\nu}'} d''^{ij(0)}_{\tilde{\nu}'\tilde{b}''} \tag{3.100}$$

$$\mathcal{F}^{ij,\boldsymbol{\lambda}}_{\tilde{a}''\tilde{b}''} = \sum_{\tilde{\mu}'\tilde{\nu}'} d''^{ij(0)*}_{\tilde{\mu}'\tilde{a}''} F^{\boldsymbol{\lambda}}_{\tilde{\mu}'\tilde{\nu}'} d''^{ij(0)}_{\tilde{\nu}'\tilde{b}''} \tag{3.101}$$

eq. 3.99 is once again solved in the pseudo-canonical NPAO basis. Next, the perturbed PNO constraint gives the PNO-CPNO block of $\boldsymbol{\theta}^{ij,\boldsymbol{\lambda}}$:

$$\begin{aligned}\sum_{\tilde{c}} \breve{D}^{ij}_{\tilde{a}\tilde{c}} \theta^{ij,\boldsymbol{\lambda}}_{\tilde{b}'\tilde{c}} - \sum_{\tilde{c}'} \theta^{ij,\boldsymbol{\lambda}}_{\tilde{c}'\tilde{a}} \breve{D}^{ij}_{\tilde{c}'\tilde{b}'} = \Big(& \widetilde{\widehat{\mathbf{T}}}^{ij,\boldsymbol{\lambda}*} \widehat{\mathbf{T}}^{ji} + \widetilde{\widehat{\mathbf{T}}}^{ji,\boldsymbol{\lambda}*} \widehat{\mathbf{T}}^{ij} + \widetilde{\widehat{\mathbf{T}}}^{ij*} \widehat{\mathbf{T}}^{ji,\boldsymbol{\lambda}} + \widetilde{\widehat{\mathbf{T}}}^{ji*} \widehat{\mathbf{T}}^{ij,\boldsymbol{\lambda}} \\ & - \breve{\mathbf{D}}^{ij} \boldsymbol{\mathcal{S}}^{ij,\boldsymbol{\lambda}*} - \widetilde{\widehat{\mathbf{T}}}^{ij*} \boldsymbol{\mathcal{S}}^{ij,\boldsymbol{\lambda}} \widehat{\mathbf{T}}^{ji} - \widetilde{\widehat{\mathbf{T}}}^{ji*} \boldsymbol{\mathcal{S}}^{ij,\boldsymbol{\lambda}} \widehat{\mathbf{T}}^{ij} \Big)_{\tilde{a}\tilde{b}'}\end{aligned} \tag{3.102}$$

These equations are solved in the basis which diagonalizes $\breve{\mathbf{D}}^{ij}$. The PNO-PNO and CPNO-CPNO blocks of $\boldsymbol{\theta}^{ij,\boldsymbol{\lambda}}$ are only constrained by eq. 3.98 and can be assigned "symmetrically" analogously to eq. 3.93, although an alternative choice will be discussed in Section 3.2.2. The perturbed PNO amplitudes $\mathbf{T}^{ij,\boldsymbol{\lambda}}$ are then obtained from the perturbed PNO residual equations:

$$\begin{aligned} 0 \equiv \frac{\mathrm{d}}{\mathrm{d}\boldsymbol{\lambda}} \frac{\partial \mathcal{L}}{\partial \widetilde{T}^{ij*}_{\tilde{a}\tilde{b}}} &= X^{ij,\boldsymbol{\lambda}}_{\tilde{a}\tilde{b}} + \sum_{\tilde{c}} \left(T^{ij,\boldsymbol{\lambda}}_{\tilde{a}\tilde{c}} F^{ij}_{\tilde{b}\tilde{c}} + F^{ij}_{\tilde{a}\tilde{c}} T^{ij,\boldsymbol{\lambda}}_{\tilde{c}\tilde{b}} \right) \\ &\quad - \sum_{k\tilde{c}\tilde{d}} \left(F_{kj} S^{ij,ik}_{\tilde{a}\tilde{c}} T^{ik,\boldsymbol{\lambda}}_{\tilde{c}\tilde{d}} S^{ik,ij*}_{\tilde{d}\tilde{b}} + F_{ki} S^{ij,kj}_{\tilde{a}\tilde{c}} T^{kj,\boldsymbol{\lambda}}_{\tilde{c}\tilde{d}} S^{kj,ij*}_{\tilde{d}\tilde{b}} \right) \end{aligned} \tag{3.103}$$

$$X^{ij,\boldsymbol{\lambda}}_{\tilde{a}\tilde{b}} = K^{ij,\boldsymbol{\lambda}*}_{\tilde{a}\tilde{b}} + \sum_{\tilde{c}} \left(T^{ij}_{\tilde{a}\tilde{c}} F^{ij,\boldsymbol{\lambda}}_{\tilde{b}\tilde{c}} + F^{ij,\boldsymbol{\lambda}}_{\tilde{a}\tilde{c}} T^{ij}_{\tilde{c}\tilde{b}} \right) \tag{3.104}$$

$$- \sum_{k\tilde{c}\tilde{d}} \left[\left(F_{kj} S^{ij,ik}_{\tilde{a}\tilde{c}} S^{ik,ij*}_{\tilde{d}\tilde{b}} \right)^{\boldsymbol{\lambda}} T^{ik}_{\tilde{c}\tilde{d}} + \left(F_{ki} S^{ij,kj}_{\tilde{a}\tilde{c}} S^{kj,ij*}_{\tilde{d}\tilde{b}} \right)^{\boldsymbol{\lambda}} T^{kj}_{\tilde{c}\tilde{d}} \right] \tag{3.105}$$

which can be solved iteratively with the same solver as eq. 3.55. The prescreening contributions to the response density, $\mathbf{D}^{\mathrm{o(Pre)},\boldsymbol{\lambda}}$ and $\mathbf{D}^{\mathrm{v(Pre)},\boldsymbol{\lambda}}$ require the NPAO response coefficients $\boldsymbol{\theta}^{i,\boldsymbol{\lambda}}$, which are only constrained by the perturbed NPAO orthonormality condition with the possible solution:

$$\theta^{i,\boldsymbol{\lambda}}_{\tilde{\mu}\tilde{\nu}} = \theta^{i,\boldsymbol{\lambda}*}_{\tilde{\nu}\tilde{\mu}} = -\frac{1}{2} \mathcal{S}^{i,\boldsymbol{\lambda}}_{\tilde{\mu}\tilde{\nu}} \quad \text{with} \quad \mathcal{S}^{i,\boldsymbol{\lambda}}_{\tilde{\mu}\tilde{\nu}} = \sum_{\tilde{\mu}'\tilde{\nu}'} \pi^{i(0)*}_{\tilde{\mu}'\tilde{\mu}} \widetilde{S}^{\boldsymbol{\lambda}}_{\tilde{\mu}'\tilde{\nu}'} \pi^{i(0)}_{\tilde{\nu}'\tilde{\nu}} \tag{3.106}$$

Also required are the perturbed prescreening amplitudes, obtained from the equations $\frac{\mathrm{d}}{\mathrm{d}\boldsymbol{\lambda}} \frac{\partial \mathcal{L}}{\partial \mathbf{t}^{ij*}} = 0$ giving:

$$\begin{aligned} t^{ij,\boldsymbol{\lambda}}_{\tilde{\mu}\tilde{\nu}} = (F_{ii} + F_{jj} - F^i_{\tilde{\mu}} - F^i_{\tilde{\nu}})^{-1} \Big[& M^{ij,\boldsymbol{\lambda}*}_{\tilde{\mu}\tilde{\nu}} \\ & - (F^{\boldsymbol{\lambda}}_{ii} + F^{\boldsymbol{\lambda}}_{jj}) t^{ij}_{\tilde{\mu}\tilde{\nu}} + \sum_{\tilde{\eta}} \Big(F^{i,\boldsymbol{\lambda}}_{\tilde{\mu}\tilde{\eta}} t^{ij}_{\tilde{\eta}\tilde{\nu}} + t^{ij}_{\tilde{\mu}\tilde{\eta}} F^{j,\boldsymbol{\lambda}}_{\tilde{\nu}\tilde{\eta}} \Big) \Big] \end{aligned} \tag{3.107}$$

$$\begin{aligned} M^{ij,\lambda_x}_{\tilde{\mu}\tilde{\nu}} = & \frac{\mathbf{r}^{\lambda_x}_{i\tilde{\mu}} \mathbf{r}_{j\tilde{\nu}} + \mathbf{r}_{i\tilde{\mu}} \mathbf{r}^{\lambda_x}_{j\tilde{\nu}}}{|\mathbf{R}_{ij}|^3} - 3 \frac{\left(\mathbf{r}^{\lambda_x}_{i\tilde{\mu}} \mathbf{R}_{ij}\right) \left(\mathbf{r}_{j\tilde{\nu}} \mathbf{R}_{ij}\right) + \left(\mathbf{r}_{i\tilde{\mu}} \mathbf{R}_{ij}\right) \left(\mathbf{r}^{\lambda_x}_{j\tilde{\nu}} \mathbf{R}_{ij}\right)}{|\mathbf{R}_{ij}|^5} \\ & - 3 \frac{\left(\mathbf{r}_{i\tilde{\mu}} \mathbf{R}^{\lambda_x}_{ij}\right) \left(\mathbf{r}_{j\tilde{\nu}} \mathbf{R}_{ij}\right) + \left(\mathbf{r}_{i\tilde{\mu}} \mathbf{R}_{ij}\right) \left(\mathbf{r}_{j\tilde{\nu}} \mathbf{R}^{\lambda_x}_{ij}\right)}{|\mathbf{R}_{ij}|^5} \\ & - 3 \left(\mathbf{R}_{ij} \mathbf{R}^{\lambda_x}_{ij}\right) \left(\frac{\mathbf{r}_{i\tilde{\mu}} \mathbf{r}_{j\tilde{\nu}}}{|\mathbf{R}_{ij}|^5} - 5 \frac{\left(\mathbf{r}_{i\tilde{\mu}} \mathbf{R}_{ij}\right) \left(\mathbf{r}_{j\tilde{\nu}} \mathbf{R}_{ij}\right)}{|\mathbf{R}_{ij}|^7} \right) \end{aligned} \tag{3.108}$$

For magnetic perturbations $\mathbf{R}^{\boldsymbol{\lambda}}_{ij} = 0$. The perturbed Lagrange multipliers $\mathbf{w}^{ij,\boldsymbol{\lambda}}$ are obtained from the equations:

$$\sum_{\tilde{c}''} \left(w^{ij,\boldsymbol{\lambda}}_{\tilde{a}''\tilde{c}''} F^{ij}_{\tilde{c}''\tilde{b}''} + F^{ij}_{\tilde{c}''\tilde{a}''} w^{ij,\boldsymbol{\lambda}}_{\tilde{c}''\tilde{b}''} \right) - \left(F_{ii} + F_{jj}\right) w^{ij,\boldsymbol{\lambda}}_{\tilde{a}''\tilde{b}''} = -W^{ij,\boldsymbol{\lambda}}_{\tilde{a}''\tilde{b}''} \tag{3.109}$$

which are solved in the pseudo-canonical NPAO basis with

$$\begin{aligned} \mathbf{W}^{ij,\boldsymbol{\lambda}} = \frac{\mathrm{d}}{\mathrm{d}\boldsymbol{\lambda}} \Bigg\{ \boldsymbol{\theta}^{ij*} \Bigg[& \mathbf{F}^{ij*} \mathbf{w}^{ij(0)} + \mathbf{w}^{ij(0)} \mathbf{F}^{ij} - \left(F_{ii} + F_{jj}\right) \mathbf{w}^{ij(0)} \\ & + \frac{2}{1+\delta_{ij}} \left(2\mathbf{K}^{ij} - \mathbf{K}^{ji} - 2\mathbf{N}^{ij}\mathbf{K}^{ij}\mathbf{N}^{ij} + \mathbf{N}^{ij}\mathbf{K}^{ji}\mathbf{N}^{ij} \right) \\ & + \widetilde{\overline{\mathbf{T}}}^{ij*} \mathbf{v}^{ij,\mathrm{T}} + \mathbf{v}^{ij} \widetilde{\overline{\mathbf{T}}}^{ij*} \Bigg] \boldsymbol{\theta}^{ij\dagger} \Bigg\} \end{aligned} \tag{3.110}$$

The equations for the perturbed multipliers $\mathbf{v}^{ij,\boldsymbol{\lambda}}$ are derived in Appendix D and have the form:

$$\sum_{\tilde{c}} v^{ij,\boldsymbol{\lambda}}_{\tilde{c}\tilde{b}'} \overline{D}^{ij}_{\tilde{c}\tilde{a}} - \sum_{\tilde{c}'} \overline{D}^{ij}_{\tilde{b}'\tilde{c}'} v^{ij,\boldsymbol{\lambda}}_{\tilde{a}\tilde{c}'} = -V^{ij,\boldsymbol{\lambda}}_{\tilde{b}'\tilde{a}} \tag{3.111}$$

with

$$\begin{aligned} V^{ij,\boldsymbol{\lambda}}_{\tilde{b}'\tilde{a}} = \frac{\mathrm{d}}{\mathrm{d}\boldsymbol{\lambda}} \Big[& \mathbf{v}^{ij(0),\mathrm{T}} \overline{\mathbf{D}}^{ij} - \overline{\mathbf{D}}^{ij} \mathbf{v}^{ij(0),\mathrm{T}} \\ & + \mathbf{K}^{ji}\mathbf{N}^{ij}\widetilde{\overline{\mathbf{T}}}^{ij} + \mathbf{K}^{ij}\mathbf{N}^{ij}\widetilde{\overline{\mathbf{T}}}^{ji} + \widetilde{\overline{\mathbf{T}}}^{ij*}\mathbf{N}^{ij}\mathbf{K}^{ji*} + \widetilde{\overline{\mathbf{T}}}^{ji*}\mathbf{N}^{ij}\mathbf{K}^{ij*} \\ & - 2\left(\mathbf{K}^{ji}\widetilde{\mathbf{T}}^{ij} + \mathbf{K}^{ij}\widetilde{\mathbf{T}}^{ji} + \mathbf{F}^{ij*}\mathbf{D}^{ij} - \mathbf{d}''^{ij,\mathrm{T}}\widetilde{\mathbf{S}}^{*}\boldsymbol{\tau}^{ij\dagger} \right) \Big]_{\tilde{b}'\tilde{a}} \end{aligned} \tag{3.112}$$

The perturbed localization condition multiplier $\mathbf{l}^{\boldsymbol{\lambda}}$ is obtained from the perturbed Z-CPL equations:

$$R^{\mathrm{loc}}_{ij}[\mathbf{l}^{\boldsymbol{\lambda}}] - \left(R^{\mathrm{loc}}_{ji}[\mathbf{l}^{\boldsymbol{\lambda}}]\right)^{*} = \left(R^{\mathrm{loc},\boldsymbol{\lambda}}_{ji}[\mathbf{l}^{(0)}]\right)^{*} - R^{\mathrm{loc},\boldsymbol{\lambda}}_{ij}[\mathbf{l}^{(0)}] - L^{\boldsymbol{\lambda}}_{ij} \tag{3.113}$$

where $L^{\boldsymbol{\lambda}}_{ij}$ and $R^{\mathrm{loc},\boldsymbol{\lambda}}_{ij}[\mathbf{l}^{(0)}]$ are straightforwardly derived from eqs. 3.62 and 3.63. The derivatives of the prescreening contributions $y^{\alpha,x}_{i\tilde{\mu}'}$ and $y^{\beta,x}_{i}$ are somewhat more involved, so we provide them here:

$$\begin{aligned} y^{\alpha,x,\boldsymbol{\lambda}}_{i\tilde{\mu}'} = 8 \sum_{j} 1_{\mathrm{S}}(ij) \sum_{\tilde{\nu}\tilde{\eta}} \Bigg\{ & \left(\pi^{i}_{\tilde{\mu}'\tilde{\nu}} t^{ij}_{\tilde{\nu}\tilde{\eta}}\right)^{\boldsymbol{\lambda}} \left[\frac{r^{x}_{j\tilde{\eta}}}{\left|\mathbf{R}_{ij}\right|^{3}} - 3\frac{R^{x}_{ij}\left(\mathbf{r}_{j\tilde{\eta}}\mathbf{R}_{ij}\right)}{\left|\mathbf{R}_{ij}\right|^{5}} \right] \\ & + \pi^{i}_{\tilde{\mu}'\tilde{\nu}} t^{ij}_{\tilde{\nu}\tilde{\eta}} \left[\frac{r^{x,\boldsymbol{\lambda}}_{j\tilde{\eta}}}{\left|\mathbf{R}_{ij}\right|^{3}} - 3\frac{R^{x,\boldsymbol{\lambda}}_{ij}\left(\mathbf{r}_{j\tilde{\eta}}\mathbf{R}_{ij}\right) + R^{x}_{ij}\left(\mathbf{r}^{\boldsymbol{\lambda}}_{j\tilde{\eta}}\mathbf{R}_{ij} + \mathbf{r}_{j\tilde{\eta}}\mathbf{R}^{\boldsymbol{\lambda}}_{ij}\right)}{\left|\mathbf{R}_{ij}\right|^{5}} \right] \\ & - \pi^{i}_{\tilde{\mu}'\tilde{\nu}} t^{ij}_{\tilde{\nu}\tilde{\eta}} \left[3\frac{r^{x}_{j\tilde{\eta}}}{\left|\mathbf{R}_{ij}\right|^{5}} - 15\frac{R^{x}_{ij}\left(\mathbf{r}_{j\tilde{\eta}}\mathbf{R}_{ij}\right)}{\left|\mathbf{R}_{ij}\right|^{7}} \right] \left(\mathbf{R}^{\boldsymbol{\lambda}}_{ij}\mathbf{R}_{ij}\right) \Bigg\} \end{aligned} \tag{3.114}$$

$$\begin{aligned} y^{\beta,x,\boldsymbol{\lambda}}_{i} = 48 \sum_{j} 1_{\mathrm{S}}(ij) \sum_{\tilde{\mu}\tilde{\nu}} \Bigg\{ & t^{ij,\boldsymbol{\lambda}}_{\tilde{\mu}\tilde{\nu}} \Bigg[\left(\frac{\mathbf{r}_{i\tilde{\mu}}\mathbf{r}_{j\tilde{\nu}}}{\left|\mathbf{R}_{ij}\right|^{5}} - 5\frac{\left(\mathbf{r}_{i\tilde{\mu}}\mathbf{R}_{ij}\right)\left(\mathbf{r}_{j\tilde{\nu}}\mathbf{R}_{ij}\right)}{\left|\mathbf{R}_{ij}\right|^{7}} \right) R^{x}_{ji} \\ & - \frac{r^{x}_{i\tilde{\mu}}\left(\mathbf{r}_{j\tilde{\nu}}\mathbf{R}_{ij}\right) + r^{x}_{j\tilde{\nu}}\left(\mathbf{r}_{i\tilde{\mu}}\mathbf{R}_{ij}\right)}{\left|\mathbf{R}_{ij}\right|^{5}} \Bigg] \end{aligned}$$

$$
\begin{aligned}
&+ t^{ij}_{\tilde{\mu}\tilde{\nu}} \Bigg[\left(\frac{\mathbf{r}_{i\tilde{\mu}} \mathbf{r}_{j\tilde{\nu}}}{|\mathbf{R}_{ij}|^5} - 5 \frac{(\mathbf{r}_{i\tilde{\mu}} \mathbf{R}_{ij})\,(\mathbf{r}_{j\tilde{\nu}} \mathbf{R}_{ij})}{|\mathbf{R}_{ij}|^7} \right) R^{x,\boldsymbol{\lambda}}_{ji} \\
&\quad - \frac{r^{x,\boldsymbol{\lambda}}_{i\tilde{\mu}} (\mathbf{r}_{j\tilde{\nu}} \mathbf{R}_{ij}) + r^{x,\boldsymbol{\lambda}}_{j\tilde{\nu}} (\mathbf{r}_{i\tilde{\mu}} \mathbf{R}_{ij})}{|\mathbf{R}_{ij}|^5} \\
&\quad + \left(\frac{(\mathbf{r}_{i\tilde{\mu}} \mathbf{r}_{j\tilde{\nu}})^{\boldsymbol{\lambda}}}{|\mathbf{R}_{ij}|^5} - 5 \frac{(\mathbf{r}_{i\tilde{\mu}} \mathbf{R}_{ij})^{\boldsymbol{\lambda}}\,(\mathbf{r}_{j\tilde{\nu}} \mathbf{R}_{ij}) + (\mathbf{r}_{i\tilde{\mu}} \mathbf{R}_{ij})\,(\mathbf{r}_{j\tilde{\nu}} \mathbf{R}_{ij})^{\boldsymbol{\lambda}}}{|\mathbf{R}_{ij}|^7} \right) R^{x}_{ji} \\
&\quad - \frac{r^{x}_{i\tilde{\mu}} (\mathbf{r}_{j\tilde{\nu}} \mathbf{R}_{ij})^{\boldsymbol{\lambda}} + r^{x}_{j\tilde{\nu}} (\mathbf{r}_{i\tilde{\mu}} \mathbf{R}_{ij})^{\boldsymbol{\lambda}}}{|\mathbf{R}_{ij}|^5} \Bigg] \\
&- t^{ij}_{\tilde{\mu}\tilde{\nu}} \Bigg[\left(5 \frac{\mathbf{r}_{i\tilde{\mu}} \mathbf{r}_{j\tilde{\nu}}}{|\mathbf{R}_{ij}|^7} - 35 \frac{(\mathbf{r}_{i\tilde{\mu}} \mathbf{R}_{ij})\,(\mathbf{r}_{j\tilde{\nu}} \mathbf{R}_{ij})}{|\mathbf{R}_{ij}|^9} \right) R^{x}_{ji} \\
&\quad - 5 \frac{r^{x}_{i\tilde{\mu}} (\mathbf{r}_{j\tilde{\nu}} \mathbf{R}_{ij}) + r^{x}_{j\tilde{\nu}} (\mathbf{r}_{i\tilde{\mu}} \mathbf{R}_{ij})}{|\mathbf{R}_{ij}|^7} \Bigg] \left(\mathbf{R}^{\boldsymbol{\lambda}}_{ji} \mathbf{R}_{ji} \right) \Bigg\}
\end{aligned}
\tag{3.115}
$$

The perturbed Z-CV equations have the form:

$$
\sum_k \bar{z}^{\boldsymbol{\lambda}}_{mk} F_{jk} - \sum_n F_{nm} \bar{z}^{\boldsymbol{\lambda}}_{nj} = \sum_n F^{\boldsymbol{\lambda}}_{nm} \bar{z}_{nj} - \sum_k \bar{z}_{mk} F^{\boldsymbol{\lambda}}_{jk} + L^{\mathrm{CV},\boldsymbol{\lambda}}_{mj} \tag{3.116}
$$

where $L^{\mathrm{CV},\boldsymbol{\lambda}}_{mj}$ is the derivative of eq. 3.71. Finally, the perturbed Z-CPSCF equations must be solved for $\mathbf{z}^{\boldsymbol{\lambda}}$:

$$
\sum_b z^{\boldsymbol{\lambda}}_{ib} F_{ab} - \sum_j F_{ji} z^{\boldsymbol{\lambda}}_{ja} + 2 g_{ai}\left[\mathbf{z}^{\boldsymbol{\lambda}}\right] = L^{\boldsymbol{\lambda}}_{ia} - \sum_b z_{ib} F^{\boldsymbol{\lambda}}_{ab} + \sum_j F^{\boldsymbol{\lambda}}_{ji} z_{ja} - 2 \left(g_{ai}\left[\mathbf{z}^{(0)}\right] \right)^{\boldsymbol{\lambda}} \tag{3.117}
$$

Thus, the full response density can be assembled and contracted with the property integrals to obtain the second derivative.

At the end of this section, we briefly summarize the order of computational steps needed to obtain the DLPNO-MP2 response density in Table 3.2. The actual procedure used in our implementation is given in more detail in Section 3.3.

Table 3.2: Interdependencies between the main Lagrange multipliers and target quantities with references to relevant equations. Some terms are excluded for brevity, e.g. those related to the prescreening correction. Wherever a perturbed quantity is required as input (e.g. $\mathbf{c}^{\boldsymbol{\lambda}}$), so is the unperturbed one (i.e. $\mathbf{c}$).

In	Equations	Out
	SCF, FB-loc.	$\rightarrow \mathbf{c}, E_{\mathrm{HF}}$
$\mathbf{c} \rightarrow$	LMP2 guess (3.15–3.17)	$\rightarrow \breve{\mathbf{T}}^{ij}, \mathbf{d}''^{ij}, \Delta E_{\mathrm{PNO}}$
$\mathbf{d}^{ij} \rightarrow$	LMP2 iter. (3.55)	$\rightarrow \mathbf{T}^{ij}, E_2^{\mathrm{DLPNO}}$
$\breve{\mathbf{T}}^{ij}, \mathbf{d}''^{ij}, \mathbf{T}^{ij} \rightarrow$	PNO cond. (3.60)	$\rightarrow \mathbf{v}^{ij}$
$\breve{\mathbf{T}}^{ij}, \mathbf{d}''^{ij}, \mathbf{v}^{ij} \rightarrow$	SC cond. (3.58)	$\rightarrow \mathbf{w}^{ij}$
$\breve{\mathbf{T}}^{ij}, \mathbf{d}''^{ij}, \mathbf{T}^{ij}, \mathbf{w}^{ij} \rightarrow$	eq. 3.64	$\rightarrow \boldsymbol{\Gamma}^{K}$
$\mathbf{c}, \breve{\mathbf{T}}^{ij}, \mathbf{d}''^{ij}, \mathbf{T}^{ij}, \mathbf{w}^{ij} \rightarrow$	eq. 3.48	$\rightarrow \mathbf{D}'$
$\mathbf{D}', \boldsymbol{\Gamma}^{K} \rightarrow$	Z-CPL (3.61)	$\rightarrow \mathbf{l}$
$\mathbf{l}, \boldsymbol{\Gamma}^{K} \rightarrow$	Z-CV (3.70)	$\rightarrow \bar{\mathbf{z}}$
$\mathbf{c}, \mathbf{l}, \boldsymbol{\Gamma}^{K}, \mathbf{D}', \bar{\mathbf{z}} \rightarrow$	Z-CPSCF (3.72)	$\rightarrow \mathbf{z}$
$\mathbf{c}, \mathbf{D}', \bar{\mathbf{z}}, \mathbf{z} \rightarrow$	eq. 3.47	$\rightarrow \mathbf{D}$
$\mathbf{c} \rightarrow$	CPSCF (3.86), CV (3.87), CPL (3.88), $C^{\boldsymbol{\lambda}}_{\mathrm{MOO}}$ (3.85)	$\rightarrow \mathbf{U}^{\boldsymbol{\lambda}}, \mathbf{c}^{\boldsymbol{\lambda}}$
$\mathbf{c}^{\boldsymbol{\lambda}}, \breve{\mathbf{T}}^{ij}, \mathbf{d}''^{ij} \rightarrow$	PNO resp. (3.99,3.102,3.98)	$\rightarrow \breve{\mathbf{T}}^{ij,\boldsymbol{\lambda}}, \boldsymbol{\theta}^{ij,\boldsymbol{\lambda}}, \mathbf{d}''^{ij,\boldsymbol{\lambda}}$
$\mathbf{d}^{ij,\boldsymbol{\lambda}}, \mathbf{T}^{ij} \rightarrow$	eq. 3.103	$\rightarrow \mathbf{T}^{ij,\boldsymbol{\lambda}}$
$\breve{\mathbf{T}}^{ij,\boldsymbol{\lambda}}, \mathbf{d}''^{ij,\boldsymbol{\lambda}}, \mathbf{T}^{ij,\boldsymbol{\lambda}}, \mathbf{v}^{ij} \rightarrow$	Pert. PNO cond. (3.111)	$\rightarrow \mathbf{v}^{ij,\boldsymbol{\lambda}}$
$\breve{\mathbf{T}}^{ij,\boldsymbol{\lambda}}, \mathbf{d}''^{ij,\boldsymbol{\lambda}}, \mathbf{v}^{ij,\boldsymbol{\lambda}}, \mathbf{w}^{ij} \rightarrow$	Pert. SC cond. (3.109)	$\rightarrow \mathbf{w}^{ij,\boldsymbol{\lambda}}$
$\breve{\mathbf{T}}^{ij,\boldsymbol{\lambda}}, \mathbf{d}''^{ij,\boldsymbol{\lambda}}, \mathbf{T}^{ij,\boldsymbol{\lambda}}, \mathbf{w}^{ij,\boldsymbol{\lambda}} \rightarrow$	Deriv. of eq. 3.64	$\rightarrow \boldsymbol{\Gamma}^{K,\boldsymbol{\lambda}}$
$\mathbf{c}^{\boldsymbol{\lambda}}, \breve{\mathbf{T}}^{ij,\boldsymbol{\lambda}}, \mathbf{d}''^{ij,\boldsymbol{\lambda}}, \mathbf{T}^{ij,\boldsymbol{\lambda}}, \mathbf{w}^{ij,\boldsymbol{\lambda}} \rightarrow$	Deriv. of eq. 3.48	$\rightarrow \mathbf{D}'^{\boldsymbol{\lambda}}$
$\mathbf{D}'^{\boldsymbol{\lambda}}, \boldsymbol{\Gamma}^{K,\boldsymbol{\lambda}}, \mathbf{l} \rightarrow$	Pert. Z-CPL (3.113)	$\rightarrow \mathbf{l}^{\boldsymbol{\lambda}}$
$\mathbf{l}^{\boldsymbol{\lambda}}, \boldsymbol{\Gamma}^{K,\boldsymbol{\lambda}}, \bar{\mathbf{z}} \rightarrow$	Pert. Z-CV (3.116)	$\rightarrow \bar{\mathbf{z}}^{\boldsymbol{\lambda}}$
$\mathbf{c}^{\boldsymbol{\lambda}}, \mathbf{l}^{\boldsymbol{\lambda}}, \boldsymbol{\Gamma}^{K,\boldsymbol{\lambda}}, \mathbf{D}'^{\boldsymbol{\lambda}}, \bar{\mathbf{z}}^{\boldsymbol{\lambda}}, \mathbf{z} \rightarrow$	Pert. Z-CPSCF (3.117)	$\rightarrow \mathbf{z}^{\boldsymbol{\lambda}}$
$\mathbf{c}^{\boldsymbol{\lambda}}, \mathbf{D}'^{\boldsymbol{\lambda}}, \bar{\mathbf{z}}^{\boldsymbol{\lambda}}, \mathbf{z}^{\boldsymbol{\lambda}} \rightarrow$	Deriv. of eq. 3.47	$\rightarrow \mathbf{D}^{\boldsymbol{\lambda}}$
$\mathbf{c}^{\boldsymbol{\lambda}}, \mathbf{D}^{\boldsymbol{\lambda}} \rightarrow$	Property eqs. 3.2,3.1,3.83	$\rightarrow \boldsymbol{\alpha}, \boldsymbol{\sigma}^{A}$

3.2 Treatment of numerical instabilities

3.2.1 Localization response singularities

It was discussed at some length in ref. 192 that for some systems the Z-CPL (as well as the CPL and perturbed Z-CPL) equations can be (near-)singular. In other words, the left-hand side matrix $\mathbf{A}^{\mathrm{loc},\pm}$ can have (near-)zero eigenvalues. This happens when a continuous degeneracy exists among the LMOs, i.e. when some subset of the localized orbitals can be arbitrarily rotated without changing the value of the localization sum. Formally, continuous degeneracies are only possible for certain point groups,[304–306] however even local pseudosymmetry can result in small eigenvalues of $\mathbf{A}^{\mathrm{loc},\pm}$ and thus prevent convergence of the CPL/Z-CPL equations or negatively impact the results, as shown for the $(CH_3)_3P(CO)_4Os\cdots Cr(CO)_5$ molecule (reference code KAMDOR)[307] in ref. 192. To systematically treat this problem here we take the same approach as for the DLPNO-MP2 gradient, namely, to modify the Lagrangian so as to obtain a nonsingular problem with the nullspace projected out. Note that the matrix $\mathbf{A}^{\mathrm{loc},-}$, which occurs in the Z-CPL equations (3.61) and in the CPL (3.88) and perturbed Z-CPL (3.113) equations for electric perturbations, is different from the matrix $\mathbf{A}^{\mathrm{loc},+}$, which occurs in the CPL and perturbed Z-CPL equations for magnetic perturbations. Thus, the two matrices have different eigenvalues and eigenvectors. In order to ensure both types of equations are properly treated, it is most convenient to reformulate the localization constraint in the Lagrangian using separate real and imaginary terms:

$$C_{\mathrm{Loc}}^{\mathrm{valence}} = \sum_{i<j}^{\mathrm{valence}} \left(l_{ij}^{\Re} \Re[s_{ij}] + l_{ij}^{\Im} \Im[s_{ij}] \right) = \frac{1}{2} \sum_{i<j}^{\mathrm{valence}} \left[l_{ij}^{\Re} \left(s_{ij} + s_{ij}^* \right) + \mathrm{i} l_{ij}^{\Im} \left(s_{ij} - s_{ij}^* \right) \right] \tag{3.118}$$

$$= \frac{1}{2} \sum_{i<j}^{\mathrm{valence}} \left[\underbrace{\left(l_{ij}^{\Re} + \mathrm{i} l_{ij}^{\Im} \right)}_{l_{ij}} s_{ij} + \underbrace{\left(l_{ij}^{\Re} - \mathrm{i} l_{ij}^{\Im} \right)}_{l_{ij}^*} s_{ij}^* \right] \tag{3.119}$$

where the equivalence of the two formulations is demonstrated for the valence orbitals. The core orbital terms are analogous, so for simplicity we will omit them in this section. Note that both of the newly introduced Lagrange multiplier matrices $\mathbf{l}^{\Re}$ and $\mathbf{l}^{\Im}$ are real by definition. Using this definition of C_{Loc}, eq. 3.94 becomes

$$\sum_{k<l} l_{ij}^{\Re} A_{ij,kl}^{\mathrm{loc},\Re} + \mathrm{i} \sum_{k<l} l_{kl}^{\Im} A_{ij,kl}^{\mathrm{loc},\Im} = -L_{ij} \tag{3.120}$$

where

$$A_{ij,kl}^{\mathrm{loc},\Re} = \left[\frac{\mathrm{d}s_{kl}}{\mathrm{d}U_{ij}} + \left(\frac{\mathrm{d}s_{lk}}{\mathrm{d}U_{ji}} \right)^* - \frac{\mathrm{d}s_{lk}}{\mathrm{d}U_{ij}} - \left(\frac{\mathrm{d}s_{kl}}{\mathrm{d}U_{ji}} \right)^* \right] \tag{3.121}$$

$$A_{ij,kl}^{\mathrm{loc},\Im} = \left[\frac{\mathrm{d}s_{kl}}{\mathrm{d}U_{ij}} + \left(\frac{\mathrm{d}s_{lk}}{\mathrm{d}U_{ji}} \right)^* + \frac{\mathrm{d}s_{lk}}{\mathrm{d}U_{ij}} + \left(\frac{\mathrm{d}s_{kl}}{\mathrm{d}U_{ji}} \right)^* \right] \tag{3.122}$$

The real and imaginary parts of eq. 3.120 can be separated and the latter yields $\mathbf{l}^{\Im} = 0$ because L_{ij} is real. Note that as the unperturbed quantities are purely real, $\mathbf{A}^{\mathrm{loc},\Re}$ coincides with $A^{\mathrm{loc},-}$ and $A^{\mathrm{loc},\Im}$ – with $A^{\mathrm{loc},+}$. We then define the eigendecompositions of these matrices as:

$$\sum_{i<j} A_{kl,ij}^{\mathrm{loc},\Re} u_{ij,u''}^{\Re} = u_{kl,u''}^{\Re} \omega_{u''}^{\Re} \tag{3.123}$$

$$\sum_{i<j} A^{\mathrm{loc},\Im}_{kl,ij}\, u^{\Im}_{ij,u''} = u^{\Im}_{kl,u''}\omega^{\Im}_{u''} \tag{3.124}$$

where the index u'' denotes the eigenvectors of either matrix (determined from context), u' denotes those with (near-)zero eigenvalues and u denotes the rest. We change the Lagrangian constraint to

$$\begin{aligned} C^{\text{valence}}_{\text{Loc}} &= \sum_{u}^{\Re} l^{\Re}_{u}\Re[s_u] + \sum_{u}^{\Im} l^{\Im}_{u}\Im[s_u] + \sum_{u'}^{\Re} l^{\Re}_{u'}\Re[U_{u'}] + \sum_{u'}^{\Im} l^{\Im}_{u'}\Im[U_{u'}] \\ &= \frac{1}{2}\sum_{i<j}^{\text{valence}}\sum_{k<l}^{\text{valence}} \Big[l^{\Re}_{ij}\left(\delta_{ij,kl} - \mathcal{O}^{\Re}_{ij,kl}\right)\left(s_{kl} + s^*_{kl}\right) + \mathrm{i} l^{\Im}_{ij}\left(\delta_{ij,kl} - \mathcal{O}^{\Im}_{ij,kl}\right)\left(s_{kl} - s^*_{kl}\right) \\ &\quad + l^{\Re}_{ij}\mathcal{O}^{\Re}_{ij,kl}\left(U_{kl} + U^*_{kl}\right) + \mathrm{i} l^{\Im}_{ij}\mathcal{O}^{\Im}_{ij,kl}\left(U_{kl} - U^*_{kl}\right) \Big] \end{aligned} \tag{3.125}$$

where $\delta_{ij,kl} = \delta_{ik}\delta_{jl}$ and the projectors onto the nullspace of $\mathbf{A}^{\mathrm{loc},\Re/\Im}$ are:

$$\mathcal{O}^{\Re/\Im}_{ij,kl} = \sum_{u'} u^{\Re/\Im}_{ij,u'} u^{\Re/\Im}_{kl,u'} \tag{3.126}$$

Thus, the Z-CPL equations become:

$$\sum_{k<l} l^{\Re}_{kl}\tilde{A}^{\mathrm{loc},\Re}_{ij,kl} + \mathrm{i}\sum_{k<l} l^{\Im}_{kl}\tilde{A}^{\mathrm{loc},\Im}_{ij,kl} = -L_{ij} \tag{3.127}$$

where

$$\tilde{\mathbf{A}}^{\mathrm{loc},\Re} = \left(\mathbf{I} - \boldsymbol{\mathcal{O}}^{\Re}\right)\mathbf{A}^{\mathrm{loc},\Re}\left(\mathbf{I} - \boldsymbol{\mathcal{O}}^{\Re}\right) + \boldsymbol{\mathcal{O}}^{\Re} \tag{3.128}$$

$$\tilde{\mathbf{A}}^{\mathrm{loc},\Im} = \left(\mathbf{I} - \boldsymbol{\mathcal{O}}^{\Im}\right)\mathbf{A}^{\mathrm{loc},\Im}\left(\mathbf{I} - \boldsymbol{\mathcal{O}}^{\Im}\right) + \boldsymbol{\mathcal{O}}^{\Im} \tag{3.129}$$

Once again, $\mathbf{l}^{\Im}$ is zero, while the contributions of $\mathbf{l}^{\Re}$ to eqs. 3.71, 3.76, 3.116, and 3.117 must be calculated with the projected matrix:

$$\tilde{l}^{\Re}_{ij} = \sum_{k<l}\left(\delta_{ij,kl} - \mathcal{O}^{\Re}_{ij,kl}\right) l^{\Re}_{kl} \tag{3.130}$$

The electric/magnetic CPL equations become:

$$\sum_{k<l} U^{\boldsymbol{\lambda}}_{kl}\tilde{A}^{\mathrm{loc},\Re/\Im}_{kl,ij} = -\sum_{k<l}\left(\mathbf{I} - \boldsymbol{\mathcal{O}}^{\Re/\Im}\right)_{ij,kl} B^{\mathrm{loc},\boldsymbol{\lambda}}_{kl} \tag{3.131}$$

$$\begin{aligned} B^{\mathrm{loc},\boldsymbol{\lambda}}_{ij} &= s^{(\boldsymbol{\lambda})}_{ij} - \sum_{k<l}\left[\frac{\mathrm{d}s_{ij}}{\mathrm{d}U_{lk}} S^{(\boldsymbol{\lambda})}_{lk} - \left(\frac{\mathrm{d}s_{ji}}{\mathrm{d}U_{lk}}\right)^* S^{(\boldsymbol{\lambda})*}_{lk}\right] \\ &\quad + \sum_{pk}\left(\delta_{pm} + \delta_{pa}\right)\left[\frac{\mathrm{d}s_{ij}}{\mathrm{d}U_{pk}} U^{\boldsymbol{\lambda}}_{pk} - \left(\frac{\mathrm{d}s_{ji}}{\mathrm{d}U_{pk}}\right)^* U^{\boldsymbol{\lambda}*}_{pk}\right] \end{aligned} \tag{3.132}$$

I.e., the nullspace must first be projected out of the right-hand side in eq. 3.131, the equations are solved, and afterwards, the nullspace is also projected out of the solution before the perturbed orthonormality constraint is used to obtain the upper triangle of the matrix:

$$\tilde{U}^{\boldsymbol{\lambda}}_{ij} = \sum_{k<l}\left(\delta_{ij,kl} - \mathcal{O}^{\Re/\Im}_{ij,kl}\right) U^{\boldsymbol{\lambda}}_{kl} \tag{3.133}$$

The perturbed Z-CPL equations become:

$$\sum_{k<l} l_{kl}^{\Re,\boldsymbol{\lambda}} \tilde{A}_{ij,kl}^{\mathrm{loc},\Re} + \mathrm{i} \sum_{k<l} l_{kl}^{\Im,\boldsymbol{\lambda}} \tilde{A}_{ij,kl}^{\mathrm{loc},\Im} = -\sum_{k<l} \tilde{l}_{kl}^{\Re} A_{ij,kl}^{\mathrm{loc},\Re,\boldsymbol{\lambda}} - L_{ij}^{\boldsymbol{\lambda}} \tag{3.134}$$

with

$$\begin{aligned} A_{pq,ij}^{\mathrm{loc},\Re,\boldsymbol{\lambda}} = \big[&\left(r_{ij} + r_{ij}^*\right) \left(\delta_{pj} r_{qj} + \delta_{qi} r_{ip} - \delta_{pi} r_{qi} - \delta_{qj} r_{jp}\right) \\ &+ \left(r_{ii} - r_{jj}\right) \left(\delta_{qj} r_{ip} + \delta_{qi} r_{jp} - \delta_{pi} r_{qj} - \delta_{pj} r_{qi}\right) \big]^{\boldsymbol{\lambda}} \end{aligned} \tag{3.135}$$

eq. 3.134 is separated into real and imaginary parts, of which only the former/latter yields a nonzero solution for electric/magnetic perturbations, respectively. Note that for magnetic perturbations $\left(r_{ii} - r_{jj}\right)^{\boldsymbol{\lambda}} = 0$ and $\left(r_{ij} + r_{ij}^*\right)^{\boldsymbol{\lambda}} = 0$. The contributions of $\mathbf{l}^{\Re/\Im,\boldsymbol{\lambda}}$ to eqs. 3.116 and 3.117 must be calculated with the projected matrices:

$$\tilde{l}_{ij}^{\Re/\Im,\boldsymbol{\lambda}} = \sum_{k<l} \left(\delta_{ij,kl} - \mathcal{O}_{ij,kl}^{\Re/\Im}\right) l_{kl}^{\Re/\Im,\boldsymbol{\lambda}} \tag{3.136}$$

Table 3.3: (Maximum) absolute errors vs RI-MP2 in the isotropic polarizability (α) and ^{19}F shielding (σ_{F}) for the systems SF_6 and SeF_6 from frozen-core (FC) and all-electron (AE) NormalPNO calculations with and without projection of the localization response nullspace.

System	SF_6		SeF_6	
	FC	AE	FC	AE
$\mathbf{A}^{\mathrm{loc},\Re}$ nullspace	6	9	16	22
$\mathbf{A}^{\mathrm{loc},\Im}$ nullspace	0	0	10	10
	Errors without projection:			
$\lvert\Delta\alpha\rvert$/Å^3	8×10^5	—[a]	17	—[a]
max($\lvert\Delta\sigma_{\mathrm{F}}\rvert$)/ppm	0.26	0.28	2.1	29
	Errors with projection:			
$\lvert\Delta\alpha\rvert$/Å^3	<0.001	<0.001	<0.001	<0.001
max($\lvert\Delta\sigma_{\mathrm{F}}\rvert$)/ppm	0.26	0.28	0.47	0.55

[a]The calculation did not converge.

Finally, we demonstrate the numerical instabilities which can occur if the localization response matrix, $\mathbf{A}^{\mathrm{loc},\Re}$ or $\mathbf{A}^{\mathrm{loc},\Im}$, is singular, as well as the effectiveness of the procedure to remove the near-zero eigenvalues. We chose the octahedral molecules SF_6 and SeF_6 with bond lengths 1.560 and 1.688 Å, respectively. SF_6 has 6 eigenvalues of $\mathbf{A}^{\mathrm{loc},\Re}$ smaller than 10^{-4} due to a continuous degeneracy in the FB LMOs among the 18 fluorine sp^3-hybridized orbitals (3 on each F atom) directed away from the S atom. A further 3 singular eigenvalues are associated with the sulfur 2sp shell, which is treated as core orbitals. In addition to these, SeF_6 has a further 10 singular eigenvalues in the valence and 3 in the core region, associated with the 3d and 3sp shells, respectively. The magnetic response matrix $\mathbf{A}^{\mathrm{loc},\Im}$ only has 10 singular eigenvalues for SeF_6, due to the 3d orbitals, and none for SF_6. Table 3.3 shows that if no measures are taken to remove the singularities, the iterative solution of the perturbed CPL, Z-CPL, or PNO amplitude equations may not converge, or large errors may occur in the calculated properties, which is arguably worse. However, if the singular eigenvectors are projected out, the iterative solutions are stable and the results are in line with the expected accuracy for DLPNO-MP2.

3.2.2 PAO domain redundancy

While testing our initial implementation, we discovered large errors due to numerical instabilities related to the domain truncation. After thorough investigation, we found that the source was the appearance of near-linear dependencies in the "non-redundant" PAO domains. Recall that the full PAO space is linearly dependent because it is of the same size as the full AO basis, N_{AO}, but it only represents the N_{virt} virtual orbitals. Therefore there are exactly N_{occ} redundant PAOs. However, any subset (domain) of PAOs is not *exactly* linearly dependent, which becomes obvious when inspecting the eigenvalue spectrum of the overlap matrix of a domain of PAOs - see Figure 3.1. While the spectrum

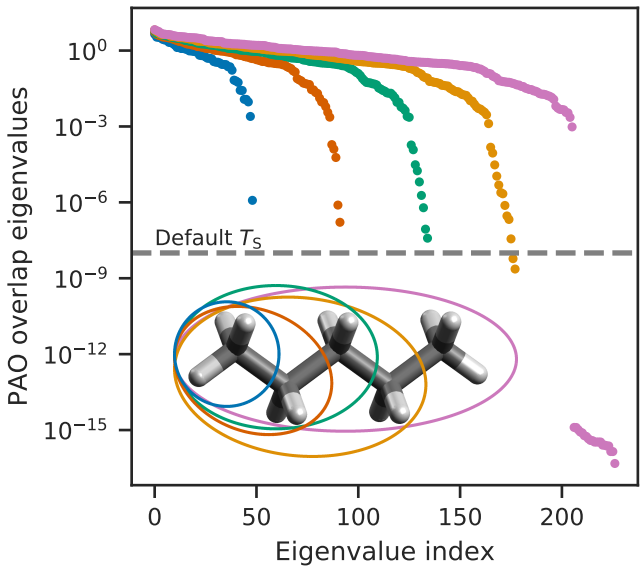

Figure 3.1: Eigenvalues of the PAO domain overlap matrix, for different domains in a pentane molecule with the def2-TZVP basis set. The atoms included in each domain are depicted graphically with matching colors.

of the full overlap matrix clearly reveals the N_{occ} redundant eigenvectors, all smaller domains have virtually continuous eigenvalue spectra, i.e. the matrix is ill-conditioned. By default, eigenvectors with eigenvalues greater than $T_{\text{S}} = 10^{-8}$ form the NPAO domain. It is apparent that the lowest remaining eigenvalue s_n will be very close to the threshold, and thus the normalization coefficient of that eigenvector will be $s_n^{-\frac{1}{2}} \approx 10^4$. This is not cause for concern, and indeed the energy and gradient calculations do not suffer. It is, however, a problem for second derivatives due to the perturbed PNO/CPNO coefficients $\mathbf{d}''^{ij,\boldsymbol{\lambda}}$. To illustrate this, we express the latter as:

$$\mathbf{d}''^{ij,\boldsymbol{\lambda}} = \mathbf{U}^{\text{S}}\mathbf{s}^{-\frac{1}{2}}\mathbf{U}^{\text{SD}}\boldsymbol{\theta}^{ij,\boldsymbol{\lambda}} \tag{3.137}$$

where $\mathbf{U}^{\text{S}}$ is the unitary matrix that diagonalizes the PAO domain overlap matrix, $\mathbf{s}$ is the diagonal matrix of eigenvalues, and $\mathbf{U}^{\text{SD}}$ is a unitary transformation from the overlap eigenbasis to the SC pair density eigenbasis. We will drop the ij indices in the rest of this section for simplicity of notation. Let us also assume for now that no PNO truncation is used, thus using eq. 3.98 we can express:

$$\boldsymbol{\theta}^{\boldsymbol{\lambda}} = -\frac{1}{2}\mathbf{d}''^{(0)\dagger}\widetilde{\mathbf{S}}^{\boldsymbol{\lambda}}\mathbf{d}''^{(0)} = -\frac{1}{2}\mathbf{U}^{\text{SD}\dagger}\mathbf{s}^{-\frac{1}{2}}\mathbf{U}^{\text{S}\dagger}\widetilde{\mathbf{S}}^{\boldsymbol{\lambda}}\mathbf{U}^{\text{S}}\mathbf{s}^{-\frac{1}{2}}\mathbf{U}^{\text{SD}} \propto \mathbf{s}^{-1} \approx 10^8 \tag{3.138}$$

and therefore

$$\mathbf{d}''^{\boldsymbol{\lambda}} \propto \mathbf{s}^{-\frac{3}{2}} \approx 10^{12} \tag{3.139}$$

The largest elements of the matrices are estimated based on $\mathbf{s}^{-\frac{1}{2}} \approx T_{\mathrm{S}}^{-\frac{1}{2}} = 10^4$. These large numbers lead to a loss of numerical precision, which gets amplified during the multiple iterative procedures, especially the solution of the CPSCF equations. An example of this problem in its purest form is illustrated in Table 3.4 for a toy model of two water molecules in a triangular prism configuration with C_{2v} symmetry at a distance of 10.5 Bohr between the two molecular planes. No truncations were used other than the domain truncation with $T_{\mathrm{CutDO}} = 10^{-2}$. Ignoring the line "Analytic v2" for now, the large error in the analytic

Table 3.4: Isotropic polarizability (Bohr^3) of the water dimer model (see text) calculated semi-numerically and analytically using RI-MP2 and DLPNO-MP2 with the "symmetric" solution for $\theta^{ij}_{\tilde{a}''\tilde{b}''}$ (v1) or the alternative solution discussed in the text (v2). Only the domain truncation was used. The maximal absolute deviation of the MP2 density matrix elements ($\max(|\Delta D_{\mu\nu}|)$) is also given.

	$T_{\mathrm{S}} = 10^{-8}$	$T_{\mathrm{S}} = 10^{-7}$	$T_{\mathrm{S}} = 10^{-6}$	$T_{\mathrm{S}} = 10^{-5}$	RI-MP2
Numeric	19.1393	19.0770	19.1034	19.1146	19.1190
Analytic v1	17.5287	19.0675	19.0973	19.1149	19.1190
Analytic v2	19.1033	19.0688	19.0974	19.1149	
$\max(\lvert\Delta D_{\mu\nu}\rvert)$	0.0117	0.0110	0.0055	0.0010	

polarizability at $T_{\mathrm{S}} = 10^{-8}$ is apparent. This disappears at higher values of the cutoff and at $T_{\mathrm{S}} = 10^{-5}$, there is very good agreement with both the semi-numeric polarizability (calculated from analytic dipole moment calculations with an explicit electric field of 10^{-4} a.u.), and the RI-MP2 value. Note that even the errors in the relaxed MP2 density get larger with lower values of T_{S}, hinting at the underlying numerical instability, although of course these errors are negligible.

After some experimentation, we found an alternative solution for eq. 3.98, which partially alleviates the problem and results in the line "Analytic v2" in Table 3.4. First we express $\boldsymbol{\theta}^{\boldsymbol{\lambda}}$ as

$$\boldsymbol{\theta}^{\boldsymbol{\lambda}} = -\frac{1}{2}\mathbf{d}''^{(0)\dagger}\widetilde{\mathbf{S}}^{\boldsymbol{\lambda}}\mathbf{d}''^{(0)} + \boldsymbol{\theta}^{1,\boldsymbol{\lambda}} + \boldsymbol{\theta}^{2,\boldsymbol{\lambda}} \tag{3.140}$$

where both $\boldsymbol{\theta}^{1,\boldsymbol{\lambda}}$ and $\boldsymbol{\theta}^{2,\boldsymbol{\lambda}}$ are defined as skew-Hermitian matrices and the latter only has elements in the PNO-CPNO block. Thus the first and last terms in eq. 3.140 are used to ensure that the perturbed orthonormality, and SC conditions (eqs. 3.98 and 3.102) are fulfilled, respectively, while the second term is arbitrary. We got the best results by choosing it so as to minimize the norm of the perturbed PNO/CPNO coefficients, excluding the $\boldsymbol{\theta}^{2,\boldsymbol{\lambda}}$ part:

$$\left|\mathbf{U}^{\mathrm{S}}\mathbf{s}^{-\frac{1}{2}}\mathbf{U}^{\mathrm{SD}}\left(-\frac{1}{2}\mathbf{d}''^{(0)\dagger}\widetilde{\mathbf{S}}^{\boldsymbol{\lambda}}\mathbf{d}''^{(0)} + \boldsymbol{\theta}^{1,\boldsymbol{\lambda}}\right)\right|^2 \to \min \tag{3.141}$$

which is solved in the overlap eigenbasis as:

$$\left(\mathbf{U}^{\mathrm{SD}}\boldsymbol{\theta}^{1,\boldsymbol{\lambda}}\mathbf{U}^{\mathrm{SD}\dagger}\right)_{\tilde{\mu}\tilde{\nu}} = \frac{(s_{\tilde{\nu}} - s_{\tilde{\mu}})}{2\sqrt{s_{\tilde{\mu}}s_{\tilde{\nu}}}\,(s_{\tilde{\nu}} + s_{\tilde{\mu}})}\left(\mathbf{U}^{\mathrm{S}\dagger}\widetilde{\mathbf{S}}^{\boldsymbol{\lambda}}\mathbf{U}^{\mathrm{S}}\right)_{\tilde{\mu}\tilde{\nu}} \tag{3.142}$$

All of the above also applies to the orbital-specific PAO domains used for the prescreening contributions and their response parametrized by $\boldsymbol{\theta}^{i,\boldsymbol{\lambda}}$. Of course, in that case $\boldsymbol{\theta}^{i,2,\boldsymbol{\lambda}} = 0$.

This approach basically serves to better distribute the large floating point numbers throughout $\mathbf{d}''^{\boldsymbol{\lambda}}$, and seems to reduce the error in the calculated properties as evidenced by

the toy example in Table 3.4. However, agreement with the numeric polarizability is still not perfect, and in fact large, unpredictable errors still occur in calculations for realistic systems when the default value of T_S is used, as will be shown in Section 3.4. Therefore, in addition to the "Analytic v2" ansatz presented above, we have settled on a cutoff of $T_S = 10^{-5}$, with which the issue no longer occurs. The reduced NPAO domains do lead to a slightly increased error in the correlation energy, but the difference is negligible compared to the deviations due to the domain and PNO approximations, which are themselves sufficiently small by design, so as to obtain results with chemical accuracy.

We note in passing that the entire problem disappears if a linearly independent set of virtual orbitals is used, such as FB-localized MOs. In fact, we implemented this option and confirmed the instability does not occur. However, on the one hand, localizing virtual orbitals to a true maximum, rather than a saddle point, of the FB condition is very difficult and time-consuming, even with the augmented Hessian solver used in our implementation. On the other hand, much larger domains were necessary to obtain accurate results, corroborating recent observations.[308,309] Therefore, we will not discuss this approach further.

A final approach to mention here is to perform the entire calculation with extended numerical precision for the floating point numbers, i.e. more than 64 bit IEEE 754 double precision. Unfortunately, this is not supported by any linear algebra libraries and only by some C++ compilers. Attempting, as a proof of concept, to convert only the DLPNO-MP2 response density module to quadruple precision, using the hand-coded linear algebra routines available in ORCA, did not resolve the problem. It is possible that converting the entire DLPNO-MP2 code might be successful but this was not attempted. In any case, it would be very inefficient.

3.2.3 PNO response singularities

To solve eqs. 3.60, 3.102, and 3.111, which follow from the PNO constraint $\breve{D}^{ij}_{\tilde{a}\tilde{b}'}$, it is necessary to divide by the difference $(n^{ij}_{\tilde{a}} - n^{ij}_{\tilde{b}'})$ between occupation numbers of PNOs and CPNOs. Evidently, if this difference approaches zero, the equations become near-singular, which may lead to numeric instability. Usually, the eigenvalue spectrum of $\breve{\mathbf{D}}^{ij}$ is nearly continuous and thus, both the smallest PNO and the largest CPNO occupation numbers are of the same order of magnitude as T_{CutPNO}, and it is not uncommon for the threshold to fall between two nearly degenerate PNOs. In our tests, we found rare cases, where this instability caused spurious, sometimes very large, errors in the calculated properties. In all of these cases, the smallest relative difference $(n^{ij}_{\tilde{a}} - n^{ij}_{\tilde{b}'})/n^{ij}_{\tilde{a}}$ was smaller than 10^{-2}, which can be taken as a necessary, but not sufficient, condition for problems to occur. Clearly, it is necessary to treat this problem systematically, since it is not possible to know when the results will be, or indeed have been, affected, without reference calculations, e.g. at other values of T_{CutPNO}.

We investigated two approaches, which were both successful in alleviating the problem in all cases, where we observed it. The first one is likely not always applicable in general and is only described here for completeness. It consists of a pair-specific adjustment of T_{CutPNO}, within a narrow range, so as to find the largest gap between occupation numbers in that range. I.e., we find

$$n^{ij}_{\tilde{a}} - n^{ij}_{\tilde{a}+1} \to \max, \quad \text{for} \quad n^{ij}_{\tilde{a}} \geq n^{ij}_{\tilde{a}+1} \quad \text{and} \quad f_{\mathrm{range}} T_{\mathrm{CutPNO}} > n^{ij}_{\tilde{a}} > f^{-1}_{\mathrm{range}} T_{\mathrm{CutPNO}} \tag{3.143}$$

and keep PNOs up to and including the index $\tilde{a}$. This is illustrated in Figure 3.2. f_{range} is

an input parameter greater than 1 – we used 1.1. On the one hand, f_{range} should be small, so as to keep the cutoff threshold close to the chosen value of T_{CutPNO}. On the other hand, the wider the range, the more likely it is to find two sequential PNO occupation numbers suitably far apart. In fact, there is no guarantee that two such PNOs exist for every occupied orbital pair of every system, particularly if large basis sets are used. Thus, even though this solution requires no modification of the Lagrangian and avoids the instability problem entirely, it is rather ad hoc and is not guaranteed to work so we will not discuss it further (except for the proof-of-concept example in Figure 3.3).

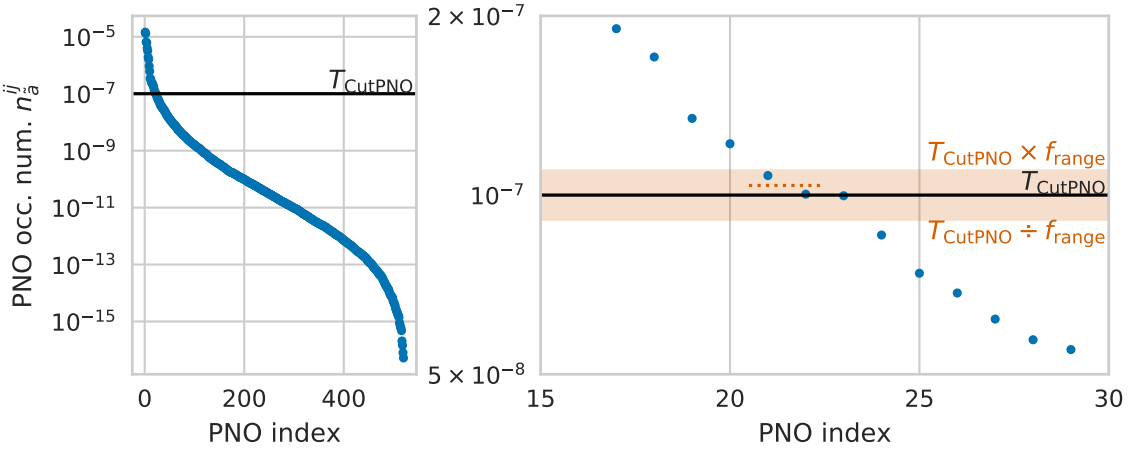

Figure 3.2: PNO/CPNO occupation numbers in a single pair domain of caffeine with LoosePNO settings. The right subplot illustrates the range-based adjustment of T_{CutPNO} (see text).

The second approach we propose is to introduce a level shift ε in the denominator of eqs. 3.60, 3.102, and 3.111, thus ensuring that $(n_{\tilde{a}}^{ij} - n_{\tilde{b}'}^{ij} + \varepsilon) > \varepsilon$. To that end, we modify the PNO condition as follows:

$$C_{\text{PNO}} = \frac{1}{2} \sum_{i \geq j} \sum_{\tilde{a}\tilde{b}'} \left[v_{\tilde{a}\tilde{b}'}^{ij} \left(\breve{D}_{\tilde{a}\tilde{b}'}^{ij} + \Xi_{\tilde{a}\tilde{b}'}^{ij} \right) + v_{\tilde{a}\tilde{b}'}^{ij*} \left(\breve{D}_{\tilde{a}\tilde{b}'}^{ij*} + \Xi_{\tilde{a}\tilde{b}'}^{ij*} \right) \right] \tag{3.144}$$

$$\boldsymbol{\Xi}^{ij} = \boldsymbol{\theta}^{ij*} \boldsymbol{\Xi}^{ij} \boldsymbol{\theta}^{ij,\mathrm{T}} \tag{3.145}$$

$$\Xi_{\tilde{a}''\tilde{b}''}^{ij} = \sum_{\tilde{c}} \delta_{\tilde{c}\tilde{a}''} \delta_{\tilde{c}\tilde{b}''} \varepsilon \tag{3.146}$$

In effect, we shift all kept PNO occupation numbers up by ε. This modification has no effect on the DLPNO-MP2 energy, as the occupation numbers are only used for PNO truncation. It does, however, lead to extra terms in the right-hand sides of eqs. 3.102 and 3.111 (given below in the pair density-diagonalizing basis):

$$\begin{aligned} \left(n_{\tilde{a}}^{ij} - n_{\tilde{b}'}^{ij} + \varepsilon \right) \theta_{\tilde{b}'\tilde{a}}^{ij,\boldsymbol{\lambda}} = &- \left(n_{\tilde{a}}^{ij} + \varepsilon \right) \mathcal{S}_{\tilde{b}'\tilde{a}}^{ij,\boldsymbol{\lambda}} - \Big(\widetilde{\mathbf{T}}^{ij*} \boldsymbol{\mathcal{S}}^{ij,\boldsymbol{\lambda}} \widehat{\mathbf{T}}^{ji} + \widetilde{\mathbf{T}}^{ji*} \boldsymbol{\mathcal{S}}^{ij,\boldsymbol{\lambda}} \widehat{\mathbf{T}}^{ij} \\ &- \widetilde{\mathbf{T}}^{ij,\boldsymbol{\lambda}*} \widehat{\mathbf{T}}^{ji} - \widetilde{\mathbf{T}}^{ji,\boldsymbol{\lambda}*} \widehat{\mathbf{T}}^{ij} - \widetilde{\mathbf{T}}^{ij*} \widehat{\mathbf{T}}^{ji,\boldsymbol{\lambda}} - \widetilde{\mathbf{T}}^{ji*} \widehat{\mathbf{T}}^{ij,\boldsymbol{\lambda}} \Big)_{\tilde{a}\tilde{b}'} \end{aligned} \tag{3.147}$$

$$\left(n_{\tilde{a}}^{ij} - n_{\tilde{b}'}^{ij} + \varepsilon \right) v_{\tilde{a}\tilde{b}'}^{ij,\boldsymbol{\lambda}} = -V_{\tilde{b}'\tilde{a}}^{ij,\boldsymbol{\lambda}} + \varepsilon \sum_{\tilde{c}} \mathcal{S}_{\tilde{a}\tilde{c}}^{ij,\boldsymbol{\lambda}} v_{\tilde{c}\tilde{b}'}^{ij} \tag{3.148}$$

An appropriate value of the level shift parameter ε must be chosen: if it is too low, it will have no effect. However, if it is too large, it can introduce additional round-off

errors. It makes sense to choose a value proportional to T_{CutPNO}, i.e. $\varepsilon = \varepsilon_{\mathrm{scale}} \times T_{\mathrm{CutPNO}}$. After some experimentation (see below) we found that $\varepsilon_{\mathrm{scale}} = 0.1$ provides stable results without introducing additional errors. Note that because the value of T_{CutPNO} is different for occupied pairs, which include core orbitals, the value of ε reflects that. In principle, it is also possible for the level shift to be pair-specific, e.g. only applied to "problematic" domains, but we did not find that to be necessary.

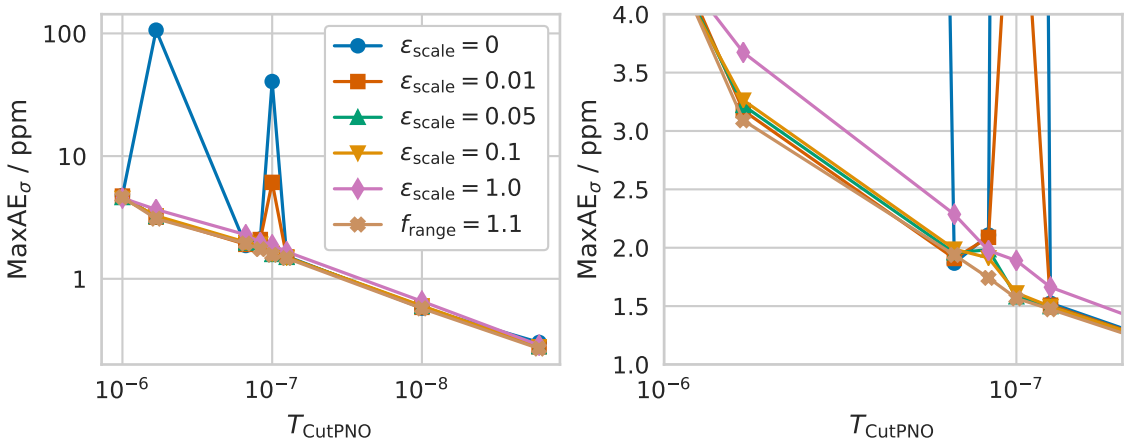

Figure 3.3: Maximum absolute errors vs RI-MP2 in the shieldings of caffeine from LoosePNO calculations with varying T_{CutPNO} and different level shift scaling parameters $\varepsilon_{\mathrm{scale}}$ in the PNO response equations ($\varepsilon_{\mathrm{scale}} = 0$ is equivalent to no level shift), or using the range-based adjustment. The legend applies to both subplots.

We demonstrate a rather extreme example of the instability discussed above in Figure 3.3. In shielding calculations for caffeine with LoosePNO default thresholds, $T_{\mathrm{S}} = 10^{-5}$, and $T_{\mathrm{CutPNO}} = 10^{-7}$, as well as with $T_{\mathrm{CutPNO}} = 5.96 \times 10^{-7}$, the maximal absolute errors with respect to RI-MP2 are huge (40.5 and 106.3 ppm, respectively). The level shift scheme with $\varepsilon_{\mathrm{scale}}$ in the range 0.05–0.1 is successful in resolving the problem and producing a smooth curve. A value of 0.01 is not sufficient to remove the singularity at $T_{\mathrm{CutPNO}} = 10^{-7}$, while $\varepsilon_{\mathrm{scale}} = 1.0$ results in a smooth curve but with an additional small deviation for all values of T_{CutPNO}. Thus, we consider $\varepsilon_{\mathrm{scale}} = 0.1$ to be an appropriate value. We mention in passing that the range-based adjustment of T_{CutPNO} discussed above is also successful for this system.

Initially, no adjustment or level shift was applied to the calculations in sections 3.4.2 and 3.4.3. Consequently, we encountered several calculations with conspicuously large errors, which are discussed whenever they occur in the following sections. In all of these cases the level shift approach (with $\varepsilon_{\mathrm{scale}} = 0.1$) was successful in reducing the errors to within the expected bounds.

3.3 Implementation

We have implemented the DLPNO-MP2 response density calculation in the ORCA package,[221] closely following the algorithm for the DLPNO-MP2 gradient.[192] The code is structured as follows:

1. First the SCF equations are solved.

2. Then, the DLPNO-MP2 energy and relaxed density calculation is performed. The PNO coefficients $\mathbf{d}^{ij}$ and amplitudes $\mathbf{T}^{ij}$ are kept on disk, as well as the list of active orbital pairs and the domain information.

3. Next, the SCF-level property calculation is performed and the CPSCF solution $U_{ai}^{\boldsymbol{\lambda}}$ is stored.

4. The remaining blocks of $\mathbf{U}^{\boldsymbol{\lambda}}$ are calculated, according to eqs. 3.85, 3.87, 3.88, and 3.93. $\mathbf{F}^{\boldsymbol{\lambda}}$ and $\mathbf{c}^{\boldsymbol{\lambda}}$ are completed, as well as $\widetilde{\mathbf{P}}^{\boldsymbol{\lambda}}$.

5. The 3-index integrals $(i\tilde{\mu}'|K)$ and $(i\tilde{\mu}'|K)^{\boldsymbol{\lambda}}$ are calculated and stored.

6. In a loop over orbital pairs, the CPNO coefficients $\mathbf{d}'^{ij}$ are reconstructed, and $\breve{\mathbf{T}}^{ij}$ and $\widehat{\mathbf{T}}^{ij,\boldsymbol{\lambda}}$ are calculated according to eqs. 3.16 and 3.99. $\boldsymbol{\theta}^{ij,\boldsymbol{\lambda}}$ are computed and the perturbed PNO coefficients $\mathbf{d}^{ij,\boldsymbol{\lambda}}$ are stored on disk.

7. The perturbed PNO amplitude equations, 3.103 are solved iteratively, separately for each perturbation.

8. The contributions to the response density matrix from D_{ij}, $\mathbf{D}^{ij}$, and their derivatives is calculated.

9. The PNO-dependent terms are evaluated in a loop over orbital pairs:

   9.1. The full $\mathbf{d}''^{ij}$, $\breve{\mathbf{T}}^{ij}$, $\mathbf{d}''^{ij,\boldsymbol{\lambda}}$, and $\breve{\mathbf{T}}^{ij,\boldsymbol{\lambda}}$ are reconstructed.

   9.2. The intermediates $\boldsymbol{\tau}^{ij}$ and $\boldsymbol{\tau}^{ij,\boldsymbol{\lambda}}$ are calculated.

   9.3. eqs. 3.60 and 3.111 are solved to obtain $\mathbf{v}^{ij}$ and $\mathbf{v}^{ij,\boldsymbol{\lambda}}$.

   9.4. eqs. 3.58 and 3.109 are solved to obtain $\mathbf{w}^{ij}$ and $\mathbf{w}^{ij,\boldsymbol{\lambda}}$. Their contributions to $\mathbf{D}'^{\mathrm{o}}$, $\mathbf{D}'^{ij}$, and their derivatives are evaluated.

   9.5. $\mathbf{G}^{i(ij)}$, $\mathbf{G}^{j(ij)}$, $\mathbf{G}^{i(ij),\boldsymbol{\lambda}}$, and $\mathbf{G}^{j(ij),\boldsymbol{\lambda}}$ and their contributions to $\boldsymbol{\Gamma}^{K}$, $\boldsymbol{\xi}^{ij}$, $\mathbf{Y}^{\gamma}$, and their derivatives are computed.

   9.6. Terms related to $\boldsymbol{\xi}^{ij}$ and $\boldsymbol{\tau}^{ij}$ and their derivatives are added to $\mathbf{Y}^{\delta}$ and $\mathbf{Y}^{\delta,\boldsymbol{\lambda}}$.

10. $\boldsymbol{\Gamma}^{K}$ and $\boldsymbol{\Gamma}^{K,\boldsymbol{\lambda}}$ are read from disk and their contributions to $L_{ij}^{\boldsymbol{\lambda}}$, $L_{mj}^{\boldsymbol{\lambda}}$, $\mathbf{Y}^{\alpha,\boldsymbol{\lambda}}$, $\mathbf{Y}^{\beta}$, and $\mathbf{Y}^{\beta,\boldsymbol{\lambda}}$ are evaluated in the AO basis by generating the required 3-index integrals on the fly.

11. The prescreening contributions to $L_{ij}^{\boldsymbol{\lambda}}$, $L_{mj}^{\boldsymbol{\lambda}}$, $L_{ia}^{\boldsymbol{\lambda}}$, and $\mathbf{D}'$ are calculated.

12. $L_{mj}^{\boldsymbol{\lambda}}$ is completed and the Z-CV eqs. 3.116 are solved to obtain $z_{mj}^{\boldsymbol{\lambda}}$.

13. $L_{ij}^{\boldsymbol{\lambda}}$ is completed and the Z-CPL eqs. 3.113 are solved to obtain $z_{ij}^{\boldsymbol{\lambda}}$. In our implementation a conjugate gradient solver is used.

14. $L_{ia}^{\boldsymbol{\lambda}}$ is completed and the Z-CPSCF eqs. 3.72 are solved to obtain $z_{ia}^{\boldsymbol{\lambda}}$. This is most conveniently done in the CMO basis using a standard CPSCF solver.

15. The full response density $\mathbf{D}^{\boldsymbol{\lambda}}$ is assembled and the DLPNO-MP2-level properties are calculated.

As the goal here is the calculation of field-response properties, the algorithm has been optimized for a small number of perturbations. The loop over the three Cartesian components of the external field is the innermost one in most cases, such that the unperturbed and a single perturbed quantity are kept in memory at any given time. In some situations, e.g. step 9.2., it is faster to calculate all perturbed quantities at the same time, at the cost of higher memory usage. Likewise, all intermediates which are stored on disk – such as $(i\tilde{\mu}'|K)^{\boldsymbol{\lambda}}$, $\mathbf{d}^{ij,\boldsymbol{\lambda}}$, and $\mathbf{T}^{ij,\boldsymbol{\lambda}}$ – are kept for all perturbations simultaneously. For these reasons, the implemented algorithm is not suitable for a number of perturbations that grows with the system size, e.g. nuclear Hessians.

It is also worth pointing out that the NPAO domains and the SC amplitudes are calculated four times in total – in steps 2. (twice), 6., and 9.1. – while their response is calculated twice – in steps 6., and 9.1.. This is not an insignificant computational overhead, as shown in Section 3.4.4, but is done intentionally to avoid the storage and I/O of quantities in the full NPAO domains, which are much larger than the PNO domains. Taking the vancomycin example from that section, with 22 265 kept pairs and average NPAO and PNO domain sizes of 1007 and 22, respectively: about 1.2 TB of disk space was required in total, of which the PNO coefficients ($\mathbf{d}^{ij}$ and $\mathbf{d}^{ij,\mathbf{B}}$) were about 12.8 GB and the PNO amplitudes ($\mathbf{T}^{ij}$ and $\mathbf{T}^{ij,\boldsymbol{\lambda}}$) – about 960 MB. A back-of-the-envelope estimate suggests that if the NPAO coefficients ($\mathbf{d}''^{ij}$ and $\mathbf{d}''^{ij,\mathbf{B}}$) and SC amplitudes ($\widehat{\mathbf{T}}^{ij}$ and $\widehat{\mathbf{T}}^{ij,\boldsymbol{\lambda}}$) were stored in addition, a further 2.5 TB of disk space would be required just for those quantities. In the end, less than 20 % of the total computation time would be saved, at the cost of additional I/O overhead.

The asymptotic scaling behavior of the DLPNO-MP2 gradient algorithm was discussed in ref. 192 and that discussion applies here as well. Briefly, the number of orbital pairs that survive the dipole-based prescreening scales linearly with system size in the asymptotic limit, while the PAO correlation domains reach a finite size for large systems. This allows for asymptotic linear scaling of most major steps in the algorithm, provided sparsity is properly exploited using the sparse maps infrastructure introduced in ref. 144. In particular, the RI integral transformation, PNO generation, and iterative solution of the amplitude equations are asymptotically linear scaling. Two-electron contributions coming from the Fock matrix, e.g. in the CPSCF and Z-CPSCF equations, can be calculated with effective quadratic scaling using the RIJCOSX approximation.[113] The calculation of terms involving $(K|ip)$ integrals in the Z-CPSCF equations (eq. 3.77) right-hand sides asymptotically scales as $\mathcal{O}(N^2)$. Together with the $(i\tilde{\mu}'|K)$ contributions (eq. 3.78) these terms take about 10–15% of the computation time for the largest systems discussed here. Contributions from the screened-out pairs scale quadratically, while localization, CPL, and Z-CPL equations scale as $\mathcal{O}(N^3)$ but these steps constitute a very small part of the overall computation time.

Alongside MP2, the implementation can be used for DHDFT – the relevant modifications are identical to the RI-MP2 case, discussed in Section 2.1.4. Spin-component scaling is also implemented.[51] Implicit solvent effects can be included using CPCM,[245,246] as discussed in Section 2.1.5

3.4 Results and discussion

3.4.1 Computational details

To examine how quickly DLPNO-MP2 response properties converge towards the RI-MP2 results as the various thresholds are tightened, we performed a series of polarizability and NMR shielding calculations on the molecules depicted in Figure 3.4.

For the shielding calculations, the pcSseg-2[284] basis set was used, along with the cc-pwCVTZ/C[111,290,310] auxiliary basis set, which was shown to be an appropriate combination in Chapter 2. RI was used only for Coulomb integrals in all Fock matrix builds with no approximation for the exchange integrals, while RIJK was used for the perturbed two-electron integrals over GIAOs. In both cases, the def2-JK[115] auxiliary basis set was employed. All orbitals were included in the MP2 treatment.

For the polarizability calculations, we used the def2-TZVPD[311,312] basis set together with the aug-cc-pVTZ/C[111] auxiliary basis set. Once again, def2-JK[115] was used for Coulomb fitting and all electrons were correlated.

In order to isolate the influences of the different DLPNO parameters, we performed several sets of calculations as follows:

1. Varying T_{CutPNO} for the valence orbitals with very conservative values of $T_{\mathrm{CutPNO}} = 10^{-12}$ for the core orbitals and $F_{\mathrm{Cut}} = 10^{-8}$. We set $T_{\mathrm{S}} = 10^{-8}$ and all other DLPNO thresholds to 0.

2. Varying T_{CutPNO} for the core orbitals with $T_{\mathrm{CutPNO}} = 10^{-10}$ for the valence orbitals, $F_{\mathrm{Cut}} = 10^{-8}$, $T_{\mathrm{S}} = 10^{-8}$ and all other DLPNO thresholds equal to 0.

3. Varying F_{Cut} with $T_{\mathrm{CutPNO}} = 10^{-12}$ for the core and $T_{\mathrm{CutPNO}} = 10^{-10}$ for the valence orbitals, $T_{\mathrm{S}} = 10^{-8}$ and all other DLPNO thresholds equal to 0.

4. Same as above but also fixing $F_{\mathrm{Cut}} = 10^{-5}$ and varying T_{CutDO}. Two values were used for T_{S} to examine the numerical stability: 10^{-8} and 10^{-5}.

5. Same as above but also fixing $T_{\mathrm{CutDO}} = 10^{-3}$, $T_{\mathrm{CutDOPre}} = 0.03$, and $T_{\mathrm{S}} = 10^{-5}$ and varying T_{CutPre}. We set $T_{\mathrm{CutDOij}} = 0.05$, a large value, so as to allow as many pairs as possible to be screened out without the dipole approximation breaking down.

6. Setting all thresholds to the default ("NormalPNO") values used for energy and gradient calculations: $T_{\mathrm{CutPNO}} = 10^{-8}$ (10^{-10} for core orbitals), $F_{\mathrm{Cut}} = 10^{-5}$, $T_{\mathrm{CutDO}} = 10^{-2}$, $T_{\mathrm{CutDOPre}} = 0.03$, $T_{\mathrm{CutDOij}} = 10^{-5}$, $T_{\mathrm{CutPre}} = 10^{-6}$, $T_{\mathrm{CutMKN}} = 10^{-3}$, $T_{\mathrm{CutC}} = 10^{-3}$, but with $T_{\mathrm{S}} = 10^{-5}$ and a PNO level shift $\varepsilon_{\mathrm{scale}} = 0.1$.

7. Same as above with the "LoosePNO" default thresholds: $T_{\mathrm{CutPNO}} = 10^{-7}$ (10^{-9} for core orbitals) and $T_{\mathrm{CutDO}} = 2 \times 10^{-2}$.

8. We also performed shielding calculations with RI-MP2, NormalPNO, LoosePNO, and TightPNO ($T_{\mathrm{CutPNO}} = 10^{-9}$ for valence and 10^{-11} for core orbitals, $T_{\mathrm{CutDO}} = 5 \times 10^{-3}$), together with the RIJCOSX approximation to see how the COSX and DLPNO errors stack up. The keyword `DefGrid3` was used to choose finer COSX integration grids than the default. Note that the grids in ORCA were updated for version 5 of the program and the `DefGrid3` settings are similar to the "RIJCOSX-XL" settings used in Chapter 2.

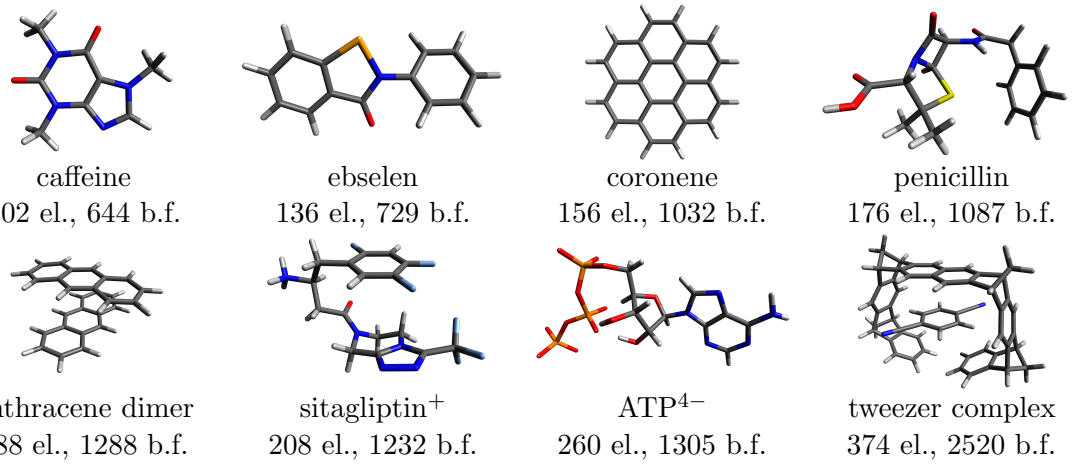

Figure 3.4: Models of the benchmark systems with number of electrons and pcSseg-2 basis functions.[268]

To investigate the efficiency of the implementation for larger system sizes, we used idealized glycine chains in either a linear ($\phi = 180°$, $\psi = 180°$) or α-helix ($\phi = -57°$, $\psi = -47°$) conformation. The neutral form of the molecules was used, rather than the zwitterion. The structures were generated using Gabedit.[313] As above, these calculations were performed with NormalPNO (and RI-MP2) and RIJCOSX. These calculations ran in a node-exclusive fashion on 8 Intel Xeon E5-2690v2@3.00GHz CPU cores with 6 GB of RAM per core.

To showcase all the capabilities of the implementation, another large shielding calculation was performed on the vancomycin molecule using the DSD-PBEP86 DHDFT functional,[85] NormalPNO thresholds, RIJCOSX, frozen core orbitals, and CPCM for implicit solvation in dimethylsulfoxide (DMSO). This calculation ran on 12 Intel Xeon E5-2687Wv4@3.00GHz CPU cores with 15 GB RAM per core.

Finally, a series of DLPNO-MP2 polarizability calculations were performed on [n]helicene ($n = 7, 9, 11, 13, 15$) molecules using the aug-cc-pVTZ,[265,314] aug-cc-pVTZ/C, and def2-JK basis sets, NormalPNO thresholds, frozen core orbitals, and RIJCOSX. The geometries were optimized with RI-MP2 (for n=7–11) and DLPNO-MP2 (for n=13–15) using the cc-pVTZ[265,315] and cc-pVTZ/C[111] basis sets. These calculations ran on 12 Intel Xeon E5-2687Wv3@3.10GHz CPU cores with 8 GB of RAM per core.

3.4.2 Accuracy: NMR shieldings

In this section we use some of the systems in Figure 3.4 to examine how much the DLPNO-MP2 isotropic shielding constants deviate from the RI-MP2 values, as we tighten the DLPNO thresholds. The mean absolute errors (MAEs) vs RI-MP2 for different values of T_{CutPNO} are shown in Figure 3.5a for the different nuclides in the systems ATP^{4-}, caffeine, ebselen, and penicillin. We note that the errors diminish rapidly with decreasing T_{CutPNO} and at the default value of 10^{-8} for valence orbitals, they are much lower than the inherent error in MP2. For example, the MAE for C is 0.1 ppm, which is an order of magnitude smaller than the average deviation from CCSD(T) (see Section 2.3.3 and ref. 47). It is also noteworthy that the results are insensitive to core PNO truncation, except for the heavier elements, particularly P and Se. This may be in part because the pcSseg-2 basis set does not fully capture core correlation effects (see Section 2.3.6).

For simplicity in the discussion we want a single measure of the DLPNO error, however,

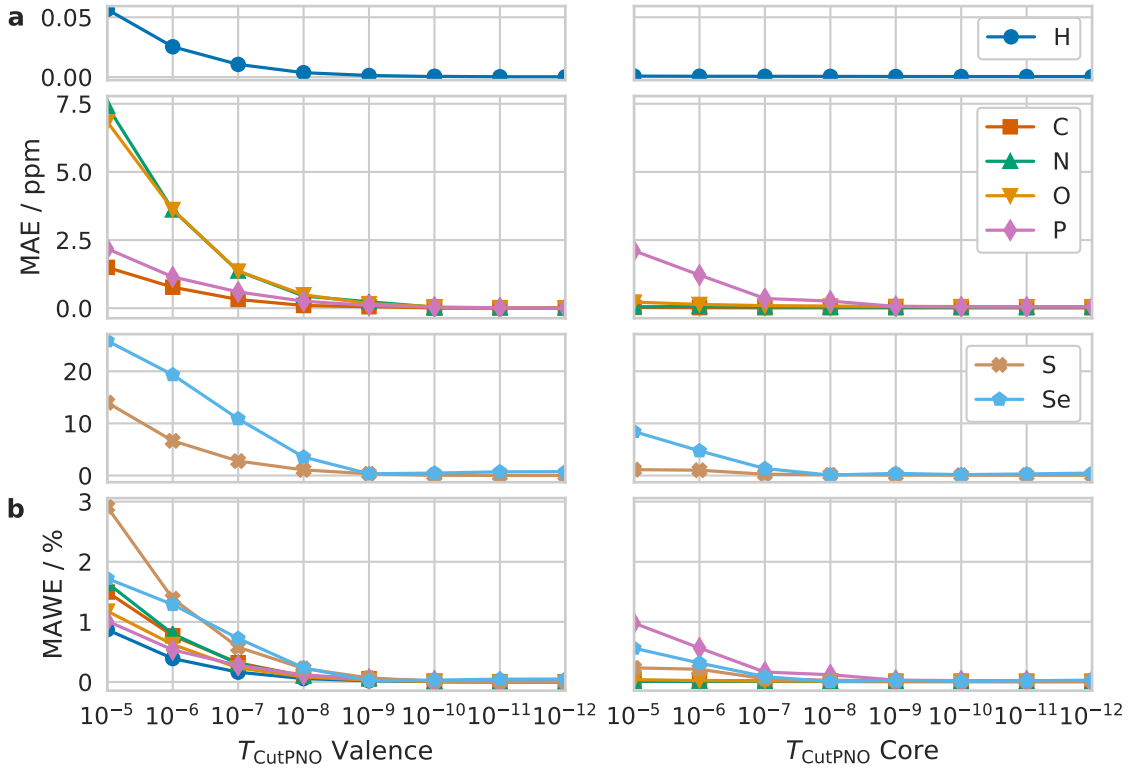

Figure 3.5: Mean absolute error (a) and mean absolute weighted error (b) vs RI-MP2 in the shieldings of different nuclei in the systems ATP^{4-}, caffeine, ebselen, and penicillin. T_{CutPNO} was varied for either the valence (left) or core (right) orbitals, with the other parameter set to 10^{-12} and 10^{-10}, respectively. The line and marker styles in the legend apply to all subplots.

the shielding constants have very different magnitudes for different nuclides. Thus, we define an absolute weighted error (AWE), whereby we scale the error in the calculated isotropic shielding (e.g. vs RI-MP2) by a factor w_A, derived from the experimental range of chemical shifts for nuclide A:

$$\mathrm{AWE} = \frac{\left|\sigma_i^{\text{DLPNO-MP2}} - \sigma_i^{\text{RI-MP2}}\right|}{\mathrm{w}_A} \times 100\%, \quad i \in A \tag{3.149}$$

$$\mathrm{w}_A = \frac{1}{2}\left(\delta^A_{\max} - \delta^A_{\min}\right) \tag{3.150}$$

We use the values for $\delta^A_{\min}$ and $\delta^A_{\max}$ shown in Table 3.5. A reasonable target accuracy is a mean AWE (MAWE) below 0.5%, which corresponds to 0.5 ppm for ^{13}C, 0.03 ppm for ^{1}H, and about 1 ppm for ^{15}N and ^{17}O. As can be seen from Figure 3.5b, the MAWE

Table 3.5: Experimental chemical shift ranges (ppm) for different nuclides used for scaling in MAWE calculations.

A	$\delta^A_{\min}$	$\delta^A_{\max}$	w_A
^{1}H	-1	12	6.5
^{13}C	0	200	100
^{15}N	0	900	450
^{17}O	-40	1120	580
^{19}F	-300	400	350
^{33}S	-290	670	480
^{31}P	-180	250	215
^{77}Se	-1000	2000	1500

faithfully represents the trends in Figure 3.5a, while also allowing us to combine the data for different nuclides, as they now have the same order of magnitude. The same data

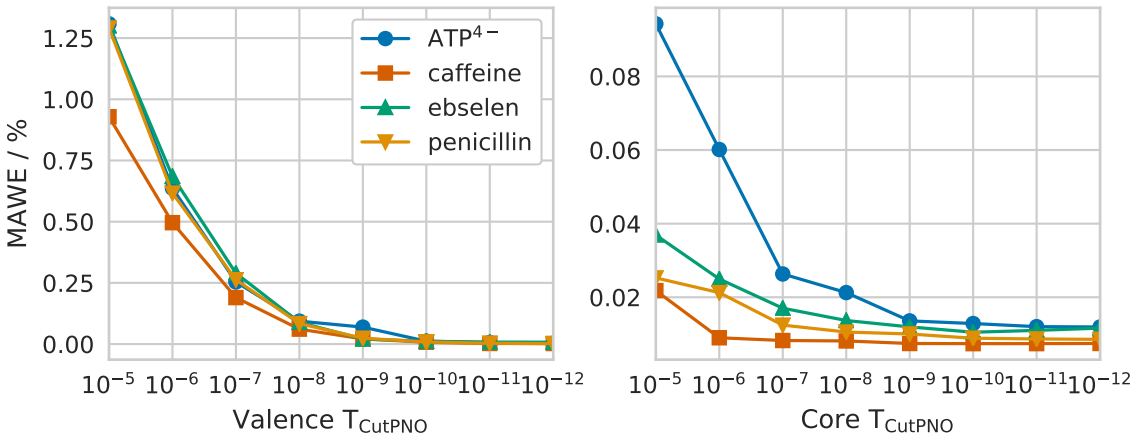

Figure 3.6: Mean absolute weighted error vs RI-MP2 in the shieldings of the systems ATP^{4-}, caffeine, ebselen, and penicillin. T_{CutPNO} was varied for either the valence (left) or core (right) orbitals, with the other parameter set to 10^{-12} and 10^{-10}, respectively. The line and marker styles in the legend apply to both subplots.

are displayed in Figure 3.6, separating the different systems and averaging over all nuclei. Here we can see that ATP^{4-} is slightly more sensitive to core PNO truncation, probably because it contains all the phosphorus atoms in the dataset. The same system also suffers

from a PNO response instability at valence $T_{\mathrm{CutPNO}} = 10^{-9}$ with MaxAE = 1.51 ppm for ^{15}N vs 0.59 and 0.04 ppm for the same nucleus at $T_{\mathrm{CutPNO}} = 10^{-8}$ and $T_{\mathrm{CutPNO}} = 10^{-10}$, respectively. With the level shift-based adjustment (see Section 3.2.3), this error drops to 0.17 ppm at valence $T_{\mathrm{CutPNO}} = 10^{-9}$.

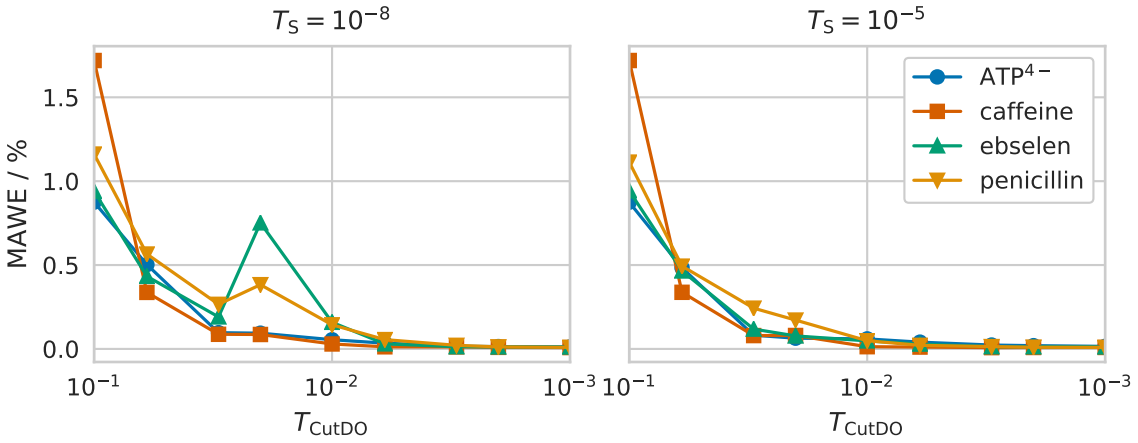

Figure 3.7: Mean absolute weighted error vs RI-MP2 in the shieldings of the systems ATP^{4-}, caffeine, ebselen, and penicillin. T_{CutDO} was varied and T_{S} was set to either 10^{-8} (left) or 10^{-5} (right). The line and marker styles in the legend apply to both subplots.

The influence of T_{CutDO} (at a conservative value of T_{CutPNO}) is shown in Figure 3.7 for the same set of molecules. In the left subplot the redundant PAO domains were truncated with the default eigenvalue threshold $T_{\mathrm{S}} = 10^{-8}$, which leads to some numerical issues, as discussed in Section 3.2.2, seen in the figure as large kinks in the curves for some molecules. In the right subplot a value of $T_{\mathrm{S}} = 10^{-5}$ was used which leads to smooth convergence of the results towards the RI-MP2 reference. At the default value of $T_{\mathrm{CutDO}} = 10^{-2}$, the MAWE over the whole dataset is under 0.05%.

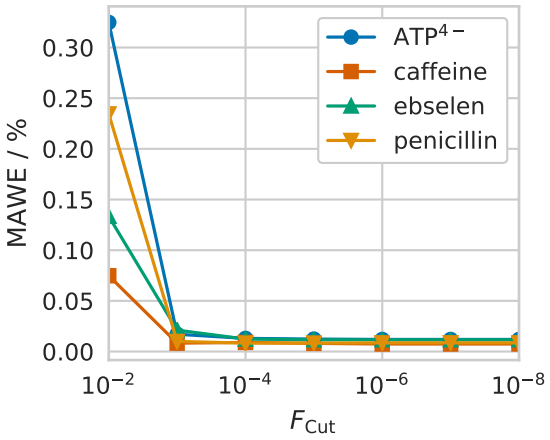

Figure 3.8: Mean absolute weighted error vs RI-MP2 in the shieldings of the systems ATP^{4-}, caffeine, ebselen, and penicillin with varying F_{Cut}.

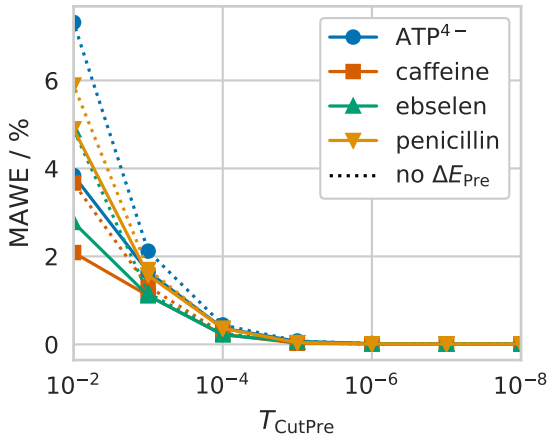

Figure 3.9: Mean absolute weighted error vs RI-MP2 in the shieldings of the systems ATP^{4-}, caffeine, ebselen, and penicillin. T_{CutPre} was varied and dipole estimate-based contributions from the screened-out pairs were either included (solid lines) or excluded (dotted lines).

Setting T_{CutPNO} to a conservative value, we examine the effect of F_{Cut} in Figure 3.8.

Apparently, it imparts negligible errors on the shieldings, especially at the default value of 10^{-5}.

Turning to the pair prescreening threshold T_{CutPre}, its effect on the shielding MAWE is shown in Figure 3.9. Despite the relatively small systems, using a large $T_{\mathrm{DOij}} = 0.05$ leads a significant number of pairs to be screened-out: 50–80% at $T_{\mathrm{CutPre}} = 10^{-4}$ and 20–50% at $T_{\mathrm{CutPre}} = 10^{-6}$. Even so, the effect on the shieldings is minor. Neglecting the contributions from the prescreening correction ΔE_{Pre} also does not worsen the results significantly for $T_{\mathrm{CutPre}} \leq 10^{-4}$, however, calculating these contributions takes a very small proportion of the computation time, so there are no savings to be made by skipping them. On the other hand, the default threshold values of $T_{\mathrm{DOij}} = 10^{-5}$ and $T_{\mathrm{CutPre}} = 10^{-6}$ might be too conservative for NMR shielding calculations.

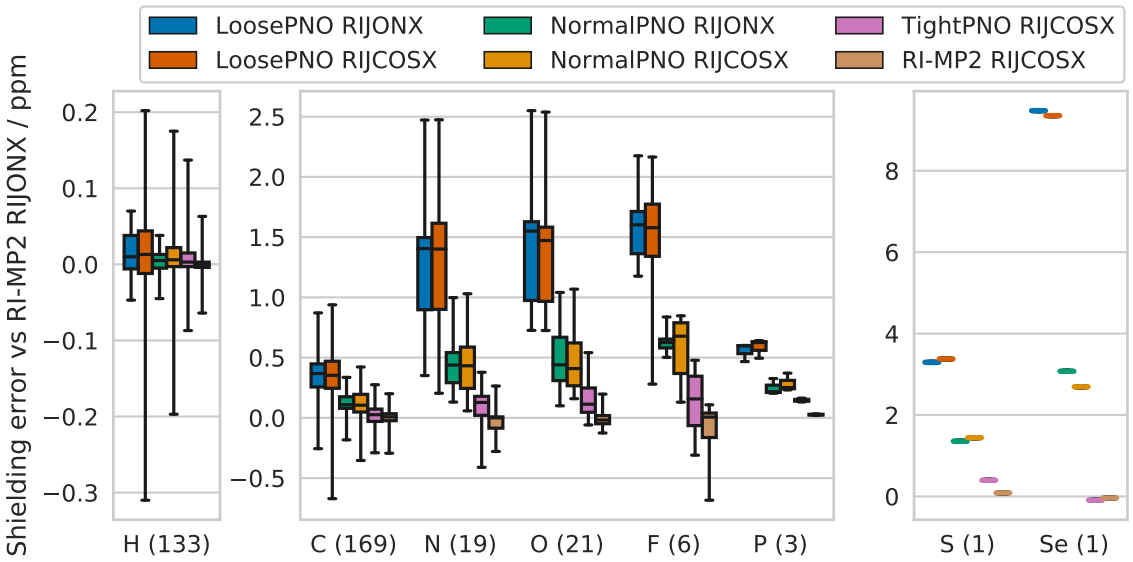

Figure 3.10: Distribution of errors in the shieldings for the systems: $(\mathrm{anth})_2$, ATP^{4-}, caffeine, coronene, ebselen, penicillin, and tweezer complex. Calculations were performed (from left to right, respectively) using LoosePNO thresholds without and with the COSX approximation, using NormalPNO thresholds without and with COSX, and using TightPNO and RI-MP2 with COSX, and the errors were calculated against RI-MP2 without COSX for all datasets. The lines, boxes, and whiskers denote the median, interquartile range, and minimum/maximum values, respectively. The number of nuclei of each element are indicated in parentheses.

Having separately examined the effects of the most important DLPNO parameters on the shieldings, we now see what happens when all parameters are set to their default (NormalPNO) values. Figure 3.10 shows the error distributions for different nuclides over all 8 test systems in Figure 3.4. The NormalPNO/RIJONX distributions are fairly narrow and both the medians and the ranges (which are more relevant for chemical shift calculations) are much smaller than the inherent error in MP2. There is an overall bias towards overestimation of the shielding constants, so some error compensation can be expected in chemical shift calculations. The same figure also contains results with the LoosePNO threshold settings, which produce both larger systematic deviations and wider error distributions, at the borderline of what we may consider tolerable.

All calculations discussed so far were performed using the RIJONX approximation. In practice, it is preferable to also approximate the exchange part of the Fock matrix, e.g. using the COSX approximation, as this significantly reduces the computation time.

However, the semi-numerical integration used in COSX introduces additional errors and numerical noise to the calculation, which may get amplified in DLPNO calculations. Therefore, we have included in Figure 3.10 the error distributions from calculations employing the RIJCOSX approximation with a rather large set of integration grids (corresponding to the `DefGrid3` keyword). Though the DLPNO and COSX errors are basically cumulative, the latter are fairly small so the conclusions from the previous paragraph still apply for the most part. One exception is the ^{1}H shieldings, where the combined NormalPNO and COSX errors lead to a maximum deviation of 0.2 ppm and a spread of almost 0.4 ppm, which is larger than the method error and could in principle lead to a wrong assignment, compared to RI-MP2. This can be remedied by using larger COSX grids, in particular for the CPSCF and Z-CPSCF equations, which appear to be the main source of the deviations. As expected, tightening T_{CutPNO} and T_{CutDO} from LoosePNO to NormalPNO to TightPNO systematically reduces the errors towards the RI-MP2 reference.

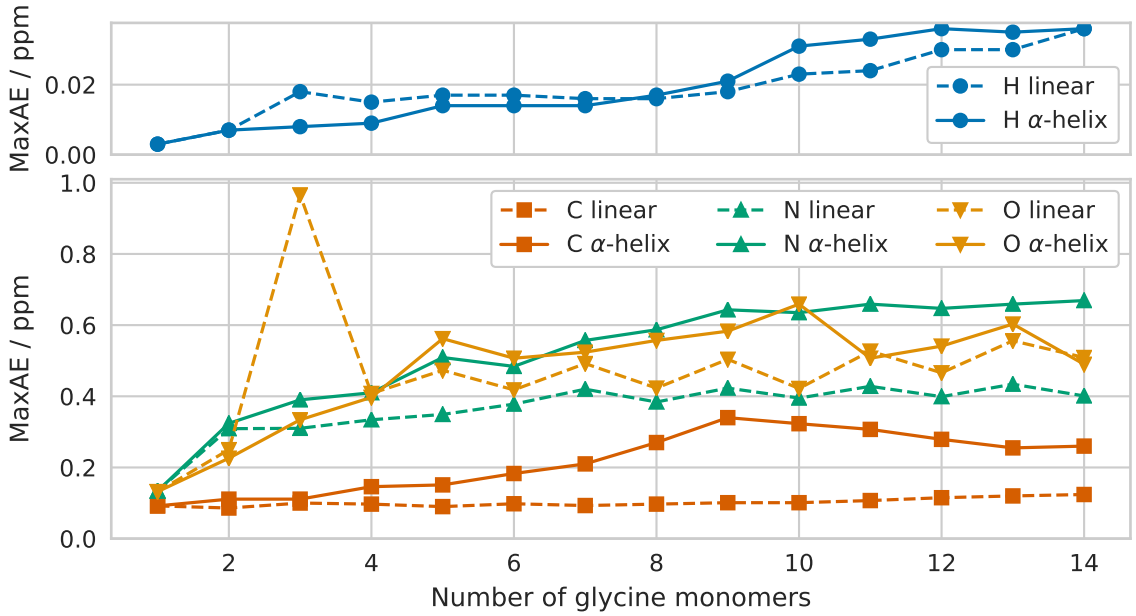

Figure 3.11: Maximum absolute errors in the shieldings of different nuclides from NormalPNO calculations vs RI-MP2 for polyglycine chains in either linear (dotted lines) or α-helix conformation (solid lines). RIJCOSX was used throughout.

As the effect of the local approximations becomes more significant with increasing system size, the relative error in the properties can also be expected to increase, up to the point where all approximations are fully active: orbital domains have reached a constant size, etc. For an intrinsic (i.e. local) property like NMR shielding this means that absolute errors should also reach an upper limit for large enough systems. To examine this relationship, we use the calculations on the glycine chain systems, discussed in Section 3.4.4. Figure 3.11 shows the maximum absolute errors in the shieldings of different nuclides, as a function of the chain length. Apparently, the errors do increase slightly with the system size and the effect is more pronounced for the less sparse α-helix conformation. However, the errors do not grow indefinitely, leveling off around $(\mathrm{gly})_{10}$, and are within the ranges shown in Figure 3.10. A notable outlier is an oxygen nucleus in linear $(\mathrm{gly})_3$ with a rather large error of 0.97 ppm for ^{17}O vs 0.25 and 0.41 ppm for $(\mathrm{gly})_2$ and $(\mathrm{gly})_4$, respectively. Using the level shift-based adjustment, discussed in Section 3.2.3, the MaxAE for ^{17}O in linear $(\mathrm{gly})_3$ is reduced to 0.42 ppm, consistent with the slightly oscillating trend.

3.4.3 Accuracy: dipole polarizabilities

As evident from Section 3.1, the same general procedure can be used to calculate both magnetic shielding and dipole polarizability tensors. It is worth noting, that the polarizability is an extensive global property of the system and as such is less useful to obtain for large molecules, which are the main targets of local correlation methods. Nonetheless, we have included the capability in our implementation and will evaluate the accuracy of the DLPNO-MP2 polarizabilities in this section. It is most convenient to use the relative error (RE) in the isotropic polarizability:

$$\mathrm{RE} = \frac{\alpha^{\text{DLPNO-MP2}} - \alpha^{\text{RI-MP2}}}{\alpha^{\text{RI-MP2}}} \times 100\% \tag{3.151}$$

and its absolute value (ARE). This should be compared to the inherent error of MP2 vs more accurate methods such as CCSD(T), which is around 2% for closed-shell species.[91] DHDFT performs slightly better but still over 1%. Therefore, we consider a DLPNO error of up to 0.5% to be reasonable.

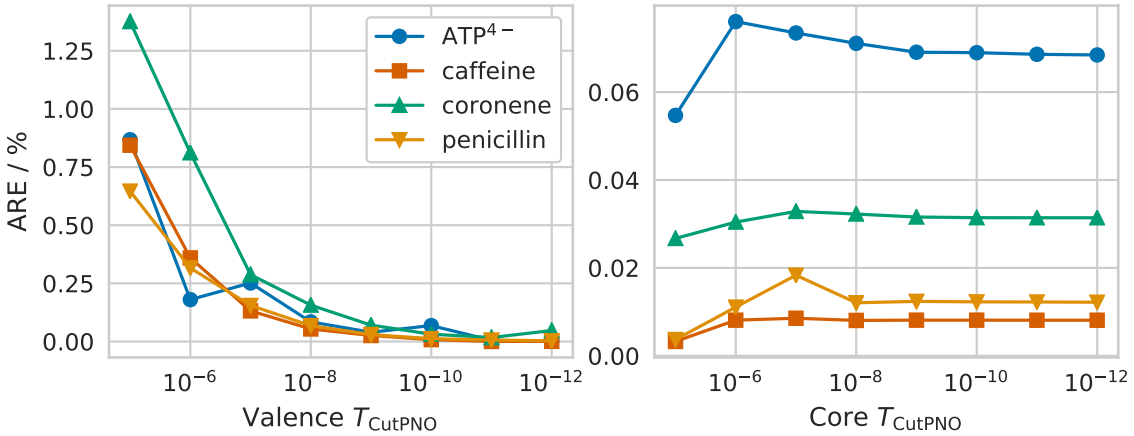

Figure 3.12: Absolute relative errors vs RI-MP2 in the isotropic polarizability of the systems ATP^{4-}, caffeine, coronene, and penicillin. T_{CutPNO} was varied for either the valence (left) or core (right) orbitals, with the other parameter set to 10^{-12} and 10^{-10}, respectively. T_{S} was set to 10^{-5}. The line and marker styles in the legend apply to both subplots.

Figure 3.12 shows the dependence of the error on T_{CutPNO} for several molecules. The DLPNO-MP2 polarizabilities correctly converge towards the RI-MP2 reference values and are accurate enough for $T_{\text{CutPNO}} \leq 10^{-7}$. The influence of PNO truncation for core electrons is almost negligible, which is to be expected, since they do not contribute significantly to the polarizability, especially since we did not include core-polarization basis functions in these calculations. We also note a number of kinks in the curves on the left – one for coronene at $T_{\text{CutPNO}} = 10^{-12}$ and two for ATP^{4-} at 10^{-7} and 10^{-10} (the latter also leads to the slightly larger error in the right subplot). We associate these discrepancies with numerical instabilities due to small differences in the occupation numbers of PNOs and CPNOs, as discussed in Section 3.2.3. Indeed, applying the level shift introduced in that section reduces these errors to fit the downwards trend (see Table F.55).

The effect of domain truncation on the polarizability is shown in Figure 3.13. As for the shieldings, a low value of T_{S} results in erratic behavior and huge errors, especially for coronene. At $T_{\text{S}} = 10^{-5}$, however, convergence towards the RI-MP2 reference is

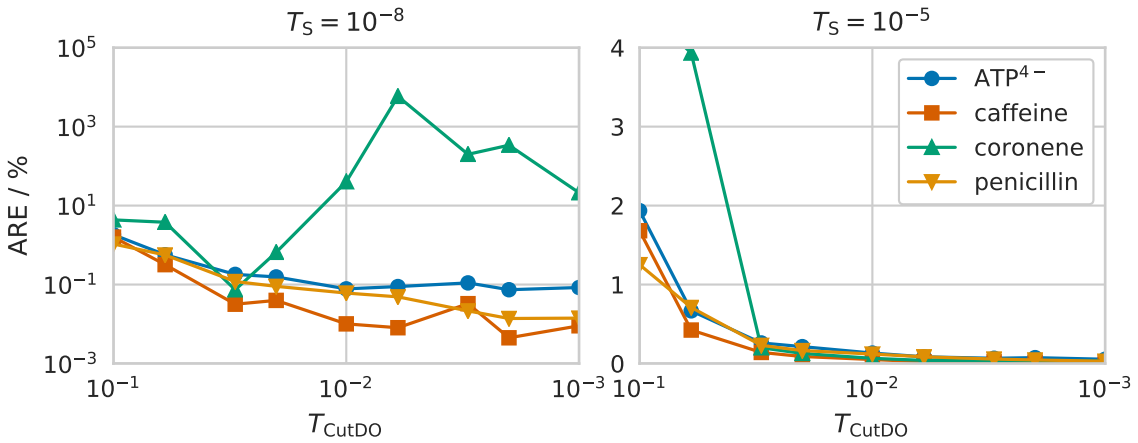

Figure 3.13: Absolute relative errors vs RI-MP2 in the isotropic polarizability of the systems ATP^{4-}, caffeine, coronene, and penicillin. T_{CutDO} was varied and T_{S} was set to either 10^{-8} (left) or 10^{-5} (right). The line and marker styles in the legend apply to both subplots.

much smoother and the errors are already sufficiently small at $T_{\mathrm{CutDO}} = 3 \times 10^{-2}$. The issue is exacerbated by near-linear dependencies in the AO basis: the threshold used for the orthonormalization of the MOs was 10^{-8} and the lowest AO overlap eigenvalues for caffeine, penicillin, coronene, and ATP^{4-} were 2.7×10^{-7}, 4.2×10^{-7}, 2.2×10^{-8}, and 4.6×10^{-7} respectively. Increasing this threshold to 10^{-6} results in smooth convergence of the error for coronene, even with $T_{\mathrm{S}} = 10^{-8}$ (see Table F.56).

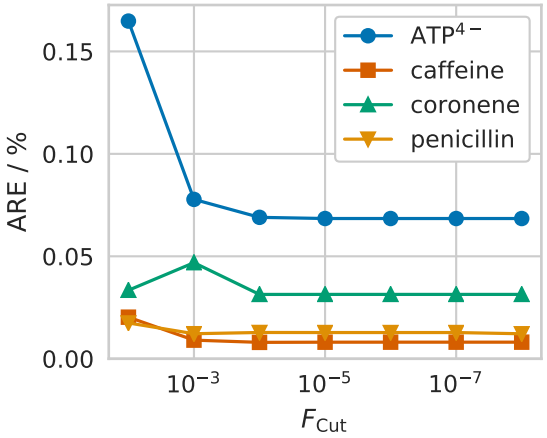

Figure 3.14: Absolute relative errors vs RI-MP2 in the isotropic polarizability of the systems ATP^{4-}, caffeine, coronene, and penicillin with varying F_{Cut}.

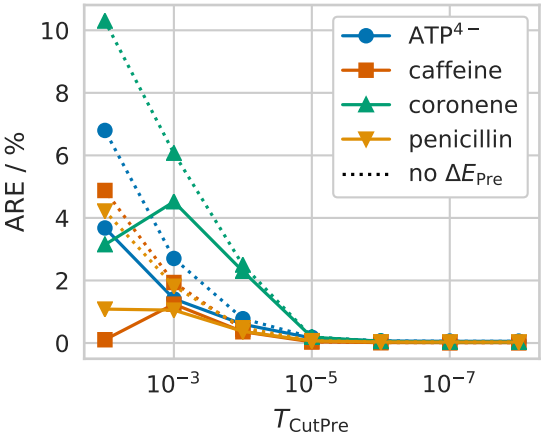

Figure 3.15: Absolute relative errors vs RI-MP2 in the isotropic polarizability of the systems ATP^{4-}, caffeine, coronene, and penicillin. T_{CutPre} was varied and dipole estimate-based contributions from the screened-out pairs were either included (solid lines) or excluded (dotted lines).

The influence of F_{Cut} on the polarizability, shown in Figure 3.14, is rather small. Apparently, the default value of 10^{-5} is more than conservative enough.

Convergence with the pair prescreening threshold T_{CutPre}, as well as the significance of the terms derived from ΔE_{Pre}, is shown in Figure 3.15. With the default parameters, only 18% of pairs are skipped for the largest system, ATP^{4-}, however with the high value of

T_{CutDOij} used here, between 35 and 67% of pairs are screened out already at $T_{\text{CutPre}} = 10^{-5}$ and the errors in the polarizability are below 0.2%. As for the shieldings, the dipole-based correction terms only make a difference for very high values of the threshold. The somewhat larger errors for coronene at $T_{\text{CutPre}} \geq 10^{-4}$ are probably due to the strong delocalization in the system, together with the large value of T_{CutDOij}.

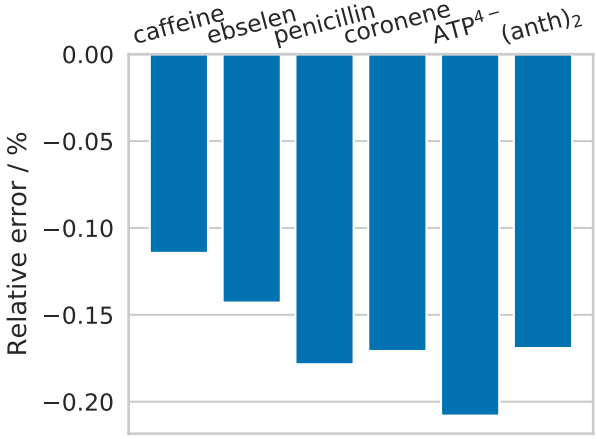

Figure 3.16: Relative errors in the isotropic polarizability from NormalPNO calculations vs RI-MP2 for the systems caffeine, ebselen, penicillin, coronene, ATP^{4-}, and $(anth)_2$, ordered by increasing polarizability.

The combined effect of all DLPNO approximations with the default NormalPNO parameters (and $T_S = 10^{-5}$, $\varepsilon_{\text{scale}} = 0$) is shown in Figure 3.16. The signed error is plotted to illustrate that DLPNO-MP2 consistently underestimates the RI-MP2 polarizabilities. In turn, MP2 tends towards overestimation with respect to CCSD(T),[91] so some fortuitous error compensation can be expected with DLPNO-MP2. In any case, the DLPNO-MP2 values only deviate from the RI-MP2 reference by 0.1–0.2%, which is well within our 0.5% tolerance.

3.4.4 Computational efficiency

To compare the efficiency of our RI-MP2 and DLPNO-MP2 implementations, we performed calculations on a series of polyglycine chains in both linear and α-helical conformations (see Figure 3.17). The latter are much denser and expected to be a bigger challenge for the local approximations. The total wall-clock times for the shielding calculations, including SCF and CPSCF solutions, are presented in Figure 3.18a. The steep scaling of the RI-MP2 calculations is apparent and there is no difference between the two conformations, which is expected, as sparsity is not exploited apart from basic and rather conservative prescreening. In contrast, both series of DLPNO calculations achieve quadratic effective scaling, although the prefactor for the helical conformation is about 4.5 times higher. The crossover point between RI- and DLPNO-MP2 is thus surpassed at $(gly)_5$ (38 atoms, 160 electrons, 994 basis functions) and $(gly)_9$ (66 atoms, 280 electrons, 1738 basis functions) in the linear and helical series, respectively. In other words, calculations that take more than a day or two (on 8 cores) with RI-MP2 can be performed more efficiently with DLPNO-MP2. For the largest system reported here – $(gly)_{15}$ (108 atoms, 460 electrons, 3040 basis functions) – the difference is substantial: 1–3 days with DLPNO-MP2 (depending on the conformation) vs 36 days with RI-MP2. Before the crossover point, the DLPNO-MP2 calculation is at most 2 times slower (for the helical $(gly)_5$) than

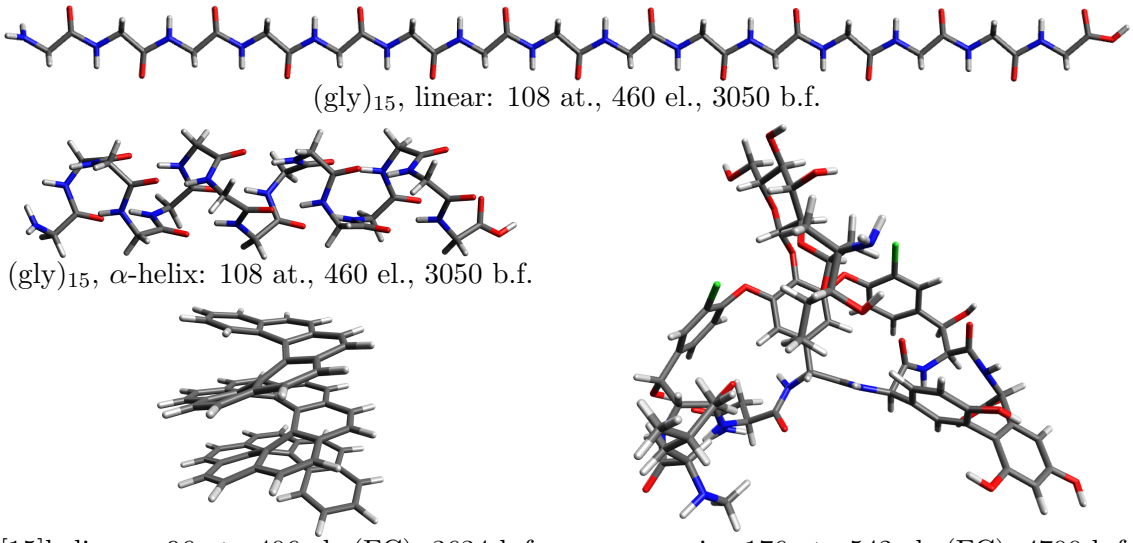

Figure 3.17: Models of some of the large systems used to test the efficiency of the implementation.[268] The numbers of atoms, correlated electrons (frozen-core is indicated), and basis functions (aug-cc-pVTZ for [15]helicene, pcSseg-2 for the rest) are given.

the RI-MP2 one. Another worthwhile comparison is given in Figure 3.18b, namely, how much more expensive a shielding calculation is at the MP2-level vs the SCF-level (HF or hybrid DFT). Apparently, with NormalPNO and RIJCOSX, the DLPNO-MP2 shieldings are obtained at only 5–20 times the cost of the preceding HF shielding calculation (the latter is included in the DLPNO-MP2 timings) and the ratio is still going down at $(gly)_{15}$. This is in stark contrast to RI-MP2, where the calculations with 400 correlated electrons are already more than 100 times more expensive than HF or hybrid DFT and hardly feasible beyond that. Based on the calculations performed for Figure 3.10, the TightPNO (LoosePNO) settings increase (decrease) the total computation time by a factor of 1.3–2.2, compared to NormalPNO.

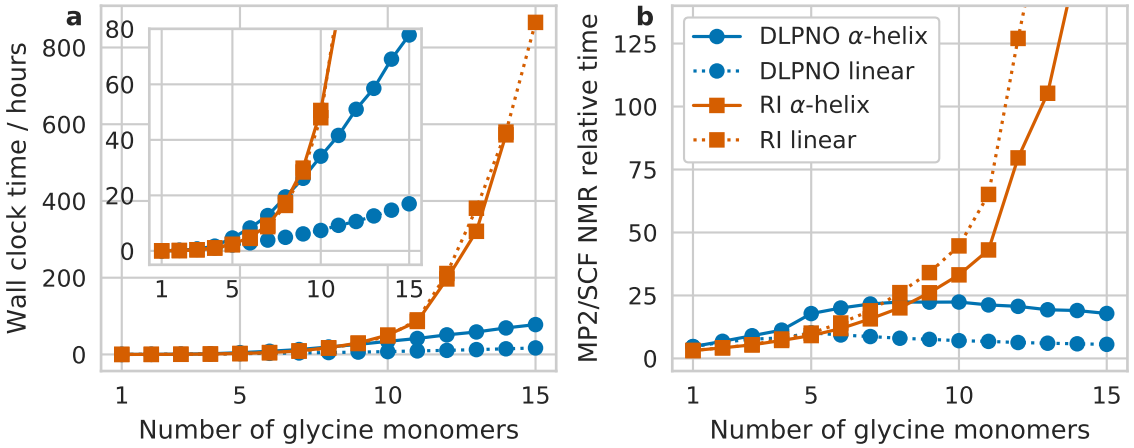

Figure 3.18: (a) Wall clock times (on 8 CPU cores) for shielding calculations on polyglycine chains in either linear (dotted lines) or α-helix (solid lines) conformation using either DLPNO-MP2 with NormalPNO or RI-MP2. (b) Ratio of the wall clock times for MP2 vs HF shielding calculations on the same systems. The legend applies to both plots. RIJCOSX was used throughout.

An in-depth look at the computational cost of different parts of the DLPNO-MP2

response density calculation for the linear polyglicine chains is presented in Figure 3.19. Based on these data, one can see that most major contributions to the wall-clock time (left plot) – the construction of $\widehat{\mathbf{T}}^{ij,\boldsymbol{\lambda}}$ and $\mathbf{d}''^{ij,\boldsymbol{\lambda}}$, the PNO-specific contributions to the Z-CPSCF RHS, the construction of the two-body density, the NPAO space reconstruction, and the PNO amplitude equations – reach an effective scaling (right plot) better than $\mathcal{O}(N_{\mathrm{gly}}^{1.5})$. The Fock response terms scale as $\mathcal{O}(N_{\mathrm{gly}}^{2})$, as expected for RIJCOSX. The transformations involving three-index integrals only achieve $\mathcal{O}(N_{\mathrm{gly}}^{2.5})$ scaling, which suggests that either $(\mathrm{gly})_{15}$ is not a large enough system, or some improvements to the algorithm are possible for these terms. Somewhat surprising is the worse-than-cubic scaling of the Z-CPSCF solution, which should, in principle, match the scaling of the Fock response terms. The source of this discrepancy might be hardware-related or an issue in the CPSCF module of ORCA. Either way, it is not directly related to the implementation described in the present work.

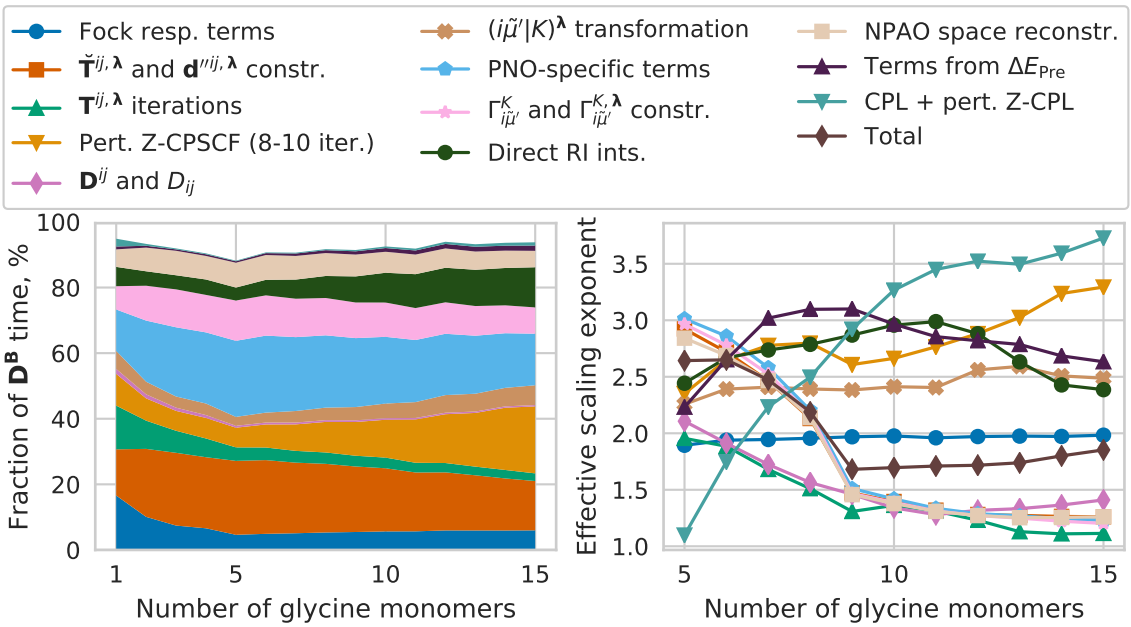

Figure 3.19: Left: contributions to the wall clock time for the DLPNO-MP2 response density calculation on linear polyglycine chains. Right: effective scaling of different calculation parts, as estimated by the slope of a linear fit (on a log–log scale) for the five preceding data points, i.e. the datum at $n = 10$ is based on the data for $n = 6$–10. The colors in the legend apply to both plots.

Detailed information on the most time-consuming steps for an even larger system – the vancomycin molecule – are given in Table 3.6. In this case a frozen-core calculation was performed with a DHDFT functional (DSD-PBEP86), also including implicit solvent (DMSO) effects using CPCM. Some key takeaways from the data are: (1) The total time for the DLPNO-DHDFT calculation is only 8 times longer than an equivalent hybrid DFT calculation (SCF plus SCF-level NMR timings). (2) The cost to calculate the DLPNO-MP2 response densities is roughly 6 times higher than the DLPNO-MP2 energy and density calculation. (3) Reconstructing the SC amplitudes, NPAO space, and the perturbed (C)PNO coefficients twice, takes about a third of the DLPNO-MP2 response time. (4) The equations related to orbital localization make up less than 1% of the computational time. (5) Timings for the evaluation of DFT functional, CPCM, and dipole-based prescreening terms are almost negligible and therefore not shown.

Table 3.6: System size indicators and wall-clock times (min) for a frozen-core DLPNO-DSD-PBEP86 NMR shielding calculation on vancomycin using RIJCOSX. The calculation was performed on 12 Intel Xeon E5-2687Wv4@3.00GHz CPU cores with 15 GB RAM per core. Subparts of calculation steps are marked with "→".

Atoms	176	→ $\breve{\mathbf{T}}^{ij}$ and $\mathbf{d}^{ij}$ construction	88
Basis size (pcSseg-2)	4700	→ PNO amplitude iterations	35
AuxJ size (def2-JK)	9097	→ NPAO space reconstruction	163
AuxC size (cc-pwCVTZ/C)	13591	→ PNO-specific terms	70
Core electrons	218	→ $\Gamma^{K}_{i\tilde{\mu}'}$ contributions	84
Valence electrons	542	→ Fock response terms	10
Kept orbital pairs	22265	→ Z-CPSCF (10 cycles)	56
Mean PAO domain size	1013	→ Localization + Z-CPL	5
Mean PNO domain size	22		
Mean AuxC domain size	1852	DLPNO-MP2 response density	3603
		→ $(i\tilde{\mu}'\|K)^{\boldsymbol{\lambda}}$ transformation	276
Total time	4791	→ $\widehat{\mathbf{T}}^{ij,\boldsymbol{\lambda}}$ and $\mathbf{d}''^{ij,\boldsymbol{\lambda}}$ construction	809
SCF (15 cycles)	355	→ $\mathbf{T}^{ij,\boldsymbol{\lambda}}$ iterations	160
		→ NPAO space reconstruction	270
SCF-level NMR	242	→ PNO-specific terms	671
→ CPSCF right-hand size	56	→ $\Gamma^{K}_{i\tilde{\mu}'}$ and $\Gamma^{K,\boldsymbol{\lambda}}_{i\tilde{\mu}'}$ contributions	748
→ CPSCF (8 cycles)	175	→ Fock response terms	127
		→ Perturbed Z-CPSCF (8 cycles)	176
DLPNO-MP2 energy+density	579	→ CPL + perturbed Z-CPL	27
→ $(i\tilde{\mu}'\|K)$ transformation	23		

Table 3.7: Isotropic polarizability (α_{iso}/Bohr^3) and wall-clock time (t/hours) for calculations on [n]helicene using DLPNO-MP2, compared to RI-MP2 data from ref. 123. The number of (aug-cc-pVTZ) basis functions (N_{bas}) is also given.

		DLPNO-MP2		RI-MP2[123]	
n	N_{bas}	α_{iso}	t^a	α_{iso}	t^b
7	1794	357.7	11	357	65
9	2254	436.4	30	437	134
11	2714	516.5	66	518	425
13	3174	596.5	104		
15	3634	675.7	150		

[a] On 12 Intel Xeon E5-2687Wv3@3.10GHz CPU cores with 8 GB of RAM per core.
[b] On 12 Intel Xeon X5670@2.93GHz CPU cores.

A final test is shown in Table 3.7. Here, DLPNO-MP2 polarizability calculations were carried out for a series of [n]helicene molecules. The results are compared to those obtained by Friese et. al. with their Laplace-based RI-MP2 implementation.[123] The calculated isotropic polarizabilities agree to within 0.3%, as expected. It is not fair to compare the timings directly due to the different computer architectures, but we can look at the trends and effective scaling of both implementations with system size. Based on the calculations for n=7–11, the RI-MP2 algorithm scales as $\mathcal{O}(N_{\text{bas}}^{4.5})$, roughly equivalent to the $\mathcal{O}(N_{\text{bas}}^{4.3})$ scaling of our DLPNO-MP2 code for the same systems. The poor performance of the DLPNO approximations here can be explained by the high degree of delocalization in the helicenes, combined with the diffuse basis sets, which leads to large correlation domains, and to practically all occupied orbital pairs surviving the dipole-based prescreening. Regardless, the performance of DLPNO-MP2 improves for the larger systems and the effective scaling for n=11-15 drops to $\mathcal{O}(N_{\text{bas}}^{2.8})$.

Chapter 4

Conclusion

This thesis encompasses several complementary approaches, which aim to reduce the computational cost of NMR shielding calculations, whilst preserving or improving the accuracy of the results. We focused on the SCF level of theory – HF and DFT – as well as methods including PT2 correlation – MP2 and DHDFT. Chapter 2 recapitulates the known theory of NMR shielding tensors as analytic derivatives of the SCF or MP2 energies. The de facto standard GIAO approach was used to deal with the gauge origin problem. With small modifications, we generalized the GIAO-NMR theory to DHDFT for the first time (a previously reported implementation could only handle a common gauge origin,[94] which is not appropriate for NMR shielding). We discussed the RI and COS approximations to the two-electron terms of the Fock operator, which comprise the computational bottleneck at the SCF level, as well as the RI approximation applied to the MP2 correlation contributions, which also leads to a large speedup compared to a canonical implementation. Similar work has been done before: for example, the linear and sub-linear scaling GIAO-SCF implementations of Ochsenfeld and coworkers,[105,108,109] and the RI-based GIAO-HF program of Loibl et al.[117] In the context of reducing the computational cost of MP2 response property calculations, one should mention the integral-direct GIAO-MP2 implementation for NMR shieldings of Kollwitz, Häser, and Gauss,,[120,121] the derivation of RI-MP2 second derivatives in combination with COSX,[94] and the Laplace-based approaches of Ochsenfeld, Hättig and their coworkers.[122,123]

When examining the accuracy of the various approximations, we compared them to the other error sources in NMR chemical shift calculations – primarily due to the method itself and basis set incompleteness. For this purpose, a benchmark set of 15 small molecules was assembled, comprising 34 ^{1}H, ^{13}C, ^{15}N,^{17}O, ^{19}F, and ^{31}P shielding constants, which were calculated at the CCSD(T)/pcSseg-4 level. The accuracy of standard DFT functionals – as measured by the MARE$_\delta$ – varied greatly in the range of 4–18 %, while MP2 and its SCS variants is somewhat more robust at about 4 %, which is in agreement with other similar benchmarks.[47,73] DHDFT stands out in comparison with errors between 1.5 and 4.3 %, depending on the functional, the most accurate being revDSD-PBEP86 (closely followed by its slightly different parameterizations).

When it comes to basis set convergence, it is unsurprisingly faster for SCF- than for PT2-based methods: HF and DFT shieldings are already sufficiently converged at the pcSseg-2 level with a residual error of about 0.8 %, while MP2 still has a significant 1.9 % error with this basis, reduced to 0.4 % with pcSseg-3. DHDFT (DSD-PBEP86) has intermediate basis set errors of 1.1 % and 0.2 % at the pcSseg-2 and pcSseg-3 levels, respectively.

An appropriate target for the error due to the two-electron integral approximations is thus an order of magnitude lower than the basis set errors and it is readily achieved with either the RIJK or RIJCOSX approximations in combination with the def2-JK auxiliary basis set and appropriate COSX grids. The cc-pwCV[T,Q,5]Z/C RI-MP2 fitting basis sets were shown to be appropriate for the pcSseg-[2,3,4] orbital basis sets, respectively.

The efficiency of the algorithms was tested on realistic systems between 10 and 100 atoms, as well as on idealized linear alkane chains. The RIJK method is hence recommended for calculations on small molecules (up to about 100 electrons and 1000 basis functions), while for larger systems, the RIJCOSX method is more efficient. RI-MP2 (and DHDFT) NMR shielding calculations were shown to be feasible for systems of up to about 400 electrons with the present implementation within a few days of computation time.

Chapter 3 focused on a way to relax this restriction and enable MP2 and DHDFT chemical shift calculations for even larger systems via the DLPNO-MP2 approximation. We discussed the theory and implementation of the DLPNO-MP2 response density, based on previous work on the energy and gradient.[144,191–193] Similar efforts by others to apply local correlation approaches to NMR shielding calculations have yielded a proof-of-concept GIAO-LMP2 implementation,[178] as well as an efficient RI-based version of the latter.[179,180] However, the present work describes the first complete analytic second derivative implementation for a PNO-based method.

The present derivation is applicable both to NMR shieldings and other analytic second derivatives, for which the AOs are independent of at least one of the two perturbations, such as dipole polarizabilities. Based on a benchmark set of several medium-sized molecules, we assessed the errors due to the DLPNO approximations and found them to be sufficiently small. Setting the relevant thresholds to the default ("NormalPNO") values used in energy and gradient calculations results in errors in the calculated shieldings an order of magnitude smaller than the inherent error of MP2. For example, the maximum absolute deviations from the RI-MP2 reference for ^{13}C and ^{1}H shieldings in the test set are 0.3 and 0.04 ppm, respectively. The DLPNO-MP2 isotropic polarizabilities with default thresholds are also within 0.2% of the RI-MP2 reference values

Comparing the computational cost of DLPNO-MP2 and RI-MP2 property calculations for linear and helical polyglycine, we found that the DLPNO-MP2 implementation becomes more efficient for systems larger than 38 atoms/160 electrons and 66 atoms/280 electrons, respectively. Due to the asymptotic linear scaling of the major post-SCF steps, DLPNO-MP2 property calculations are never more than about 20 times more expensive than equivalent HF or hybrid DFT calculations. The largest DLPNO-MP2 NMR shielding calculation reported here – on vancomycin (176 atoms, 542 correlated electrons, 4700 basis functions) – took 80 hours on 12 CPU cores, compared to 10 hours for hybrid DFT. Thus, the implementation allows accurate MP2 and DHDFT property calculations for virtually all systems that could be treated at the hybrid DFT level.

It is important to note that MP2, DHDFT, and any approximate variants thereof can fail fundamentally for certain systems, such as those with a small HOMO-LUMO gap (e.g. transition metal complexes) or high degree of static correlation, whereas many of these cases can be treated accurately with coupled cluster methods. In this regard, the developments presented here set the stage for analytic second derivatives of higher level local correlation methods such as DLPNO-CCSD. In particular, the pitfalls encountered here and their proposed solutions, discussed in Section 3.2, are also likely relevant for other local correlation methods.

Another avenue of interest is multi-layer schemes like those reported in ref. 316, in which some orbital pair interactions are treated with lower accuracy in the DLPNO approximations or completely neglected in the correlation treatment. Such an approach may be particularly well suited to NMR shielding calculations of solvated systems, or cluster models of molecular crystals. Fragment-based and QM/MM schemes can also be applied on top of the approximations discussed in this thesis, further increasing the size of the systems within reach.

List of acronyms

AA	auxiliary basis set generated with AutoAux
AE	absolute error
AIMD	ab initio molecular dynamics
AO	atomic orbital
ATP	adenosine triphosphate
AuxC	auxiliary basis set used for the RI-MP2 approximation
AuxJ	auxiliary basis set used for the RIJ approximation
AWE	absolute weighted error
B2GP-PLYP	"general purpose" version of the B2PLYP functional by J.M.L. Martin and coworkers
B2K-PLYP	version of the B2PLYP functional for kinetics by J.M.L. Martin and coworkers
B2PLYP	double-hybrid functional based on BLYP by S. Grimme
B2T-PLYP	version of the B2PLYP functional for thermochemistry by J.M.L. Martin and coworkers
B3LYP	three-parameter hybrid functional, based on BLYP
B97-D3	version of the Becke 1997 functional by S. Grimme
BLYP	combination of Becke 1988 exchange and Lee–Yang–Parr 1988 correlation functionals
CBS	complete basis set
CC	coupled cluster theory
CC2	second order approximate coupled cluster method
CCSD(T)	coupled cluster theory with single, double, and perturbative triple excitations
CDFT	current density functional theory
CFOUR	electronic structure program
CI	configuration interaction
CMO	canonical molecular orbital
COS	chain-of-spheres (approximation)
COSJ	chain-of-spheres for Coulomb
COSJX	chain-of-spheres for Coulomb and exchange
COSX	chain-of-spheres for exchange
CPCM	conductor-like polarizable continuum model
CPL	coupled perturbed localization
CPNO	complementary pair natural orbitals
CPSCF	coupled perturbed self-consistent field
CPU	central processing unit
CV	core–valence

D3BJ	S. Grimme's empirical dispersion correction with Becke–Johnson damping
DF	density functional
DFT	density functional theory
DHDF	double-hybrid density functional
DHDFT	double-hybrid density functional theory
DLPNO	domain-based local pair natural orbital (approximation)
DSD	dispersion-corrected spin-component-scaled double-hybrid
DSD-BLYP	DSD functional based on BLYP by J.M.L. Martin and coworkers
DSD-PBEP86	DSD functional based on PBE exchange and Perdew 1986 correlation by J.M.L. Martin and coworkers
FB	Foster–Boys (orbital localization method)
FC	frozen core (approximation)
FCI	full configuration interaction
GGA	generalized gradient approximation
GIAO	gauge-including atomic orbitals
GTO	Gaussian-type orbital
HF	Hartree–Fock method
HFC	hyperfine coupling
HOMO	highest occupied molecular orbital
I/O	input/output
IQR	interquartile range
IQRE	interquartile range of errors
IQRRE	interquartile range of relative errors
KS-DFT	Kohn–Sham density functional theory
KT2, KT3	Keal–Tozer functionals for NMR shielding
LHS	left-hand side
LMO	localized molecular orbital
LMP2	local (approximate) MP2
LUMO	lowest unoccupied molecular orbital
M06, M06-2X	Minnesota 2006 hybrid functionals by D. Truhlar and coworkers
M06-L	Minnesota 2006 local functional by D. Truhlar and coworkers
MAE	mean absolute error
MARE	mean absolute relative error
MAWE	mean absolute weighted error
ME	mean error
MD	molecular dynamics
MO	molecular orbital
MP2	second order Møller–Plesset perturbation theory
MRE	mean relative error
MRRE	mean range of relative errors
NMR	nuclear magnetic resonance
NPAO	non-redundant projected atomic orbitals
OBS	orbital basis set
ONIOM	"our own n-layered integrated molecular orbital and molecular mechanics" method by K. Morokuma and coworkers
ORCA	electronic structure program
OS	opposite-spin

PAO	projected atomic orbital
PBE	Perdew–Burke–Ernzerhof 1996 density functional
PBE0	hybrid functional based on PBE
PNO	pair natural orbital
PT2	second order perturbation theory
QM/MM	quantum mechanics/molecular mechanics
RAID	redundant array of independent disks
RAM	random-access memory
RHS	right-hand side
RI	resolution of the identity
RIJ	RI approximation for Coulomb
RIJCOSX	RI approximation for Coulomb and chain-of-spheres for exchange
RIJCOSX-S	RIJCOSX using “small” grid settings
RIJCOSX-L	RIJCOSX using “large” grid settings
RIJCOSX-XL	RIJCOSX using “extra large” grid settings
RIJK	RI approximation for Coulomb and exchange
RIJONX	RI approximation for Coulomb and analytic exchange
RIK	RI approximation for exchange
RI-MP2	RI-based MP2 method
S2-MP2	variant of SCS-MP2 with different parameters
SCF	self-consistent field
SCS	spin-component scaling
SCS-MP2	spin-component-scaled MP2
SDRE	standard deviation of relative errors
SOS-MP2	spin-opposite-scaled MP2
SS	same-spin
TPSS	Tao–Perdew–Staroverov–Scuseria 2003 density functional
VPT2	second order vibrational perturbation theory
VS98	Van Voorhis–Scuseria 1998 density functional
VV10	Vydrov–Van Voorhis 2010 non-local density functional
XC	exchange–correlation
Z-CPL	coupled perturbed localization z-vector (equations)
Z-CPSCF	coupled perturbed self-consistent field z-vector (equations)
Z-CV	core–valence z-vector (equations)

Appendices

Appendix A Coordinates of the test set molecules from Chapter 2

The coordinates below are given in Angstrøm in XYZ format. All systems are neutral singlets. The CCSD(T)/pcSseg-4 shieldings (in ppm) are provided in the comment line.

```
9
C4H4O O(64.82) C2,3(47.36) C4,5(81.67) H6,7(24.03) H8,9(25.02)
   O   0.000000   0.000000  -1.132414
   C   0.000000   1.089600  -0.317680
   C   0.000000  -1.089600  -0.317680
   C   0.000000   0.716737   0.986182
   C   0.000000  -0.716737   0.986182
   H   0.000000  -2.041237  -0.808438
   H   0.000000   2.041237  -0.808438
   H   0.000000  -1.371142   1.834814
   H   0.000000   1.371142   1.834814

5
CF4 C(64.96) F(267.58)
   F   0.000000  -1.074800   0.759998
   C   0.000000   0.000000   0.000000
   F   0.000000   1.074800   0.759998
   F   1.074800   0.000000  -0.759998
   F  -1.074800   0.000000  -0.759998

10
CH3COCH3 O(-297.91) C2(-10.84) C3,4(162.88) H5,6(29.70) H7-10(29.44)
   O   0.000000   0.000000   1.312747
   C   0.000000   0.000000   0.100560
   C   0.000000   1.280014  -0.697250
   C   0.000000  -1.280014  -0.697250
   H   0.000000   2.132916  -0.028110
   H   0.000000  -2.132916  -0.028110
   H   0.876773   1.314696  -1.342826
   H  -0.876773   1.314696  -1.342826
   H  -0.876773  -1.314696  -1.342826
   H   0.876773  -1.314696  -1.342826

5
CH4 C(199.39) H(31.39)
   H   0.000000  -0.884131   0.625175
   C   0.000000   0.000000   0.000000
   H   0.000000   0.884131   0.625175
   H   0.884131   0.000000  -0.625175
   H  -0.884131   0.000000  -0.625175

2
CO C(2.56) O(-55.42)
   C   0.000000   0.000000   0.646590
   O   0.000000   0.000000  -0.485097
```

```
3
F2O F(-24.28) O(-446.32)
   O   0.000000   0.000000   0.615029
   F   0.000000  -1.102008  -0.258899
   F   0.000000   1.102008  -0.258899

2
F2 F(-192.76)
   F   0.000000   0.000000   0.706799
   F   0.000000   0.000000  -0.706799

3
H2O O(337.63) H(30.65)
   O   0.000000   0.000000   0.066196
   H   0.000000  -0.753371  -0.525286
   H   0.000000   0.753371  -0.525286

2
HF F(419.91) H(28.82)
   H   0.000000   0.000000   0.870030
   F   0.000000   0.000000  -0.046153

3
N2O N1(11.74) N2(106.22) O(198.77)
   N   0.000000   0.000000  -0.071438
   N   0.000000   0.000000  -1.200428
   O   0.000000   0.000000   1.113481

2
N2 N(-61.16)
   N   0.000000   0.000000   0.550296
   N   0.000000   0.000000  -0.550296

4
NH3 N(270.40) H(31.44)
   N   0.000000   0.000000   0.069289
   H   0.807968   0.466482  -0.320910
   H   0.000002  -0.932962  -0.320910
   H  -0.807969   0.466479  -0.320910

4
PF3 P(224.80) F(231.81)
   P   0.000000   0.506017   0.000000
   F   0.683058  -0.274992   1.183091
   F  -1.366116  -0.274992   0.000000
   F   0.683058  -0.274992  -1.183091

4
PH3 P(604.51) H(29.46)
   P   0.068293   0.000000   0.000000
   H  -0.699620   0.593802  -1.028495
   H  -0.699620  -1.187603   0.000000
   H  -0.699620   0.593802   1.028495

2
PN P(51.61) N(-344.71)
   P   0.000000   0.000000   0.468029
   N   0.000000   0.000000  -1.035245
```

Appendix B Benchmark data from Chapter 2

Table B.2: Isotropic NMR shieldings (ppm) calculated with CCSD(T) and variants of MP2 and the pcSseg-4 basis set.

Element	Nucleus	CCSD(T)	ae-MP2	fc-MP2	ae-SCS-MP2	ae-S2-MP2
^{1}H	furan (at C2/5)	24.03	23.78	23.82	24.10	23.90
	furan (at C3/4)	25.02	24.77	24.83	25.11	24.90
	HF	28.82	28.55	28.59	28.72	28.66
	PH_3	29.46	29.45	29.52	29.52	29.47
	$(CH_3)_2CO$	29.53	29.46	29.49	29.63	29.51
	H_2O	30.65	30.40	30.43	30.56	30.47
	CH_4	31.39	31.35	31.38	31.42	31.37
	NH_3	31.43	31.28	31.31	31.40	31.32
^{13}C	$(CH_3)_2\underline{C}O$	-10.84	-10.63	-7.59	-7.30	-8.27
	CO	2.56	7.68	11.15	8.69	10.21
	furan (C2/5)	47.36	46.03	48.68	48.69	47.79
	CF_4	65.96	62.76	64.48	65.02	62.93
	furan (C3/4)	81.67	81.20	83.67	83.13	82.48
	$(\underline{C}H_3)_2CO$	162.88	163.16	164.19	163.58	163.39
	CH_4	199.39	201.06	201.61	199.30	200.59
^{15}N	PN	-344.70	-259.92	-245.40	-255.09	-243.15
	N_2	-61.16	-44.01	-40.24	-41.58	-38.72
	N$\underline{\text{N}}$O	11.74	29.34	32.19	28.75	32.83
	$\underline{\text{N}}$NO	106.22	128.78	131.93	127.04	131.89
	NH_3	270.40	275.85	276.29	273.14	275.39
^{17}O	OF_2	-446.32	-468.62	-463.25	-431.49	-452.61
	$(CH_3)_2CO$	-297.91	-274.33	-267.48	-265.20	-266.71
	CO	-55.42	-48.72	-45.20	-42.01	-43.12
	furan	64.82	46.88	50.05	66.33	55.21
	NNO	198.77	216.33	218.68	217.77	219.48
	H_2O	337.63	345.53	345.83	342.55	345.19
^{19}F	F_2	-192.76	-177.27	-173.27	-170.63	-174.36
	OF_2	-24.28	-15.88	-12.96	-9.67	-15.05
	PF_3	231.81	231.79	235.29	240.79	234.59
	CF_4	267.58	268.35	269.63	273.49	269.94
	HF	419.91	425.36	425.46	423.17	424.99
^{31}P	PN	51.61	106.63	135.14	119.14	124.92
	PF_3	224.80	215.96	230.57	224.70	217.71
	PH_3	604.50	609.03	615.63	599.59	606.15

Table B.3: Isotropic NMR shieldings (ppm) calculated with CCSD(T) and different DHDFs and the pcSseg-4 basis set.

Element	Nucleus	CCSD(T)	ae-B2PLYP	ae-B2GP-PLYP	ae-DSD-BLYP	ae-DSD-PBEP86	fc-DSD-PBEP86	ae-NoDSD-PBEP86	ae-revDSD-PBEP86	fc-rev-DSD-PBEP86	ae-ωB97X-2	fc-ωB97X-2	ae-rev-ωB97X-2	fc-rev-ωB97X-2
^{1}H	furan (at C2/5)	24.03	23.94	23.93	23.94	23.97	23.90	23.99	24.04	24.05	23.90	23.92	23.97	23.99
	furan (at C3/4)	25.02	24.94	24.92	24.93	24.96	24.88	24.98	25.04	25.06	24.90	24.93	24.96	24.99
	HF	28.82	28.99	28.81	28.70	28.89	28.80	28.89	28.96	28.97	29.03	29.05	29.09	29.11
	PH_3	29.46	29.57	29.54	29.53	29.48	29.46	29.51	29.50	29.53	29.56	29.60	29.57	29.61
	$(CH_3)_2CO$	29.53	29.55	29.55	29.56	29.54	29.50	29.55	29.58	29.59	29.57	29.59	29.60	29.62
	H_2O	30.65	30.78	30.66	30.60	30.70	30.64	30.71	30.75	30.75	30.77	30.79	30.81	30.82
	CH_4	31.39	31.50	31.47	31.45	31.45	31.42	31.46	31.46	31.47	31.50	31.52	31.51	31.53
	NH_3	31.43	31.54	31.48	31.45	31.49	31.45	31.50	31.52	31.52	31.54	31.56	31.56	31.58
^{13}C	$(CH_3)_2\underline{C}O$	-10.84	-26.08	-23.18	-20.96	-17.27	-17.41	-16.13	-16.80	-15.79	-21.04	-19.49	-19.86	-18.38
	CO	2.56	-10.30	-8.75	-7.07	-3.27	-3.27	-2.00	-2.65	-1.52	-4.24	-2.54	-2.84	-1.21
	furan (C2/5)	47.36	35.57	37.53	39.15	42.15	42.01	43.12	42.62	43.51	39.03	40.37	39.85	41.13
	CF_4	65.96	53.23	56.88	59.84	59.94	60.37	60.66	60.17	60.80	57.65	58.61	57.62	58.55
	furan (C3/4)	81.67	70.60	72.77	74.60	76.68	76.75	77.60	77.14	77.97	74.83	76.08	75.43	76.64
	$(\underline{C}H_3)_2CO$	162.88	155.33	157.38	159.00	159.67	160.00	160.08	159.74	160.11	159.22	159.77	159.28	159.81
	CH_4	199.39	193.92	195.43	196.56	197.06	197.78	197.28	196.62	196.81	197.74	198.03	197.46	197.74
^{15}N	PN	-344.70	-371.20	-361.97	-354.57	-336.88	-335.73	-332.03	-335.92	-331.50	-353.86	-347.41	-345.55	-339.28
	N_2	-61.16	-76.50	-74.03	-71.63	-65.74	-65.86	-64.36	-64.74	-63.51	-68.10	-66.32	-65.38	-63.65
	N$\underline{N}$O	11.74	3.24	4.81	6.45	12.48	12.92	13.51	12.66	13.59	7.92	9.25	9.65	10.94
	$\underline{N}$NO	106.22	99.32	101.60	103.08	108.12	108.81	109.26	107.84	108.85	106.45	107.92	108.17	109.59
	NH_3	270.40	265.56	267.18	268.66	268.94	269.82	269.12	268.44	268.59	269.74	269.95	269.53	269.73
^{17}O	OF_2	-446.32	-542.16	-520.66	-501.40	-490.94	-495.38	-488.83	-481.09	-479.20	-504.00	-501.28	-495.91	-493.28
	$(CH_3)_2CO$	-297.91	-315.02	-308.61	-305.90	-298.57	-298.79	-295.97	-299.08	-296.81	-308.15	-304.65	-303.97	-300.61
	CO	-55.42	-72.47	-69.92	-66.99	-62.64	-63.43	-61.30	-60.74	-59.53	-66.56	-64.89	-63.71	-62.07
	furan	64.82	33.42	38.15	42.83	48.01	45.26	49.25	52.06	53.22	37.57	39.17	41.41	42.98
	NNO	198.77	189.28	192.85	195.44	198.50	198.93	199.42	198.65	199.53	199.62	200.65	201.28	202.32
	H_2O	337.63	333.05	334.89	336.72	336.68	337.69	336.83	336.11	336.23	337.81	337.94	337.67	337.80
^{19}F	F_2	-192.76	-225.17	-212.82	-202.60	-201.79	-200.20	-200.27	-201.01	-199.67	-195.40	-193.35	-193.90	-191.94
	OF_2	-24.28	-51.99	-39.58	-29.69	-29.47	-28.10	-28.32	-28.92	-27.86	-31.89	-30.37	-31.34	-29.86
	PF_3	231.81	213.79	220.45	225.80	224.61	224.32	226.05	226.02	227.42	216.06	217.98	217.40	219.28
	CF_4	267.58	253.27	258.28	262.20	262.22	262.31	262.78	262.87	263.43	257.38	258.06	258.16	258.84
	HF	419.91	416.45	417.98	419.35	418.70	419.49	418.79	418.26	418.32	419.41	419.46	419.22	419.27
^{31}P	PN	51.61	10.06	17.54	24.05	44.38	43.04	54.32	47.38	56.06	17.07	31.02	26.30	39.55
	PF_3	224.80	191.99	200.82	207.99	209.12	209.32	214.76	210.03	215.07	196.40	204.50	197.07	204.76
	PH_3	604.50	580.92	586.31	590.53	594.52	597.48	596.98	592.57	594.58	594.21	597.72	592.61	595.89

Table B.4: Isotropic NMR shieldings (ppm) calculated with CCSD(T), HF, and different hybrid functionals and the pcSseg-4 basis set.

Element	Nucleus	CCSD(T)	HF	B3LYP	PBE0	TPSSh	M06	M06-2X	ωB97X-D3BJ	ωB97X-V
^{1}H	furan (at C2/5)	24.03	24.28	24.00	23.83	24.22	23.97	23.22	24.02	23.99
	furan (at C3/4)	25.02	25.30	25.00	24.81	25.29	24.85	24.07	25.01	24.98
	HF	28.82	28.11	29.34	29.25	29.74	28.95	28.71	29.33	29.32
	PH_3	29.46	29.68	29.64	29.47	29.67	29.63	29.50	29.60	29.58
	$(CH_3)_2CO$	29.53	29.95	29.57	29.44	29.75	29.64	29.30	29.65	29.63
	H_2O	30.65	30.49	31.05	30.97	31.41	30.86	30.49	31.03	31.03
	CH_4	31.39	31.64	31.59	31.51	31.77	31.70	31.40	31.60	31.59
	NH_3	31.43	31.57	31.72	31.66	32.04	31.70	31.28	31.73	31.73
^{13}C	$(CH_3)_2\underline{C}O$	-10.84	-24.95	-39.81	-33.95	-25.90	-51.84	-64.32	-30.04	-29.93
	CO	2.56	-28.07	-22.94	-21.33	-6.22	-46.00	-57.90	-16.10	-15.94
	furan (C2/5)	47.36	36.85	26.50	31.69	40.04	14.17	6.14	34.12	34.24
	CF_4	65.96	77.82	44.64	51.23	51.06	38.98	46.60	55.12	55.19
	furan (C3/4)	81.67	74.51	61.64	66.43	73.35	51.42	44.73	69.67	69.89
	$(\underline{C}H_3)_2CO$	162.88	162.51	148.83	153.45	156.02	145.99	142.44	156.53	156.65
	CH_4	199.39	195.13	188.84	192.87	194.17	186.38	183.53	194.54	194.80
^{15}N	PN	-344.70	-511.98	-448.36	-446.50	-400.48	-532.81	-603.90	-430.57	-430.64
	N_2	-61.16	-116.14	-97.32	-96.95	-77.57	-140.84	-154.69	-88.56	-88.41
	$N\underline{N}O$	11.74	-35.81	-14.54	-9.89	0.89	-33.55	-43.51	-10.30	-10.21
	$\underline{N}NO$	106.22	60.96	79.03	81.60	91.63	59.25	47.37	85.15	85.37
	NH_3	270.40	262.08	259.70	262.84	264.04	257.62	254.46	263.88	264.18
^{17}O	OF_2	-446.32	-449.03	-594.65	-567.82	-529.24	-661.19	-666.43	-527.18	-526.57
	$(CH_3)_2CO$	-297.91	-333.41	-356.15	-357.38	-316.75	-377.66	-496.74	-336.78	-338.14
	CO	-55.42	-92.00	-88.12	-89.37	-69.34	-116.70	-154.71	-77.19	-77.29
	furan	64.82	58.15	15.02	19.10	32.06	3.69	-23.56	34.01	33.70
	NNO	198.77	173.25	171.29	172.67	176.52	149.44	134.43	182.66	183.11
	H_2O	337.63	327.58	326.56	328.98	331.53	324.88	319.44	330.58	330.81
^{19}F	F_2	-192.76	-174.56	-260.45	-247.88	-219.84	-300.28	-301.34	-225.02	-224.34
	OF_2	-24.28	19.51	-76.86	-59.60	-53.74	-78.98	-73.47	-42.87	-42.80
	PF_3	231.81	255.25	198.89	202.93	208.49	203.44	193.36	211.46	210.19
	CF_4	267.58	281.91	241.29	245.67	250.16	244.97	233.35	251.41	250.92
	HF	419.91	414.32	411.49	412.90	414.58	411.59	406.05	414.15	414.25
^{31}P	PN	51.61	-110.39	-71.26	-72.02	-2.00	-195.36	-255.65	-68.22	-67.99
	PF_3	224.80	255.52	168.12	182.81	197.76	160.85	156.57	191.56	191.15
	PH_3	604.50	583.52	561.38	582.47	588.47	547.76	547.82	580.69	582.14

Table B.5: Isotropic NMR shieldings (ppm) calculated with CCSD(T) and different pure DFT methods and the pcSseg-4 basis set.

Element	Nucleus	CCSD(T)	BLYP	PBE	KT2	KT3	TPSS	r^{2}SCAN	M06-L	B97-D3
^{1}H	furan (at C2/5)	24.03	24.02	23.80	23.78	23.97	24.25	24.45	24.68	24.04
	furan (at C3/4)	25.02	25.03	24.79	24.89	25.07	25.33	25.45	25.73	25.07
	HF	28.82	29.81	29.77	29.83	29.92	29.96	29.80	30.09	29.73
	PH_3	29.46	29.70	29.50	29.57	29.70	29.70	29.69	29.86	29.65
	$(CH_3)_2CO$	29.53	29.53	29.34	29.43	29.60	29.76	29.78	30.12	29.56
	H_2O	30.65	31.30	31.23	31.29	31.39	31.54	31.48	31.93	31.28
	CH_4	31.39	31.65	31.55	31.60	31.68	31.81	31.82	32.11	31.66
	NH_3	31.43	31.84	31.76	31.80	31.89	32.11	32.11	32.48	31.85
^{13}C	$(CH_3)_2\underline{C}O$	-10.84	-42.27	-36.99	-18.33	-18.28	-26.15	-10.94	-11.18	-31.88
	CO	2.56	-19.20	-17.24	3.27	1.75	-3.42	7.97	2.37	-11.08
	furan (C2/5)	47.36	25.17	30.00	43.03	43.38	40.40	51.12	50.16	33.11
	CF_4	65.96	36.05	41.05	52.26	52.84	47.68	59.76	60.12	44.35
	furan (C3/4)	81.67	59.63	63.90	77.62	77.12	73.25	82.18	80.22	66.58
	$(\underline{C}H_3)_2CO$	162.88	145.04	148.99	156.23	155.53	154.86	162.75	160.82	149.17
	CH_4	199.39	186.49	190.57	195.22	192.79	193.64	202.17	191.60	188.18
^{15}N	PN	-344.70	-426.12	-419.72	-378.39	-375.19	-388.08	-345.51	-365.59	-401.33
	N_2	-61.16	-90.09	-88.59	-64.66	-66.29	-73.09	-55.33	-65.30	-82.00
	N$\underline{N}$O	11.74	-7.63	-1.22	8.58	10.11	4.97	16.84	13.22	1.63
	$\underline{N}$NO	106.22	85.33	89.22	99.55	98.96	95.08	106.86	105.31	90.34
	$\underline{N}H_3$	270.40	258.47	261.89	264.52	261.85	263.89	270.73	254.14	258.86
^{17}O	OF_2	-446.32	-647.49	-635.45	-544.24	-555.13	-546.86	-475.19	-457.26	-622.30
	$(CH_3)_2CO$	-297.91	-350.92	-352.38	-305.22	-298.48	-311.92	-253.91	-233.13	-324.00
	CO	-55.42	-83.95	-84.92	-63.17	-61.02	-66.41	-43.70	-50.69	-71.81
	furan	64.82	8.09	10.20	27.06	29.74	30.41	51.49	59.99	19.75
	NNO	198.77	172.20	174.11	175.61	173.38	177.18	195.41	195.16	173.03
	H_2O	337.63	325.53	328.28	328.58	326.29	331.49	340.39	327.17	325.71
^{19}F	F_2	-192.76	-280.23	-274.22	-218.45	-233.03	-225.05	-171.71	-162.39	-275.00
	OF_2	-24.28	-105.32	-94.37	-70.03	-73.42	-64.71	-22.78	-11.85	-89.95
	PF_3	231.81	182.48	181.38	185.25	195.76	201.76	228.86	236.75	195.56
	CF_4	267.58	229.92	231.05	237.15	241.28	245.70	264.90	268.15	238.31
	HF	419.91	409.96	411.42	411.92	410.60	414.14	421.80	420.01	410.34
^{31}P	PN	51.61	-49.46	-47.15	32.29	34.21	12.25	63.92	46.58	-23.07
	PF_3	224.80	149.17	159.14	197.09	207.07	191.50	230.52	240.87	175.22
	PH_3	604.50	553.65	575.62	595.68	588.28	587.02	622.10	615.52	565.70

Table B.6: Isotropic NMR shielding constants, calculated with different methods and the pcSseg-4 basis set (denoted "pS4") and deviations from these values due to smaller basis sets (ΔpSn). All values are in ppm. No RI/COS approximations were employed for the two-electron integrals.

		HF			B3LYP			TPSS			DSD-PBEP86			MP2		
	Nucleus	pS4	ΔpS3	ΔpS2	pS4	ΔpS3	ΔpS2	pS4	ΔpS3	ΔpS2	pS4	ΔpS3	ΔpS2	pS4	ΔpS3	ΔpS2
^{1}H	PH_3	29.68	−0.00	0.05	29.64	0.00	0.01	29.70	0.02	0.05	29.48	0.02	0.09	29.45	0.04	0.15
	HF	28.12	0.01	0.14	29.34	0.01	0.11	29.96	−0.16	−0.03	28.89	0.04	0.20	28.55	0.06	0.31
	H_2O	30.49	0.00	0.11	31.05	0.00	0.10	31.54	−0.13	0.00	30.70	0.03	0.18	30.40	0.04	0.27
	NH_3	31.57	0.00	0.10	31.72	0.01	0.12	32.11	−0.09	0.05	31.49	0.02	0.16	31.28	0.03	0.23
	CH_4	31.64	−0.00	0.04	31.60	−0.00	0.03	31.81	−0.04	0.04	31.45	0.00	0.07	31.35	0.01	0.10
	$(CH_3)_2CO$	29.95	−0.00	0.07	29.57	0.00	0.08	29.76	−0.04	0.08	29.54	0.01	0.13	29.46	0.02	0.18
	furan (at C2/5)	24.28	0.00	0.06	24.00	0.00	0.09	24.25	−0.01	0.09	23.97	−0.00	0.12	23.78	0.03	0.19
	furan (at C3/4)	25.30	−0.00	0.05	25.00	0.00	0.06	25.33	−0.05	0.05	24.96	0.00	0.10	24.77	0.02	0.16
^{13}C	$(CH_3)_2\underline{C}O$	−24.95	−0.08	1.54	−39.81	0.05	1.10	−26.15	0.34	0.77	−17.27	−0.04	2.43	−10.63	0.30	4.50
	CO	−28.07	−0.09	1.50	−22.94	−0.01	0.68	−3.42	−0.38	−0.31	−3.27	0.32	2.68	7.68	0.34	4.69
	CF_4	77.82	−0.01	1.15	44.64	0.06	0.73	47.68	−0.21	0.01	59.94	0.11	1.62	62.76	0.12	2.44
	furan (C2/5)	36.85	−0.06	1.27	26.50	0.04	0.79	40.40	−0.25	−0.02	42.15	0.02	1.83	46.03	0.22	3.31
	furan (C3/4)	74.51	−0.06	1.02	61.64	0.04	0.62	73.25	0.65	0.63	76.68	0.11	1.66	81.20	0.16	2.75
	$(\underline{C}H_3)_2CO$	162.51	−0.03	0.96	148.83	0.03	0.64	154.86	0.86	0.76	159.67	0.14	1.23	163.16	0.06	1.76
	CH_4	195.14	−0.00	0.60	188.84	0.04	0.35	193.64	0.21	−0.19	197.07	−0.03	0.52	201.06	−0.04	0.78
^{15}N	PN	−511.98	−2.29	−9.20	−448.36	−2.20	−6.69	−388.08	−0.89	−4.02	−336.88	−1.58	2.04	−259.92	−1.53	11.92
	N_2	−116.14	−0.43	1.28	−97.32	−0.64	0.22	−73.09	−0.16	0.25	−65.74	−0.14	2.59	−44.01	−0.10	4.81
	$N\underline{N}O$	−35.81	−0.05	1.05	−14.54	0.12	0.98	4.97	0.80	1.34	12.49	0.09	2.23	29.34	0.41	4.11
	$\underline{N}NO$	60.96	−0.07	0.71	79.04	0.15	0.46	95.08	0.90	0.84	108.12	0.46	2.18	128.78	0.50	3.95
	NH_3	262.09	−0.01	1.45	259.70	0.05	2.01	263.89	1.03	2.57	268.94	−0.07	1.71	275.85	0.00	2.16
^{17}O	OF_2	−449.03	0.32	4.15	−594.65	0.60	3.40	−546.86	−0.01	1.79	−490.94	1.30	9.66	−468.62	2.15	16.30
	$(CH_3)_2CO$	−333.41	−0.49	−2.33	−356.16	−0.18	−2.76	−311.92	0.24	−2.72	−298.58	−1.15	−2.65	−274.33	−0.45	0.30
	CO	−92.00	−0.33	1.10	−88.12	−0.19	0.27	−66.41	0.25	2.22	−62.64	0.24	2.30	−48.72	−0.03	3.87
	furan	58.15	−0.15	0.28	15.02	0.02	1.02	30.41	−0.39	0.47	48.01	−0.37	1.86	46.88	0.09	4.76
	NNO	173.25	−0.20	−0.02	171.29	−0.07	−0.36	177.18	−0.07	0.06	198.50	−0.49	0.70	216.33	0.13	2.55
	H_2O	327.59	−0.07	1.21	326.56	−0.07	1.98	331.49	0.43	2.98	336.68	−0.16	1.54	345.53	−0.17	2.04
^{19}F	F_2	−174.56	1.28	3.58	−260.46	1.86	2.78	−225.05	1.07	1.89	−201.79	1.92	6.24	−177.27	2.56	10.52
	OF_2	19.51	0.88	2.86	−76.86	1.66	4.16	−64.71	1.34	4.02	−29.47	1.54	5.77	−15.88	2.03	8.90
	PF_3	255.25	0.04	3.26	198.89	0.24	4.45	201.76	−0.02	3.90	224.61	0.35	6.02	231.79	0.82	8.42
	CF_4	281.91	−0.09	0.55	241.29	0.04	1.15	245.70	−0.42	0.49	262.22	0.00	1.93	268.35	0.21	3.19
	HF	414.32	−0.14	0.16	411.49	−0.21	−0.20	414.14	−0.09	1.14	418.70	−0.12	−0.13	425.36	−0.42	−0.38
^{31}P	PN	−110.40	−2.26	−17.16	−71.26	−2.94	−10.39	12.25	−2.33	−7.24	44.38	−1.69	−6.55	106.63	−0.92	−1.74
	PF_3	255.52	−0.13	0.97	168.12	−0.64	0.37	191.50	−0.54	0.82	209.12	0.64	2.55	215.96	1.33	3.94
	PH_3	583.52	0.15	2.25	561.38	−0.28	0.38	587.02	−0.02	0.73	594.52	−0.12	−1.73	609.04	−0.06	−3.85

Table B.7: Isotropic NMR shielding constants, calculated at the HF/pcSseg-2 and HF/pcSseg-3 levels and errors due to different approximations for the two-electron integrals. All values are in ppm.

		HF/pcSseg-2				HF/pcSseg-3			
	Nucleus	Exact	ΔRIJ-COSX-S	ΔRIJ-COSX-L	ΔRIJK	Exact	ΔRIJ-COSX-S	ΔRIJ-COSX-L	ΔRIJK
^{1}H	PH_3	29.73	−0.02	−0.00	−0.00	29.68	−0.01	−0.00	0.00
	HF	28.26	−0.00	0.00	−0.00	28.12	−0.00	0.00	−0.00
	H_2O	30.61	−0.00	0.00	0.00	30.49	−0.00	0.00	0.00
	NH_3	31.67	−0.00	0.00	−0.00	31.57	0.00	0.00	0.00
	CH_4	31.67	−0.00	0.00	0.00	31.63	0.00	0.00	−0.00
	$(CH_3)_2CO$	30.02	−0.00	0.00	0.00	29.94	0.00	0.00	0.00
	furan (at C2/5)	24.34	0.00	−0.01	−0.01	24.28	0.00	0.00	−0.00
	furan (at C3/4)	25.35	−0.01	0.00	0.00	25.30	0.00	0.00	0.00
^{13}C	$(CH_3)_2\underline{C}O$	−23.41	0.04	0.00	−0.01	−25.03	0.00	0.01	−0.01
	CO	−26.57	−0.01	−0.01	−0.03	−28.16	0.00	0.00	−0.03
	CF_4	78.97	0.03	0.00	−0.01	77.82	0.02	0.01	−0.01
	furan (C2/5)	38.12	0.03	0.04	−0.02	36.79	0.01	−0.01	−0.01
	furan (C3/4)	75.53	0.17	0.01	−0.00	74.45	−0.00	−0.01	0.00
	$(\underline{C}H_3)_2CO$	163.47	0.02	0.01	0.01	162.48	−0.02	−0.00	0.01
	CH_4	195.74	0.09	0.04	0.01	195.13	−0.01	0.02	0.01
^{15}N	PN	−521.17	0.03	0.04	−0.04	−514.26	−0.03	−0.00	−0.04
	N_2	−114.86	−0.01	0.00	−0.01	−116.57	0.01	0.01	0.01
	$N\underline{N}O$	−34.76	−0.00	−0.01	−0.00	−35.86	0.00	0.01	0.02
	$\underline{N}NO$	61.66	−0.01	−0.02	−0.01	60.89	0.00	0.01	−0.00
	NH_3	263.53	−0.35	0.07	0.00	262.08	0.10	−0.00	0.01
^{17}O	OF_2	−444.88	0.03	0.05	−0.04	−448.72	−0.01	0.07	−0.02
	$(CH_3)_2CO$	−335.73	−0.25	0.08	0.03	−333.90	0.19	0.02	0.07
	CO	−90.90	−0.02	−0.02	−0.03	−92.33	0.02	0.02	−0.02
	furan	58.42	0.09	−0.04	0.03	58.00	−0.03	0.01	0.05
	NNO	173.23	−0.05	−0.05	−0.03	173.05	0.01	0.01	−0.03
	H_2O	328.79	0.42	0.04	−0.01	327.52	0.41	0.04	−0.00
^{19}F	F_2	−170.97	0.00	0.12	−0.03	−173.27	−0.02	0.04	−0.02
	OF_2	22.37	−0.13	0.00	0.00	20.39	−0.02	0.00	0.01
	PF_3	258.51	−0.09	−0.03	0.13	255.29	−0.02	−0.01	0.17
	CF_4	282.46	−0.05	−0.03	0.07	281.82	−0.01	0.01	0.10
	HF	414.48	0.00	−0.03	−0.01	414.18	0.01	−0.01	−0.01
^{31}P	PN	−127.56	0.05	0.00	−0.09	−112.66	−0.04	0.00	−0.13
	PF_3	256.49	−0.02	−0.03	0.05	255.39	−0.02	−0.01	0.05
	PH_3	585.77	−3.09	−0.25	−0.10	583.67	−1.30	−0.13	−0.10

Table B.8: Isotropic NMR shielding constants, calculated at the B3LYP/pcSseg-2 and B3LYP/pcSseg-3 levels and errors due to different approximations for the two-electron integrals. All values are in ppm.

		B3LYP/pcSseg-2				B3LYP/pcSseg-3			
	Nucleus	Exact	ΔRIJ-COSX-S	ΔRIJ-COSX-L	ΔRIJK	Exact	ΔRIJ-COSX-S	ΔRIJ-COSX-L	ΔRIJK
^{1}H	PH_3	29.66	−0.01	−0.00	−0.00	29.64	−0.00	0.00	0.00
	HF	29.45	0.00	0.00	0.00	29.35	−0.00	0.00	0.00
	H_2O	31.15	0.00	0.00	0.00	31.05	−0.00	0.00	0.00
	NH_3	31.84	0.00	0.00	0.00	31.73	0.00	0.00	0.00
	CH_4	31.63	0.00	0.00	0.00	31.59	0.00	0.00	0.00
	$(CH_3)_2CO$	29.65	0.00	0.00	0.00	29.57	0.00	0.00	0.00
	furan (at C2/5)	24.09	0.00	0.00	0.00	24.00	0.00	0.00	0.00
	furan (at C3/4)	25.06	0.00	0.00	0.00	25.00	0.00	0.00	0.00
^{13}C	$(CH_3)_2\underline{C}O$	−38.71	0.01	0.00	−0.00	−39.76	0.00	0.00	0.00
	CO	−22.26	0.00	0.00	−0.01	−22.95	0.00	0.01	−0.00
	CF_4	45.37	0.01	0.00	0.00	44.70	0.01	0.01	0.01
	furan (C2/5)	27.29	0.00	0.01	0.00	26.54	0.01	0.00	0.00
	furan (C3/4)	62.25	0.04	0.01	0.00	61.67	0.01	0.00	0.01
	$(\underline{C}H_3)_2CO$	149.47	0.01	0.01	0.01	148.86	0.01	0.01	0.01
	CH_4	189.20	0.03	0.02	0.02	188.88	0.02	0.02	0.02
^{15}N	PN	−455.05	0.00	0.00	−0.01	−450.56	0.00	0.01	0.01
	N_2	−97.10	−0.01	−0.00	−0.00	−97.96	0.01	0.01	0.01
	N$\underline{N}$O	−13.56	−0.00	−0.00	−0.00	−14.42	0.00	0.00	0.01
	$\underline{N}$NO	79.50	−0.00	−0.01	−0.00	79.19	0.00	0.00	0.00
	NH_3	261.70	−0.07	0.02	0.01	259.74	0.04	0.00	0.01
^{17}O	OF_2	−591.24	0.06	0.07	0.04	−594.04	0.08	0.10	0.08
	$(CH_3)_2CO$	−358.92	−0.05	0.03	0.02	−356.33	0.07	0.03	0.03
	CO	−87.85	−0.00	−0.00	−0.00	−88.31	0.02	0.02	0.01
	furan	16.04	0.03	−0.00	0.01	15.04	−0.00	0.01	0.02
	NNO	170.93	−0.01	−0.01	−0.01	171.22	0.01	0.01	0.00
	H_2O	328.54	0.13	0.02	0.01	326.48	0.12	0.02	0.01
^{19}F	F_2	−257.67	−0.00	0.02	−0.01	−258.60	0.02	0.03	0.01
	OF_2	−72.69	−0.05	−0.02	−0.03	−75.19	−0.01	−0.01	−0.01
	PF_3	203.34	−0.03	−0.01	0.02	199.12	0.00	0.00	0.04
	CF_4	242.44	−0.01	−0.01	0.01	241.33	0.01	0.01	0.03
	HF	411.29	0.01	0.00	0.00	411.29	0.02	0.01	0.01
^{31}P	PN	−81.65	0.01	−0.00	−0.01	−74.20	0.00	0.01	0.00
	PF_3	168.49	−0.01	−0.01	0.01	167.48	−0.01	−0.00	0.01
	PH_3	561.76	−0.70	−0.07	−0.06	561.09	−0.27	−0.02	−0.03

Table B.9: Isotropic NMR shielding constants, calculated at the TPSS/pcSseg-2 and TPSS/pcSseg-3 levels and errors due to RI approximation for the two-electron integrals with the def2-J (RI/J) or def2-JK (RI/JK) auxiliary basis sets. All values are in ppm.

		TPSS/pcSseg-2			TPSS/pcSseg-3		
	Nucleus	Exact	ΔRI/J	ΔRI/JK	Exact	ΔRI/J	ΔRI/JK
^{1}H	PH_3	29.75	−0.01	−0.00	29.72	−0.01	−0.00
	HF	29.93	−0.01	0.00	29.81	−0.01	0.00
	H_2O	31.54	−0.01	0.00	31.41	−0.01	0.00
	NH_3	32.17	−0.00	0.00	32.02	−0.00	0.00
	CH_4	31.85	−0.00	0.00	31.77	−0.00	0.00
	$(CH_3)_2CO$	29.84	−0.00	0.00	29.72	−0.00	0.00
	furan (at C2/5)	24.34	−0.00	0.00	24.24	−0.00	0.00
	furan (at C3/4)	25.39	−0.00	0.00	25.29	−0.00	0.00
^{13}C	$(CH_3)_2\underline{C}O$	−25.38	−0.01	0.00	−25.81	−0.00	0.00
	CO	−3.73	0.00	0.00	−3.80	0.01	0.00
	CF_4	47.69	−0.00	0.00	47.48	0.00	0.01
	furan (C2/5)	40.37	0.00	0.00	40.15	−0.01	0.01
	furan (C3/4)	73.89	−0.01	0.01	73.90	−0.01	0.01
	$(\underline{C}H_3)_2CO$	155.61	0.00	0.01	155.72	−0.01	0.01
	CH_4	193.45	−0.03	0.02	193.84	−0.05	0.03
^{15}N	PN	−392.10	0.55	−0.01	−388.97	0.70	0.01
	N_2	−72.85	0.09	−0.00	−73.25	0.10	0.00
	$N\underline{N}O$	6.31	0.02	−0.00	5.77	0.02	0.00
	$\underline{N}NO$	95.92	−0.03	−0.00	95.99	−0.02	0.00
	NH_3	266.46	−0.04	0.01	264.91	−0.05	0.01
^{17}O	OF_2	−545.07	0.77	0.06	−546.87	0.75	0.10
	$(CH_3)_2CO$	−314.64	−0.04	0.02	−311.69	−0.03	0.03
	CO	−64.20	0.04	0.00	−66.17	0.05	0.02
	furan	30.88	−0.01	0.00	30.02	0.00	0.01
	NNO	177.24	−0.00	−0.00	177.12	0.00	0.01
	H_2O	334.47	−0.03	0.01	331.92	−0.05	0.02
^{19}F	F_2	−223.16	0.53	−0.01	−223.98	0.44	0.02
	OF_2	−60.69	0.30	−0.03	−63.38	0.25	−0.01
	PF_3	205.66	0.20	−0.01	201.75	0.23	0.00
	CF_4	246.19	0.03	−0.00	245.29	0.03	0.01
	HF	415.28	−0.02	0.01	414.06	−0.00	0.03
^{31}P	PN	5.01	0.68	0.00	9.92	0.81	0.01
	PF_3	192.31	−0.01	−0.00	190.96	−0.03	0.00
	PH_3	587.75	−0.48	−0.10	587.00	−0.48	−0.11

Table B.10: Isotropic NMR shielding constants, calculated at the RI-MP2/pcSseg-2 and RI-MP2/pcSseg-3 levels and errors due to different approximations for the two-electron Fock matrix contributions. All values are in ppm.

		MP2 pcSseg-2 cc-pwCVQZ/C					MP2 pcSseg-3 cc-pwCV5Z/C				
	Nucleus	Exact	ΔRIJ-COSX-S	ΔRIJ-COSX-L	ΔRIJ-COSX-XL	ΔRIJK	Exact	ΔRIJ-COSX-S	ΔRIJ-COSX-L	ΔRIJ-COSX-XL	ΔRIJK
^{1}H	PH_3	29.61	−0.02	−0.00	−0.00	−0.00	29.49	−0.00	−0.00	0.00	−0.00
	HF	28.86	0.01	0.01	0.00	0.00	28.62	0.01	0.00	−0.01	0.00
	H_2O	30.67	−0.00	0.00	0.00	0.00	30.45	0.01	0.01	0.00	0.00
	NH_3	31.51	−0.00	0.00	0.00	0.00	31.31	0.00	0.01	0.00	0.00
	CH_4	31.45	−0.00	0.00	0.00	0.00	31.36	0.01	0.00	0.00	0.00
	$(CH_3)_2CO$	29.64	−0.00	0.00	0.00	0.00	29.48	0.01	−0.01	0.00	0.00
	furan (at C2/5)	23.97	0.02	−0.00	−0.01	0.00	23.81	−0.00	−0.01	−0.01	0.00
	furan (at C3/4)	24.93	−0.02	−0.00	0.00	0.00	24.80	−0.07	−0.01	0.01	0.00
^{13}C	$(CH_3)_2\underline{C}O$	−6.13	0.01	0.00	−0.00	−0.01	−10.33	0.47	0.48	0.06	−0.02
	CO	12.36	−0.00	0.00	0.01	−0.01	8.02	0.01	0.01	0.00	−0.03
	CF_4	65.20	0.02	−0.01	0.00	0.00	62.88	−0.03	−0.01	0.01	0.02
	furan (C2/5)	49.34	−0.05	0.02	0.02	−0.01	46.25	−0.54	−0.22	−0.01	−0.02
	furan (C3/4)	83.96	0.14	0.02	0.02	0.00	81.36	0.52	−0.04	−0.02	0.00
	$(\underline{C}H_3)_2CO$	164.91	0.08	0.01	0.00	0.01	163.22	0.39	0.24	0.04	−0.00
	CH_4	201.84	0.09	0.05	0.05	0.01	201.02	0.23	0.16	0.05	0.01
^{15}N	PN	−248.00	0.03	0.01	−0.00	0.04	−261.45	0.03	0.04	0.04	0.03
	N_2	−39.20	−0.00	0.01	−0.01	−0.00	−44.11	−0.09	−0.07	0.01	0.02
	$N\underline{N}O$	33.44	−0.01	−0.02	−0.01	0.00	29.75	−0.11	−0.09	−0.00	0.04
	$\underline{N}NO$	132.73	0.02	0.03	−0.00	−0.01	129.28	0.02	−0.02	0.01	0.03
	NH_3	278.01	−0.31	0.08	0.07	0.00	275.86	−0.36	−0.17	−0.07	0.00
^{17}O	OF_2	−452.33	0.03	0.02	0.03	−0.06	−466.48	−0.11	−0.23	0.01	−0.04
	$(CH_3)_2CO$	−274.04	0.14	0.17	0.12	0.03	−274.78	1.61	2.17	0.49	−0.01
	CO	−44.85	0.06	0.07	−0.00	−0.01	−48.75	0.07	0.06	0.00	−0.07
	furan	51.64	0.58	−0.10	−0.01	0.02	46.98	1.58	−0.05	−0.15	0.04
	NNO	218.89	−0.00	−0.01	−0.01	−0.01	216.46	0.27	0.10	0.01	−0.02
	H_2O	347.57	0.43	0.03	0.02	−0.01	345.37	0.51	−0.13	0.06	−0.01
^{19}F	F_2	−166.75	−0.02	0.10	0.01	−0.04	−174.71	−0.38	−0.23	0.03	−0.04
	OF_2	−6.98	−0.11	−0.01	−0.01	−0.00	−13.85	0.24	0.20	0.05	0.01
	PF_3	240.21	−0.09	−0.04	−0.02	0.15	232.62	0.10	−0.11	−0.06	0.20
	CF_4	271.54	−0.10	−0.11	0.01	0.08	268.56	−0.47	−0.39	0.01	0.13
	HF	424.98	0.06	0.03	0.05	−0.01	424.94	0.11	−0.03	0.21	−0.01
^{31}P	PN	104.89	−0.01	−0.04	−0.00	0.02	105.71	−0.06	−0.03	0.05	0.00
	PF_3	219.90	−0.02	−0.03	−0.00	0.07	217.29	0.00	−0.03	−0.03	0.09
	PH_3	605.18	−2.86	−0.25	−0.16	−0.06	608.98	−1.26	−0.05	−0.01	−0.02

Table B.11: Isotropic NMR shielding constants, calculated at the RI-DSD-PBEP86/pcSseg-2 and RI-DSD-PBEP86/pcSseg-3 levels and errors due to different approximations for the two-electron Fock matrix contributions. All values are in ppm.

		DSD-PBEP86 pcSseg-2 cc-pwCVQZ/C					DSD-PBEP86 pcSseg-3 cc-pwCV5Z/C				
	Nucleus	Exact	ΔRIJ-COSX-S	ΔRIJ-COSX-L	ΔRIJ-COSX-XL	ΔRIJK	Exact	ΔRIJ-COSX-S	ΔRIJ-COSX-L	ΔRIJ-COSX-XL	ΔRIJK
^{1}H	PH_3	29.57	−0.01	−0.00	−0.00	−0.00	29.50	−0.01	−0.00	−0.00	0.00
	HF	29.08	0.00	0.00	0.00	0.00	28.92	0.00	−0.00	−0.00	0.00
	H_2O	30.88	−0.00	0.00	0.00	0.00	30.73	0.00	0.00	0.00	0.00
	NH_3	31.65	−0.00	0.00	0.00	0.00	31.50	0.00	0.00	0.00	0.00
	CH_4	31.51	0.00	0.00	0.00	0.00	31.45	0.00	0.00	0.00	0.00
	$(CH_3)_2CO$	29.66	−0.00	0.00	0.00	0.00	29.54	0.00	−0.00	0.00	0.00
	furan (at C2/5)	24.09	0.01	−0.00	−0.00	0.00	23.97	0.00	−0.00	0.00	0.00
	furan (at C3/4)	25.06	−0.01	0.00	0.00	0.00	24.96	−0.02	0.00	0.01	0.00
^{13}C	$(CH_3)_2\underline{C}O$	−14.83	0.01	−0.00	−0.00	−0.01	−17.31	0.17	0.16	0.02	−0.01
	CO	−0.59	−0.00	−0.00	0.00	−0.01	−2.95	0.00	0.01	0.00	−0.01
	CF_4	61.56	0.02	−0.00	0.00	0.00	60.06	−0.00	0.00	0.01	0.01
	furan (C2/5)	43.98	−0.02	0.02	0.02	−0.00	42.16	−0.18	−0.05	0.00	−0.01
	furan (C3/4)	78.34	0.10	0.01	0.01	0.00	76.79	0.17	−0.01	−0.01	0.01
	$(\underline{C}H_3)_2CO$	160.90	0.03	0.01	0.00	0.01	159.81	0.09	0.06	0.01	0.01
	CH_4	197.58	0.06	0.03	0.04	0.01	197.04	0.06	0.05	0.03	0.02
^{15}N	PN	−334.84	0.01	0.01	−0.00	0.01	−338.46	−0.00	0.01	0.02	0.02
	N_2	−63.15	−0.01	0.00	−0.01	−0.00	−65.88	−0.02	−0.02	0.01	0.01
	$N\underline{N}O$	14.72	−0.00	−0.01	−0.01	0.00	12.58	−0.04	−0.03	0.00	0.02
	$\underline{N}NO$	110.30	0.00	0.00	−0.00	−0.01	108.59	0.02	0.00	0.01	0.01
	NH_3	270.66	−0.21	0.06	0.05	0.01	268.87	−0.02	−0.04	−0.01	0.01
^{17}O	OF_2	−481.29	0.08	0.09	0.04	−0.01	−489.65	−0.02	−0.02	0.06	0.01
	$(CH_3)_2CO$	−301.23	−0.06	0.09	0.09	0.03	−299.73	0.53	0.68	0.16	0.03
	CO	−60.34	0.01	0.02	−0.00	−0.01	−62.40	0.03	0.03	0.01	−0.02
	furan	49.87	0.24	−0.03	0.00	0.02	47.64	0.39	−0.05	−0.07	0.04
	NNO	199.20	−0.02	−0.02	−0.01	−0.02	198.01	0.10	0.05	0.01	−0.01
	H_2O	338.23	0.33	0.03	0.02	0.00	336.53	0.35	−0.01	0.04	0.00
^{19}F	F_2	−195.55	−0.02	0.06	0.01	−0.03	−199.87	−0.13	−0.06	0.03	−0.03
	OF_2	−23.71	−0.11	−0.04	−0.02	−0.02	−27.93	0.07	0.06	0.01	−0.01
	PF_3	230.64	−0.07	−0.02	−0.01	0.10	224.97	0.03	−0.04	−0.02	0.13
	CF_4	264.16	−0.05	−0.05	0.01	0.05	262.23	−0.17	−0.13	0.01	0.08
	HF	418.58	0.03	0.01	0.03	−0.00	418.58	0.06	−0.00	0.08	0.00
^{31}P	PN	37.83	0.00	−0.02	0.00	−0.01	42.70	−0.04	−0.01	0.03	−0.01
	PF_3	211.67	−0.01	−0.02	−0.00	0.04	209.76	−0.01	−0.01	−0.02	0.06
	PH_3	592.79	−2.01	−0.19	−0.13	−0.08	594.40	−0.82	−0.07	−0.05	−0.05

Table B.12: Isotropic NMR shielding constants, calculated at the canonical MP2 level ("Exact") with different pcSseg-n basis sets and deviations from these reference values due to the RI-MP2 approximation with different auxiliary basis sets ("AA", "AA3l", "cw$n$C"). All values are in ppm.

		pcSseg-2						pcSseg-3					pcSseg-4			
	Nucleus	Exact	Δcw3C	Δcw4C	Δcw5C	ΔAA	ΔAA3l	Exact	Δcw4C	Δcw5C	ΔAA	ΔAA3l	Exact	Δcw5C	ΔAA	ΔAA3l
^{1}H	PH_3	29.61	0.00	0.00	0.00	0.00	0.00	29.49	−0.00	0.00	0.00	0.00	29.45	0.00	0.00	0.00
	HF	28.86	0.00	−0.00	0.00	0.00	0.00	28.62	−0.00	0.00	0.00	0.00	28.55	−0.00	0.00	0.00
	H_2O	30.67	0.00	0.00	0.00	0.00	0.00	30.45	−0.00	0.00	0.00	0.00	30.40	0.00	0.00	0.00
	NH_3	31.51	0.00	0.00	0.00	0.00	0.00	31.31	−0.00	0.00	0.00	0.00	31.28	0.00	0.00	0.00
	CH_4	31.45	0.00	0.00	0.00	0.00	0.00	31.36	−0.00	0.00	0.00	0.00	31.35	0.00	0.00	0.00
	$(CH_3)_2CO$	29.64	−0.00	−0.00	−0.00	−0.00	−0.00	29.48	−0.00	0.00	0.00	0.00	29.46	−0.00	0.00	0.00
	furan (at C2/5)	23.97	0.00	0.00	0.00	0.00	0.00	23.81	−0.00	0.00	0.00	0.00	23.78	0.00	0.00	0.00
	furan (at C3/4)	24.93	−0.00	0.00	0.00	−0.00	0.00	24.80	−0.00	0.00	0.00	0.00	24.77	0.00	0.00	0.00
^{13}C	$(CH_3)_2\underline{C}O$	−6.13	−0.04	−0.00	0.00	−0.02	−0.00	−10.33	−0.02	0.00	−0.01	0.00	−10.62	−0.01	−0.01	−0.00
	CO	12.37	−0.03	−0.00	−0.00	−0.01	−0.00	8.02	−0.02	−0.00	−0.01	−0.00	7.69	−0.01	−0.01	−0.00
	CF_4	65.20	−0.00	0.00	0.00	−0.00	0.00	62.88	−0.01	−0.00	−0.00	0.00	62.76	−0.00	−0.00	0.00
	furan (C2/5)	49.34	−0.02	−0.00	0.00	−0.01	−0.00	46.25	−0.02	−0.00	−0.00	0.00	46.04	−0.01	−0.00	−0.00
	furan (C3/4)	83.96	−0.03	−0.00	0.00	−0.01	0.00	81.36	−0.02	0.00	−0.00	0.00	81.21	−0.01	−0.00	0.00
	$(\underline{C}H_3)_2CO$	164.91	−0.02	−0.00	−0.00	−0.01	−0.00	163.22	0.00	−0.00	−0.00	−0.00	163.16	−0.00	−0.00	−0.00
	CH_4	201.84	−0.01	−0.00	−0.00	−0.01	−0.01	201.01	0.03	0.00	0.00	0.00	201.06	0.00	0.00	0.00
^{15}N	PN	−247.98	−0.11	−0.02	−0.00	−0.01	−0.02	−261.44	−0.06	−0.01	−0.03	−0.01	−259.88	−0.04	−0.03	−0.01
	N_2	−39.19	−0.03	−0.01	−0.00	−0.01	−0.00	−44.10	−0.02	−0.00	−0.01	−0.00	−44.00	−0.01	−0.00	0.00
	$N\underline{N}O$	33.44	0.00	0.00	−0.00	0.00	−0.00	29.75	−0.00	0.00	−0.00	0.00	29.34	−0.00	−0.00	−0.00
	$\underline{N}NO$	132.74	−0.02	−0.01	−0.00	−0.00	−0.00	129.28	−0.01	0.00	−0.00	0.00	128.79	−0.01	−0.00	−0.00
	NH_3	278.02	−0.04	−0.00	−0.00	−0.01	−0.01	275.85	0.03	0.00	0.00	0.00	275.85	0.00	−0.00	−0.00
^{17}O	OF_2	−452.30	−0.27	−0.02	−0.00	−0.09	−0.00	−466.46	−0.09	−0.02	−0.04	−0.00	−468.57	−0.05	−0.04	−0.02
	$(CH_3)_2CO$	−274.02	−0.24	−0.02	0.00	−0.07	−0.01	−274.77	−0.08	−0.01	−0.03	−0.00	−274.28	−0.06	−0.02	−0.01
	CO	−44.84	−0.06	−0.01	−0.00	−0.01	−0.00	−48.75	−0.04	−0.00	−0.01	−0.00	−48.69	−0.03	−0.01	−0.00
	furan	51.65	−0.09	−0.01	−0.01	−0.04	−0.01	46.98	−0.06	−0.01	−0.02	−0.01	46.91	−0.03	−0.01	−0.01
	NNO	218.88	−0.00	0.00	0.01	−0.01	0.00	216.46	−0.01	−0.00	−0.01	0.00	216.34	−0.01	−0.00	0.00
	H_2O	347.58	−0.04	−0.00	−0.01	−0.01	−0.01	345.37	0.03	−0.00	0.00	0.00	345.53	0.00	0.00	0.00
^{19}F	F_2	−166.74	−0.05	−0.01	0.01	−0.05	−0.01	−174.70	−0.02	−0.01	−0.02	−0.00	−177.25	−0.02	−0.02	−0.01
	OF_2	−6.98	0.05	−0.00	0.00	−0.03	0.00	−13.84	0.00	−0.01	−0.01	0.00	−15.86	−0.01	−0.01	−0.00
	PF_3	240.22	−0.08	−0.01	−0.00	−0.04	−0.01	232.63	−0.04	−0.01	−0.02	−0.01	231.82	−0.03	−0.02	−0.01
	CF_4	271.54	−0.04	−0.00	−0.00	−0.02	−0.00	268.56	−0.03	−0.01	−0.02	−0.00	268.37	−0.02	−0.01	−0.01
	HF	424.98	0.00	0.00	−0.00	−0.01	−0.01	424.94	0.02	0.00	0.00	0.00	425.36	0.01	0.01	0.01
^{31}P	PN	104.91	−0.09	−0.01	−0.00	−0.02	−0.01	105.72	−0.05	−0.00	−0.03	0.00	106.67	−0.04	−0.02	−0.01
	PF_3	219.90	−0.02	−0.01	−0.00	−0.03	−0.01	217.29	−0.02	−0.00	−0.01	−0.00	215.98	−0.02	−0.02	−0.01
	PH_3	605.17	−0.06	0.01	−0.00	−0.02	−0.01	608.98	0.08	−0.00	−0.01	−0.01	609.05	−0.01	−0.01	−0.01

Table B.13: Isotropic NMR shielding constants, calculated at the DSD-PBEP86 level with the pcSseg-2 and pcSseg-3 basis sets and a large AutoAux-generated AuxC basis ("AA3l"), as well as deviations from these reference values due to smaller auxiliary basis sets ("cw$n$C"). All values are in ppm.

		pcSseg-2			pcSseg-3		
	Nucleus	AA3l	Δcw3C	Δcw4C	AA3l	Δcw4C	Δcw5C
^{1}H	PH_3	29.57	0.00	−0.00	29.50	−0.00	0.00
	HF	29.08	0.00	−0.00	28.92	−0.00	0.00
	H_2O	30.88	0.00	0.00	30.73	−0.00	0.00
	NH_3	31.65	0.00	0.00	31.50	−0.00	0.00
	CH_4	31.51	0.00	−0.00	31.45	−0.00	0.00
	$(CH_3)_2CO$	29.66	0.00	0.00	29.54	−0.00	0.00
	furan (at C2/5)	24.09	0.00	0.00	23.97	−0.00	0.00
	furan (at C3/4)	25.06	0.00	0.00	24.96	−0.00	0.00
^{13}C	$(CH_3)_2\underline{C}O$	−14.83	−0.02	0.00	−17.31	−0.01	0.00
	CO	−0.59	−0.02	−0.00	−2.95	−0.01	0.00
	CF_4	61.56	−0.01	−0.00	60.06	−0.00	0.00
	furan (C2/5)	43.98	−0.01	0.00	42.16	−0.01	0.00
	furan (C3/4)	78.35	−0.01	−0.00	76.80	−0.01	−0.00
	$(\underline{C}H_3)_2CO$	160.90	−0.01	0.00	159.81	0.00	0.00
	CH_4	197.58	−0.00	0.00	197.04	0.01	0.00
^{15}N	PN	−334.83	−0.12	−0.01	−338.46	−0.05	−0.00
	N_2	−63.15	−0.03	−0.01	−65.87	−0.01	−0.00
	$N\underline{N}O$	14.71	−0.01	0.00	12.58	−0.00	0.00
	$\underline{N}NO$	110.31	−0.02	−0.00	108.59	−0.01	−0.00
	NH_3	270.66	−0.03	0.00	268.87	0.01	0.00
^{17}O	OF_2	−481.27	−0.11	−0.01	−489.64	−0.04	−0.01
	$(CH_3)_2CO$	−301.22	−0.16	−0.01	−299.72	−0.05	−0.00
	CO	−60.33	−0.05	−0.00	−62.40	−0.03	−0.00
	furan	49.88	−0.05	−0.00	47.64	−0.03	−0.00
	NNO	199.20	−0.03	0.00	198.01	−0.01	−0.00
	H_2O	338.23	−0.03	0.00	336.53	0.01	−0.00
^{19}F	F_2	−195.54	−0.10	−0.01	−199.86	−0.03	−0.01
	OF_2	−23.70	−0.05	−0.00	−27.93	−0.02	−0.00
	PF_3	230.64	−0.06	−0.00	224.97	−0.02	−0.00
	CF_4	264.16	−0.03	−0.00	262.23	−0.01	−0.01
	HF	418.58	−0.01	0.00	418.58	0.00	0.00
^{31}P	PN	37.83	−0.10	0.00	42.70	−0.04	−0.00
	PF_3	211.67	−0.04	−0.00	209.76	−0.02	−0.00
	PH_3	592.78	−0.04	0.00	594.41	0.04	−0.01

Table B.14: Isotropic NMR shielding constants (in ppm), calculated at the RI-DSD-PBEP86 and RI-MP2 levels with different basis sets (pcSseg-n, denoted pSn, and cc-pwCVnZ/C, denoted cw$n$C) and with either all electrons correlated (AE) or with a frozen core (FC).

		MP2						DSD-PBEP86					
		pS2 cwQC		pS3 cw5C		pS4 cw5C		pS2 cwQC		pS3 cw5C		pS4 cw5C	
	Nucleus	FC	AE	FC	AE	FC	AE	FC	AE	FC	AE	FC	AE
^{1}H	PH_3	29.65	29.61	29.55	29.49	29.52	29.45	29.59	29.57	29.53	29.50	29.51	29.48
	HF	28.87	28.86	28.65	28.62	28.59	28.55	29.08	29.08	28.93	28.92	28.89	28.89
	H_2O	30.68	30.67	30.48	30.45	30.44	30.40	30.88	30.88	30.74	30.73	30.71	30.70
	NH_3	31.52	31.51	31.34	31.31	31.31	31.28	31.65	31.65	31.51	31.50	31.50	31.49
	CH_4	31.47	31.45	31.39	31.36	31.38	31.35	31.52	31.51	31.46	31.45	31.46	31.45
	$(CH_3)_2CO$	29.66	29.64	29.51	29.48	29.49	29.46	29.67	29.66	29.56	29.54	29.55	29.54
	furan (at C2/5)	24.00	23.97	23.85	23.81	23.82	23.78	24.10	24.09	23.99	23.97	23.99	23.97
	furan (at C3/4)	24.97	24.93	24.85	24.80	24.83	24.77	25.07	25.06	24.98	24.96	24.98	24.96
^{13}C	$(CH_3)_2\underline{C}O$	−4.99	−6.13	−7.58	−10.33	−7.59	−10.63	−14.49	−14.83	−16.30	−17.31	−16.13	−17.27
	CO	13.30	12.36	11.19	8.02	11.15	7.68	−0.35	−0.59	−1.81	−2.95	−2.00	−3.27
	CF_4	65.95	65.20	64.44	62.88	64.48	62.76	61.83	61.56	60.69	60.06	60.66	59.94
	furan (C2/5)	50.39	49.34	48.66	46.25	48.68	46.03	44.31	43.98	43.04	42.16	43.12	42.15
	furan (C3/4)	84.96	83.96	83.61	81.36	83.67	81.20	78.67	78.34	77.62	76.79	77.60	76.68
	$(\underline{C}H_3)_2CO$	165.29	164.91	164.16	163.22	164.19	163.16	161.03	160.90	160.18	159.81	160.08	159.67
	CH_4	202.00	201.84	201.51	201.02	201.61	201.06	197.63	197.58	197.23	197.04	197.28	197.07
^{15}N	PN	−240.75	−248.00	−248.16	−261.45	−245.40	−259.92	−332.72	−334.84	−334.10	−338.46	−332.03	−336.88
	N_2	−38.24	−39.20	−40.83	−44.11	−40.24	−44.01	−62.92	−63.15	−64.73	−65.88	−64.36	−65.74
	$N\underline{N}O$	34.32	33.44	32.21	29.75	32.19	29.34	14.96	14.72	13.43	12.58	13.51	12.49
	$\underline{N}NO$	133.81	132.73	132.07	129.28	131.93	128.78	110.62	110.30	109.55	108.59	109.26	108.12
	NH_3	278.12	278.01	276.22	275.86	276.29	275.85	270.70	270.66	269.01	268.87	269.12	268.94
^{17}O	OF_2	−451.31	−452.33	−461.96	−466.48	−463.25	−468.62	−481.08	−481.29	−487.94	−489.65	−488.84	−490.94
	$(CH_3)_2CO$	−271.61	−274.04	−268.75	−274.78	−267.48	−274.33	−300.53	−301.23	−297.56	−299.73	−295.97	−298.58
	CO	−43.86	−44.85	−45.72	−48.75	−45.20	−48.72	−60.06	−60.34	−61.30	−62.40	−61.30	−62.64
	furan	52.90	51.64	49.79	46.98	50.05	46.88	50.30	49.87	48.74	47.64	49.25	48.01
	NNO	219.76	218.89	218.54	216.46	218.68	216.33	199.52	199.20	198.81	198.01	199.42	198.50
	H_2O	347.62	347.57	345.60	345.37	345.83	345.53	338.26	338.23	336.63	336.53	336.83	336.68
^{19}F	F_2	−166.03	−166.75	−171.41	−174.71	−173.27	−177.27	−195.44	−195.55	−198.68	−199.87	−200.27	−201.79
	OF_2	−6.36	−6.98	−11.41	−13.85	−12.96	−15.88	−23.55	−23.71	−27.01	−27.93	−28.32	−29.47
	PF_3	242.35	240.21	235.77	232.62	235.29	231.79	231.53	230.64	226.26	224.97	226.05	224.61
	CF_4	272.05	271.54	269.68	268.56	269.64	268.35	264.36	264.16	262.71	262.23	262.78	262.22
	HF	424.98	424.98	425.01	424.94	425.47	425.36	418.60	418.58	418.64	418.58	418.79	418.70
^{31}P	PN	127.07	104.89	131.73	105.71	135.14	106.63	45.30	37.83	51.57	42.70	54.32	44.38
	PF_3	230.88	219.90	230.28	217.29	230.57	215.96	215.78	211.67	214.68	209.76	214.76	209.12
	PH_3	610.74	605.18	614.86	608.98	615.63	609.04	594.83	592.79	596.55	594.40	596.98	594.52

Appendix C Additional data for Chapter 2

Table C.15: Parameters of the used double-hybrid functionals (see eq. 2.71 for definitions).

Functional	c_X	c_C	c_O	c_S	Ref.
B2PLYP	0.53	0.73	0.27	0.27	78
B2GP-PLYP	0.65	0.64	0.36	0.36	281
DSD-BLYP	0.71	0.54	0.47	0.40	85
DSD-PBEP86	0.69	0.44	0.52	0.22	85
NoDSD-PBEP86	0.72	0.44	0.51	0.36	85
revDSD-PBEP86	0.69	0.4296	0.5785	0.0799	89
ωB97X-2	0.636158[a]	1.00[b]	0.447105	0.529319	282
revωB97X-2	0.636158[a]	0.9518[b]	0.5123	0.4294	89

[a] At long range; 0.315503 at short range; $\omega = 0.3$.

[b] DFT correlation also scaled via internal functional parameters.

Table C.16: Number of angular grid points per radial shell belonging to one of the five atomic regions. Smaller grid sizes are used for H and He.

	H–He					Li–Lr				
gn	Innermost				Outermost	Innermost				Outermost
g1	12	26	26	26	26	12	26	50	50	26
g2	12	12	26	50	26	12	26	50	110	50
g3	12	26	50	110	50	26	50	110	194	110
g4	26	50	110	194	110	26	110	194	302	194
g5	50	110	194	302	194	50	194	302	434	302
g6	50	194	302	434	302	50	302	434	590	434
g7	110	302	434	590	434	110	434	590	770	590

Table C.17: Shielding constants, calculated with HF using different basis sets: pcSseg-4, extrapolated aug-cc-pCV[TQ]Z with extrapolation exponent $\alpha = 1.63$ ([TQ1.63]),[73] extrapolated aug-cc-pCV[TQ]Z with $\alpha = 1.05$ ([TQ1.05])[73,287] and a large multiwavelet basis set (MW6).[287] ME and MAE with respect to MW6 are given in ppm and MRE and MARE are given in percent

	Nucleus	pcSseg-4	[TQ1.63]	[TQ1.05]	MW6
^{1}H	PH_3	29.68			
	HF	28.12	28.15	28.09	28.12
	H_2O	30.49	30.55	30.49	30.51
	NH_3	31.57	31.68	31.65	31.59
	CH_4	31.64	31.60	31.60	31.55
	$(CH_3)_2CO$	29.95			
	furan (at C2/5)	24.28			
	furan (at C3/4)	25.30			
^{13}C	$(CH_3)_2\underline{C}O$	−24.95			
	CO	−28.07	−27.40	−28.38	−28.41
	CF_4	77.82			
	furan (C2/5)	36.85			
	furan (C3/4)	74.51			
	$(\underline{C}H_3)_2CO$	162.51			
	CH_4	195.14	194.73	194.41	194.61
^{15}N	PN	−511.98	−508.57	−511.08	−511.80
	N_2	−116.14	−114.39	−115.84	−116.07
	$N\underline{N}O$	−35.81	−34.37	−35.55	−35.73
	$\underline{N}NO$	60.96	61.97	61.09	61.04
	NH_3	262.09	262.41	262.17	262.23
^{17}O	OF_2	−449.03	−445.85	−448.32	−449.10
	$(CH_3)_2CO$	−333.41			
	CO	−92.00	−90.84	−92.58	−92.83
	furan	58.15			
	NNO	173.25	174.19	173.45	173.41
	H_2O	327.59	327.93	327.72	327.78
^{19}F	F_2	−174.56			
	OF_2	19.51	21.08	19.49	19.38
	PF_3	255.25			
	CF_4	281.91			
	HF	414.32	414.63	414.54	414.56
^{31}P	PN	−110.40	−107.79	−107.05	−109.37
	PF_3	255.52			
	PH_3	583.52			
	ME	0.01	−1.01	−0.25	
	MAE	0.23	1.01	0.29	
	MRE	−0.09	−1.41	−0.23	
	MARE	0.29	1.41	0.27	

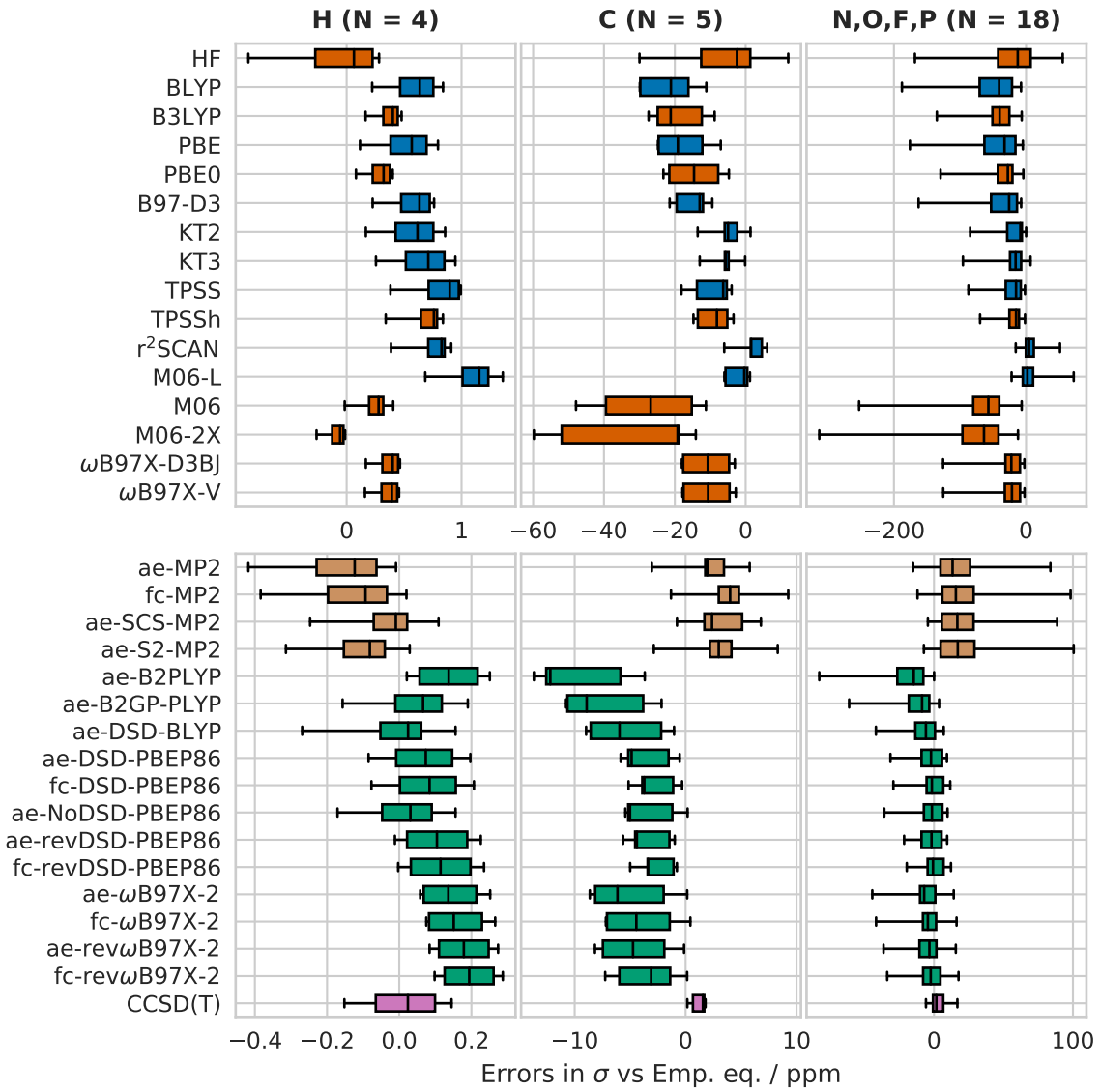

Figure C.1: Deviations of isotropic shielding constants (ppm) for groups of nuclei, calculated using different methods and the pcSseg-4 basis set, from empirical equilibrium values. The number of nuclei in each group is given in parentheses. Boxes show the IQRE_σ, whiskers show the MinE_σ and MaxE_σ, and lines show the MedE_σ. Pure functionals are shown in blue, hybrids and HF in orange, MP2 variants in yellow, and DHDFs in green. Note the different scales used for the abscissa.

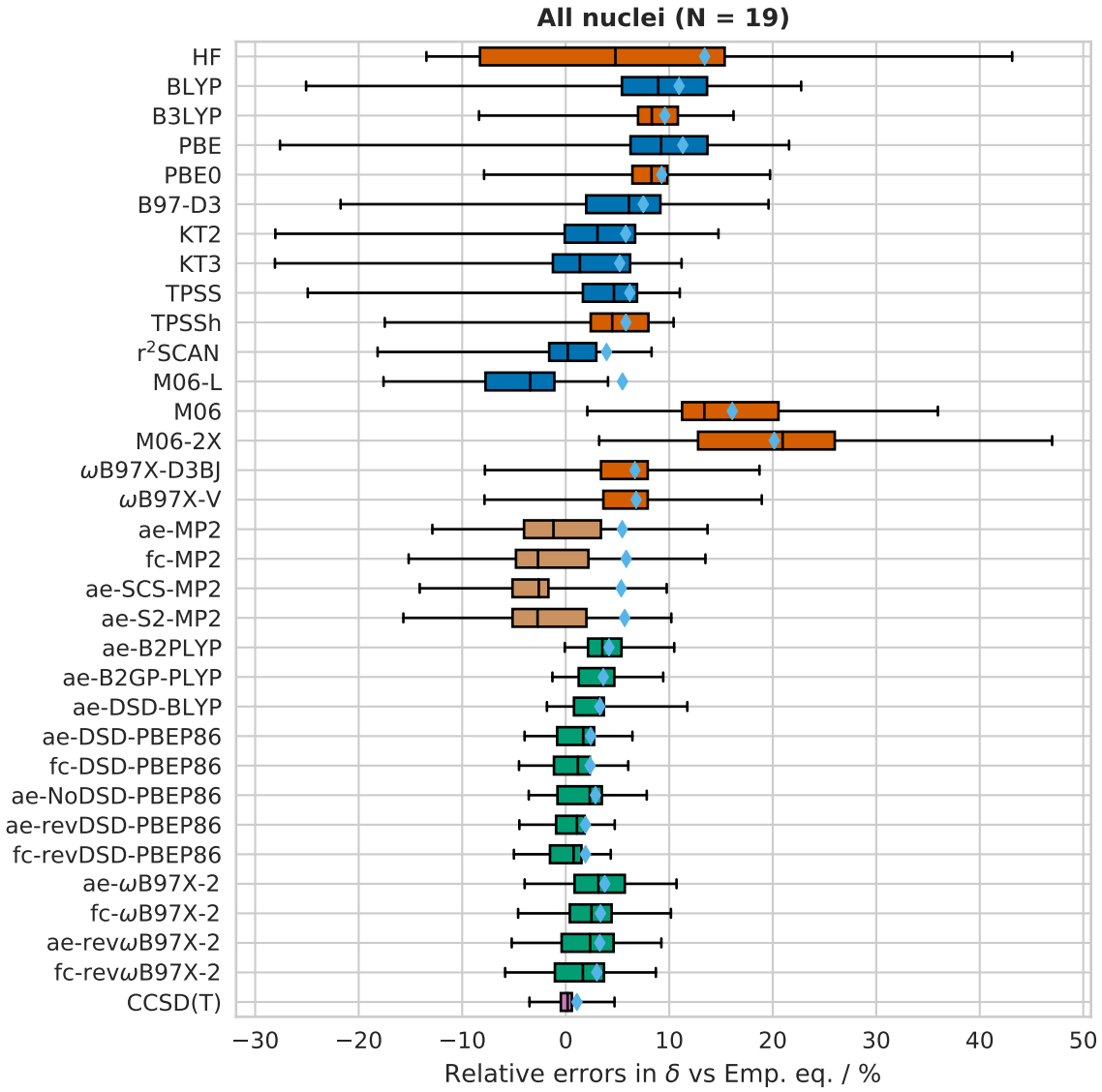

Figure C.2: Relative deviations of chemical shifts (%), calculated using different methods and the pcSseg-4 basis set, from empirical equilibrium values. The number of data points is given in parentheses. Excluded: $N\underline{H}_3$ and $\underline{H}_2O$. Boxes show the $IQRRE_\delta$, whiskers show the $MinRE_\delta$ and $MaxRE_\delta$, lines show the $MedRE_\delta$, and diamonds show the $MARE_\delta$. Pure functionals are shown in blue, hybrids and HF in orange, MP2 variants in yellow, and DHDFs in green.

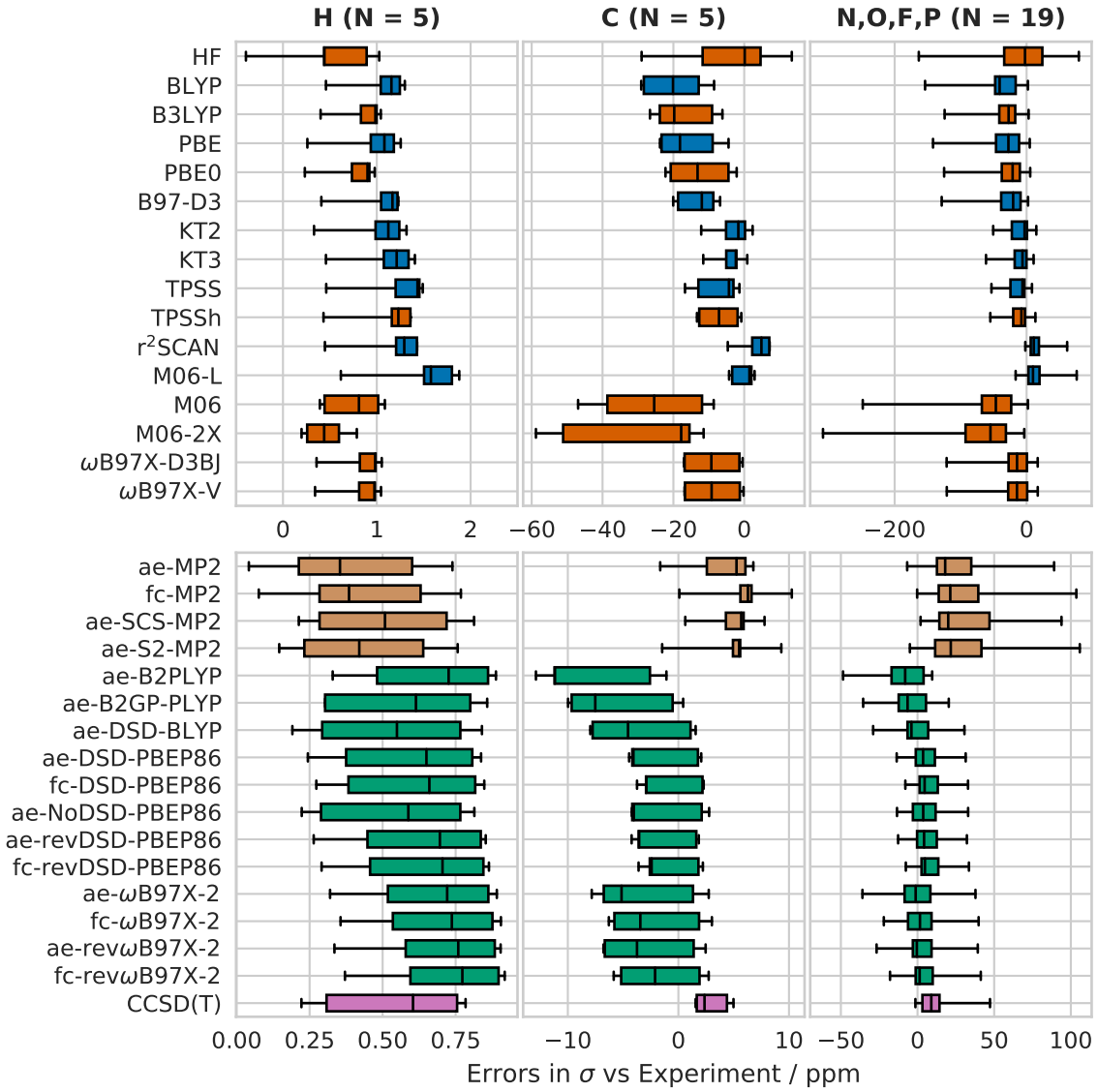

Figure C.3: Deviations of isotropic shielding constants (ppm) for groups of nuclei, calculated using different methods and the pcSseg-4 basis set, from experimental values. The number of nuclei in each group is given in parentheses. Boxes show the IQRE_σ, whiskers show the MinE_σ and MaxE_σ, and lines show the MedE_σ. Pure functionals are shown in blue, hybrids and HF in orange, MP2 variants in yellow, and DHDFs in green. Note the different scales used for the abscissa.

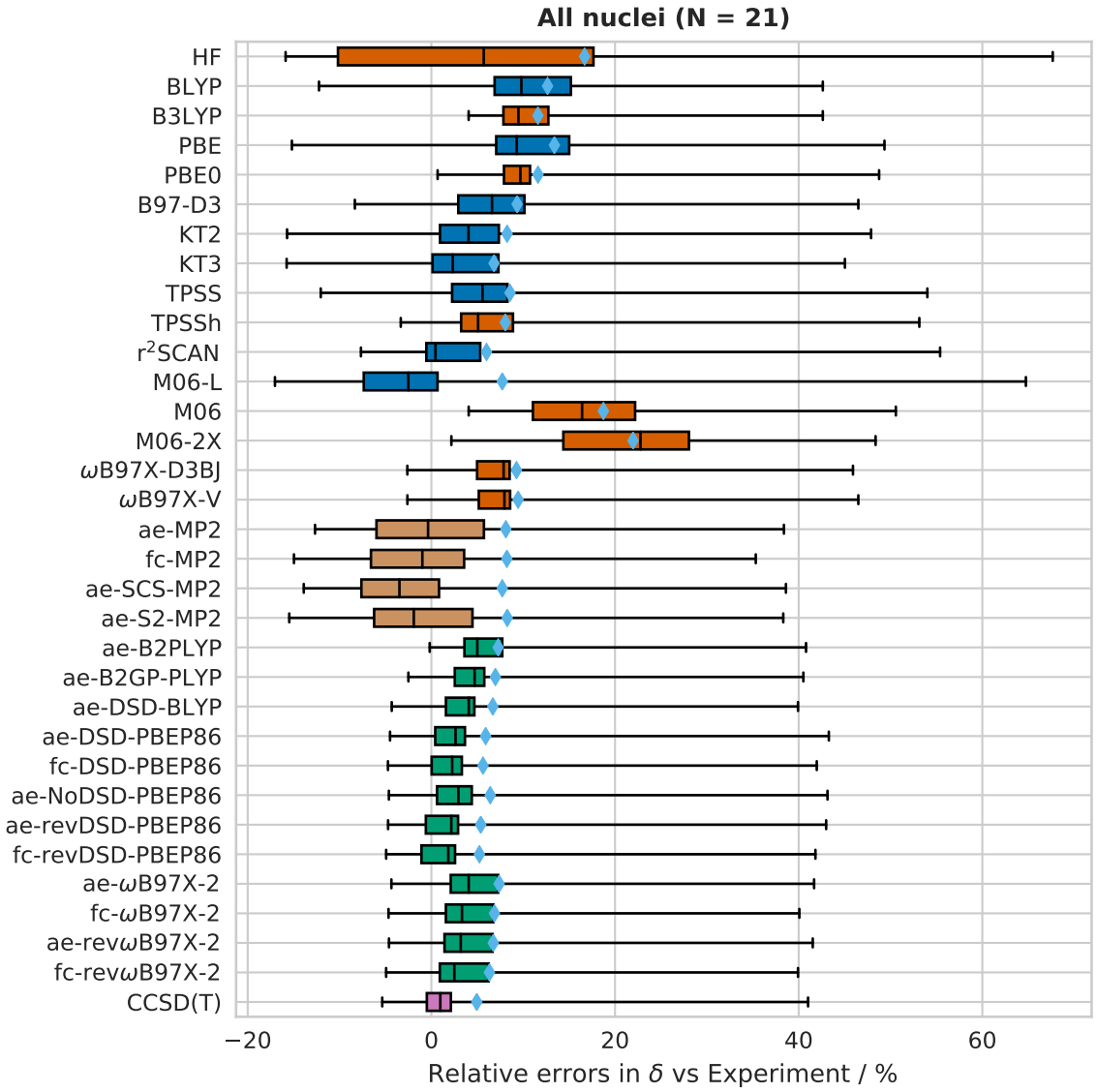

Figure C.4: Relative deviations of chemical shifts (%), calculated using different methods and the pcSseg-4 basis set, from experimental values. The number of data points is given in parentheses. Excluded: $N\underline{H}_3$ and $\underline{H}_2O$. Boxes show the $IQRRE_\delta$, whiskers show the $MinRE_\delta$ and $MaxRE_\delta$, lines show the $MedRE_\delta$, and diamonds show the $MARE_\delta$. Pure functionals are shown in blue, hybrids and HF in orange, MP2 variants in yellow, and DHDFs in green.

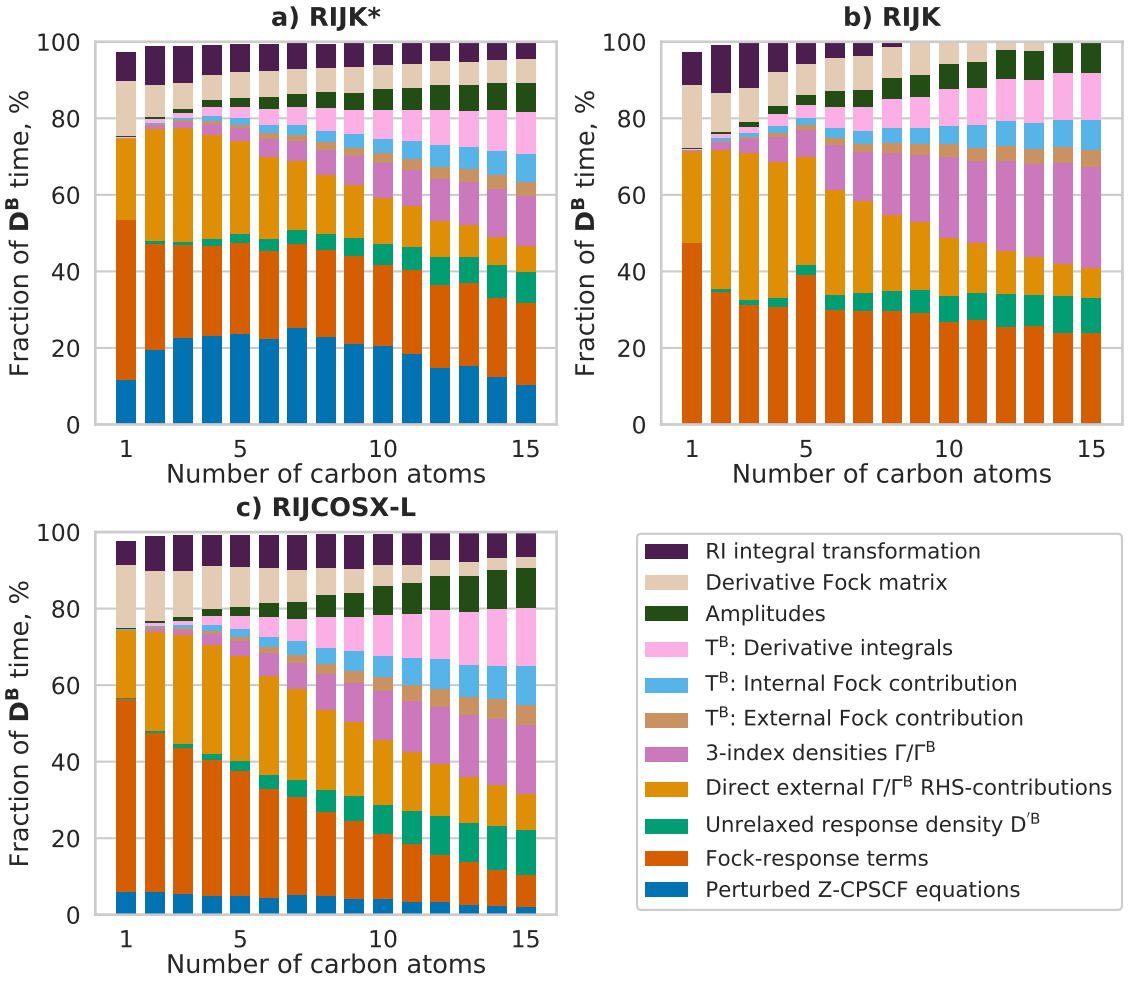

Figure C.5: Contributions, adding up to over 97 % of the total $\mathbf{D^B}$ computation time at the DSD-PBEP86/pS2/cw3C level for linear alkane chains ($C_nH_{(2n+2)}$), using different approximations for the Fock matrix two-electron integrals (see Table 2.6). The calculations were performed on 8 Intel Xeon E7-8837 2.67 GHz cores with 8 GB RAM per core. The legend applies to all subplots.

Appendix D Derivation of the PNO rotation stationarity conditions

In Chapter 3, the MO and PNO response is parametrized using full, complex-valued matrices, constrained with an explicit orthonormality condition, in contrast to the exponential parametrization used previously for DLPNO-MP2.[192] This has the consequence that the final working equations for electric/magnetic perturbations, which are purely real/imaginary, must be obtained as linear combinations of several Lagrangian stationarity conditions. In this section we show a detailed derivation of the equations related to PNO rotations and briefly discuss the analogous treatment of MO rotations.

The PNO rotation stationarity conditions have the following form:

$$0 \equiv \frac{\partial \mathcal{L}}{\partial \boldsymbol{\theta}^{ij}} = \frac{\partial E_2^{\mathrm{DLPNO}}}{\partial \boldsymbol{\theta}^{ij}} + \frac{\partial \Delta E_{\mathrm{PNO}}}{\partial \boldsymbol{\theta}^{ij}} + \frac{\partial C_{\mathrm{PNO}}}{\partial \boldsymbol{\theta}^{ij}} + \frac{\partial C_{\mathrm{PNOO}}}{\partial \boldsymbol{\theta}^{ij}} + \frac{\partial C_{\mathrm{SC}}}{\partial \boldsymbol{\theta}^{ij}} \tag{D.1}$$

$$0 \equiv \frac{\partial \mathcal{L}}{\partial \boldsymbol{\theta}^{ij\dagger}} = \left(\frac{\partial \mathcal{L}}{\partial \boldsymbol{\theta}^{ij}}\right)^{\dagger} \tag{D.2}$$

The separate terms are as follows:

$$\frac{\partial E_2^{\mathrm{DLPNO}}}{\partial \boldsymbol{\theta}^{ij}} = \boldsymbol{\mathcal{K}}^{ji}\boldsymbol{\theta}^{ij}\widetilde{\mathbf{T}}^{ij} + \boldsymbol{\mathcal{K}}^{ij}\boldsymbol{\theta}^{ij}\widetilde{\mathbf{T}}^{ji} + \boldsymbol{\mathcal{F}}^{ij*}\boldsymbol{\theta}^{ij*}\mathbf{D}^{ij} - \mathbf{d}''^{ij(0),\mathrm{T}}\widetilde{\mathbf{S}}^{*}\boldsymbol{\tau}^{ij\dagger} \tag{D.3}$$

$$\begin{aligned}\frac{\partial \Delta E_{\mathrm{PNO}}}{\partial \boldsymbol{\theta}^{ij}} = {}& \frac{1}{2}\Big(\boldsymbol{\mathcal{K}}^{ji}\boldsymbol{\theta}^{ij}\widetilde{\breve{\mathbf{T}}}^{ij} + \boldsymbol{\mathcal{K}}^{ij}\boldsymbol{\theta}^{ij}\widetilde{\breve{\mathbf{T}}}^{ji} + \widetilde{\widehat{\mathbf{T}}}^{ij*}\boldsymbol{\theta}^{ij}\mathbf{K}^{ji*} + \widetilde{\widehat{\mathbf{T}}}^{ji*}\boldsymbol{\theta}^{ji}\mathbf{K}^{ij*}\Big) \\ & - \frac{1}{2}\Big(\boldsymbol{\mathcal{K}}^{ji}\boldsymbol{\theta}^{ij}\mathbf{N}^{ij}\widetilde{\breve{\mathbf{T}}}^{ij} + \boldsymbol{\mathcal{K}}^{ij}\boldsymbol{\theta}^{ij}\mathbf{N}^{ij}\widetilde{\breve{\mathbf{T}}}^{ji} \\ & + \widetilde{\widehat{\mathbf{T}}}^{ij*}\boldsymbol{\theta}^{ij}\mathbf{N}^{ij}\mathbf{K}^{ji*} + \widetilde{\widehat{\mathbf{T}}}^{ji*}\boldsymbol{\theta}^{ji}\mathbf{N}^{ij}\mathbf{K}^{ij*}\Big)\mathbf{N}^{ij}\end{aligned} \tag{D.4}$$

$$\frac{\partial C_{\mathrm{PNO}}}{\partial \boldsymbol{\theta}^{ij}} = \frac{1}{2}\widetilde{\widehat{\mathbf{T}}}^{ij*}\boldsymbol{\theta}^{ij}\left(\breve{\mathbf{T}}^{ji}\mathbf{v}^{ij,\mathrm{T}} + \mathbf{v}^{ij}\breve{\mathbf{T}}^{ji}\right) + \frac{1}{2}\widetilde{\widehat{\mathbf{T}}}^{ji*}\boldsymbol{\theta}^{ij}\left(\breve{\mathbf{T}}^{ij}\mathbf{v}^{ij,\mathrm{T}} + \mathbf{v}^{ij}\breve{\mathbf{T}}^{ij}\right) \tag{D.5}$$

$$\frac{\partial C_{\mathrm{PNOO}}}{\partial \boldsymbol{\theta}^{ij}} = \boldsymbol{\mathcal{S}}^{ij*}\boldsymbol{\theta}^{ij*}\mathbf{x}^{ij} \tag{D.6}$$

$$\begin{aligned}\frac{\partial C_{\mathrm{SC}}}{\partial \boldsymbol{\theta}^{ij}} = \frac{1}{2}\Big[& \boldsymbol{\mathcal{F}}^{ij*}\boldsymbol{\theta}^{ij*}\mathbf{w}^{ij,\mathrm{T}}\breve{\mathbf{T}}^{ij} + \boldsymbol{\mathcal{F}}^{ij*}\boldsymbol{\theta}^{ij*}\mathbf{w}^{ij}\breve{\mathbf{T}}^{ji} + \widehat{\mathbf{T}}^{ji*}\boldsymbol{\theta}^{ij}\mathbf{w}^{ij*}\mathbf{F}^{ij*} \\ & + \widehat{\mathbf{T}}^{ij*}\boldsymbol{\theta}^{ij}\mathbf{w}^{ij\dagger}\mathbf{F}^{ij*} + \widehat{\mathbf{R}}^{ij*}\boldsymbol{\theta}^{ij}\mathbf{w}^{ij\dagger} + \widehat{\mathbf{R}}^{ij\dagger}\boldsymbol{\theta}^{ij}\mathbf{w}^{ij*}\Big]\end{aligned} \tag{D.7}$$

where quantities in the full PNO+CPNO basis are expanded as

$$\mathbf{K}^{ij} = \boldsymbol{\theta}^{ij,\mathrm{T}}\boldsymbol{\mathcal{K}}^{ij}\boldsymbol{\theta}^{ij} \tag{D.8}$$

$$\breve{\mathbf{R}}^{ij} = \boldsymbol{\theta}^{ij\dagger}\widehat{\mathbf{R}}^{ij}\boldsymbol{\theta}^{ij*} \tag{D.9}$$

$$\mathbf{S}^{ij} = \boldsymbol{\theta}^{ij\dagger}\boldsymbol{\mathcal{S}}^{ij}\boldsymbol{\theta}^{ij} = \boldsymbol{\theta}^{ij\dagger}\mathbf{d}''^{ij(0)\dagger}\widetilde{\mathbf{S}}\mathbf{d}''^{ij(0)}\boldsymbol{\theta}^{ij} \tag{D.10}$$

$$\mathbf{F}^{ij} = \boldsymbol{\theta}^{ij\dagger}\boldsymbol{\mathcal{F}}^{ij}\boldsymbol{\theta}^{ij} \tag{D.11}$$

The index $\tilde{\mu}'$ of the intermediate $\tau^{ij}_{\tilde{a}\tilde{\mu}'}$ spans the PAO domains of all pairs ik and jk included in the sum, i.e. those for which $|\,F_{kj}\,|$ or $|\,F_{ki}\,|$, respectively, is greater than F_{Cut}. Note also that the amplitudes $\mathbf{T}^{ij}$ are implicitly non-zero only in the PNO block. To obtain equations for $\mathbf{v}^{ij}$, we take the following linear combination, where the contributions from

C_{SC} and C_{PNOO} drop out:

$$\begin{aligned} 0 \equiv \left[\frac{\partial \mathcal{L}}{\partial \boldsymbol{\theta}^{ij}} - \frac{\partial \mathcal{L}}{\partial \boldsymbol{\theta}^{ij\dagger}}\right]\Bigg|_{\boldsymbol{\lambda}=0} = \Bigg[\frac{\partial E_2^{\mathrm{DLPNO}}}{\partial \boldsymbol{\theta}^{ij}} - \frac{\partial E_2^{\mathrm{DLPNO}}}{\partial \boldsymbol{\theta}^{ij\dagger}} \\ + \frac{\partial \Delta E_{\mathrm{PNO}}}{\partial \boldsymbol{\theta}^{ij}} - \frac{\partial \Delta E_{\mathrm{PNO}}}{\partial \boldsymbol{\theta}^{ij\dagger}} + \frac{\partial C_{\mathrm{PNO}}}{\partial \boldsymbol{\theta}^{ij}} - \frac{\partial C_{\mathrm{PNO}}}{\partial \boldsymbol{\theta}^{ij\dagger}}\Bigg]\Bigg|_{\boldsymbol{\lambda}=0} \end{aligned} \tag{D.12}$$

Only rotations between PNOs and CPNOs result in the non-zero equations shown in eq. 3.60. In addition, we use eq. 3.57 (at $\boldsymbol{\lambda} = 0$) to express eq. D.5 as

$$\begin{aligned} \frac{\partial C_{\mathrm{PNO}}}{\partial \boldsymbol{\theta}^{ij}} = \frac{1}{2}\Big[&\widetilde{\widehat{\mathbf{T}}}^{ij*}\boldsymbol{\theta}^{ij}\left(\mathbf{N}^{ij}\mathbf{K}^{ji*}\mathbf{N}^{ij} - \mathbf{K}^{ji*}\right) + \widetilde{\widehat{\mathbf{T}}}^{ji*}\boldsymbol{\theta}^{ij}\left(\mathbf{N}^{ij}\mathbf{K}^{ij*}\mathbf{N}^{ij} - \mathbf{K}^{ij*}\right) \\ &+ \widehat{\mathbf{T}}^{ij*}\boldsymbol{\theta}^{ij}\left(\mathbf{w}^{ij\dagger}\left(F_{jj} + F_{ii}\right) - \mathbf{F}^{ij}\mathbf{w}^{ij\dagger} - \mathbf{w}^{ij\dagger}\mathbf{F}^{ij*}\right) \\ &+ \widehat{\mathbf{T}}^{ji*}\boldsymbol{\theta}^{ij}\left(\mathbf{w}^{ij*}\left(F_{jj} + F_{ii}\right) - \mathbf{F}^{ij}\mathbf{w}^{ij*} - \mathbf{w}^{ij*}\mathbf{F}^{ij*}\right)\Big] \end{aligned} \tag{D.13}$$

and after expanding the semi-canonical residuals in eq. D.7 we obtain a different expression for eq. D.1:

$$\begin{aligned} 0 \equiv \frac{\partial \mathcal{L}}{\partial \boldsymbol{\theta}^{ij}} = \frac{1}{2}\boldsymbol{\mathcal{K}}^{ji}\boldsymbol{\theta}^{ij}\mathbf{g}^{ij} + \frac{1}{2}\boldsymbol{\mathcal{K}}^{ij}\boldsymbol{\theta}^{ij}\mathbf{g}^{ij,\mathrm{T}} + \boldsymbol{\mathcal{F}}^{ij*}\boldsymbol{\theta}^{ij*}\mathbf{D}''^{ij} - \mathbf{d}''^{ij(0),\mathrm{T}}\widetilde{\mathbf{S}}^{*}\boldsymbol{\tau}^{ij\dagger} \\ + \boldsymbol{\mathcal{S}}^{ij*}\boldsymbol{\theta}^{ij*}\mathbf{x}^{ij} \end{aligned} \tag{D.14}$$

where, padding $\mathbf{D}^{ij}$ with zeros up to the full PNO+CPNO basis, we have substituted

$$\mathbf{D}''^{ij} = \mathbf{D}^{ij} + \frac{1}{2}\left(\mathbf{w}^{ij}\breve{\mathbf{T}}^{ji} + \mathbf{w}^{ij,\mathrm{T}}\breve{\mathbf{T}}^{ij} + \breve{\mathbf{T}}^{ji*}\mathbf{w}^{ij*} + \breve{\mathbf{T}}^{ij*}\mathbf{w}^{ij\dagger}\right) \tag{D.15}$$

If we define $\mathcal{L}_{-\mathrm{PNOO}} = \mathcal{L} - C_{\mathrm{PNOO}}$ we obtain a solution for $\mathbf{x}^{ij}$:

$$\mathbf{x}^{ij} = -\left.\frac{\partial \mathcal{L}_{-\mathrm{PNOO}}}{\partial \boldsymbol{\theta}^{ij}}\right|_{\boldsymbol{\lambda}=0} = -\frac{1}{2}\boldsymbol{\mathcal{K}}^{ji}\mathbf{g}^{ij} - \frac{1}{2}\boldsymbol{\mathcal{K}}^{ij}\mathbf{g}^{ij,\mathrm{T}} - \boldsymbol{\mathcal{F}}^{ij*}\mathbf{D}''^{ij} + \mathbf{d}''^{ij(0),\mathrm{T}}\widetilde{\mathbf{S}}^{*}\boldsymbol{\tau}^{ij\dagger} \tag{D.16}$$

Note that we obtain a different expression from the Hermitian conjugate:

$$\mathbf{x}^{ij} = -\left.\frac{\partial \mathcal{L}_{-\mathrm{PNOO}}}{\partial \boldsymbol{\theta}^{ij\dagger}}\right|_{\boldsymbol{\lambda}=0} = -\frac{1}{2}\mathbf{g}^{ij\dagger}\boldsymbol{\mathcal{K}}^{ij*} - \frac{1}{2}\mathbf{g}^{ij*}\boldsymbol{\mathcal{K}}^{ji*} - \mathbf{D}''^{ij}\boldsymbol{\mathcal{F}}^{ij*} + \boldsymbol{\tau}^{ij}\widetilde{\mathbf{S}}^{*}\mathbf{d}''^{ij(0)*} \tag{D.17}$$

but both equations are equivalent, provided that eq. D.12 is fulfilled.

To obtain the perturbed multipliers $\mathbf{v}^{ij,\boldsymbol{\lambda}}$, we first express the perturbed PNO/CPNO stationarity conditions as:

$$\begin{aligned} 0 \equiv \frac{\mathrm{d}}{\mathrm{d}\boldsymbol{\lambda}}\frac{\partial \mathcal{L}}{\partial \boldsymbol{\theta}^{ij}} = \frac{\mathrm{d}}{\mathrm{d}\boldsymbol{\lambda}}\left(\frac{\partial \mathcal{L}_{-\mathrm{PNOO}}}{\partial \boldsymbol{\theta}^{ij}} + \boldsymbol{\mathcal{S}}^{ij*}\boldsymbol{\theta}^{ij*}\mathbf{x}^{ij}\right) \\ = \frac{\mathrm{d}}{\mathrm{d}\boldsymbol{\lambda}}\frac{\partial \mathcal{L}_{-\mathrm{PNOO}}}{\partial \boldsymbol{\theta}^{ij}} + \boldsymbol{\theta}^{ij,\boldsymbol{\lambda},\mathrm{T}}\frac{\partial \mathcal{L}_{-\mathrm{PNOO}}}{\partial \boldsymbol{\theta}^{ij}} + \mathbf{x}^{ij,\boldsymbol{\lambda}} \end{aligned} \tag{D.18}$$

$$0 \equiv \frac{\mathrm{d}}{\mathrm{d}\boldsymbol{\lambda}}\frac{\partial \mathcal{L}}{\partial \boldsymbol{\theta}^{ij\dagger}} = \frac{\mathrm{d}}{\mathrm{d}\boldsymbol{\lambda}}\frac{\partial \mathcal{L}_{-\mathrm{PNOO}}}{\partial \boldsymbol{\theta}^{ij\dagger}} + \frac{\partial \mathcal{L}_{-\mathrm{PNOO}}}{\partial \boldsymbol{\theta}^{ij\dagger}}\boldsymbol{\theta}^{ij,\boldsymbol{\lambda}*} + \mathbf{x}^{ij,\boldsymbol{\lambda}} \tag{D.19}$$

where we have used eqs. D.16, D.17, and 3.98. We then take the linear combination

$$0 \equiv \frac{\mathrm{d}}{\mathrm{d}\boldsymbol{\lambda}}\left(\frac{\partial \mathcal{L}}{\partial \boldsymbol{\theta}^{ij}} - \frac{\partial \mathcal{L}}{\partial \boldsymbol{\theta}^{ij\dagger}}\right) \tag{D.20}$$

in which $\mathbf{x}^{ij,\boldsymbol{\lambda}}$ cancels out to obtain eq. 3.111. A solution for $\mathbf{x}^{ij,\boldsymbol{\lambda}}$ can also be obtained from eq. D.18:

$$\mathbf{x}^{ij,\boldsymbol{\lambda}} = \frac{\mathrm{d}}{\mathrm{d}\boldsymbol{\lambda}} \left(-\frac{1}{2}\mathbf{K}^{ji}\mathbf{g}^{ij} - \frac{1}{2}\mathbf{K}^{ij}\mathbf{g}^{ij,\mathrm{T}} - \mathbf{F}^{ij*}\mathbf{D}''^{ij} + \mathbf{d}''^{ij,\mathrm{T}}\widetilde{\mathbf{S}}^{*}\boldsymbol{\tau}^{ij\dagger} \right) \tag{D.21}$$

This is equal to the Hermitian conjugate, obtained from eq. D.19, if eq. D.20 is fulfilled.

The derivation of the MO rotation stationarity conditions in analogous to the above and to that given for RI-MP2 in Section 2.1.3: the contributions from C_{MOO} cancel in the linear combination:

$$0 \equiv \left[\frac{\partial \mathcal{L}}{\partial \mathbf{U}} - \frac{\partial \mathcal{L}}{\partial \mathbf{U}^{\dagger}} \right] \Bigg|_{\boldsymbol{\lambda}=0} \tag{D.22}$$

which gives the Z-CPL, Z-CV, and Z-CPSCF equations 3.61, 3.70, and 3.72, respectively, while solutions for $\mathbf{x}$ can be obtained from either equation separately:

$$\mathbf{x} = \frac{\partial \mathcal{L}_{-\mathrm{MOO}}}{\partial \mathbf{U}} \Bigg|_{\boldsymbol{\lambda}=0} \tag{D.23}$$

$$\mathbf{x} = -\frac{\partial \mathcal{L}_{-\mathrm{MOO}}}{\partial \mathbf{U}^{\dagger}} \Bigg|_{\boldsymbol{\lambda}=0} \tag{D.24}$$

$$\mathcal{L}_{-\mathrm{MOO}} \equiv \mathcal{L} - C_{\mathrm{MOO}} \tag{D.25}$$

which are equivalent, provided that eq. D.22 is fulfilled. The second derivatives are also treated analogously – we first express the stationarity conditions as:

$$0 \equiv \frac{\mathrm{d}}{\mathrm{d}\boldsymbol{\lambda}} \frac{\partial \mathcal{L}}{\partial \mathbf{U}} = \frac{\mathrm{d}}{\mathrm{d}\boldsymbol{\lambda}} \frac{\partial \mathcal{L}_{-\mathrm{MOO}}}{\partial \mathbf{U}} + \mathbf{U}^{\boldsymbol{\lambda},\mathrm{T}} \frac{\partial \mathcal{L}_{-\mathrm{MOO}}}{\partial \mathbf{U}} + \mathbf{x}^{\boldsymbol{\lambda}} \tag{D.26}$$

$$0 \equiv \frac{\mathrm{d}}{\mathrm{d}\boldsymbol{\lambda}} \frac{\partial \mathcal{L}}{\partial \mathbf{U}^{\dagger}} = \frac{\mathrm{d}}{\mathrm{d}\boldsymbol{\lambda}} \frac{\partial \mathcal{L}_{-\mathrm{MOO}}}{\partial \mathbf{U}^{\dagger}} + \frac{\partial \mathcal{L}_{-\mathrm{MOO}}}{\partial \mathbf{U}^{\dagger}} \mathbf{U}^{\boldsymbol{\lambda}*} + \mathbf{x}^{\boldsymbol{\lambda}} \tag{D.27}$$

and then obain the perturbed Z-CPL, Z-CV, and Z-CPSCF equations 3.113, 3.116, and 3.117, respectively, from the linear combination in which $\mathbf{x}^{\boldsymbol{\lambda}}$ cancels:

$$0 \equiv \frac{\mathrm{d}}{\mathrm{d}\boldsymbol{\lambda}} \left(\frac{\partial \mathcal{L}}{\partial \mathbf{U}} - \frac{\partial \mathcal{L}}{\partial \mathbf{U}^{\dagger}} \right) \tag{D.28}$$

Equivalent solutions for $\mathbf{x}^{\boldsymbol{\lambda}}$ can be obtained from either eq. D.26 or eq. D.27, however, this is not necessary for the properties discussed in the present work.

Appendix E Coordinates of the test set molecules from Chapter 3

The coordinates below are given in Angstrøm in XYZ format. All systems are closed-shell; the charge, if any, is given in the comment line. In the interest of space, the coordinates of the glycine chains, [n]helicenes, and vancomycin are not included here. However, they are published in the supplementary material of ref. 317.

Toy systems

These are the pentane and water dimer examples from Section 3.2.2.

```
17
C5H12
   H  -0.629312   0.000000  -0.889981
   C   0.000000   0.000000   0.000000
   H   0.629312   0.889981   0.000000
   H   0.629312  -0.889981   0.000000
   C  -0.889120   0.000000   1.257405
   H  -1.518432   0.889981   1.257405
   H  -1.518432  -0.889981   1.257405
   C   0.000000   0.000000   2.514809
   H   0.629312   0.889981   2.514809
   H   0.629312  -0.889981   2.514809
   C  -0.889120   0.000000   3.772214
   H  -1.518432   0.889981   3.772214
   H  -1.518432  -0.889981   3.772214
   C   0.000000   0.000000   5.029618
   H   0.629312   0.889981   5.029618
   H   0.629312  -0.889981   5.029618
   H  -0.629312   0.000000   5.919599
6
H2O dimer
   O   0.000000   0.066196   0.000000
   H  -0.753371  -0.525286   0.000000
   H   0.753371  -0.525286   0.000000
   O   0.000000   0.066196   5.556361
   H  -0.753371  -0.525286   5.556361
   H   0.753371  -0.525286   5.556361
```

Benchmark systems

Below are the systems shown in Figure 3.4.

```
48
anthracene dimer
   C   -0.014583    0.019296    0.019945
   C    0.015588   -0.068948    1.443598
   C    1.208832   -0.159702    2.117976
   C    2.443170   -0.148967    1.406576
   C    2.456414   -0.051249    0.036071
   C    1.238642    0.023672   -0.703387
   H   -0.933051   -0.091030    1.982926
   H    1.217494   -0.244434    3.206160
   H    3.381052   -0.219349    1.959877
   H    3.399668   -0.054392   -0.513591
   C    1.217474    0.034863   -2.103734
   C    0.014635    0.019250   -2.819884
   C   -0.015532   -0.068969   -4.243543
   C   -1.208778   -0.159768   -4.917910
   C   -2.443113   -0.149069   -4.206502
   C   -2.456361   -0.051288   -2.836005
   C   -1.238592    0.023661   -2.096550
   H    0.933094   -0.090928   -4.782895
```

```
H   -1.217449   -0.244447   -6.006098
H   -3.380994   -0.219490   -4.759800
H   -3.399615   -0.054408   -2.286346
C   -1.217421    0.034906   -0.696204
H    2.162529   -0.004165   -2.650377
H   -2.162476   -0.004140   -0.149558
C   -0.703878   -3.284869   -2.617432
C    0.696466   -3.273651   -2.638699
C    1.435837   -3.198719   -3.856521
C    2.806340   -3.100991   -3.843368
C    3.517838   -3.090271   -2.609087
C    2.843545   -3.181031   -1.415797
C    1.419887   -3.269194   -1.385525
H    0.886131   -3.195668   -4.799748
H    3.359574   -3.030627   -4.781292
H    4.606024   -3.005588   -2.617834
H    3.382930   -3.158990   -0.467189
C    0.703825   -3.284846   -0.182633
C   -0.696518   -3.273661   -0.161364
C   -1.435880   -3.198650    1.056460
C   -2.806382   -3.100920    1.043305
C   -3.517886   -3.090313   -0.190975
C   -2.843602   -3.181112   -1.384269
C   -1.419936   -3.269212   -1.414541
H   -0.886171   -3.195567    1.999686
H   -3.359614   -3.030494    1.981225
H   -4.606081   -3.005735   -0.182223
H   -3.383030   -3.159234   -2.332856
H   -1.250586   -3.245821   -3.562449
H    1.250536   -3.245742    0.762382
```

```
43
ATP 4-
   C   -1.576263   -0.517809    2.519624
   C   -0.276695   -0.324338    1.699527
   C    0.170085    1.053123    2.240267
   C   -2.160128    0.906512    2.443712
   O   -0.961931    1.740809    2.672654
   H   -2.549650    1.151734    1.447172
   C   -3.179900    1.261980    3.507566
   O   -2.362141   -1.588395    2.126323
   H   -1.280915   -0.686451    3.579680
   O   -0.480541   -0.246479    0.331972
   H    0.486952   -1.093046    1.950055
   H    0.744435    1.609638    1.483768
   N    1.072530    0.921789    3.426385
   H   -3.413428    2.339915    3.440196
   O   -4.339268    0.485202    3.376433
   H   -2.739445    1.051486    4.507253
   C    2.433704    0.794584    3.432716
   C    0.678306    0.933581    4.733082
   P   -5.562986    1.005339    2.269894
   C    2.793834    0.731090    4.803949
   N    1.691462    0.821820    5.609339
   H   -0.373020    1.058708    4.979027
   N    3.305034    0.780254    2.407718
   C    4.572584    0.696625    2.806657
   N    5.049509    0.632133    4.080068
   H    5.332192    0.683992    2.018977
   C    4.169548    0.645449    5.085612
   N    4.630466    0.560140    6.397104
   H    5.563089    0.940948    6.512641
   H    3.953764    0.903838    7.072690
   H   -2.781009   -1.312077    1.228226
   H   -1.493075   -0.342211    0.068413
   O   -6.811305    0.290873    2.778470
   O   -5.095988    0.288930    0.880527
   P   -4.028231    0.482544   -0.456995
   O   -5.465387    2.528477    2.257689
   O   -3.424283    1.878520   -0.399735
   O   -4.974096    0.073789   -1.626388
```

```
   O   -2.950942   -0.644556   -0.135518
   P   -5.029839   -0.194823   -3.536341
   O   -6.271131    0.660424   -3.886431
   O   -5.234160   -1.727200   -3.590803
   O   -3.663597    0.342050   -4.008795


24
caffeine
   C   -0.490943   -0.681235   -0.009146
   C    0.886732   -0.693286   -0.028792
   N    1.611792    0.468546   -0.022553
   C    0.956284    1.689004   -0.021661
   O    1.570890    2.738760   -0.043216
   N   -0.446090    1.663514    0.014463
   C   -1.269203    0.515951    0.008722
   O   -2.489808    0.585225    0.019443
   N   -0.865045   -2.015012    0.001624
   N    1.372812   -1.959365   -0.041383
   C    0.286618   -2.723561   -0.022453
   C   -2.224959   -2.528249    0.017743
   C    3.068854    0.463776   -0.034295
   C   -1.094299    2.973845    0.050119
   H    0.295187   -3.802474   -0.024229
   H   -2.198207   -3.579230    0.300206
   H   -2.815272   -1.966459    0.736260
   H   -2.687554   -2.420281   -0.963490
   H    3.444711    0.803847   -1.000088
   H    3.399593   -0.552853    0.156699
   H    3.440040    1.137974    0.733649
   H   -2.142240    2.817758    0.283048
   H   -0.612916    3.591470    0.803892
   H   -0.996979    3.472333   -0.914563


36
coronene
   C   -0.515149   -1.337548    0.000025
   C    0.900713   -1.114666    0.000032
   C   -1.415886   -0.222738    0.000019
   C    1.415903    0.222760    0.000031
   C   -0.900696    1.114688    0.000018
   C    0.515165    1.337570    0.000025
   C   -1.030023   -2.674617    0.000026
   C    1.801114   -2.229165    0.000038
   C   -2.831321   -0.445493    0.000013
   C    2.831338    0.445515    0.000038
   C   -1.801097    2.229187    0.000012
   C    1.030040    2.674639    0.000024
   C   -0.107792   -3.767248    0.000032
   C   -2.446919   -2.866601    0.000020
   C    1.259004   -3.552179    0.000038
   C    3.208445   -1.976781    0.000044
   C   -3.316572   -1.790447    0.000013
   C   -3.705806    0.685730    0.000006
   C    3.705822   -0.685708    0.000044
   C    3.316588    1.790469    0.000037
   C   -3.208428    1.976803    0.000006
   C   -1.258987    3.552201    0.000011
   C    2.446935    2.866624    0.000030
   C    0.107809    3.767270    0.000017
   H   -0.507491   -4.793413    0.000033
   H   -2.838757   -3.895787    0.000020
   H    1.954169   -4.406366    0.000043
   H    3.897339   -2.835959    0.000049
   H   -4.405014   -1.957667    0.000009
   H   -4.793104    0.511169    0.000002
   H    4.793120   -0.511146    0.000049
   H    4.405030    1.957689    0.000042
   H   -3.897322    2.835981    0.000000
   H   -1.954152    4.406388    0.000006
   H    2.838774    3.895810    0.000030
   H    0.507508    4.793435    0.000017
```

```
25
ebselen
   N    2.481307   -0.087176   -0.031100
  Se    1.673417   -1.784765   -0.135544
   C    0.204002    0.510065    0.032788
   C    0.018085   -0.867037   -0.051633
   C    1.600713    0.987318    0.041298
   C   -1.253926   -1.427248   -0.066799
   C   -2.345689   -0.573089    0.003615
   C   -2.173916    0.811611    0.090274
   C   -0.900103    1.355753    0.105849
   O    1.949332    2.152132    0.109884
   C    5.912907    1.128072   -0.731882
   C    6.680949    0.137548   -0.129669
   C    6.047907   -0.918836    0.513168
   C    4.661836   -0.981277    0.557670
   C    3.892898    0.009082   -0.055316
   C    4.526533    1.070054   -0.706499
   H   -1.396692   -2.498164   -0.132061
   H   -3.344909   -0.989678   -0.008681
   H   -3.040350    1.456986    0.145706
   H   -0.732819    2.423244    0.173681
   H    6.395528    1.955790   -1.236071
   H    7.761742    0.189355   -0.160562
   H    6.630775   -1.695455    0.991602
   H    4.174955   -1.792896    1.083471
   H    3.934759    1.842863   -1.169308


41
penicillin
   C    1.814441   -2.014653    1.677276
   C    2.751715   -1.233401   -0.388794
   C    2.138807   -0.809522    2.284277
   C    3.076985   -0.022979    0.216660
   C    2.771540    0.191161    1.553980
   C    1.667551   -3.521913   -0.329014
   C   -1.714202    2.521143    0.690571
   C   -3.479206    1.266532    1.963304
   H    0.150356   -1.582582   -0.862633
   C    2.113751   -2.242055    0.332194
   O   -5.627607    0.713883   -0.467330
   O   -2.166551   -0.749140   -2.976585
   O   -0.476631   -4.627656   -0.401192
   O   -4.671233    2.731713   -0.745328
   C   -4.643931    1.384928   -0.596520
   C    0.152359   -3.597655   -0.540633
   C   -3.207780    0.891835   -0.586697
   C   -1.832471   -2.216218   -0.915471
   C   -2.363871   -1.101738   -1.850571
   H   -5.602901    3.003190   -0.725273
   N   -0.422818   -2.411369   -0.907075
   C   -2.469567   -1.344879    0.220884
   C   -2.501996    1.217551    0.787368
   S   -1.322527   -0.193886    1.048091
   N   -3.110169   -0.530400   -0.817715
   H   -2.675547    1.406914   -1.389084
   H   -3.148162   -1.834275    0.915601
   H   -2.397423    3.345792    0.482727
   H   -1.199947    2.732300    1.629140
   H   -0.972750    2.473656   -0.107075
   H   -4.057133    0.346832    2.052516
   H   -2.921831    1.414721    2.887730
   H   -4.179599    2.098053    1.854934
   H   -2.326034   -3.178111   -1.039800
   H    2.144610   -3.638712   -1.305126
   H    1.931147   -4.394226    0.267425
   H    1.307948   -2.785701    2.246264
   H    2.994348   -1.393576   -1.432788
   H    1.886752   -0.644752    3.323995
   H    3.569692    0.750455   -0.358844
   H    3.026828    1.131279    2.025928
```

```
44
sitagliptin 1+
   C    5.189277    7.529162   33.837135
   C    4.952310    7.809722   31.072724
   C    4.049120    8.441443   31.922171
   C    4.168620    8.308206   33.293071
   H    3.439273    8.803646   33.921066
   F    4.822361    7.952372   29.757234
   F    3.062560    9.172486   31.402763
   C    5.353161    7.336853   35.321380
   H    4.456410    7.696293   35.833185
   H    5.451570    6.268227   35.536210
   H    5.972194    8.007749   37.896298
   C    5.457028   11.892804   34.133521
   C    4.558883   12.008786   32.946245
   N    5.025834   11.848874   31.675758
   C    6.372742   11.391942   31.334068
   N    3.287724   12.308961   32.944339
   C    3.922966   12.077753   30.894698
   N    2.883913   12.358035   31.630456
   C    3.956979   12.010358   29.398295
   F    4.812174   12.935152   28.902639
   F    4.420070   10.805396   28.990833
   F    2.762899   12.208794   28.866922
   H    5.485610    9.929321   35.880900
   H    4.902225   11.437253   34.945177
   H    6.333434   10.337672   31.059197
   C    6.069540    6.911136   32.957517
   C    5.979025    7.035584   31.586267
   H    6.678915    6.539084   30.929260
   F    7.055534    6.149250   33.477532
   C    6.583223    8.073538   35.853990
   N    6.761310    7.691696   37.326331
   O    8.078408    9.381641   33.965184
   H    7.490145    7.726135   35.361439
   H    7.614767    8.102524   37.712143
   H    6.828689    6.675295   37.425510
   C    6.507131    9.589957   35.728672
   C    7.125094   10.018088   34.384829
   N    6.639653   11.118856   33.767324
   C    7.282801   11.599246   32.539926
   H    7.127003   10.076431   36.489591
   H    5.763491   12.889939   34.468088
   H    6.743097   11.956428   30.479901
   H    8.214693   11.060749   32.402233
   H    7.501144   12.662034   32.669261


92
tweezer complex
   N    5.323376    8.894292   15.683438
   H    6.008335    5.939395   14.844914
   H    6.728273    6.998069   12.237493
   H    6.392142    9.727046   13.165319
   C    6.262998    8.852781   16.387144
   H    6.051308    5.626441   20.711084
   H    5.997106    6.772760   23.401417
   H    5.617173    9.514511   22.461966
   H    6.237570    8.810903   19.088449
   H    6.792653   12.530158   13.779448
   H    6.146629   12.155297   16.583965
   H    5.919504   12.377819   21.940614
   H    5.887650   12.104602   19.050723
   C    9.377810    6.257590   14.164567
   C    9.926215    5.682276   15.310076
   H   11.016157    5.625785   15.456396
   C    9.043718    5.168591   16.287568
   H    9.453991    4.700972   17.193732
   C    7.653156    5.254527   16.118705
   H    6.982243    4.857714   16.895181
   C    7.098333    5.850326   14.964286
   C    7.971701    6.334060   13.992072
```

C	7.734770	7.093126	12.681579
C	10.002059	6.977921	12.959177
H	11.070414	6.772643	12.766310
C	8.962299	6.579807	11.862203
H	9.107111	7.132495	10.912229
H	8.930308	5.487680	11.674779
C	9.615596	8.451991	13.149839
C	10.361156	9.570561	13.551983
H	11.450394	9.514603	13.705777
C	9.647310	10.759931	13.767308
C	8.238262	10.815569	13.615030
C	7.489468	9.695039	13.230985
C	8.207833	8.518363	12.984638
C	9.822090	8.807060	17.515059
H	10.830319	8.810852	17.079487
C	8.704796	8.801295	16.680516
H	8.825175	8.794557	15.590961
C	7.409615	8.815193	17.246689
N	11.744423	8.894566	20.484590
C	7.689681	6.257865	22.003064
C	7.141251	5.682810	20.857440
C	8.023735	5.169353	19.879815
H	7.613453	4.702048	18.973497
C	9.414299	5.255172	20.048710
H	10.085188	4.858583	19.272100
C	9.969149	5.850705	21.203255
H	11.059154	5.939670	21.322668
C	9.095797	6.334290	22.175558
C	9.332758	7.093158	23.486168
H	10.339256	6.998017	23.930233
C	7.065467	6.978023	23.208564
C	7.451967	8.452089	23.018039
C	6.706388	9.570635	22.615891
C	7.420209	10.760032	22.400636
C	8.829257	10.815687	22.552950
C	9.578069	9.695153	22.936969
H	10.675398	9.727174	23.002606
C	8.859721	8.518453	23.183282
C	7.245799	8.807116	18.652873
C	8.363097	8.801538	19.487410
H	8.242844	8.795009	20.576979
C	9.658272	8.815336	18.921232
C	10.804862	8.853097	19.780803
C	8.105225	6.579754	24.305478
H	7.960428	7.132316	25.255527
H	8.137203	5.487602	24.492756
C	7.801513	12.203787	14.087750
C	10.077315	12.123644	14.325068
H	11.148005	12.377749	14.227276
C	9.032288	13.039536	13.608919
H	9.029798	14.077357	13.998843
H	9.146406	13.040106	12.506286
C	9.500504	12.159341	15.745115
C	10.085405	12.124874	16.993644
H	11.179915	12.104696	17.117201
C	7.813286	12.136269	18.007769
C	7.242342	12.157645	16.694460
C	8.075197	12.193467	15.595946
C	9.265995	12.203911	22.080216
H	10.274844	12.530296	22.388538
C	6.990201	12.123729	21.842854
C	8.035195	13.039648	22.559005
H	8.037675	14.077461	22.169059
H	7.921053	13.040238	23.661635
C	7.567042	12.159396	20.422822
C	6.982154	12.124844	19.174292
C	9.254279	12.136280	18.160177
C	9.825212	12.157730	19.473495
H	10.920926	12.155458	19.583996
C	8.992346	12.193556	20.572007

Appendix F Benchmark data from Chapter 3

In the following tables, the data a grouped by element and indexed according to the order in the structures given in Appendix E.

F.1 RI-MP2 NMR shieldings and DLPNO-MP2 errors

Table F.18: Isotropic NMR shieldings (in ppm) for the anthracene dimer calculated with RI-MP2/RIJONX and deviations due to COSX and DLPNO-MP2 using the LoosePNO, NormalPNO, and TightPNO settings, with or without COSX.

El.	Ind.	RI-MP2 RIJONX	RI-MP2 RIJCOSX	LoosePNO RIJONX	LoosePNO RIJCOSX	NormalPNO RIJONX	NormalPNO RIJCOSX	TightPNO RIJCOSX
^{1}H	7	23.513	-0.006	-0.006	-0.021	0.011	0.010	0.010
	8	23.474	0.001	0.047	0.060	0.014	0.021	0.004
	9	23.474	-0.004	0.049	0.028	0.016	0.008	-0.010
	10	23.508	-0.001	-0.002	-0.012	0.010	-0.003	0.011
	18	23.510	-0.004	0.000	0.012	0.012	0.021	0.010
	19	23.470	0.003	0.056	0.081	0.016	0.029	0.008
	20	23.472	-0.006	0.056	0.040	0.016	0.011	-0.010
	21	23.508	0.002	0.002	0.000	0.013	0.001	0.023
	23	24.437	-0.009	-0.007	-0.045	-0.011	-0.053	-0.022
	24	24.438	-0.005	-0.016	-0.072	-0.010	-0.048	-0.019
	32	23.504	0.001	-0.003	-0.010	0.010	-0.019	0.017
	33	23.471	-0.005	0.048	0.030	0.023	0.026	-0.009
	34	23.471	0.003	0.048	0.081	0.018	0.032	0.007
	35	23.510	-0.001	-0.006	0.011	0.008	0.022	0.016
	43	23.508	-0.003	0.004	-0.016	0.009	-0.026	0.018
	44	23.474	-0.008	0.055	0.026	0.019	0.022	-0.011
	45	23.472	0.006	0.054	0.091	0.021	0.034	0.014
	46	23.509	-0.001	-0.002	0.023	0.007	0.030	0.015
	47	24.432	-0.002	-0.017	0.000	-0.016	-0.033	-0.026
	48	24.436	0.002	-0.007	-0.013	-0.013	-0.024	-0.012
^{13}C	1	57.591	-0.026	0.345	0.288	0.113	0.055	-0.047
	2	62.189	-0.014	0.317	0.283	0.103	0.085	0.023
	3	67.346	0.008	0.442	0.440	0.204	0.167	0.034
	4	67.292	0.041	0.446	0.506	0.198	0.272	0.101
	5	62.300	-0.052	0.308	0.240	0.092	0.029	-0.045
	6	57.624	-0.051	0.355	0.324	0.101	0.082	-0.026
	11	67.319	-0.040	0.384	0.251	0.122	-0.009	-0.077
	12	57.591	-0.028	0.479	0.466	0.147	0.151	0.008
	13	62.189	0.007	0.326	0.294	0.094	0.062	0.026
	14	67.345	0.002	0.500	0.538	0.223	0.230	0.073
	15	67.292	0.039	0.497	0.537	0.221	0.242	0.061
	16	62.301	-0.030	0.340	0.344	0.104	0.111	-0.008
	17	57.621	-0.034	0.470	0.402	0.165	0.101	-0.041
	22	67.320	-0.049	0.381	0.329	0.130	0.104	0.042
	25	67.314	-0.089	0.373	0.188	0.118	-0.082	-0.140
	26	57.623	-0.058	0.353	0.295	0.107	0.081	-0.035
	27	62.298	-0.054	0.317	0.245	0.092	-0.025	-0.070
	28	67.293	0.060	0.444	0.534	0.202	0.274	0.112
	29	67.344	-0.014	0.448	0.467	0.204	0.160	0.016
	30	62.186	0.005	0.306	0.331	0.098	0.102	0.048
	31	57.587	-0.019	0.354	0.272	0.093	0.043	-0.053
	36	67.314	-0.083	0.392	0.302	0.128	0.068	-0.004
	37	57.621	-0.043	0.477	0.378	0.136	0.064	-0.078
	38	62.298	-0.019	0.325	0.305	0.092	0.055	0.004
	39	67.294	0.042	0.497	0.516	0.219	0.215	0.053
	40	67.344	-0.008	0.496	0.549	0.232	0.246	0.077
	41	62.186	0.000	0.337	0.307	0.098	0.066	0.006
	42	57.590	-0.028	0.477	0.432	0.161	0.158	0.018

Table F.19: Isotropic NMR shieldings (in ppm) for the ATP^{4-} anion calculated with RI-MP2/RIJONX and deviations due to COSX and DLPNO-MP2 using the LoosePNO, NormalPNO, and TightPNO settings, with or without COSX.

El.	Ind.	RI-MP2 RIJONX	RI-MP2 RIJCOSX	LoosePNO RIJONX	LoosePNO RIJCOSX	NormalPNO RIJONX	NormalPNO RIJCOSX	TightPNO RIJCOSX
^{1}H	6	23.457	-0.010	0.033	0.033	0.038	0.032	0.008
	9	27.740	-0.004	0.033	0.036	0.018	0.014	0.006
	11	27.843	-0.005	0.018	0.015	0.009	0.000	0.006
	12	25.194	-0.004	0.008	0.008	0.010	-0.004	0.003
	14	25.934	0.001	0.038	0.039	0.028	0.030	0.013
	16	28.322	0.002	0.019	0.021	0.022	0.022	0.008
	22	22.261	-0.011	0.007	-0.004	0.004	-0.010	-0.005
	26	23.194	0.000	0.000	-0.002	0.001	-0.002	-0.001
	29	27.971	0.004	0.011	0.016	0.004	0.010	0.006
	30	26.499	0.000	0.010	0.011	0.005	0.005	0.002
	31	18.947	-0.001	0.005	0.009	0.009	0.008	0.006
	32	16.596	-0.019	-0.003	-0.025	0.017	0.001	-0.023
^{13}C	1	105.419	0.007	0.555	0.568	0.244	0.258	0.106
	2	101.577	0.003	0.484	0.490	0.190	0.187	0.079
	3	89.349	0.025	0.529	0.551	0.208	0.237	0.102
	4	107.791	0.002	0.474	0.476	0.195	0.192	0.078
	7	118.635	0.001	0.397	0.399	0.157	0.154	0.065
	17	41.294	0.027	-0.099	-0.061	-0.115	-0.073	-0.050
	18	44.344	0.044	-0.256	-0.223	-0.142	-0.120	-0.039
	20	60.801	0.019	0.599	0.626	0.205	0.246	0.090
	24	48.234	0.020	-0.029	0.007	-0.049	-0.033	-0.009
	27	37.560	0.005	-0.061	-0.047	-0.114	-0.102	-0.051
^{15}N	13	38.796	0.003	1.841	1.854	0.671	0.673	0.187
	21	35.050	-0.084	0.778	0.683	0.213	0.129	-0.063
	23	-6.911	-0.007	1.973	1.943	0.656	0.618	0.178
	25	15.556	0.005	1.405	1.401	0.430	0.432	0.081
	28	207.756	0.045	0.597	0.649	0.213	0.266	0.115
^{17}O	5	262.737	0.018	2.550	2.538	1.041	1.025	0.384
	8	309.005	-0.126	1.588	1.472	0.689	0.545	0.156
	10	284.746	0.053	1.736	1.791	0.778	0.852	0.393
	15	246.285	0.019	1.721	1.725	0.801	0.813	0.328
	33	215.724	0.054	0.726	0.795	0.100	0.159	0.090
	34	161.339	-0.055	1.611	1.560	0.669	0.622	0.161
	36	219.767	-0.049	0.891	0.853	0.440	0.409	0.141
	37	189.743	-0.018	1.555	1.511	0.614	0.582	0.248
	38	159.565	-0.052	1.628	1.583	0.598	0.557	0.119
	39	173.954	-0.018	1.893	1.872	0.794	0.781	0.257
	41	198.226	-0.046	0.905	0.861	0.309	0.266	0.068
	42	198.466	-0.023	0.974	0.967	0.399	0.388	0.113
	43	199.661	-0.048	0.765	0.725	0.284	0.244	0.067
^{31}P	19	327.365	0.033	0.601	0.641	0.326	0.371	0.163
	35	332.481	0.020	0.598	0.625	0.217	0.251	0.144
	40	283.618	0.026	0.467	0.495	0.204	0.232	0.132

Table F.20: Isotropic NMR shieldings (in ppm) for the caffeine molecule calculated with RI-MP2/RIJONX and deviations due to COSX and DLPNO-MP2 using the LoosePNO, NormalPNO, and TightPNO settings, with or without COSX.

El.	Ind.	RI-MP2 RIJONX	RI-MP2 RIJCOSX	LoosePNO RIJONX	LoosePNO RIJCOSX	NormalPNO RIJONX	NormalPNO RIJCOSX	TightPNO RIJCOSX
^{1}H	15	24.380	0.001	0.006	0.002	-0.002	-0.003	0.000
	16	27.905	0.001	0.010	0.014	0.001	0.005	0.001
	17	27.029	0.002	0.038	0.037	0.006	0.005	0.003
	18	27.710	0.003	0.021	0.020	0.006	0.007	0.005
	19	28.497	0.001	0.002	0.003	0.002	0.003	0.003
	20	27.211	0.000	0.002	0.000	0.000	-0.002	0.000
	21	28.131	0.000	0.006	0.006	0.001	0.000	0.002
	22	27.031	0.000	-0.018	-0.009	0.003	0.003	-0.002
	23	28.427	0.000	0.001	0.005	0.003	0.002	0.001

Continued on next page

Continued from previous page

El.	Ind.	RI-MP2 RIJONX	RI-MP2 RIJCOSX	LoosePNO RIJONX	LoosePNO RIJCOSX	NormalPNO RIJONX	NormalPNO RIJCOSX	TightPNO RIJCOSX
	24	28.906	0.000	-0.002	-0.004	0.004	0.004	0.002
^{13}C	1	79.290	0.009	0.463	0.461	0.118	0.129	0.033
	2	42.996	0.031	0.214	0.248	0.020	0.050	-0.004
	4	39.940	0.016	-0.066	-0.058	-0.054	-0.033	-0.047
	7	35.484	0.028	0.098	0.119	0.005	0.036	0.007
	11	58.463	0.009	-0.147	-0.123	-0.130	-0.127	-0.063
	12	158.823	0.004	0.279	0.281	0.100	0.102	0.030
	13	163.889	0.003	0.285	0.282	0.097	0.095	0.034
	14	166.511	0.000	0.301	0.276	0.115	0.113	0.038
^{15}N	3	144.119	0.001	1.613	1.629	0.574	0.574	0.174
	6	103.247	-0.012	1.470	1.471	0.469	0.451	0.143
	9	95.032	0.011	1.169	1.159	0.382	0.378	0.132
	10	18.531	-0.042	1.048	1.029	0.293	0.251	0.008
^{17}O	5	37.086	0.012	0.867	0.798	0.305	0.305	-0.005
	8	-3.137	-0.067	1.558	1.472	0.379	0.323	0.000

Table F.21: Isotropic NMR shieldings (in ppm) for the coronene molecule calculated with RI-MP2/RIJONX and deviations due to COSX and DLPNO-MP2 using the LoosePNO, NormalPNO, and TightPNO settings, with or without COSX.

El.	Ind.	RI-MP2 RIJONX	RI-MP2 RIJCOSX	LoosePNO RIJONX	LoosePNO RIJCOSX	NormalPNO RIJONX	NormalPNO RIJCOSX	TightPNO RIJCOSX
^{1}H	25	21.554	0.003	0.038	0.064	0.011	0.019	-0.012
	26	21.554	0.005	0.050	0.051	0.015	0.028	-0.014
	27	21.553	0.000	0.040	0.044	0.012	0.011	0.026
	28	21.554	0.002	0.046	0.041	0.013	0.030	0.023
	29	21.554	0.009	0.053	0.080	0.019	0.017	0.037
	30	21.555	0.000	0.051	0.066	0.013	0.024	0.012
	31	21.555	-0.002	0.051	0.065	0.013	0.024	0.011
	32	21.554	0.008	0.053	0.079	0.019	0.015	0.036
	33	21.554	0.001	0.046	0.040	0.013	0.029	0.021
	34	21.553	0.003	0.040	0.045	0.012	0.013	0.028
	35	21.554	0.006	0.050	0.053	0.015	0.030	-0.013
	36	21.554	0.001	0.038	0.062	0.011	0.019	-0.014
^{13}C	1	64.829	0.017	0.194	0.235	0.098	0.086	-0.016
	2	64.835	-0.042	0.190	0.100	0.101	0.085	-0.078
	3	64.832	0.021	0.179	0.188	0.098	0.115	0.034
	4	64.831	0.027	0.180	0.193	0.099	0.124	0.039
	5	64.835	-0.031	0.190	0.114	0.101	0.102	-0.067
	6	64.829	0.012	0.194	0.228	0.098	0.083	-0.022
	7	58.397	0.022	0.385	0.453	0.169	0.184	0.070
	8	58.409	-0.011	0.383	0.353	0.162	0.092	-0.055
	9	58.406	0.009	0.391	0.329	0.169	0.166	-0.012
	10	58.406	0.026	0.391	0.348	0.169	0.185	0.005
	11	58.409	-0.020	0.383	0.346	0.162	0.087	-0.061
	12	58.397	0.031	0.385	0.463	0.169	0.191	0.078
	13	63.311	-0.062	0.413	0.347	0.181	0.069	-0.044
	14	63.313	0.087	0.401	0.460	0.175	0.219	0.107
	15	63.326	0.119	0.408	0.529	0.179	0.281	0.169
	16	63.313	0.024	0.400	0.442	0.179	0.215	0.067
	17	63.329	-0.004	0.421	0.427	0.171	0.168	0.065
	18	63.329	0.032	0.425	0.428	0.172	0.195	0.068
	19	63.329	0.039	0.425	0.435	0.173	0.204	0.074
	20	63.329	-0.005	0.421	0.427	0.171	0.174	0.063
	21	63.313	0.065	0.400	0.477	0.179	0.254	0.107
	22	63.327	0.084	0.407	0.499	0.178	0.245	0.135
	23	63.313	0.060	0.401	0.430	0.175	0.201	0.080
	24	63.311	-0.036	0.413	0.377	0.181	0.095	-0.018

Table F.22: Isotropic NMR shieldings (in ppm) for the ebselen molecule calculated with RI-MP2/RIJONX and deviations due to COSX and DLPNO-MP2 using the LoosePNO, NormalPNO, and TightPNO settings, with or without COSX.

El.	Ind.	RI-MP2 RIJONX	RI-MP2 RIJCOSX	LoosePNO RIJONX	LoosePNO RIJCOSX	NormalPNO RIJONX	NormalPNO RIJCOSX	TightPNO RIJCOSX
^{1}H	17	23.561	0.001	0.012	0.011	0.008	0.012	0.004
	18	23.683	0.001	0.002	0.004	0.010	0.010	0.003
	19	23.630	0.001	0.019	0.017	0.005	0.005	0.004
	20	22.956	0.000	-0.014	-0.014	0.008	0.002	0.002
	21	23.760	0.007	0.021	0.027	0.005	0.009	0.002
	22	23.983	0.005	0.013	0.014	0.000	-0.003	-0.003
	23	23.825	0.005	0.016	0.015	-0.009	0.000	0.003
	24	23.940	0.000	-0.005	-0.009	-0.010	-0.001	0.006
	25	22.646	0.000	0.020	0.014	0.005	-0.001	0.000
^{13}C	3	59.074	0.026	0.229	0.252	0.015	0.040	0.003
	4	50.287	0.015	0.504	0.517	0.123	0.145	0.034
	5	28.897	0.011	-0.149	-0.122	-0.111	-0.098	-0.048
	6	67.139	0.022	0.358	0.383	0.093	0.124	0.029
	7	63.404	0.000	0.144	0.141	0.045	0.040	0.001
	8	63.808	0.013	0.352	0.357	0.102	0.111	0.021
	9	64.699	0.010	0.236	0.253	0.058	0.066	0.030
	11	64.249	0.019	0.264	0.270	0.032	0.039	0.018
	12	66.635	-0.033	0.365	0.330	0.101	0.069	-0.016
	13	64.510	0.014	0.267	0.286	0.057	0.070	0.016
	14	68.853	0.017	0.341	0.336	0.083	0.125	0.028
	15	49.589	0.011	0.362	0.369	0.112	0.132	0.032
	16	65.060	0.000	0.281	0.284	0.109	0.119	0.014
^{15}N	1	138.602	0.004	2.472	2.474	0.998	1.030	0.378
^{17}O	10	3.671	-0.077	1.339	1.134	0.410	0.252	0.021
^{77}Se	2	960.699	-0.040	9.478	9.355	3.074	2.693	-0.094

Table F.23: Isotropic NMR shieldings (in ppm) for the penicillin molecule calculated with RI-MP2/RIJONX and deviations due to COSX and DLPNO-MP2 using the LoosePNO, NormalPNO, and TightPNO settings, with or without COSX.

El.	Ind.	RI-MP2 RIJONX	RI-MP2 RIJCOSX	LoosePNO RIJONX	LoosePNO RIJCOSX	NormalPNO RIJONX	NormalPNO RIJCOSX	TightPNO RIJCOSX
^{1}H	9	26.163	-0.003	-0.046	-0.049	-0.007	-0.010	-0.007
	20	25.599	0.005	-0.001	0.001	-0.002	0.003	0.005
	26	27.470	-0.001	0.004	0.000	0.018	0.016	0.001
	27	26.339	0.002	0.014	0.014	0.012	0.019	0.000
	28	29.646	-0.001	-0.005	-0.008	-0.010	-0.013	0.002
	29	30.240	-0.001	0.013	0.013	0.013	0.012	0.002
	30	30.378	-0.001	-0.002	-0.003	0.003	0.004	0.002
	31	29.918	0.001	-0.012	-0.017	0.014	0.015	0.003
	32	30.237	0.000	0.007	0.005	-0.002	-0.004	0.003
	33	30.434	0.002	0.013	0.010	0.005	0.006	0.004
	34	25.730	0.001	-0.003	-0.008	0.003	0.005	-0.003
	35	28.061	0.001	-0.017	-0.023	0.008	0.004	0.003
	36	27.885	-0.002	-0.023	-0.023	0.013	0.004	0.002
	37	23.890	0.002	-0.019	-0.012	0.001	0.006	0.006
	38	23.919	0.000	-0.003	-0.007	-0.005	-0.004	-0.003
	39	23.747	0.001	0.055	0.052	0.003	0.002	0.003
	40	23.759	0.001	-0.014	-0.019	-0.001	0.000	0.000
	41	23.838	0.000	0.045	0.049	0.006	0.007	-0.001
^{13}C	1	61.737	-0.010	0.171	0.173	0.053	0.048	-0.028
	2	62.156	0.014	0.115	0.134	0.019	0.039	-0.023
	3	62.013	0.043	0.286	0.329	0.057	0.105	0.052
	4	63.031	0.000	0.249	0.252	0.075	0.074	0.004
	5	64.463	-0.005	0.313	0.322	0.064	0.070	-0.003
	6	147.085	-0.014	0.330	0.326	0.124	0.111	0.025
	7	165.032	-0.005	0.294	0.287	0.134	0.129	0.040
	8	165.168	0.004	0.256	0.257	0.110	0.117	0.039
	10	53.703	-0.008	0.227	0.226	0.088	0.080	0.008

Continued on next page

Continued from previous page

El.	Ind.	RI-MP2 RIJONX	RI-MP2 RIJCOSX	LoosePNO RIJONX	LoosePNO RIJCOSX	NormalPNO RIJONX	NormalPNO RIJCOSX	TightPNO RIJCOSX
	15	25.590	0.022	0.059	0.062	-0.015	0.001	0.005
	16	24.368	0.009	-0.160	-0.150	-0.116	-0.099	-0.042
	17	119.831	0.014	0.515	0.518	0.206	0.214	0.054
	18	131.744	-0.008	0.384	0.377	0.122	0.116	0.033
	19	19.618	0.018	-0.072	-0.028	-0.055	-0.020	-0.021
	22	116.919	-0.010	0.660	0.644	0.246	0.232	0.063
	23	123.580	-0.007	0.852	0.839	0.333	0.321	0.089
^{15}N	21	148.137	0.000	1.299	1.307	0.524	0.533	0.179
	25	91.492	0.018	1.497	1.510	0.470	0.484	0.128
^{17}O	11	-49.917	0.035	1.304	1.287	0.450	0.429	0.036
	12	-53.145	-0.005	1.550	1.512	0.316	0.236	-0.059
	13	-42.477	0.023	1.139	1.218	0.299	0.312	0.056
	14	154.944	-0.016	1.003	1.034	0.230	0.239	0.046
^{33}S	24	397.143	0.087	3.293	3.377	1.355	1.442	0.396

Table F.24: Isotropic NMR shieldings (in ppm) for the sitagliptin cation calculated with RI-MP2/RIJONX and deviations due to COSX and DLPNO-MP2 using the LoosePNO, NormalPNO, and TightPNO settings, with or without COSX.

El.	Ind.	RI-MP2 RIJONX	RI-MP2 RIJCOSX	LoosePNO RIJONX	LoosePNO RIJCOSX	NormalPNO RIJONX	NormalPNO RIJCOSX	TightPNO RIJCOSX
^{1}H	5	24.706	0.008	-0.047	-0.074	-0.015	-0.064	-0.009
	9	29.167	0.011	-0.033	0.024	-0.017	-0.014	0.006
	10	28.051	0.010	-0.024	-0.036	0.004	0.006	0.011
	11	26.990	0.020	-0.011	0.031	-0.005	0.019	0.027
	23	28.357	0.021	-0.023	0.045	-0.023	0.003	0.024
	24	26.626	0.052	-0.032	0.037	-0.027	0.039	0.050
	25	28.524	0.005	-0.001	0.016	0.011	0.005	0.003
	28	24.132	0.001	0.022	0.093	0.014	0.019	0.018
	33	26.037	-0.004	-0.042	-0.038	-0.028	0.006	0.011
	34	26.741	-0.003	-0.019	-0.042	-0.005	-0.012	0.000
	35	26.638	-0.004	-0.016	-0.018	-0.011	-0.021	-0.013
	40	29.463	0.043	-0.007	0.030	-0.001	0.034	0.023
	41	26.980	0.024	-0.006	0.013	-0.009	0.020	0.014
	42	27.421	0.001	0.027	0.120	0.018	0.066	0.008
	43	26.781	-0.021	-0.005	-0.052	-0.001	-0.036	-0.039
	44	28.573	0.036	-0.009	-0.007	-0.007	0.038	0.038
^{13}C	1	81.234	-0.109	0.469	0.406	0.183	0.086	-0.104
	2	34.188	0.097	0.172	0.321	0.015	0.062	0.069
	3	38.789	0.040	0.368	0.437	0.099	0.095	0.052
	4	75.593	0.020	0.137	0.198	-0.012	-0.008	-0.056
	8	155.175	-0.121	0.365	0.229	0.178	0.008	-0.073
	12	147.474	-0.032	0.388	0.399	0.121	0.052	-0.004
	13	50.795	0.038	-0.192	-0.085	-0.116	-0.071	-0.047
	15	148.616	0.071	0.415	0.510	0.195	0.254	0.105
	17	47.149	0.073	0.122	0.206	-0.030	0.023	0.028
	19	64.867	0.003	0.329	0.341	0.152	0.158	0.063
	26	30.790	0.027	0.233	0.224	0.093	0.085	0.012
	27	83.066	0.047	0.445	0.517	0.141	0.136	0.087
	30	133.212	0.093	0.331	0.445	0.146	0.260	0.139
	36	157.909	-0.195	0.300	0.207	0.102	0.004	-0.148
	37	34.091	0.127	-0.101	0.097	-0.084	0.018	0.069
	39	151.780	0.119	0.420	0.586	0.168	0.320	0.191
^{15}N	14	90.036	-0.138	1.481	1.414	0.511	0.358	0.033
	16	-62.997	0.264	1.016	1.657	0.247	0.601	0.298
	18	-72.654	-0.156	1.496	1.355	0.396	0.238	-0.096
	31	211.277	-0.088	0.351	0.204	0.131	0.078	-0.078
	38	146.346	0.121	1.445	1.602	0.560	0.667	0.304
^{17}O	32	-21.919	0.197	1.724	2.262	0.512	1.068	0.541
^{19}F	6	329.991	-0.684	1.716	1.648	0.652	0.284	-0.310

Continued on next page

Continued from previous page

El.	Ind.	RI-MP2 RIJONX	RI-MP2 RIJCOSX	LoosePNO RIJONX	LoosePNO RIJCOSX	NormalPNO RIJONX	NormalPNO RIJCOSX	TightPNO RIJCOSX
	7	342.186	0.051	2.175	2.165	0.837	0.736	0.478
	20	261.626	-0.220	1.316	1.285	0.598	0.620	-0.104
	21	261.293	0.006	1.704	1.816	0.574	0.807	0.374
	22	279.560	0.108	1.176	1.508	0.654	0.847	0.260
	29	326.760	0.006	1.501	0.280	0.502	0.130	0.054

Table F.25: Isotropic NMR shieldings (in ppm) for the tweezer complex calculated with RI-MP2/RIJONX and deviations due to COSX and DLPNO-MP2 using the LoosePNO, NormalPNO, and TightPNO settings, with or without COSX.

El.	Ind.	RI-MP2 RIJONX	RI-MP2 RIJCOSX	LoosePNO RIJONX	LoosePNO RIJCOSX	NormalPNO RIJONX	NormalPNO RIJCOSX	TightPNO RIJCOSX
^{1}H	2	23.563	-0.009	0.050	0.081	0.005	0.043	0.051
	3	26.633	-0.038	0.036	0.085	-0.008	0.005	0.005
	4	23.083	-0.048	0.051	-0.057	0.006	-0.029	0.019
	6	24.007	-0.027	0.062	0.117	0.035	0.033	-0.038
	7	26.744	-0.034	0.017	-0.060	-0.019	-0.140	-0.041
	8	23.534	-0.025	-0.011	0.035	-0.006	0.000	-0.024
	9	25.602	-0.064	-0.021	0.202	0.019	0.081	0.017
	10	26.739	-0.006	0.030	-0.069	-0.006	-0.087	-0.031
	11	23.830	-0.016	-0.010	0.060	-0.007	-0.064	0.024
	12	26.810	-0.003	0.016	-0.045	-0.017	-0.088	-0.053
	13	23.943	-0.011	0.010	-0.031	0.013	-0.042	-0.024
	16	23.987	0.030	0.054	0.068	0.021	0.031	0.043
	18	24.581	0.014	-0.019	0.040	-0.008	0.105	0.114
	20	24.526	-0.017	0.018	0.037	0.014	-0.006	0.015
	25	26.745	0.002	0.018	0.065	-0.006	0.019	0.031
	27	28.292	-0.007	0.050	-0.059	0.032	-0.046	0.007
	28	28.385	-0.022	0.043	0.036	0.026	0.028	0.019
	31	23.526	0.005	-0.004	-0.052	-0.019	-0.029	-0.017
	37	25.583	0.058	0.003	-0.310	-0.006	-0.197	-0.062
	39	29.413	-0.025	-0.045	-0.091	-0.043	-0.097	-0.060
	45	24.597	-0.010	-0.017	-0.069	0.019	0.011	0.025
	47	24.526	0.008	0.025	-0.012	0.016	0.043	0.028
	49	23.538	-0.006	0.045	0.101	0.014	0.048	0.040
	52	26.571	0.039	0.015	-0.014	-0.012	0.005	0.056
	59	23.039	0.037	0.021	0.197	-0.004	0.175	0.031
	63	29.439	-0.001	-0.042	-0.009	-0.045	-0.061	-0.087
	67	28.227	-0.015	0.029	0.176	0.005	0.103	-0.005
	68	28.347	0.001	0.039	0.077	-0.004	0.064	0.021
	71	26.803	0.015	0.012	0.116	0.003	0.068	0.024
	73	28.538	-0.010	0.036	0.038	0.004	-0.027	-0.025
	74	28.356	-0.002	0.070	-0.050	0.008	-0.100	-0.028
	77	23.921	0.063	-0.003	-0.030	0.001	0.107	0.137
	82	26.688	0.035	0.015	0.103	-0.023	0.091	0.010
	85	28.530	0.027	0.042	0.044	-0.021	-0.018	-0.014
	86	28.294	0.030	0.042	0.188	0.011	0.146	0.026
	91	23.801	0.022	-0.012	-0.062	-0.023	-0.026	-0.040
^{13}C	5	64.124	-0.012	-0.062	-0.671	0.014	-0.354	-0.117
	14	36.176	0.045	0.328	0.413	0.083	0.150	0.089
	15	68.217	-0.071	0.368	0.470	0.112	0.184	0.048
	17	64.900	-0.138	0.242	0.167	0.097	0.098	0.050
	19	64.271	-0.114	0.262	0.146	0.082	0.040	-0.030
	21	65.133	-0.018	0.374	0.399	0.084	0.091	0.015
	22	35.801	0.020	0.370	0.481	0.065	0.052	0.037
	23	134.514	0.070	0.858	0.938	0.311	0.422	0.211
	24	134.154	0.006	0.825	0.847	0.330	0.229	0.158
	26	120.594	-0.055	0.571	0.386	0.181	0.084	-0.012
	29	38.203	-0.126	0.549	0.287	0.201	-0.078	-0.158
	30	73.221	0.125	0.270	0.461	-0.016	0.182	0.169
	32	39.663	0.028	0.368	0.575	0.096	0.292	-0.017
	33	39.602	-0.040	0.228	0.327	-0.045	0.046	-0.086
	34	68.107	-0.023	0.339	0.248	0.051	-0.056	-0.035
	35	37.813	-0.076	0.449	0.476	0.088	0.037	-0.106

Continued on next page

Continued from previous page

El.	Ind.	RI-MP2 RIJONX	RI-MP2 RIJCOSX	LoosePNO RIJONX	LoosePNO RIJCOSX	NormalPNO RIJONX	NormalPNO RIJCOSX	TightPNO RIJCOSX
	36	60.976	-0.030	0.155	-0.244	-0.069	-0.129	-0.006
	38	60.968	0.018	0.358	0.195	0.175	0.142	0.063
	40	75.953	-0.102	-0.129	-0.010	-0.183	-0.031	-0.075
	42	36.166	-0.030	0.370	0.331	0.099	0.060	-0.055
	43	68.217	0.034	0.403	0.383	0.128	0.068	-0.070
	44	64.872	0.200	0.208	0.353	0.091	0.253	0.202
	46	64.257	0.106	0.259	0.377	0.093	0.154	0.119
	48	65.128	-0.011	0.394	0.465	0.079	0.111	0.037
	50	35.813	-0.024	0.400	0.331	0.093	0.139	0.041
	51	134.499	-0.095	0.835	0.840	0.303	0.224	0.042
	53	134.140	-0.112	0.844	0.802	0.308	0.247	-0.071
	54	38.169	0.050	0.581	0.411	0.206	0.032	0.041
	55	73.216	-0.053	0.291	0.231	0.047	-0.013	-0.130
	56	39.636	-0.126	0.382	0.072	0.085	-0.240	-0.256
	57	39.588	-0.002	0.224	0.226	-0.060	-0.191	-0.043
	58	68.073	0.043	0.296	0.466	0.050	0.344	0.275
	60	37.801	0.088	0.459	0.448	0.063	0.122	0.192
	61	61.002	-0.067	0.149	0.383	0.087	-0.030	-0.135
	62	60.995	0.013	0.008	0.170	-0.158	0.069	0.013
	64	75.959	0.175	0.167	0.177	0.100	0.159	0.117
	65	64.098	0.028	-0.111	0.494	-0.055	0.305	0.266
	66	120.592	0.134	0.554	0.672	0.149	0.261	0.155
	69	135.058	-0.020	0.871	0.913	0.326	0.303	0.136
	70	134.756	-0.154	0.848	0.570	0.336	0.043	-0.044
	72	122.054	0.160	0.547	0.761	0.207	0.408	0.232
	75	40.466	0.080	0.474	0.774	0.155	0.314	0.088
	76	69.527	0.073	0.444	0.635	0.149	0.314	0.125
	78	58.051	0.081	0.266	0.168	0.018	0.019	0.078
	79	67.988	0.080	0.475	0.627	0.124	0.322	0.178
	80	40.272	0.091	0.510	0.574	0.194	0.203	0.005
	81	135.043	-0.294	0.862	0.468	0.315	-0.101	-0.290
	83	134.747	-0.090	0.857	0.848	0.322	0.274	-0.048
	84	122.048	0.190	0.520	0.655	0.170	0.231	0.141
	87	40.456	0.085	0.491	0.660	0.176	0.388	0.079
	88	69.551	-0.058	0.461	0.410	0.161	0.124	-0.019
	89	58.068	0.045	0.268	0.372	0.022	0.132	0.174
	90	67.979	0.143	0.475	0.513	0.098	0.202	0.089
	92	40.291	0.085	0.550	0.604	0.200	0.273	0.203
^{15}N	1	14.811	-0.279	0.691	0.350	0.290	0.224	-0.411
	41	14.792	-0.225	0.758	0.772	0.438	0.058	0.066

F.2 NMR shielding errors due to PNO truncation

Results with different values of T_{CutPNO} for valence orbitals are shown in Tables F.26–F.29 and for core orbitals – in Tables F.30–F.33.

Table F.26: Errors (in ppm) in isotropic NMR shieldings vs RI-MP2 for the ATP^{4-} anion at different values of T_{CutPNO} for valence orbitals, with $T_{\mathrm{CutPNO}} = 10^{-12}$ for core orbitals, $F_{\mathrm{Cut}} = 10^{-8}$, $T_{\mathrm{S}} = 10^{-8}$, and all other DLPNO thresholds equal to 0.

		T_{CutPNO}(valence)							
El.	Ind.	10^{-5}	10^{-6}	10^{-7}	10^{-8}	10^{-9}	10^{-10}	10^{-11}	10^{-12}
^{1}H	6	0.073	0.033	0.014	0.007	0.000	0.000	-0.001	-0.001
	9	0.095	0.053	0.017	0.006	0.002	0.000	-0.001	-0.001
	11	0.083	0.042	0.018	0.007	0.001	0.000	0.000	0.000
	12	0.103	0.050	0.020	0.006	-0.002	0.000	0.000	0.000
	14	0.067	0.026	0.015	0.005	0.002	0.000	0.000	0.000
	16	0.054	0.034	0.011	0.003	0.001	0.000	0.000	-0.001
	22	0.030	0.007	0.006	-0.001	0.003	0.000	0.001	0.000
	26	0.130	0.042	0.006	0.000	-0.007	-0.001	0.000	0.000
	29	0.043	0.014	0.006	0.002	-0.002	0.000	0.000	0.000
	30	0.022	0.010	0.005	0.000	-0.001	0.000	0.000	0.000
	31	-0.069	-0.022	-0.006	-0.003	-0.001	-0.001	-0.001	0.000

Continued on next page

Continued from previous page

El.	Ind.	10^{-5}	10^{-6}	10^{-7}	10^{-8}	10^{-9}	10^{-10}	10^{-11}	10^{-12}
	32	-0.073	-0.023	-0.010	-0.004	-0.003	-0.001	-0.001	-0.001
^{13}C	1	2.228	1.208	0.693	0.203	0.089	0.035	0.012	0.005
	2	2.106	1.111	0.505	0.145	0.062	0.016	0.010	0.002
	3	2.473	1.214	0.542	0.202	0.067	0.019	0.011	0.000
	4	2.117	1.063	0.491	0.171	0.074	0.019	0.009	0.001
	7	1.690	1.028	0.444	0.159	0.067	0.021	0.007	0.000
	17	-0.992	-0.176	0.010	-0.062	-0.991	-0.019	-0.028	-0.012
	18	-0.922	0.022	-0.146	-0.107	0.027	-0.023	-0.007	-0.001
	20	3.516	1.757	0.599	0.115	0.085	-0.010	0.000	0.002
	24	0.640	0.199	0.026	-0.043	-0.038	0.005	-0.010	-0.004
	27	-0.230	-0.463	-0.137	-0.084	-0.065	-0.028	-0.006	-0.001
^{15}N	13	8.861	4.108	1.740	0.697	0.033	0.043	0.017	0.001
	21	4.286	3.877	0.735	-0.023	0.135	0.018	0.011	0.007
	23	13.759	6.078	1.840	0.589	-1.509	0.042	-0.020	-0.016
	25	10.077	3.820	1.383	0.415	0.126	0.070	0.010	0.004
	28	2.117	1.220	0.572	0.216	0.060	0.004	0.002	-0.001
^{17}O	5	9.910	5.103	2.346	1.030	0.403	0.164	0.036	0.013
	8	5.568	3.137	1.448	0.665	0.284	0.133	0.051	0.018
	10	6.519	3.531	1.613	0.683	0.248	0.094	0.029	0.009
	15	6.782	3.760	1.560	0.599	0.263	0.106	0.044	0.021
	33	5.762	3.179	1.066	0.399	0.133	0.044	0.013	0.004
	34	6.511	3.310	1.266	0.575	0.188	0.069	0.015	0.006
	36	5.761	3.141	1.181	0.428	0.168	0.060	0.020	0.002
	37	7.505	3.965	1.558	0.704	0.279	0.102	0.026	0.010
	38	6.712	3.464	1.294	0.533	0.171	0.056	0.022	0.008
	39	7.013	3.598	1.495	0.643	0.249	0.074	0.030	0.009
	41	5.632	3.048	0.951	0.393	0.115	0.032	0.011	0.003
	42	5.642	3.080	1.050	0.388	0.113	0.012	0.012	0.001
	43	5.686	2.992	0.783	0.325	0.140	0.035	0.005	-0.001
^{31}P	19	2.788	1.231	0.670	0.335	0.126	0.047	0.013	0.004
	35	2.357	1.112	0.623	0.263	0.092	0.051	0.015	0.005
	40	1.395	1.105	0.496	0.168	0.089	0.038	0.012	0.002

Table F.27: Errors (in ppm) in isotropic NMR shieldings vs RI-MP2 for the caffeine molecule at different values of T_{CutPNO} for valence orbitals, with $T_{\mathrm{CutPNO}} = 10^{-12}$ for core orbitals, $F_{\mathrm{Cut}} = 10^{-8}$, $T_{\mathrm{S}} = 10^{-8}$, and all other DLPNO thresholds equal to 0.

		T_{CutPNO}(valence)							
El.	Ind.	10^{-5}	10^{-6}	10^{-7}	10^{-8}	10^{-9}	10^{-10}	10^{-11}	10^{-12}
^{1}H	15	0.029	0.010	-0.001	-0.003	-0.001	0.000	0.000	0.001
	16	0.046	0.019	0.007	0.001	0.000	0.000	0.000	0.000
	17	0.060	0.027	0.012	0.005	0.002	0.001	0.000	0.000
	18	0.054	0.025	0.010	0.004	0.001	0.000	0.000	0.000
	19	0.028	0.014	0.005	0.003	0.001	0.001	0.000	0.000
	20	0.047	0.021	0.009	0.003	0.001	0.000	0.000	0.000
	21	0.049	0.025	0.008	0.003	0.001	0.000	0.000	0.000
	22	0.040	0.020	0.007	0.003	0.001	0.000	0.000	0.000
	23	0.042	0.020	0.008	0.001	0.001	0.000	0.000	0.000
	24	0.020	0.010	0.005	0.002	0.001	0.000	0.000	0.000
^{13}C	1	2.620	1.293	0.504	0.121	0.034	-0.013	-0.005	-0.004
	2	1.093	0.759	0.253	-0.006	-0.019	-0.015	-0.017	-0.009
	4	-0.037	0.312	0.150	-0.020	-0.046	-0.025	-0.009	-0.004
	7	0.283	0.400	0.069	-0.037	-0.026	-0.021	-0.008	-0.004
	11	0.138	0.032	-0.079	-0.096	-0.030	-0.022	-0.004	-0.001
	12	1.158	0.590	0.273	0.109	0.033	0.006	0.002	0.003
	13	1.167	0.641	0.283	0.104	0.023	0.008	0.001	0.000
	14	1.202	0.633	0.303	0.100	0.040	0.012	0.004	0.002
^{15}N	3	6.520	3.630	1.447	0.523	0.133	0.044	0.007	0.008
	6	6.130	3.446	1.207	0.322	0.108	0.033	0.003	0.005
	9	6.229	2.613	1.147	0.340	0.095	0.009	0.007	0.006
	10	6.163	2.758	1.069	0.303	0.035	-0.018	-0.004	-0.007

Continued on next page

Continued from previous page

El.	Ind.	10^{-5}	10^{-6}	10^{-7}	10^{-8}	10^{-9}	10^{-10}	10^{-11}	10^{-12}
^{17}O	5	6.398	3.996	-1.483	0.297	-0.009	-0.010	-0.006	0.018
	8	8.903	4.933	1.159	0.351	0.100	0.006	-0.044	-0.031

Table F.28: Errors (in ppm) in isotropic NMR shieldings vs RI-MP2 for the ebselen molecule at different values of T_{CutPNO} for valence orbitals, with $T_{\mathrm{CutPNO}} = 10^{-12}$ for core orbitals, $F_{\mathrm{Cut}} = 10^{-8}$, $T_{\mathrm{S}} = 10^{-8}$, and all other DLPNO thresholds equal to 0.

		T_{CutPNO}(valence)							
El.	Ind.	10^{-5}	10^{-6}	10^{-7}	10^{-8}	10^{-9}	10^{-10}	10^{-11}	10^{-12}
^{1}H	17	0.061	0.030	0.017	0.002	0.001	-0.001	-0.001	-0.001
	18	0.030	0.014	0.012	0.001	-0.003	0.000	0.000	0.000
	19	0.055	0.033	0.005	0.003	0.001	0.000	-0.001	-0.001
	20	0.034	0.015	0.001	0.001	-0.001	0.000	-0.001	0.000
	21	0.036	0.017	0.008	0.004	0.001	-0.001	0.000	-0.001
	22	0.070	0.027	0.012	0.001	0.001	-0.001	0.000	0.000
	23	0.041	0.019	0.007	0.005	0.000	0.001	0.001	0.001
	24	0.083	0.034	0.010	0.006	0.002	0.001	0.001	0.001
	25	0.083	0.033	0.015	0.010	0.000	0.000	0.001	0.001
^{13}C	3	1.888	0.804	0.150	0.058	0.033	0.006	-0.003	0.001
	4	1.993	1.253	0.685	0.136	0.024	-0.024	-0.020	-0.011
	5	-0.573	-0.087	-0.039	-0.049	-0.048	-0.012	-0.004	0.000
	6	1.752	1.147	0.439	0.128	0.016	-0.003	-0.001	-0.005
	7	0.669	0.464	0.264	0.030	-0.012	-0.011	-0.001	-0.002
	8	1.676	1.045	0.558	0.114	-0.007	0.010	0.002	-0.003
	9	1.047	0.704	0.205	-0.012	0.015	0.012	-0.001	-0.003
	11	0.966	0.627	0.316	0.053	0.031	-0.021	-0.002	-0.003
	12	2.057	0.932	0.360	0.116	0.047	-0.026	0.000	-0.009
	13	1.085	0.689	0.245	0.079	-0.003	-0.007	0.000	0.004
	14	2.471	1.077	0.412	0.127	0.008	-0.001	-0.007	0.006
	15	1.765	0.891	0.375	0.155	0.002	-0.007	-0.007	0.000
	16	1.941	0.931	0.317	0.107	0.005	0.007	-0.005	0.001
^{15}N	1	11.318	5.433	2.564	1.037	0.340	0.149	0.054	0.029
^{17}O	10	4.539	3.268	1.389	0.473	0.076	0.011	0.004	-0.002
^{77}Se	2	25.833	19.327	10.879	3.545	0.333	-0.471	-0.710	-0.743

Table F.29: Errors (in ppm) in isotropic NMR shieldings vs RI-MP2 for the penicillin molecule at different values of T_{CutPNO} for valence orbitals, with $T_{\mathrm{CutPNO}} = 10^{-12}$ for core orbitals, $F_{\mathrm{Cut}} = 10^{-8}$, $T_{\mathrm{S}} = 10^{-8}$, and all other DLPNO thresholds equal to 0.

		T_{CutPNO}(valence)							
El.	Ind.	10^{-5}	10^{-6}	10^{-7}	10^{-8}	10^{-9}	10^{-10}	10^{-11}	10^{-12}
^{1}H	9	0.119	0.034	0.017	0.006	0.001	0.002	0.000	0.000
	20	0.026	0.010	0.009	0.003	0.001	0.001	0.000	0.000
	26	0.082	0.041	0.019	0.006	0.003	0.000	0.000	0.000
	27	0.108	0.047	0.020	0.009	0.002	0.000	-0.001	0.000
	28	0.044	0.023	0.009	-0.007	0.001	0.000	0.000	0.000
	29	0.049	0.024	0.010	0.007	0.002	0.000	0.000	0.000
	30	0.043	0.019	0.009	0.002	0.000	0.000	0.000	0.000
	31	0.048	0.025	0.010	0.008	0.002	0.000	0.000	0.000
	32	0.043	0.023	0.010	0.004	0.001	0.001	0.000	0.000
	33	0.046	0.023	0.010	0.004	0.002	0.001	0.000	0.000
	34	0.075	0.034	0.012	0.002	0.001	0.001	0.000	0.000
	35	0.054	0.028	0.017	0.003	0.002	0.000	0.000	0.000
	36	0.061	0.029	0.014	0.004	0.001	0.001	0.000	0.000
	37	0.049	0.027	0.015	0.003	0.000	-0.001	0.000	0.000
	38	0.052	0.025	0.013	0.001	-0.001	-0.001	-0.001	-0.001
	39	0.033	0.018	0.013	0.003	0.000	0.001	0.000	0.000
	40	0.040	0.021	0.008	0.002	0.000	0.001	0.000	0.000

Continued on next page

Continued from previous page

El.	Ind.	10^{-5}	10^{-6}	10^{-7}	10^{-8}	10^{-9}	10^{-10}	10^{-11}	10^{-12}
	41	0.049	0.023	0.011	0.001	0.000	0.000	0.000	0.000
^{13}C	1	1.533	0.776	0.266	0.074	-0.024	-0.001	-0.002	-0.003
	2	1.650	0.747	0.253	0.034	0.001	-0.007	-0.011	-0.006
	3	1.046	0.620	0.299	0.066	0.007	-0.005	-0.002	-0.004
	4	1.264	0.692	0.264	0.077	0.007	0.000	-0.005	-0.004
	5	1.530	0.783	0.309	0.088	0.000	0.001	-0.003	-0.004
	6	1.587	0.795	0.354	0.132	0.036	0.010	0.004	0.001
	7	1.303	0.661	0.289	0.040	0.026	0.015	0.005	0.002
	8	1.267	0.637	0.262	0.073	0.044	0.019	0.006	0.001
	10	1.700	0.892	0.382	0.086	0.002	-0.004	-0.007	-0.002
	15	0.759	0.506	0.131	0.008	0.010	-0.001	0.002	0.002
	16	0.533	0.142	0.000	-0.086	-0.034	-0.020	-0.007	-0.004
	17	2.410	1.183	0.565	0.183	0.055	0.012	-0.002	-0.002
	18	1.949	0.958	0.419	0.131	0.056	0.000	0.007	0.003
	19	0.653	0.238	0.060	-0.065	-0.047	-0.016	-0.011	-0.004
	22	3.077	1.385	0.626	0.262	0.066	0.022	0.009	0.002
	23	3.571	1.626	0.695	0.210	0.072	0.019	0.012	0.004
^{15}N	21	6.019	2.741	1.243	0.424	0.144	0.019	0.016	0.003
	25	7.465	3.522	1.378	0.466	0.084	0.007	-0.005	0.004
^{17}O	11	8.046	4.212	1.686	0.404	0.089	0.015	0.001	-0.006
	12	9.426	4.307	1.321	0.382	0.100	-0.008	-0.034	-0.023
	13	8.501	3.547	1.631	0.370	0.147	0.035	0.002	0.001
	14	5.927	2.852	0.961	0.215	0.095	0.016	0.010	0.003
^{33}S	24	13.983	6.656	2.779	1.079	0.328	0.054	0.010	0.009

Table F.30: Errors (in ppm) in isotropic NMR shieldings vs RI-MP2 for the ATP^{4-} anion at different values of T_{CutPNO} for core orbitals, with $T_{\mathrm{CutPNO}} = 10^{-10}$ for valence orbitals, $F_{\mathrm{Cut}} = 10^{-8}$, $T_{\mathrm{S}} = 10^{-8}$, and all other DLPNO thresholds equal to 0.

		T_{CutPNO}(core)							
El.	Ind.	10^{-5}	10^{-6}	10^{-7}	10^{-8}	10^{-9}	10^{-10}	10^{-11}	10^{-12}
^{1}H	6	0.000	0.000	0.000	0.000	0.000	-0.001	0.000	0.000
	9	0.000	0.000	0.000	0.000	0.000	0.000	0.000	0.000
	11	0.001	0.001	0.000	0.000	0.000	0.000	0.000	0.000
	12	0.001	0.001	0.001	0.000	0.000	0.000	0.000	0.000
	14	0.001	0.000	0.000	0.000	0.000	0.000	0.000	0.000
	16	0.000	0.000	0.000	0.000	0.000	0.000	0.000	0.000
	22	0.000	0.000	0.000	0.000	0.000	0.000	0.000	0.000
	26	-0.002	-0.001	-0.001	-0.001	-0.001	-0.001	-0.001	-0.001
	29	0.000	0.000	0.000	0.000	0.000	0.000	0.000	0.000
	30	0.000	0.000	0.000	0.000	0.000	0.000	0.000	0.000
	31	-0.002	-0.002	-0.002	-0.002	-0.001	-0.001	-0.001	-0.001
	32	-0.001	-0.001	-0.001	-0.001	-0.001	-0.001	-0.001	-0.001
^{13}C	1	0.044	0.052	0.039	0.036	0.035	0.035	0.035	0.035
	2	0.025	0.033	0.019	0.016	0.016	0.016	0.016	0.016
	3	0.023	0.033	0.024	0.020	0.019	0.019	0.019	0.019
	4	0.018	0.034	0.024	0.020	0.019	0.019	0.019	0.019
	7	0.027	0.033	0.026	0.023	0.022	0.022	0.021	0.021
	17	-0.036	-0.018	-0.018	-0.019	-0.019	-0.019	-0.019	-0.019
	18	-0.041	-0.028	-0.021	-0.023	-0.023	-0.022	-0.023	-0.023
	20	-0.010	0.006	-0.010	-0.010	-0.010	-0.010	-0.010	-0.010
	24	-0.021	0.008	0.005	0.005	0.005	0.005	0.005	0.005
	27	-0.054	-0.032	-0.025	-0.028	-0.028	-0.028	-0.029	-0.028
^{15}N	13	0.070	0.077	0.051	0.045	0.043	0.043	0.043	0.043
	21	0.001	0.022	0.021	0.018	0.017	0.018	0.018	0.018
	23	0.007	0.081	0.040	0.044	0.042	0.042	0.042	0.042
	25	0.075	0.095	0.073	0.071	0.070	0.070	0.070	0.070
	28	0.008	0.009	0.008	0.005	0.005	0.005	0.004	0.004
^{17}O	5	0.219	0.211	0.179	0.168	0.165	0.165	0.164	0.164
	8	0.152	0.158	0.141	0.134	0.134	0.133	0.133	0.133

Continued on next page

Continued from previous page

El.	Ind.	10^{-5}	10^{-6}	10^{-7}	10^{-8}	10^{-9}	10^{-10}	10^{-11}	10^{-12}
	10	0.113	0.116	0.100	0.095	0.095	0.094	0.094	0.094
	15	0.316	0.294	0.164	0.143	0.128	0.122	0.109	0.106
	33	0.291	0.164	0.121	0.088	0.063	0.053	0.045	0.044
	34	0.409	0.280	0.157	0.122	0.110	0.094	0.068	0.069
	36	0.309	0.171	0.133	0.098	0.073	0.066	0.060	0.060
	37	0.356	0.209	0.187	0.150	0.127	0.111	0.102	0.102
	38	0.476	0.316	0.164	0.118	0.094	0.072	0.059	0.056
	39	0.289	0.218	0.136	0.111	0.095	0.077	0.075	0.074
	41	0.301	0.177	0.102	0.079	0.050	0.044	0.034	0.032
	42	0.281	0.157	0.082	0.059	0.029	0.023	0.013	0.012
	43	0.298	0.176	0.102	0.080	0.054	0.045	0.036	0.035
^{31}P	19	2.124	0.885	0.379	0.257	0.102	0.058	0.048	0.047
	35	2.209	1.826	0.404	0.263	0.083	0.049	0.052	0.051
	40	1.987	0.938	0.284	0.261	0.014	0.038	0.038	0.038

Table F.31: Errors (in ppm) in isotropic NMR shieldings vs RI-MP2 for the caffeine molecule at different values of T_{CutPNO} for core orbitals, with $T_{\mathrm{CutPNO}} = 10^{-10}$ for valence orbitals, $F_{\mathrm{Cut}} = 10^{-8}$, $T_{\mathrm{S}} = 10^{-8}$, and all other DLPNO thresholds equal to 0.

		T_{CutPNO}(core)							
El.	Ind.	10^{-5}	10^{-6}	10^{-7}	10^{-8}	10^{-9}	10^{-10}	10^{-11}	10^{-12}
^{1}H	15	-0.001	0.000	0.000	0.000	0.000	0.000	0.000	0.000
	16	0.000	0.000	0.000	0.000	0.000	0.000	0.000	0.000
	17	0.001	0.001	0.001	0.001	0.001	0.001	0.001	0.001
	18	0.000	0.000	0.000	0.000	0.000	0.000	0.000	0.000
	19	0.001	0.001	0.001	0.001	0.001	0.001	0.001	0.001
	20	0.001	0.001	0.001	0.000	0.000	0.000	0.000	0.000
	21	0.000	0.000	0.000	0.000	0.000	0.000	0.000	0.000
	22	0.001	0.001	0.001	0.001	0.000	0.000	0.000	0.000
	23	0.000	0.000	0.000	0.000	0.000	0.000	0.000	0.000
	24	0.001	0.000	0.000	0.000	0.000	0.000	0.000	0.000
^{13}C	1	-0.014	0.004	-0.012	-0.013	-0.013	-0.013	-0.013	-0.013
	2	-0.025	-0.009	-0.013	-0.015	-0.015	-0.015	-0.015	-0.015
	4	-0.025	-0.024	-0.009	-0.024	-0.024	-0.025	-0.025	-0.025
	7	-0.029	-0.021	-0.019	-0.021	-0.022	-0.021	-0.021	-0.021
	11	0.252	0.012	-0.022	-0.022	-0.022	-0.021	-0.021	-0.022
	12	0.003	0.009	0.008	0.007	0.006	0.006	0.006	0.006
	13	0.004	0.011	0.009	0.008	0.008	0.008	0.008	0.008
	14	0.008	0.015	0.013	0.012	0.012	0.012	0.012	0.012
^{15}N	3	0.079	0.072	0.057	0.047	0.044	0.044	0.044	0.044
	6	0.073	0.060	0.044	0.035	0.034	0.033	0.033	0.033
	9	0.050	0.053	0.015	0.009	0.009	0.009	0.009	0.009
	10	0.027	0.014	-0.016	-0.018	-0.018	-0.018	-0.018	-0.018
^{17}O	5	0.058	-0.024	0.003	-0.009	-0.009	-0.009	-0.010	-0.010
	8	0.059	-0.006	0.009	0.007	0.005	0.006	0.006	0.006

Table F.32: Errors (in ppm) in isotropic NMR shieldings vs RI-MP2 for the ebselen molecule at different values of T_{CutPNO} for core orbitals, with $T_{\mathrm{CutPNO}} = 10^{-10}$ for valence orbitals, $F_{\mathrm{Cut}} = 10^{-8}$, $T_{\mathrm{S}} = 10^{-8}$, and all other DLPNO thresholds equal to 0.

		T_{CutPNO}(core)							
El.	Ind.	10^{-5}	10^{-6}	10^{-7}	10^{-8}	10^{-9}	10^{-10}	10^{-11}	10^{-12}
^{1}H	17	-0.001	0.001	-0.002	0.002	-0.001	-0.001	-0.001	-0.001
	18	0.000	0.001	0.000	0.001	0.000	0.000	0.000	0.000
	19	-0.001	0.000	0.000	0.000	0.000	0.000	0.000	0.000
	20	0.000	0.000	0.000	0.000	0.000	0.000	0.000	0.000
	21	-0.001	-0.002	-0.001	-0.002	-0.001	-0.001	-0.001	-0.001
	22	-0.001	-0.001	-0.001	-0.001	-0.001	-0.001	-0.001	-0.001

Continued on next page

Continued from previous page

El.	Ind.	10^{-5}	10^{-6}	10^{-7}	10^{-8}	10^{-9}	10^{-10}	10^{-11}	10^{-12}
	23	0.001	0.001	0.002	0.000	0.001	0.001	0.001	0.001
	24	0.001	-0.001	0.002	-0.001	0.001	0.001	0.001	0.001
	25	0.001	0.000	0.001	-0.001	0.001	0.000	0.000	0.000
^{13}C	3	0.003	0.010	0.008	0.015	0.005	0.005	0.005	0.006
	4	-0.043	-0.019	-0.036	-0.022	-0.020	-0.018	-0.021	-0.024
	5	-0.018	-0.016	-0.008	-0.012	-0.012	-0.012	-0.013	-0.012
	6	-0.005	0.010	-0.002	0.007	-0.004	-0.002	-0.001	-0.003
	7	-0.025	-0.007	-0.009	-0.010	-0.011	-0.011	-0.011	-0.011
	8	0.002	0.016	0.014	0.020	0.008	0.010	0.010	0.010
	9	0.000	0.015	0.010	0.010	0.013	0.012	0.012	0.012
	11	-0.031	-0.019	-0.022	-0.024	-0.022	-0.022	-0.022	-0.021
	12	-0.036	-0.018	-0.024	-0.026	-0.026	-0.026	-0.026	-0.026
	13	-0.016	-0.004	-0.005	-0.007	-0.007	-0.007	-0.007	-0.007
	14	-0.012	0.010	0.005	-0.001	0.001	0.000	0.000	-0.001
	15	-0.016	-0.002	-0.005	-0.012	-0.006	-0.007	-0.007	-0.007
	16	-0.004	0.012	0.007	0.004	0.007	0.007	0.007	0.007
^{15}N	1	0.124	0.183	0.168	0.163	0.158	0.149	0.151	0.149
^{17}O	10	0.080	-0.012	0.033	0.042	0.009	0.013	0.013	0.011
^{77}Se	2	8.438	4.733	1.337	-0.083	-0.415	-0.168	-0.305	-0.471

Table F.33: Errors (in ppm) in isotropic NMR shieldings vs RI-MP2 for the penicillin molecule at different values of T_{CutPNO} for core orbitals, with $T_{\mathrm{CutPNO}} = 10^{-10}$ for valence orbitals, $F_{\mathrm{Cut}} = 10^{-8}$, $T_{\mathrm{S}} = 10^{-8}$, and all other DLPNO thresholds equal to 0.

		T_{CutPNO}(core)							
El.	Ind.	10^{-5}	10^{-6}	10^{-7}	10^{-8}	10^{-9}	10^{-10}	10^{-11}	10^{-12}
^{1}H	9	0.002	0.002	0.002	0.002	0.002	0.002	0.002	0.002
	20	0.002	0.001	0.001	0.001	0.001	0.001	0.001	0.001
	26	0.001	0.001	0.001	0.001	0.001	0.000	0.000	0.000
	27	0.002	0.001	0.000	0.000	0.000	0.000	0.000	0.000
	28	0.000	0.000	0.000	0.000	0.000	0.000	0.000	0.000
	29	0.001	0.001	0.000	0.000	0.000	0.000	0.000	0.000
	30	0.001	0.001	0.001	0.000	0.000	0.000	0.000	0.000
	31	0.001	0.001	0.001	0.001	0.001	0.000	0.000	0.000
	32	0.002	0.002	0.001	0.001	0.001	0.001	0.001	0.001
	33	0.001	0.001	0.001	0.001	0.001	0.001	0.001	0.001
	34	0.001	0.001	0.001	0.001	0.001	0.001	0.001	0.001
	35	0.000	0.000	0.000	0.000	0.000	0.000	0.000	0.000
	36	0.001	0.001	0.001	0.001	0.001	0.001	0.001	0.001
	37	-0.001	0.000	-0.001	-0.001	-0.001	-0.001	-0.001	-0.001
	38	-0.001	-0.001	-0.001	-0.001	-0.001	-0.001	-0.001	-0.001
	39	0.001	0.001	0.001	0.001	0.001	0.001	0.001	0.001
	40	0.000	0.001	0.001	0.001	0.001	0.001	0.001	0.001
	41	-0.001	0.000	0.000	0.000	0.000	0.000	0.000	0.000
^{13}C	1	-0.009	0.007	0.000	-0.001	-0.001	-0.001	-0.001	-0.001
	2	-0.018	0.000	-0.006	-0.007	-0.007	-0.007	-0.007	-0.007
	3	-0.016	0.000	-0.004	-0.005	-0.005	-0.005	-0.005	-0.005
	4	-0.012	0.004	0.000	0.000	0.000	0.000	0.000	0.000
	5	-0.009	0.008	0.002	0.001	0.001	0.001	0.001	0.001
	6	0.016	0.022	0.013	0.011	0.010	0.010	0.010	0.010
	7	0.020	0.023	0.018	0.016	0.015	0.015	0.015	0.015
	8	0.019	0.024	0.021	0.019	0.019	0.019	0.019	0.019
	10	-0.012	0.006	-0.001	-0.004	-0.004	-0.004	-0.004	-0.004
	15	-0.006	0.000	0.000	-0.001	-0.001	-0.002	-0.001	-0.001
	16	-0.024	-0.020	-0.019	-0.020	-0.020	-0.020	-0.020	-0.020
	17	0.028	0.034	0.020	0.015	0.014	0.013	0.013	0.012
	18	0.017	0.023	0.006	0.001	0.001	0.001	0.000	0.000
	19	-0.023	-0.014	-0.012	-0.015	-0.016	-0.015	-0.016	-0.016
	22	0.079	0.090	0.046	0.033	0.030	0.026	0.024	0.022
	23	0.095	0.104	0.048	0.033	0.028	0.023	0.020	0.019
^{15}N	21	0.041	0.041	0.024	0.021	0.020	0.019	0.019	0.019

Continued on next page

Continued from previous page

El.	Ind.	10^{-5}	10^{-6}	10^{-7}	10^{-8}	10^{-9}	10^{-10}	10^{-11}	10^{-12}
	25	0.056	0.058	0.030	0.015	0.012	0.009	0.008	0.007
^{17}O	11	0.112	0.004	0.023	0.018	0.016	0.015	0.015	0.015
	12	0.095	-0.022	-0.003	-0.004	-0.007	-0.007	-0.008	-0.008
	13	0.118	0.015	0.029	0.035	0.035	0.035	0.035	0.035
	14	0.161	0.027	0.019	0.017	0.017	0.016	0.016	0.016
^{33}S	24	1.129	1.020	0.257	0.143	0.090	0.064	0.056	0.054

F.3 NMR shielding errors due to Fock matrix-based screening

Table F.34: Errors (in ppm) in isotropic NMR shieldings vs RI-MP2 for the ATP^{4-} anion at different values of F_{Cut}, with $T_{\mathrm{CutPNO}} = 10^{-12}$ for core and $T_{\mathrm{CutPNO}} = 10^{-10}$ for valence orbitals, $T_{\mathrm{S}} = 10^{-8}$, and all other DLPNO thresholds equal to 0.

		F_{Cut}						
El.	Ind.	10^{-2}	10^{-3}	10^{-4}	10^{-5}	10^{-6}	10^{-7}	10^{-8}
^{1}H	6	-0.120	-0.003	-0.001	0.000	0.000	0.000	0.000
	9	-0.020	0.000	-0.001	0.000	0.000	0.000	0.000
	11	-0.053	-0.001	0.000	0.000	0.000	0.000	0.000
	12	-0.072	-0.003	0.000	0.001	0.000	0.000	0.000
	14	-0.012	0.000	0.000	0.000	0.000	0.000	0.000
	16	0.020	0.001	0.000	0.000	0.000	0.000	0.000
	22	0.003	0.001	0.000	0.000	0.000	0.000	0.000
	26	-0.016	-0.003	-0.001	-0.001	-0.001	-0.001	-0.001
	29	0.030	0.000	0.000	0.000	0.000	0.000	0.000
	30	0.011	0.001	0.000	0.000	0.000	0.000	0.000
	31	-0.083	-0.004	-0.002	-0.001	-0.001	-0.001	-0.001
	32	-0.105	-0.004	-0.001	-0.001	-0.001	-0.001	-0.001
^{13}C	1	-0.095	0.029	0.034	0.034	0.035	0.035	0.035
	2	-0.123	0.005	0.016	0.016	0.016	0.016	0.016
	3	-0.123	0.014	0.018	0.018	0.019	0.019	0.019
	4	-0.124	0.019	0.019	0.020	0.019	0.019	0.019
	7	-0.077	0.015	0.021	0.021	0.021	0.021	0.021
	17	-1.130	0.018	-0.022	-0.019	-0.019	-0.019	-0.019
	18	-0.513	-0.014	-0.023	-0.024	-0.023	-0.023	-0.023
	20	0.214	-0.016	-0.008	-0.010	-0.010	-0.010	-0.010
	24	-0.361	-0.020	0.008	0.005	0.005	0.005	0.005
	27	-0.448	-0.014	-0.033	-0.029	-0.028	-0.028	-0.028
^{15}N	13	0.426	0.019	0.042	0.045	0.043	0.043	0.043
	21	-0.889	-0.001	0.016	0.017	0.018	0.018	0.018
	23	2.337	-0.099	0.030	0.042	0.042	0.042	0.042
	25	1.021	0.045	0.067	0.070	0.070	0.070	0.070
	28	-0.131	0.016	0.003	0.004	0.004	0.004	0.004
^{17}O	5	0.066	0.148	0.160	0.160	0.164	0.164	0.164
	8	0.110	0.136	0.128	0.134	0.133	0.133	0.133
	10	-0.165	0.084	0.091	0.090	0.094	0.094	0.094
	15	0.233	0.077	0.106	0.106	0.106	0.106	0.106
	33	0.385	0.025	0.042	0.044	0.045	0.045	0.044
	34	-0.188	0.073	0.063	0.069	0.069	0.069	0.069
	36	0.653	0.050	0.060	0.060	0.060	0.060	0.060
	37	0.188	0.117	0.102	0.102	0.102	0.102	0.102
	38	-0.240	0.035	0.057	0.057	0.056	0.056	0.056
	39	0.236	0.071	0.072	0.074	0.074	0.074	0.074
	41	0.635	0.024	0.029	0.032	0.032	0.032	0.032
	42	0.352	0.014	0.013	0.011	0.012	0.012	0.012
	43	0.231	0.032	0.036	0.035	0.035	0.035	0.035
^{31}P	19	0.414	0.037	0.046	0.047	0.047	0.047	0.047
	35	-0.041	0.047	0.051	0.051	0.051	0.051	0.051
	40	0.985	0.033	0.039	0.039	0.038	0.038	0.038

Table F.35: Errors (in ppm) in isotropic NMR shieldings vs RI-MP2 for the caffeine molecule at different values of F_{Cut}, with $T_{\mathrm{CutPNO}} = 10^{-12}$ for core and $T_{\mathrm{CutPNO}} = 10^{-10}$ for valence orbitals, $T_{\mathrm{S}} = 10^{-8}$, and all other DLPNO thresholds equal to 0.

		F_{Cut}						
El.	Ind.	10^{-2}	10^{-3}	10^{-4}	10^{-5}	10^{-6}	10^{-7}	10^{-8}
^{1}H	15	0.002	0.000	0.000	0.000	0.000	0.000	0.000
	16	0.010	0.000	0.000	0.000	0.000	0.000	0.000
	17	0.002	0.001	0.001	0.001	0.001	0.001	0.001
	18	0.005	0.000	0.000	0.000	0.000	0.000	0.000
	19	0.002	0.001	0.001	0.001	0.001	0.001	0.001
	20	0.001	0.001	0.001	0.001	0.000	0.000	0.000
	21	0.002	0.000	0.000	0.000	0.000	0.000	0.000
	22	0.009	0.000	0.001	0.000	0.000	0.000	0.000
	23	0.003	0.000	0.000	0.000	0.000	0.000	0.000
	24	-0.003	0.000	0.000	0.000	0.000	0.000	0.000
^{13}C	1	0.073	-0.020	-0.015	-0.012	-0.013	-0.013	-0.013
	2	-0.226	-0.007	-0.015	-0.015	-0.015	-0.015	-0.015
	4	-0.204	-0.014	-0.026	-0.025	-0.025	-0.025	-0.025
	7	-0.105	-0.029	-0.024	-0.021	-0.021	-0.021	-0.021
	11	-0.262	-0.018	-0.021	-0.022	-0.022	-0.022	-0.022
	12	-0.018	0.006	0.006	0.006	0.006	0.006	0.006
	13	-0.049	0.005	0.008	0.008	0.008	0.008	0.008
	14	-0.071	0.014	0.013	0.012	0.012	0.012	0.012
^{15}N	3	0.013	0.042	0.042	0.043	0.044	0.044	0.044
	6	0.021	0.029	0.029	0.033	0.033	0.033	0.033
	9	-0.310	0.009	0.011	0.009	0.009	0.009	0.009
	10	0.074	-0.034	-0.023	-0.018	-0.018	-0.018	-0.018
^{17}O	5	-0.492	0.056	-0.011	-0.011	-0.010	-0.010	-0.010
	8	0.053	-0.025	-0.005	0.007	0.006	0.006	0.006

Table F.36: Errors (in ppm) in isotropic NMR shieldings vs RI-MP2 for the ebselen molecule at different values of F_{Cut}, with $T_{\mathrm{CutPNO}} = 10^{-12}$ for core and $T_{\mathrm{CutPNO}} = 10^{-10}$ for valence orbitals, $T_{\mathrm{S}} = 10^{-8}$, and all other DLPNO thresholds equal to 0.

		F_{Cut}						
El.	Ind.	10^{-2}	10^{-3}	10^{-4}	10^{-5}	10^{-6}	10^{-7}	10^{-8}
^{1}H	17	-0.010	-0.001	-0.001	-0.001	-0.001	-0.001	-0.001
	18	-0.001	0.000	0.000	0.000	0.000	0.000	0.000
	19	-0.003	-0.001	0.000	0.000	0.000	0.000	0.000
	20	-0.012	0.000	0.000	0.000	0.000	0.000	0.000
	21	0.012	-0.001	-0.001	-0.001	-0.001	-0.001	-0.001
	22	0.019	-0.001	-0.001	-0.001	-0.001	-0.001	-0.001
	23	0.018	0.002	0.001	0.001	0.001	0.001	0.001
	24	-0.018	0.002	0.001	0.001	0.001	0.001	0.001
	25	-0.004	0.001	0.001	0.000	0.000	0.000	0.000
^{13}C	3	-0.074	0.016	0.006	0.006	0.006	0.006	0.006
	4	-0.161	-0.030	-0.024	-0.024	-0.024	-0.024	-0.024
	5	0.171	-0.077	-0.013	-0.012	-0.012	-0.012	-0.012
	6	-0.013	-0.003	-0.003	-0.003	-0.003	-0.003	-0.003
	7	-0.114	-0.016	-0.011	-0.011	-0.011	-0.011	-0.011
	8	-0.028	0.009	0.010	0.010	0.010	0.010	0.010
	9	-0.153	0.007	0.012	0.012	0.012	0.012	0.012
	11	0.007	-0.024	-0.022	-0.022	-0.022	-0.022	-0.021
	12	-0.201	-0.020	-0.026	-0.026	-0.026	-0.026	-0.026
	13	0.037	-0.009	-0.007	-0.007	-0.007	-0.007	-0.007
	14	-0.346	0.017	0.000	0.000	0.000	0.000	-0.001
	15	-0.149	-0.015	-0.007	-0.007	-0.007	-0.007	-0.007
	16	-0.084	0.010	0.007	0.007	0.007	0.007	0.007
^{15}N	1	-0.232	0.249	0.150	0.149	0.149	0.149	0.149
^{17}O	10	0.419	-0.184	0.010	0.011	0.011	0.011	0.011
^{77}Se	2	-2.723	-0.746	-0.481	-0.477	-0.476	-0.476	-0.471

Table F.37: Errors (in ppm) in isotropic NMR shieldings vs RI-MP2 for the penicillin molecule at different values of F_{Cut}, with $T_{\mathrm{CutPNO}} = 10^{-12}$ for core and $T_{\mathrm{CutPNO}} = 10^{-10}$ for valence orbitals, $T_{\mathrm{S}} = 10^{-8}$, and all other DLPNO thresholds equal to 0.

		F_{Cut}						
El.	Ind.	10^{-2}	10^{-3}	10^{-4}	10^{-5}	10^{-6}	10^{-7}	10^{-8}
^{1}H	9	-0.097	-0.001	0.001	0.001	0.002	0.002	0.002
	20	0.019	0.001	0.001	0.001	0.001	0.001	0.001
	26	-0.056	-0.001	0.000	0.000	0.000	0.000	0.000
	27	-0.007	-0.001	0.000	0.000	0.000	0.000	0.000
	28	-0.020	-0.001	0.000	0.000	0.000	0.000	0.000
	29	-0.029	0.000	0.000	0.000	0.000	0.000	0.000
	30	-0.054	-0.001	0.000	0.000	0.000	0.000	0.000
	31	0.002	0.000	0.000	0.000	0.000	0.000	0.000
	32	-0.007	0.001	0.001	0.001	0.001	0.001	0.001
	33	0.014	0.000	0.001	0.001	0.001	0.001	0.001
	34	0.009	0.001	0.001	0.001	0.001	0.001	0.001
	35	-0.008	0.000	0.000	0.000	0.000	0.000	0.000
	36	0.023	0.001	0.001	0.001	0.001	0.001	0.001
	37	0.013	-0.001	-0.001	-0.001	-0.001	-0.001	-0.001
	38	-0.028	-0.001	-0.001	-0.001	-0.001	-0.001	-0.001
	39	0.019	0.001	0.001	0.001	0.001	0.001	0.001
	40	-0.018	0.000	0.001	0.001	0.001	0.001	0.001
	41	-0.042	-0.001	0.000	0.000	0.000	0.000	0.000
^{13}C	1	-0.181	-0.007	-0.001	-0.001	-0.001	-0.001	-0.001
	2	-0.214	-0.009	-0.007	-0.007	-0.007	-0.007	-0.007
	3	0.102	-0.006	-0.005	-0.005	-0.005	-0.005	-0.005
	4	0.107	0.000	0.000	0.000	0.000	0.000	0.000
	5	-0.191	-0.004	0.001	0.001	0.001	0.001	0.001
	6	-0.075	0.007	0.010	0.010	0.010	0.010	0.010
	7	-0.049	0.013	0.015	0.015	0.015	0.015	0.015
	8	-0.086	0.018	0.019	0.019	0.019	0.019	0.019
	10	-0.225	-0.002	-0.004	-0.004	-0.004	-0.004	-0.004
	15	-0.006	-0.009	-0.002	-0.002	-0.001	-0.001	-0.001
	16	-0.103	-0.027	-0.022	-0.022	-0.020	-0.020	-0.020
	17	-0.072	0.012	0.013	0.013	0.012	0.012	0.012
	18	-0.019	-0.001	0.001	0.001	0.000	0.000	0.000
	19	-0.313	-0.015	-0.017	-0.016	-0.016	-0.016	-0.016
	22	-0.077	0.025	0.023	0.023	0.022	0.022	0.022
	23	-0.078	0.019	0.019	0.019	0.019	0.019	0.019
^{15}N	21	-0.026	0.026	0.022	0.020	0.019	0.019	0.019
	25	-0.307	-0.014	0.007	0.007	0.007	0.007	0.007
^{17}O	11	0.227	0.030	0.016	0.016	0.015	0.015	0.015
	12	-0.995	-0.074	-0.007	-0.007	-0.008	-0.008	-0.008
	13	-0.042	0.000	0.020	0.028	0.035	0.035	0.035
	14	-0.106	0.023	0.016	0.015	0.016	0.016	0.016
^{33}S	24	-1.212	0.022	0.053	0.054	0.054	0.054	0.054

F.4 NMR shielding errors due to domain truncation

Results with $T_{\mathrm{S}} = 10^{-8}$ are shown in Tables F.38–F.41 and with $T_{\mathrm{S}} = 10^{-5}$ – in Tables F.42–F.45.

Table F.38: Errors (in ppm) in isotropic NMR shieldings vs RI-MP2 for the ATP^{4-} anion at different values of T_{CutDO}, with $T_{\mathrm{CutPNO}} = 10^{-12}$ for core and $T_{\mathrm{CutPNO}} = 10^{-10}$ for valence orbitals, $F_{\mathrm{Cut}} = 10^{-5}$, $T_{\mathrm{S}} = 10^{-8}$, and all other DLPNO thresholds equal to 0.

		T_{CutDO}								
El.	Ind.	0.001	0.002	0.003	0.006	0.010	0.020	0.030	0.060	0.100
^{1}H	6	0.000	-0.001	0.002	-0.004	0.003	0.011	0.003	-0.001	0.066
	9	0.000	-0.001	0.000	0.005	0.009	0.014	0.017	0.070	0.084
	11	0.000	0.002	0.002	0.005	0.006	0.003	0.013	0.082	0.097
	12	0.000	0.000	0.000	-0.009	-0.014	-0.018	-0.009	0.064	0.143
	14	0.000	0.000	0.001	0.004	0.015	0.026	0.023	0.034	0.100

Continued on next page

Continued from previous page

El.	Ind.	0.001	0.002	0.003	0.006	0.010	0.020	0.030	0.060	0.100
	16	0.000	-0.001	0.000	0.004	0.011	0.018	0.019	0.040	0.086
	22	0.000	-0.001	0.000	-0.002	-0.003	0.005	0.005	0.047	0.142
	26	-0.001	-0.001	0.001	0.002	0.011	-0.005	0.009	-0.024	0.011
	29	0.000	0.000	0.001	0.003	0.000	0.012	-0.004	0.020	-0.001
	30	0.000	0.001	0.001	0.004	-0.002	0.001	-0.011	0.033	0.067
	31	-0.001	-0.001	-0.002	0.005	0.012	0.012	0.024	0.018	-0.012
	32	-0.001	0.000	0.003	0.004	0.000	-0.023	-0.006	0.044	0.035
^{13}C	1	0.034	0.035	0.037	0.045	0.044	0.042	0.055	0.799	1.591
	2	0.016	0.016	0.017	0.021	0.015	0.024	0.057	0.608	1.424
	3	0.018	0.017	0.016	0.011	-0.002	-0.014	-0.028	0.346	1.357
	4	0.020	0.020	0.020	0.022	0.010	0.021	-0.001	0.559	1.176
	7	0.022	0.020	0.023	0.003	-0.002	0.015	0.018	0.493	1.280
	17	-0.022	-0.019	-0.018	-0.046	-0.053	-0.051	-0.112	-1.250	0.107
	18	-0.024	-0.024	-0.026	-0.029	-0.037	-0.069	-0.106	-0.943	0.010
	20	-0.009	-0.012	-0.011	-0.014	-0.001	0.001	-0.008	0.814	1.227
	24	0.005	0.006	-0.002	-0.008	0.006	-0.003	-0.058	-1.554	-1.987
	27	-0.027	-0.033	-0.031	-0.037	-0.035	-0.005	-0.051	-0.690	-4.421
^{15}N	13	0.046	0.044	0.041	0.031	0.021	0.142	0.247	2.004	4.992
	21	0.013	0.016	0.017	0.016	0.061	0.095	0.121	0.935	4.798
	23	0.037	0.043	0.044	0.027	0.017	0.082	0.133	2.154	-4.691
	25	0.075	0.057	0.074	0.066	0.077	0.010	-0.020	2.548	2.450
	28	0.003	0.000	0.000	0.006	0.011	0.025	0.008	0.165	1.367
^{17}O	5	0.160	0.156	0.158	0.098	0.128	0.339	0.548	2.018	5.246
	8	0.135	0.143	0.150	0.171	0.127	0.195	0.401	1.454	2.407
	10	0.092	0.087	0.096	0.145	0.237	0.281	0.492	2.021	3.502
	15	0.107	0.103	0.123	0.124	0.134	0.189	0.325	1.575	2.845
	33	0.041	0.044	0.042	0.005	-0.006	-0.021	-0.046	-0.049	0.095
	34	0.069	0.080	0.075	0.127	0.170	0.208	0.620	1.555	3.087
	36	0.063	0.072	0.081	0.031	0.058	0.014	-0.196	0.613	1.160
	37	0.102	0.103	0.122	0.180	0.128	0.053	0.103	1.874	2.277
	38	0.055	0.050	0.054	0.072	0.314	0.134	0.311	1.107	2.120
	39	0.076	0.079	0.075	0.149	0.262	0.348	0.463	2.179	5.055
	41	0.032	0.027	0.037	0.046	-0.056	0.101	0.155	0.122	0.511
	42	0.013	0.023	0.027	0.023	0.140	0.179	0.065	0.279	0.654
	43	0.034	0.034	0.037	0.081	-0.428	0.269	0.196	-0.506	-0.381
^{31}P	19	0.044	0.027	0.052	0.197	0.370	0.304	0.203	-0.269	0.492
	35	0.031	-0.041	0.053	0.157	0.191	1.887	1.131	-2.047	-1.274
	40	0.041	0.036	0.027	0.077	0.325	0.023	0.112	1.635	0.252

Table F.39: Errors (in ppm) in isotropic NMR shieldings vs RI-MP2 for the caffeine molecule at different values of T_{CutDO}, with $T_{\mathrm{CutPNO}} = 10^{-12}$ for core and $T_{\mathrm{CutPNO}} = 10^{-10}$ for valence orbitals, $F_{\mathrm{Cut}} = 10^{-5}$, $T_{\mathrm{S}} = 10^{-8}$, and all other DLPNO thresholds equal to 0.

		T_{CutDO}								
El.	Ind.	0.001	0.002	0.003	0.006	0.010	0.020	0.030	0.060	0.100
^{1}H	15	0.000	0.001	0.001	0.002	0.005	0.017	0.020	0.004	0.026
	16	0.000	-0.001	-0.002	-0.002	-0.005	0.001	0.006	0.034	0.134
	17	0.001	0.000	0.000	0.000	-0.002	0.023	0.027	0.059	0.160
	18	0.000	0.001	0.003	0.003	0.006	0.019	0.019	0.055	0.150
	19	0.001	0.001	0.000	0.001	-0.002	-0.002	-0.002	0.024	0.128
	20	0.001	0.001	0.000	0.000	-0.003	-0.005	0.000	0.029	0.147
	21	0.000	0.000	-0.001	-0.001	-0.002	-0.003	0.000	0.020	0.128
	22	0.000	0.000	0.001	0.000	-0.001	-0.027	-0.006	-0.007	0.113
	23	0.000	0.000	0.000	-0.001	-0.004	-0.010	-0.010	0.005	0.104
	24	0.000	0.000	0.001	0.000	-0.001	-0.007	-0.006	0.007	0.107
^{13}C	1	-0.012	-0.013	-0.013	-0.015	-0.027	-0.027	-0.028	0.219	1.262
	2	-0.015	-0.014	-0.015	-0.014	-0.019	-0.032	-0.073	-0.629	-1.560
	4	-0.025	-0.025	-0.025	-0.029	-0.029	-0.057	-0.107	-0.423	-3.014
	7	-0.021	-0.021	-0.021	-0.024	-0.061	-0.046	-0.079	-0.638	-3.091
	11	-0.022	-0.021	-0.020	-0.015	-0.006	-0.007	-0.043	-0.517	-1.761
	12	0.006	0.007	0.007	0.005	0.044	0.018	0.023	0.168	1.084
	13	0.008	0.008	0.007	0.008	0.004	0.005	-0.008	0.355	1.219

Continued on next page

Continued from previous page

El.	Ind.	0.001	0.002	0.003	0.006	0.010	0.020	0.030	0.060	0.100
	14	0.012	0.012	0.012	0.013	0.007	0.011	-0.023	0.250	1.214
^{15}N	3	0.043	0.043	0.042	0.046	0.046	0.098	0.168	1.071	5.808
	6	0.033	0.032	0.032	0.034	0.038	0.104	0.175	0.453	4.867
	9	0.009	0.009	0.011	0.008	0.004	0.072	0.080	0.343	5.240
	10	-0.018	-0.018	-0.016	-0.011	0.019	0.014	0.073	1.307	4.782
^{17}O	5	-0.010	-0.009	-0.008	-0.011	0.030	-0.117	-0.376	-0.450	-10.227
	8	0.007	0.008	0.012	0.012	0.030	-0.132	-0.325	-2.037	-13.229

Table F.40: Errors (in ppm) in isotropic NMR shieldings vs RI-MP2 for the ebselen molecule at different values of T_{CutDO}, with $T_{\mathrm{CutPNO}} = 10^{-12}$ for core and $T_{\mathrm{CutPNO}} = 10^{-10}$ for valence orbitals, $F_{\mathrm{Cut}} = 10^{-5}$, $T_{\mathrm{S}} = 10^{-8}$, and all other DLPNO thresholds equal to 0.

		T_{CutDO}								
El.	Ind.	0.001	0.002	0.003	0.006	0.010	0.020	0.030	0.060	0.100
^{1}H	17	-0.001	-0.001	-0.002	-0.005	-0.009	-0.045	-0.018	0.045	0.055
	18	0.000	0.000	0.000	0.003	-0.002	0.024	0.023	-0.044	0.097
	19	0.000	0.000	-0.001	-0.003	-0.006	0.060	0.040	0.044	0.049
	20	0.000	-0.001	0.000	-0.001	-0.026	-0.124	-0.047	0.002	0.132
	21	-0.001	-0.001	0.000	0.007	0.034	0.081	0.043	0.067	0.096
	22	-0.001	-0.001	-0.001	-0.001	0.041	0.176	0.019	-0.013	0.018
	23	0.001	0.001	0.002	0.010	0.042	0.196	0.012	0.033	0.112
	24	0.001	0.001	0.001	0.002	-0.024	-0.202	-0.029	0.017	0.053
	25	0.000	0.000	0.000	-0.001	-0.033	-0.166	-0.018	0.077	0.063
^{13}C	3	0.006	0.006	0.005	0.002	-0.036	-0.130	-0.072	0.570	-0.729
	4	-0.024	-0.024	-0.028	-0.025	-0.033	-0.246	-0.082	0.302	1.185
	5	-0.012	-0.013	-0.013	-0.019	-0.063	-0.183	-0.121	-0.577	-0.396
	6	-0.003	-0.003	-0.003	-0.011	-0.005	-0.047	0.016	0.490	-0.290
	7	-0.011	-0.011	-0.012	-0.015	-0.027	-0.031	0.011	-0.422	0.624
	8	0.010	0.010	0.012	0.005	0.004	0.071	0.046	0.154	-0.572
	9	0.011	0.011	0.012	0.005	-0.029	-0.130	-0.050	-0.715	1.231
	11	-0.022	-0.022	-0.020	-0.014	-0.014	-0.054	0.071	-0.222	0.976
	12	-0.026	-0.024	-0.025	-0.013	0.038	0.138	0.068	-0.283	-1.193
	13	-0.006	-0.005	-0.008	-0.001	-0.014	0.016	0.003	-0.041	1.191
	14	0.000	0.000	-0.002	-0.011	-0.085	-0.413	-0.042	-0.037	-0.663
	15	-0.007	-0.006	-0.009	-0.025	-0.115	-0.360	-0.074	-0.364	0.437
	16	0.007	0.008	0.005	-0.010	-0.089	-0.392	-0.035	0.005	-0.346
^{15}N	1	0.149	0.150	0.150	0.148	0.088	-0.021	0.229	1.758	5.261
^{17}O	10	0.011	0.010	0.008	0.019	0.029	0.031	-0.555	-3.296	-4.444
^{77}Se	2	-0.472	-0.473	-0.529	-0.834	-0.737	-0.629	-1.544	6.231	20.089

Table F.41: Errors (in ppm) in isotropic NMR shieldings vs RI-MP2 for the penicillin molecule at different values of T_{CutDO}, with $T_{\mathrm{CutPNO}} = 10^{-12}$ for core and $T_{\mathrm{CutPNO}} = 10^{-10}$ for valence orbitals, $F_{\mathrm{Cut}} = 10^{-5}$, $T_{\mathrm{S}} = 10^{-8}$, and all other DLPNO thresholds equal to 0.

		T_{CutDO}								
El.	Ind.	0.001	0.002	0.003	0.006	0.010	0.020	0.030	0.060	0.100
^{1}H	9	0.001	-0.002	-0.006	-0.024	-0.050	-0.099	-0.032	0.173	0.234
	20	0.001	0.001	0.001	-0.001	-0.006	-0.018	-0.018	0.010	0.019
	26	0.000	0.002	0.000	0.002	0.003	-0.029	-0.039	0.079	0.131
	27	0.000	-0.001	-0.004	0.000	0.001	-0.018	-0.009	0.049	0.090
	28	0.000	0.001	0.001	-0.001	-0.023	-0.016	-0.020	0.042	0.092
	29	0.000	-0.001	-0.002	0.000	0.014	-0.003	0.000	0.066	0.105
	30	0.000	0.000	-0.003	-0.007	0.003	-0.015	-0.026	0.088	0.133
	31	0.000	0.002	-0.001	-0.002	0.003	-0.046	-0.042	0.003	0.026
	32	0.001	0.001	0.000	0.000	-0.005	-0.020	-0.003	0.009	0.030
	33	0.001	0.001	0.002	0.003	-0.001	-0.007	-0.006	0.044	0.077
	34	0.000	0.000	-0.002	0.004	-0.016	-0.028	-0.035	0.062	0.124

Continued on next page

Continued from previous page

El.	Ind.	0.001	0.002	0.003	0.006	0.010	0.020	0.030	0.060	0.100
	35	0.001	-0.002	-0.002	-0.018	-0.033	-0.079	-0.037	0.026	0.103
	36	0.001	0.001	0.002	-0.013	-0.043	-0.096	-0.066	0.031	0.156
	37	-0.001	0.000	-0.003	-0.022	-0.044	-0.093	-0.048	0.009	0.057
	38	-0.001	0.000	-0.002	0.003	-0.019	-0.103	-0.043	0.023	0.043
	39	0.001	0.001	0.001	-0.005	0.003	0.020	0.055	0.008	0.083
	40	0.001	0.000	0.001	0.003	-0.002	0.080	-0.006	0.039	0.113
	41	-0.001	0.001	0.001	0.005	0.034	0.092	0.051	0.017	0.065
^{13}C	1	0.003	-0.004	-0.006	-0.031	-0.090	-0.246	-0.093	-0.131	-0.109
	2	-0.003	-0.026	-0.031	-0.025	-0.069	-0.279	-0.112	-0.274	-0.624
	3	-0.017	-0.002	-0.036	-0.100	-0.139	-0.112	0.116	-0.100	0.554
	4	-0.014	-0.001	-0.039	-0.053	-0.111	-0.004	0.045	0.146	0.805
	5	-0.006	0.007	-0.014	-0.006	0.004	-0.026	0.124	-0.150	-0.473
	6	0.010	0.008	0.003	-0.019	-0.054	-0.068	0.003	0.453	1.468
	7	0.014	0.015	0.013	0.005	0.017	-0.007	0.060	0.675	1.546
	8	0.018	0.019	0.017	0.018	0.003	-0.064	-0.036	0.603	1.440
	10	0.006	-0.018	-0.019	-0.066	-0.135	-0.258	-0.114	-0.302	0.206
	15	-0.002	-0.006	-0.002	0.000	-0.023	-0.072	-0.094	-0.074	0.163
	16	-0.022	-0.025	-0.028	-0.043	-0.060	-0.113	-0.125	0.058	-0.084
	17	0.012	0.014	0.015	0.010	0.010	-0.027	-0.043	0.507	1.745
	18	0.000	0.000	-0.005	-0.016	-0.029	-0.020	-0.032	0.542	1.295
	19	-0.016	-0.013	0.008	-0.016	-0.028	-0.044	-0.169	0.082	0.092
	22	0.022	0.022	0.017	0.006	-0.008	0.106	0.243	1.489	2.637
	23	0.019	0.018	0.020	0.028	0.036	0.126	0.275	2.100	3.038
^{15}N	21	0.019	0.018	-0.002	-0.008	0.034	0.075	0.283	1.151	3.600
	25	0.007	0.006	0.001	0.019	0.013	0.153	0.279	2.155	5.145
^{17}O	11	0.012	0.009	0.012	0.070	0.155	0.215	0.308	0.704	0.565
	12	-0.007	0.003	-0.049	0.016	0.064	0.230	0.127	1.100	1.873
	13	0.026	0.004	-0.018	0.094	-0.008	0.013	-0.253	0.390	0.614
	14	0.011	0.012	0.014	0.025	0.025	0.047	0.263	0.691	1.269
^{33}S	24	0.049	0.138	0.309	0.262	1.731	-3.487	-3.241	-11.060	-13.433

Table F.42: Errors (in ppm) in isotropic NMR shieldings vs RI-MP2 for the ATP^{4-} anion at different values of T_{CutDO}, with $T_{\mathrm{CutPNO}} = 10^{-12}$ for core and $T_{\mathrm{CutPNO}} = 10^{-10}$ for valence orbitals, $F_{\mathrm{Cut}} = 10^{-5}$, $T_{\mathrm{S}} = 10^{-5}$, and all other DLPNO thresholds equal to 0.

		T_{CutDO}								
El.	Ind.	0.001	0.002	0.003	0.006	0.010	0.020	0.030	0.060	0.100
^{1}H	6	0.001	0.003	0.005	0.014	0.032	0.018	0.006	0.015	0.073
	9	0.001	0.002	0.002	0.006	0.010	0.012	0.016	0.073	0.084
	11	0.001	0.003	0.004	0.007	0.001	0.000	0.011	0.084	0.097
	12	0.001	0.003	0.002	0.004	0.004	-0.012	-0.008	0.066	0.144
	14	0.001	0.007	0.005	0.010	0.021	0.023	0.019	0.043	0.104
	16	0.001	0.000	0.000	0.008	0.018	0.008	0.013	0.046	0.089
	22	0.002	0.003	0.005	0.005	0.004	0.005	0.002	0.049	0.143
	26	-0.001	-0.001	-0.001	-0.001	0.000	-0.009	0.009	-0.021	0.011
	29	0.000	0.000	0.000	0.001	0.002	0.005	-0.005	0.017	-0.001
	30	0.000	0.000	-0.001	0.005	0.003	0.005	-0.012	0.040	0.067
	31	-0.001	0.001	0.000	0.009	0.011	0.011	0.012	0.020	-0.016
	32	-0.001	0.000	-0.005	0.002	0.020	0.006	-0.009	0.047	0.037
^{13}C	1	0.035	0.032	0.036	0.037	0.040	0.039	0.049	0.804	1.592
	2	0.018	0.017	0.024	0.029	0.020	0.019	0.049	0.611	1.424
	3	0.019	0.018	0.020	0.014	0.018	-0.011	-0.026	0.350	1.358
	4	0.020	0.018	0.019	0.030	0.011	0.005	0.001	0.571	1.182
	7	0.020	0.023	0.022	0.018	0.004	0.002	0.021	0.502	1.284
	17	-0.024	-0.027	-0.032	-0.054	-0.055	-0.119	-0.175	-1.256	0.107
	18	-0.021	-0.018	-0.016	-0.015	-0.032	-0.075	-0.119	-0.941	0.011
	20	-0.009	0.000	0.005	0.028	-0.015	-0.032	-0.034	0.816	1.227
	24	0.008	0.013	0.016	0.025	-0.020	-0.056	-0.076	-1.563	-1.987
	27	-0.031	-0.023	-0.038	-0.051	-0.016	-0.006	-0.032	-0.696	-4.421
^{15}N	13	0.050	0.052	0.056	0.057	0.076	0.140	0.250	2.004	4.993
	21	0.019	0.026	0.028	0.035	0.042	0.097	0.124	0.929	4.797

Continued on next page

Continued from previous page

El.	Ind.	0.001	0.002	0.003	0.006	0.010	0.020	0.030	0.060	0.100
	23	0.029	0.030	0.030	0.028	0.035	-0.014	-0.012	2.144	-4.690
	25	0.070	0.085	0.065	0.063	0.036	0.002	0.011	2.546	2.450
	28	0.009	0.008	0.007	0.007	0.043	0.053	0.048	0.144	1.367
^{17}O	5	0.174	0.170	0.178	0.137	0.173	0.350	0.565	2.030	5.250
	8	0.149	0.152	0.134	0.152	0.130	0.210	0.424	1.456	2.412
	10	0.098	0.091	0.120	0.178	0.213	0.244	0.490	2.033	3.514
	15	0.116	0.095	0.108	0.164	0.192	0.229	0.521	1.601	2.829
	33	0.066	0.084	0.069	-0.098	-0.268	-0.275	-0.224	0.074	0.244
	34	0.055	0.075	0.080	0.103	0.137	0.273	0.658	1.508	3.065
	36	0.045	0.083	0.146	0.012	0.018	-0.176	-0.235	0.717	1.219
	37	0.125	0.122	0.125	0.056	0.056	0.126	0.512	1.988	2.329
	38	0.061	0.039	0.037	0.061	0.120	0.352	0.479	1.168	2.168
	39	0.099	0.110	0.136	0.169	0.285	0.470	0.648	2.238	5.119
	41	0.045	0.029	0.021	0.025	-0.017	0.020	0.063	0.305	0.606
	42	0.030	0.022	0.025	0.034	0.062	0.054	0.079	0.416	0.792
	43	-0.004	0.003	0.008	0.035	-0.009	-0.124	-0.089	-0.519	-0.350
^{31}P	19	0.043	0.048	0.040	0.068	0.070	-0.040	0.003	0.092	0.138
	35	0.051	0.053	0.051	0.040	0.016	-0.003	-0.085	0.154	-0.363
	40	0.028	0.029	0.029	0.044	0.042	0.091	0.115	0.107	0.502

Table F.43: Errors (in ppm) in isotropic NMR shieldings vs RI-MP2 for the caffeine molecule at different values of T_{CutDO}, with $T_{\mathrm{CutPNO}} = 10^{-12}$ for core and $T_{\mathrm{CutPNO}} = 10^{-10}$ for valence orbitals, $F_{\mathrm{Cut}} = 10^{-5}$, $T_{\mathrm{S}} = 10^{-5}$, and all other DLPNO thresholds equal to 0.

		T_{CutDO}								
El.	Ind.	0.001	0.002	0.003	0.006	0.010	0.020	0.030	0.060	0.100
^{1}H	15	0.000	0.000	0.001	0.002	0.000	0.009	0.018	0.004	0.026
	16	0.000	-0.001	0.000	-0.001	-0.001	0.003	0.005	0.033	0.134
	17	0.001	0.001	0.001	0.001	0.002	0.027	0.026	0.060	0.160
	18	0.000	0.000	0.000	0.000	0.001	0.010	0.017	0.055	0.150
	19	0.001	0.000	0.000	0.002	0.000	-0.004	-0.004	0.024	0.128
	20	0.001	0.001	0.000	0.000	-0.002	-0.006	0.001	0.030	0.147
	21	0.000	0.000	0.000	0.001	-0.002	-0.003	-0.001	0.020	0.128
	22	0.001	0.001	0.000	0.000	0.001	-0.024	-0.003	-0.007	0.113
	23	0.000	0.000	0.000	0.000	0.000	-0.007	-0.003	0.005	0.104
	24	0.000	0.000	0.001	0.001	0.002	-0.007	-0.003	0.007	0.107
^{13}C	1	-0.012	-0.012	-0.011	-0.019	-0.022	-0.052	-0.062	0.221	1.262
	2	-0.015	-0.014	-0.014	-0.016	-0.015	-0.029	-0.075	-0.629	-1.560
	4	-0.025	-0.025	-0.025	-0.020	-0.027	-0.083	-0.126	-0.423	-3.014
	7	-0.021	-0.020	-0.021	-0.025	-0.017	-0.053	-0.080	-0.635	-3.091
	11	-0.021	-0.023	-0.022	-0.022	-0.019	-0.046	-0.048	-0.520	-1.761
	12	0.006	0.005	0.003	0.001	0.000	0.021	0.028	0.165	1.084
	13	0.008	0.007	0.007	0.001	0.004	0.006	-0.006	0.354	1.219
	14	0.012	0.011	0.009	0.005	0.009	0.009	-0.017	0.250	1.214
^{15}N	3	0.043	0.043	0.042	0.057	0.069	0.094	0.165	1.071	5.808
	6	0.033	0.033	0.035	0.035	0.045	0.055	0.185	0.452	4.867
	9	0.009	0.009	0.009	0.014	0.033	0.056	0.085	0.340	5.240
	10	-0.018	-0.019	-0.019	-0.022	-0.005	0.020	0.073	1.310	4.782
^{17}O	5	-0.010	-0.006	0.005	0.017	0.001	-0.099	-0.309	-0.451	-10.227
	8	0.007	0.007	0.003	0.003	-0.008	-0.094	-0.315	-2.031	-13.229

Table F.44: Errors (in ppm) in isotropic NMR shieldings vs RI-MP2 for the ebselen molecule at different values of T_{CutDO}, with $T_{\mathrm{CutPNO}} = 10^{-12}$ for core and $T_{\mathrm{CutPNO}} = 10^{-10}$ for valence orbitals, $F_{\mathrm{Cut}} = 10^{-5}$, $T_{\mathrm{S}} = 10^{-5}$, and all other DLPNO thresholds equal to 0.

		T_{CutDO}								
El.	Ind.	0.001	0.002	0.003	0.006	0.010	0.020	0.030	0.060	0.100
^{1}H	17	-0.001	-0.001	0.001	0.001	0.004	0.002	-0.003	0.039	0.052
	18	0.000	0.000	0.001	0.007	0.010	0.000	0.013	-0.044	0.092
	19	0.000	0.000	0.001	0.003	0.003	0.012	0.024	0.045	0.046
	20	0.000	0.001	0.001	0.006	0.008	-0.017	-0.022	0.001	0.122
	21	0.000	-0.001	-0.001	0.000	0.003	0.016	0.033	0.069	0.094
	22	-0.001	-0.001	-0.002	-0.004	0.000	0.007	0.003	-0.011	0.018
	23	0.001	0.001	0.000	-0.003	-0.011	0.011	0.012	0.031	0.113
	24	0.002	0.001	0.000	-0.005	-0.014	-0.018	-0.024	0.032	0.057
	25	0.001	0.001	0.000	0.001	0.002	0.007	0.012	0.080	0.056
^{13}C	3	0.006	0.005	0.000	-0.016	-0.036	-0.035	-0.021	0.588	-0.796
	4	-0.017	-0.016	-0.019	-0.029	-0.044	-0.059	0.010	0.240	1.060
	5	-0.013	-0.017	-0.016	-0.020	-0.045	-0.069	-0.100	-0.609	-0.480
	6	-0.007	-0.008	-0.005	-0.005	-0.008	0.020	0.060	0.563	-0.250
	7	-0.013	-0.013	-0.014	-0.006	0.002	-0.011	0.007	-0.474	0.582
	8	0.009	0.010	0.010	0.019	0.027	0.044	0.062	0.200	-0.551
	9	0.010	0.010	0.010	0.019	0.027	0.002	-0.014	-0.761	1.190
	11	-0.021	-0.023	-0.028	0.014	-0.007	0.053	0.072	-0.218	0.987
	12	-0.026	-0.025	-0.024	0.013	-0.006	0.044	0.074	-0.261	-1.184
	13	-0.006	-0.007	-0.011	-0.016	-0.022	0.037	0.028	-0.055	1.190
	14	0.000	-0.001	-0.006	-0.004	-0.028	-0.023	0.033	-0.013	-0.686
	15	-0.006	-0.007	-0.003	0.004	0.000	-0.033	-0.039	-0.378	0.398
	16	0.008	0.006	0.000	0.013	0.025	-0.010	0.008	0.044	-0.337
^{15}N	1	0.150	0.150	0.158	0.146	0.173	0.181	0.287	2.059	5.465
^{17}O	10	0.010	0.016	0.034	0.127	0.198	0.196	-0.383	-3.425	-4.635
^{77}Se	2	-0.487	-0.453	-0.535	-0.381	-0.016	0.592	0.737	11.252	27.770

Table F.45: Errors (in ppm) in isotropic NMR shieldings vs RI-MP2 for the penicillin molecule at different values of T_{CutDO}, with $T_{\mathrm{CutPNO}} = 10^{-12}$ for core and $T_{\mathrm{CutPNO}} = 10^{-10}$ for valence orbitals, $F_{\mathrm{Cut}} = 10^{-5}$, $T_{\mathrm{S}} = 10^{-5}$, and all other DLPNO thresholds equal to 0.

		T_{CutDO}								
El.	Ind.	0.001	0.002	0.003	0.006	0.010	0.020	0.030	0.060	0.100
^{1}H	9	0.001	0.001	0.003	-0.003	-0.015	-0.065	-0.040	0.125	0.195
	20	0.001	0.000	0.002	0.001	-0.004	-0.006	-0.012	0.003	0.016
	26	0.000	0.001	0.000	0.003	0.012	-0.014	-0.022	0.027	0.081
	27	-0.001	-0.001	-0.002	-0.003	0.004	-0.006	-0.009	0.102	0.149
	28	0.000	0.000	0.000	-0.001	-0.014	-0.014	-0.003	0.019	0.076
	29	0.001	0.001	0.001	0.002	0.008	0.003	0.022	0.044	0.092
	30	0.000	0.000	-0.002	0.004	0.000	-0.011	-0.007	0.024	0.079
	31	0.001	0.001	0.001	0.000	0.010	-0.023	-0.012	0.056	0.093
	32	0.001	0.001	0.003	0.001	-0.006	-0.002	0.027	0.061	0.096
	33	0.001	0.000	0.000	0.003	0.002	0.004	0.017	0.057	0.097
	34	0.000	0.002	0.001	-0.003	0.000	-0.015	-0.047	0.054	0.117
	35	0.000	0.000	0.000	0.002	0.003	-0.029	-0.041	0.019	0.094
	36	0.001	0.002	0.003	0.002	0.009	-0.036	-0.070	0.031	0.153
	37	0.000	0.000	0.001	-0.001	-0.003	-0.028	-0.058	0.026	0.059
	38	-0.001	-0.001	-0.002	-0.002	-0.005	-0.011	-0.042	0.008	0.025
	39	0.001	0.002	0.002	0.006	0.002	0.050	0.029	0.014	0.076
	40	0.000	-0.001	0.000	0.000	-0.002	-0.020	0.002	0.024	0.093
	41	-0.001	-0.001	0.000	0.001	0.004	0.040	0.044	0.005	0.047
^{13}C	1	0.005	0.007	0.008	-0.014	-0.009	-0.078	-0.093	-0.131	-0.127
	2	-0.007	-0.008	-0.010	-0.009	-0.017	-0.118	-0.116	-0.288	-0.645
	3	-0.005	0.000	0.001	0.008	0.003	0.082	0.087	-0.108	0.528
	4	0.000	-0.003	-0.007	-0.001	0.002	0.001	0.055	0.131	0.780
	5	-0.003	-0.004	-0.009	-0.023	0.000	0.078	0.133	-0.162	-0.499
	6	0.011	0.011	0.014	0.009	0.008	0.000	-0.005	0.448	1.459
	7	0.014	0.014	0.015	0.014	0.022	0.012	0.074	0.638	1.533

Continued on next page

Continued from previous page

El.	Ind.	0.001	0.002	0.003	0.006	0.010	0.020	0.030	0.060	0.100
	8	0.018	0.019	0.015	0.012	-0.001	-0.030	0.010	0.642	1.495
	10	0.001	0.005	0.015	0.021	0.012	-0.078	-0.114	-0.306	0.195
	15	-0.002	-0.001	0.004	-0.009	-0.030	-0.074	-0.082	-0.085	0.153
	16	-0.024	-0.020	-0.013	-0.042	-0.047	-0.124	-0.138	0.051	-0.094
	17	0.015	0.015	0.006	0.001	0.022	-0.008	-0.019	0.454	1.698
	18	0.001	0.001	-0.027	0.002	-0.014	-0.031	-0.063	0.517	1.287
	19	-0.014	0.004	-0.008	-0.022	-0.037	-0.125	-0.181	0.031	0.052
	22	0.024	0.018	0.007	0.005	0.006	0.054	0.192	1.499	2.642
	23	0.021	0.021	0.022	0.027	0.061	0.147	0.289	2.076	3.013
^{15}N	21	0.021	0.023	0.019	0.062	0.089	0.099	0.267	1.136	3.586
	25	0.007	-0.002	-0.004	0.055	0.047	0.144	0.322	2.125	5.132
^{17}O	11	0.014	0.008	0.025	0.014	0.075	0.153	0.245	0.690	0.552
	12	-0.010	-0.012	0.018	0.003	0.030	0.317	0.149	1.087	1.865
	13	0.046	0.012	0.019	0.013	0.022	0.001	-0.285	0.380	0.599
	14	0.014	0.008	0.025	0.025	0.019	0.074	0.262	0.695	1.264
^{33}S	24	0.064	0.070	0.068	0.184	0.317	0.287	-1.255	3.327	7.608

F.5 NMR shielding errors due to pair prescreening

Calculations including terms due to ΔE_{Pre} are shown in Tables F.46–F.49 and those neglecting these terms – in Tables F.50–F.53.

Table F.46: Errors (in ppm) in isotropic NMR shieldings vs RI-MP2 for the ATP^{4-} anion at different values of T_{CutPre}, including terms due to ΔE_{Pre}, with $T_{\mathrm{CutPNO}} = 10^{-12}$ for core and $T_{\mathrm{CutPNO}} = 10^{-10}$ for valence orbitals, $T_{\mathrm{CutDOij}} = 0.05$, $T_{\mathrm{CutDO}} = 10^{-3}$, $F_{\mathrm{Cut}} = 10^{-5}$, $T_{\mathrm{S}} = 10^{-8}$, and the remaining DLPNO thresholds equal to 0.

		T_{CutPre}						
El.	Ind.	10^{-2}	10^{-3}	10^{-4}	10^{-5}	10^{-6}	10^{-7}	10^{-8}
^{1}H	6	0.007	0.075	0.012	0.000	0.001	0.001	0.001
	9	-0.231	0.089	0.036	0.007	0.002	0.001	0.001
	11	0.200	0.141	0.032	0.007	0.002	0.001	0.001
	12	-0.034	0.138	0.040	0.007	0.001	0.001	0.001
	14	-0.317	-0.019	0.025	0.003	0.001	0.001	0.001
	16	0.175	0.161	0.030	0.004	0.001	0.001	0.001
	22	0.140	0.114	0.036	0.007	0.002	0.002	0.002
	26	0.499	0.082	0.010	0.001	-0.001	-0.001	-0.001
	29	-0.402	-0.016	0.005	0.000	0.000	0.000	0.000
	30	0.292	0.086	0.020	0.000	0.000	0.000	0.000
	31	0.093	0.056	-0.022	-0.008	-0.001	-0.001	-0.001
	32	-1.016	-0.238	-0.070	-0.015	-0.002	-0.001	-0.001
^{13}C	1	7.291	2.557	0.719	0.107	0.036	0.035	0.035
	2	6.174	2.153	0.648	0.099	0.018	0.019	0.018
	3	4.078	2.204	0.596	0.067	0.018	0.019	0.019
	4	6.726	2.376	0.551	0.105	0.027	0.021	0.020
	7	6.681	2.093	0.669	0.064	0.024	0.020	0.020
	17	-4.177	-2.535	0.078	-0.115	-0.041	-0.025	-0.024
	18	0.264	-1.723	-0.581	-0.097	-0.031	-0.022	-0.021
	20	8.079	1.401	0.522	0.012	-0.008	-0.010	-0.009
	24	0.460	-1.932	-0.325	-0.025	0.003	0.008	0.008
	27	-2.431	-2.226	-0.161	-0.165	-0.032	-0.031	-0.031
^{15}N	13	16.616	9.455	2.117	0.190	0.068	0.049	0.050
	21	6.681	5.717	0.122	0.105	0.013	0.020	0.019
	23	37.400	10.822	1.115	0.192	0.061	0.029	0.029
	25	25.704	6.467	1.266	0.180	0.094	0.070	0.070
	28	-9.273	1.181	0.431	-0.007	0.017	0.009	0.009
^{17}O	5	14.468	9.213	2.184	0.490	0.188	0.176	0.174
	8	5.530	1.187	0.802	0.253	0.155	0.151	0.149
	10	4.652	3.339	0.895	0.246	0.104	0.100	0.098

Continued on next page

Continued from previous page

El.	Ind.	10^{-2}	10^{-3}	10^{-4}	10^{-5}	10^{-6}	10^{-7}	10^{-8}
	15	16.872	8.374	1.203	0.291	0.108	0.119	0.116
	33	-1.117	1.192	0.657	0.165	0.070	0.069	0.066
	34	29.712	13.341	0.454	0.055	0.029	0.044	0.054
	36	21.164	5.771	0.936	0.203	0.051	0.045	0.046
	37	27.581	9.639	2.730	0.287	0.134	0.129	0.125
	38	18.235	10.119	1.425	0.096	0.067	0.053	0.061
	39	17.737	9.672	1.353	0.254	0.109	0.098	0.099
	41	17.300	6.113	1.109	0.257	0.054	0.047	0.045
	42	11.231	4.870	1.003	0.223	0.037	0.034	0.031
	43	12.410	3.515	0.732	0.154	0.000	-0.001	-0.004
^{31}P	19	-7.545	-6.453	1.077	0.344	0.054	0.045	0.043
	35	-6.074	-0.760	1.924	0.291	0.072	0.055	0.051
	40	-9.875	-11.138	1.512	0.343	0.040	0.033	0.028

Table F.47: Errors (in ppm) in isotropic NMR shieldings vs RI-MP2 for the caffeine molecule at different values of T_{CutPre}, including terms due to ΔE_{Pre}, with $T_{\mathrm{CutPNO}} = 10^{-12}$ for core and $T_{\mathrm{CutPNO}} = 10^{-10}$ for valence orbitals, $T_{\mathrm{CutDOij}} = 0.05$, $T_{\mathrm{CutDO}} = 10^{-3}$, $F_{\mathrm{Cut}} = 10^{-5}$, $T_{\mathrm{S}} = 10^{-8}$, and the remaining DLPNO thresholds equal to 0.

		T_{CutPre}						
El.	Ind.	10^{-2}	10^{-3}	10^{-4}	10^{-5}	10^{-6}	10^{-7}	10^{-8}
^{1}H	15	0.300	0.058	0.009	0.001	0.000	0.000	0.000
	16	0.079	0.074	0.015	0.001	0.000	0.000	0.000
	17	0.045	0.089	0.023	0.002	0.001	0.001	0.001
	18	-0.011	0.065	0.015	0.001	0.000	0.000	0.000
	19	0.019	0.031	0.012	0.002	0.001	0.001	0.001
	20	0.188	0.079	0.020	0.002	0.001	0.001	0.001
	21	0.096	0.060	0.015	0.002	0.000	0.000	0.000
	22	0.185	0.100	0.020	0.002	0.001	0.001	0.001
	23	0.015	0.037	0.008	0.001	0.000	0.000	0.000
	24	-0.033	0.014	0.004	0.000	0.000	0.000	0.000
^{13}C	1	3.251	1.517	0.198	-0.021	-0.013	-0.013	-0.012
	2	1.070	-1.304	-0.123	-0.025	-0.020	-0.015	-0.015
	4	-0.495	-1.302	-0.158	-0.041	-0.033	-0.025	-0.025
	7	-0.357	-1.525	0.018	-0.079	-0.027	-0.022	-0.021
	11	0.808	-0.700	-0.386	-0.039	-0.030	-0.021	-0.021
	12	3.745	1.122	0.221	0.025	0.006	0.007	0.006
	13	2.599	0.965	0.359	0.026	0.009	0.008	0.008
	14	2.215	0.732	0.281	0.011	0.013	0.012	0.012
^{15}N	3	18.347	8.683	1.893	0.168	0.064	0.046	0.043
	6	21.258	7.035	1.061	0.081	0.036	0.029	0.033
	9	20.577	6.988	1.381	0.052	0.006	0.010	0.009
	10	17.380	6.027	1.584	-0.021	-0.015	-0.017	-0.018
^{17}O	5	-11.433	-7.645	0.187	-0.135	-0.053	-0.013	-0.010
	8	-8.138	-2.105	1.339	-0.134	0.014	0.003	0.007

Table F.48: Errors (in ppm) in isotropic NMR shieldings vs RI-MP2 for the ebselen molecule at different values of T_{CutPre}, including terms due to ΔE_{Pre}, with $T_{\mathrm{CutPNO}} = 10^{-12}$ for core and $T_{\mathrm{CutPNO}} = 10^{-10}$ for valence orbitals, $T_{\mathrm{CutDOij}} = 0.05$, $T_{\mathrm{CutDO}} = 10^{-3}$, $F_{\mathrm{Cut}} = 10^{-5}$, $T_{\mathrm{S}} = 10^{-8}$, and the remaining DLPNO thresholds equal to 0.

		T_{CutPre}						
El.	Ind.	10^{-2}	10^{-3}	10^{-4}	10^{-5}	10^{-6}	10^{-7}	10^{-8}
^{1}H	17	-0.043	0.037	0.008	0.000	-0.001	-0.001	-0.001
	18	0.115	-0.011	0.001	0.000	0.000	0.000	0.000
	19	0.144	0.060	0.013	0.002	0.000	0.000	0.000
	20	0.148	0.053	0.000	0.002	0.000	0.000	0.000

Continued on next page

Continued from previous page

El.	Ind.	10^{-2}	10^{-3}	10^{-4}	10^{-5}	10^{-6}	10^{-7}	10^{-8}
	21	0.099	0.107	0.012	0.004	0.000	0.000	0.000
	22	0.127	-0.016	0.007	-0.002	-0.001	-0.001	-0.001
	23	0.339	0.131	0.023	0.007	0.002	0.002	0.001
	24	0.251	-0.055	0.003	0.000	0.002	0.001	0.002
	25	-0.226	0.009	0.011	0.003	0.001	0.001	0.001
^{13}C	3	2.945	0.367	0.000	-0.091	-0.004	0.003	0.006
	4	-1.009	-0.367	-0.146	0.094	0.017	-0.011	-0.017
	5	3.838	-1.524	-0.274	-0.107	-0.024	-0.014	-0.013
	6	5.417	0.999	0.260	-0.041	-0.010	-0.008	-0.007
	7	-0.105	-0.755	0.023	-0.047	-0.025	-0.014	-0.013
	8	4.706	1.060	0.365	0.038	0.014	0.009	0.009
	9	3.249	0.528	-0.001	-0.001	0.006	0.009	0.010
	11	2.979	1.665	0.193	0.024	-0.017	-0.020	-0.021
	12	3.908	-0.369	0.455	-0.035	-0.025	-0.027	-0.026
	13	2.172	2.165	0.313	0.084	0.000	-0.005	-0.006
	14	1.543	-1.791	-0.011	-0.087	-0.005	-0.002	0.000
	15	2.897	0.993	0.354	0.063	-0.001	-0.005	-0.006
	16	-0.920	-0.387	0.032	-0.013	0.005	0.007	0.008
^{15}N	1	3.326	14.081	3.910	0.817	0.232	0.154	0.150
^{17}O	10	-17.337	-16.236	-3.304	-0.711	-0.027	0.004	0.010
^{77}Se	2	103.915	21.336	4.411	-0.826	-0.498	-0.501	-0.488

Table F.49: Errors (in ppm) in isotropic NMR shieldings vs RI-MP2 for the penicillin molecule at different values of T_{CutPre}, including terms due to ΔE_{Pre}, with $T_{\mathrm{CutPNO}} = 10^{-12}$ for core and $T_{\mathrm{CutPNO}} = 10^{-10}$ for valence orbitals, $T_{\mathrm{CutDOij}} = 0.05$, $T_{\mathrm{CutDO}} = 10^{-3}$, $F_{\mathrm{Cut}} = 10^{-5}$, $T_{\mathrm{S}} = 10^{-8}$, and the remaining DLPNO thresholds equal to 0.

		T_{CutPre}						
El.	Ind.	10^{-2}	10^{-3}	10^{-4}	10^{-5}	10^{-6}	10^{-7}	10^{-8}
^{1}H	9	0.260	0.166	0.041	0.005	0.001	0.001	0.001
	20	-0.158	-0.009	-0.016	0.001	0.001	0.001	0.001
	26	0.639	0.192	0.032	0.004	0.000	0.000	0.000
	27	0.161	0.130	0.031	0.001	-0.001	-0.001	-0.001
	28	-0.769	-0.019	0.004	0.002	0.000	0.000	0.000
	29	0.541	0.170	0.035	0.003	0.001	0.001	0.001
	30	0.379	0.106	0.020	0.001	0.000	0.000	0.000
	31	0.392	0.134	0.027	0.003	0.001	0.001	0.001
	32	0.245	0.118	0.019	0.002	0.001	0.001	0.001
	33	-0.230	0.054	0.021	0.004	0.001	0.001	0.001
	34	0.385	0.139	0.030	0.003	0.000	0.000	0.000
	35	0.027	0.083	0.021	0.002	0.000	0.000	0.000
	36	0.162	0.130	0.032	0.003	0.001	0.001	0.001
	37	0.379	0.073	0.019	0.002	0.000	0.000	0.000
	38	-0.074	-0.055	-0.009	-0.001	-0.001	-0.001	-0.001
	39	0.225	0.080	0.017	0.002	0.001	0.001	0.001
	40	0.331	0.109	0.016	0.001	0.000	0.000	0.000
	41	-0.253	-0.067	-0.012	-0.001	-0.001	-0.001	-0.001
^{13}C	1	2.157	-0.510	-0.097	-0.030	0.001	0.005	0.005
	2	-1.370	-1.483	-0.261	-0.035	-0.013	-0.007	-0.007
	3	3.065	1.324	0.257	-0.017	-0.001	-0.005	-0.005
	4	2.696	1.540	0.264	-0.008	0.005	0.000	0.000
	5	-2.603	-1.181	0.052	-0.013	-0.007	-0.004	-0.003
	6	-0.539	0.984	0.270	0.023	0.009	0.011	0.011
	7	11.267	2.154	0.485	0.030	0.013	0.014	0.014
	8	12.950	2.281	0.328	0.049	0.018	0.017	0.018
	10	3.719	1.400	0.343	0.010	0.005	0.001	0.001
	15	3.009	-0.443	0.124	-0.020	-0.002	-0.002	-0.002
	16	2.137	-0.722	-0.183	-0.067	-0.025	-0.025	-0.024
	17	8.508	3.181	0.585	0.101	0.015	0.015	0.015
	18	8.080	2.532	0.606	0.039	0.003	0.001	0.001
	19	1.407	0.110	0.236	-0.037	-0.015	-0.014	-0.014

Continued on next page

Continued from previous page

El.	Ind.	10^{-2}	10^{-3}	10^{-4}	10^{-5}	10^{-6}	10^{-7}	10^{-8}
	22	8.390	3.132	1.087	0.099	0.038	0.024	0.024
	23	12.636	4.065	1.598	0.153	0.039	0.022	0.021
^{15}N	21	14.103	5.944	1.349	0.144	0.036	0.021	0.021
	25	20.379	8.060	1.512	0.143	0.015	0.007	0.007
^{17}O	11	15.412	2.944	1.196	-0.028	0.027	0.013	0.014
	12	-9.632	-6.500	-1.092	-0.349	-0.014	-0.011	-0.010
	13	9.009	-1.442	-0.217	-0.147	0.036	0.047	0.046
	14	19.181	6.357	0.621	0.105	0.018	0.014	0.014
^{33}S	24	63.719	15.333	3.685	0.179	0.106	0.067	0.064

Table F.50: Errors (in ppm) in isotropic NMR shieldings vs RI-MP2 for the ATP^{4-} anion at different values of T_{CutPre}, neglecting terms due to ΔE_{Pre}, with $T_{\mathrm{CutPNO}} = 10^{-12}$ for core and $T_{\mathrm{CutPNO}} = 10^{-10}$ for valence orbitals, $T_{\mathrm{CutDOij}} = 0.05$, $T_{\mathrm{CutDO}} = 10^{-3}$, $F_{\mathrm{Cut}} = 10^{-5}$, $T_{\mathrm{S}} = 10^{-8}$, and the remaining DLPNO thresholds equal to 0.

		T_{CutPre}						
El.	Ind.	10^{-2}	10^{-3}	10^{-4}	10^{-5}	10^{-6}	10^{-7}	10^{-8}
^{1}H	6	0.660	0.168	0.032	0.002	0.001	0.001	0.001
	9	0.718	0.226	0.050	0.009	0.002	0.001	0.001
	11	0.623	0.183	0.039	0.008	0.002	0.001	0.001
	12	0.686	0.212	0.053	0.008	0.001	0.001	0.001
	14	0.522	0.154	0.047	0.005	0.001	0.001	0.001
	16	0.427	0.125	0.030	0.004	0.001	0.001	0.001
	22	0.455	0.098	0.034	0.007	0.002	0.002	0.002
	26	0.584	0.080	0.011	0.002	-0.001	-0.001	-0.001
	29	0.041	0.055	0.012	0.000	0.000	0.000	0.000
	30	-0.047	0.088	0.021	0.000	0.000	0.000	0.000
	31	-0.528	-0.096	-0.041	-0.009	-0.001	-0.001	-0.001
	32	-0.486	-0.122	-0.053	-0.013	-0.002	-0.001	-0.001
^{13}C	1	11.503	3.071	0.814	0.117	0.036	0.036	0.035
	2	11.538	2.980	0.784	0.114	0.019	0.019	0.018
	3	12.074	3.381	0.800	0.086	0.019	0.019	0.019
	4	9.722	2.701	0.607	0.111	0.028	0.021	0.020
	7	7.277	2.510	0.677	0.067	0.024	0.021	0.020
	17	-5.969	-3.287	0.027	-0.125	-0.043	-0.025	-0.024
	18	-2.398	-3.120	-0.749	-0.114	-0.032	-0.022	-0.021
	20	13.827	1.763	0.589	0.019	-0.007	-0.010	-0.009
	24	-3.724	-2.799	-0.419	-0.028	0.003	0.008	0.008
	27	-20.879	-3.116	-0.195	-0.193	-0.034	-0.031	-0.031
^{15}N	13	33.909	12.273	2.512	0.226	0.072	0.049	0.050
	21	8.186	6.660	0.108	0.116	0.014	0.020	0.019
	23	56.777	12.709	1.177	0.227	0.067	0.030	0.029
	25	36.615	7.745	1.424	0.189	0.096	0.070	0.070
	28	1.951	2.873	0.644	0.030	0.022	0.009	0.009
^{17}O	5	32.097	12.036	2.579	0.525	0.190	0.176	0.174
	8	13.313	4.382	1.175	0.299	0.157	0.151	0.149
	10	18.636	7.243	1.773	0.354	0.107	0.101	0.098
	15	24.689	8.088	1.057	0.302	0.108	0.120	0.116
	33	26.522	7.335	1.537	0.327	0.081	0.069	0.066
	34	35.495	12.152	0.512	0.059	0.029	0.044	0.054
	36	26.425	4.477	0.799	0.171	0.047	0.045	0.046
	37	36.822	9.213	2.691	0.290	0.134	0.129	0.125
	38	36.760	13.196	1.813	0.140	0.071	0.053	0.061
	39	32.575	11.386	1.715	0.274	0.110	0.098	0.099
	41	28.732	5.712	1.144	0.273	0.055	0.047	0.045
	42	28.988	5.696	1.157	0.252	0.039	0.034	0.031
	43	29.498	4.768	0.791	0.178	0.001	-0.001	-0.004
^{31}P	19	25.352	-6.948	1.391	0.396	0.056	0.046	0.043
	35	23.320	-0.652	2.218	0.308	0.074	0.055	0.051
	40	21.238	-14.023	1.393	0.343	0.041	0.033	0.028

Table F.51: Errors (in ppm) in isotropic NMR shieldings vs RI-MP2 for the caffeine molecule at different values of T_{CutPre}, neglecting terms due to ΔE_{Pre}, with $T_{\mathrm{CutPNO}} = 10^{-12}$ for core and $T_{\mathrm{CutPNO}} = 10^{-10}$ for valence orbitals, $T_{\mathrm{CutDOij}} = 0.05$, $T_{\mathrm{CutDO}} = 10^{-3}$, $F_{\mathrm{Cut}} = 10^{-5}$, $T_{\mathrm{S}} = 10^{-8}$, and the remaining DLPNO thresholds equal to 0.

		T_{CutPre}						
El.	Ind.	10^{-2}	10^{-3}	10^{-4}	10^{-5}	10^{-6}	10^{-7}	10^{-8}
^{1}H	15	0.229	0.029	0.006	0.001	0.000	0.000	0.000
	16	0.334	0.104	0.018	0.001	0.000	0.000	0.000
	17	0.432	0.145	0.027	0.003	0.001	0.001	0.001
	18	0.388	0.127	0.020	0.002	0.000	0.000	0.000
	19	0.144	0.069	0.015	0.002	0.001	0.001	0.001
	20	0.291	0.112	0.022	0.003	0.001	0.001	0.001
	21	0.271	0.100	0.019	0.002	0.000	0.000	0.000
	22	0.254	0.118	0.022	0.002	0.001	0.001	0.001
	23	0.197	0.069	0.010	0.001	0.001	0.000	0.000
	24	0.036	0.029	0.004	0.000	0.000	0.000	0.000
^{13}C	1	9.797	2.035	0.268	-0.020	-0.013	-0.013	-0.012
	2	3.389	-1.399	-0.107	-0.023	-0.020	-0.015	-0.015
	4	0.448	-1.233	-0.181	-0.041	-0.033	-0.025	-0.025
	7	-1.207	-1.695	0.000	-0.078	-0.027	-0.022	-0.021
	11	-1.396	-1.018	-0.424	-0.039	-0.030	-0.021	-0.021
	12	4.124	1.005	0.215	0.023	0.006	0.007	0.006
	13	2.659	0.954	0.351	0.026	0.009	0.008	0.008
	14	1.998	0.668	0.267	0.010	0.013	0.012	0.012
^{15}N	3	28.625	9.716	1.988	0.171	0.065	0.046	0.043
	6	26.007	7.387	1.123	0.080	0.036	0.029	0.033
	9	24.849	7.263	1.467	0.055	0.006	0.010	0.009
	10	19.205	6.540	1.705	-0.020	-0.015	-0.017	-0.018
^{17}O	5	-0.717	-4.560	0.560	-0.118	-0.053	-0.013	-0.010
	8	7.738	-0.068	1.609	-0.131	0.015	0.003	0.007

Table F.52: Errors (in ppm) in isotropic NMR shieldings vs RI-MP2 for the ebselen molecule at different values of T_{CutPre}, neglecting terms due to ΔE_{Pre}, with $T_{\mathrm{CutPNO}} = 10^{-12}$ for core and $T_{\mathrm{CutPNO}} = 10^{-10}$ for valence orbitals, $T_{\mathrm{CutDOij}} = 0.05$, $T_{\mathrm{CutDO}} = 10^{-3}$, $F_{\mathrm{Cut}} = 10^{-5}$, $T_{\mathrm{S}} = 10^{-8}$, and the remaining DLPNO thresholds equal to 0.

		T_{CutPre}						
El.	Ind.	10^{-2}	10^{-3}	10^{-4}	10^{-5}	10^{-6}	10^{-7}	10^{-8}
^{1}H	17	0.350	0.098	0.018	0.002	-0.001	-0.001	-0.001
	18	0.281	-0.007	0.002	-0.001	0.000	0.000	0.000
	19	0.319	0.087	0.016	0.002	0.000	0.000	0.000
	20	0.419	0.046	0.002	0.002	0.000	0.000	0.000
	21	0.340	0.105	0.017	0.004	0.000	0.000	0.000
	22	0.350	-0.010	0.008	-0.003	-0.001	-0.001	-0.001
	23	0.342	0.147	0.025	0.008	0.002	0.002	0.001
	24	0.500	-0.024	0.009	0.000	0.002	0.001	0.002
	25	0.450	0.070	0.024	0.004	0.001	0.001	0.001
^{13}C	3	5.207	0.686	0.036	-0.088	-0.003	0.003	0.006
	4	5.129	-0.295	-0.119	0.092	0.016	-0.011	-0.017
	5	-3.983	-1.360	-0.316	-0.109	-0.024	-0.014	-0.013
	6	4.496	1.408	0.323	-0.032	-0.010	-0.008	-0.007
	7	0.979	-1.043	0.019	-0.051	-0.025	-0.014	-0.013
	8	4.133	1.357	0.377	0.042	0.014	0.009	0.009
	9	3.906	0.195	0.000	-0.001	0.006	0.009	0.010
	11	2.820	1.642	0.185	0.019	-0.017	-0.020	-0.021
	12	4.423	-0.633	0.438	-0.037	-0.025	-0.027	-0.026
	13	3.071	2.482	0.373	0.093	0.000	-0.005	-0.006
	14	7.378	-1.555	0.047	-0.085	-0.005	-0.002	0.000
	15	3.365	1.281	0.384	0.062	-0.001	-0.005	-0.006
	16	3.937	-0.327	0.078	-0.007	0.005	0.007	0.008
^{15}N	1	43.368	17.632	4.400	0.845	0.234	0.154	0.150

Continued on next page

Continued from previous page

El.	Ind.	10^{-2}	10^{-3}	10^{-4}	10^{-5}	10^{-6}	10^{-7}	10^{-8}
^{17}O	10	-16.418	-3.734	-2.077	-0.600	-0.019	0.005	0.010
^{77}Se	2	77.451	18.174	3.487	-0.964	-0.505	-0.501	-0.488

Table F.53: Errors (in ppm) in isotropic NMR shieldings vs RI-MP2 for the penicillin molecule at different values of T_{CutPre}, neglecting terms due to ΔE_{Pre}, with $T_{\mathrm{CutPNO}} = 10^{-12}$ for core and $T_{\mathrm{CutPNO}} = 10^{-10}$ for valence orbitals, $T_{\mathrm{CutDOij}} = 0.05$, $T_{\mathrm{CutDO}} = 10^{-3}$, $F_{\mathrm{Cut}} = 10^{-5}$, $T_{\mathrm{S}} = 10^{-8}$, and the remaining DLPNO thresholds equal to 0.

		T_{CutPre}						
El.	Ind.	10^{-2}	10^{-3}	10^{-4}	10^{-5}	10^{-6}	10^{-7}	10^{-8}
^{1}H	9	0.571	0.177	0.038	0.005	0.001	0.001	0.001
	20	0.215	0.061	0.003	0.002	0.001	0.001	0.001
	26	0.583	0.181	0.026	0.004	0.000	0.000	0.000
	27	0.761	0.204	0.040	0.002	-0.001	-0.001	-0.001
	28	0.332	0.111	0.031	0.002	0.000	0.000	0.000
	29	0.395	0.136	0.031	0.003	0.001	0.001	0.001
	30	0.321	0.105	0.016	0.001	0.000	0.000	0.000
	31	0.398	0.138	0.024	0.003	0.001	0.001	0.001
	32	0.314	0.113	0.017	0.002	0.001	0.001	0.001
	33	0.359	0.132	0.027	0.005	0.001	0.001	0.001
	34	0.521	0.158	0.031	0.003	0.000	0.000	0.000
	35	0.352	0.121	0.028	0.002	0.000	0.000	0.000
	36	0.500	0.147	0.035	0.004	0.001	0.001	0.001
	37	0.421	0.024	0.008	0.001	0.000	0.000	0.000
	38	0.375	-0.030	-0.005	0.000	-0.001	-0.001	-0.001
	39	0.279	0.104	0.018	0.002	0.001	0.001	0.001
	40	0.315	0.112	0.015	0.001	0.000	0.000	0.000
	41	0.343	-0.007	0.005	0.000	-0.001	-0.001	-0.001
^{13}C	1	4.341	-0.924	-0.134	-0.031	0.001	0.005	0.005
	2	4.660	-1.600	-0.232	-0.032	-0.013	-0.007	-0.007
	3	1.895	1.491	0.234	-0.014	-0.001	-0.005	-0.005
	4	2.988	1.936	0.301	-0.003	0.005	0.000	0.000
	5	3.976	-0.953	0.198	-0.006	-0.007	-0.003	-0.003
	6	7.324	2.012	0.462	0.042	0.010	0.011	0.011
	7	4.937	1.270	0.306	0.025	0.012	0.014	0.014
	8	4.990	1.051	0.194	0.034	0.017	0.017	0.018
	10	3.948	1.904	0.384	0.012	0.005	0.001	0.001
	15	1.844	-0.431	0.108	-0.020	-0.001	-0.002	-0.002
	16	1.868	-0.857	-0.234	-0.072	-0.025	-0.025	-0.024
	17	11.546	3.600	0.639	0.106	0.015	0.015	0.015
	18	8.135	2.576	0.580	0.036	0.003	0.001	0.001
	19	1.812	0.173	0.215	-0.037	-0.015	-0.014	-0.014
	22	13.835	4.003	1.164	0.103	0.038	0.024	0.024
	23	18.589	5.003	1.728	0.159	0.040	0.022	0.021
^{15}N	21	20.513	6.852	1.425	0.148	0.036	0.021	0.021
	25	34.132	9.997	1.762	0.156	0.016	0.007	0.007
^{17}O	11	9.468	-2.759	0.421	-0.072	0.018	0.013	0.014
	12	11.533	0.774	0.632	-0.243	-0.009	-0.010	-0.010
	13	5.476	-2.200	-0.100	-0.140	0.038	0.047	0.046
	14	23.451	7.036	0.585	0.105	0.019	0.014	0.014
^{33}S	24	53.518	11.197	3.418	0.184	0.105	0.067	0.064

F.6 DLPNO-MP2 polarizabilities

Table F.54: Isotropic polarizabilities (in Bohr^3) for the benchmark systems calculated at the HF, RI-MP2, and DLPNO-MP2 (NormalPNO) levels using different values for the MO orthonormalization threhsold $T_{\mathrm{S,MO}}$.

Method	$T_{\mathrm{S,MO}}$	caffeine	ebselen	penicillin	coronene	ATP^{4-}	$(\mathrm{anth})_2$
HF	10^{-6}	120.19	182.80	209.80	295.52	272.93	322.47
HF	10^{-8}	120.19	182.79	209.80	295.54	272.95	322.44
RI-MP2	10^{-6}	131.56	194.16	224.98	310.76	319.42	330.42
RI-MP2	10^{-8}	131.56	194.16	224.97	310.82	319.47	330.36
DLPNO-MP2 $\varepsilon_{\mathrm{scale}} = 0$	10^{-6}	131.46	193.94	224.68	310.03	318.76	330.46
DLPNO-MP2 $\varepsilon_{\mathrm{scale}} = 0.1$	10^{-6}	131.42	193.91	224.59	310.18	318.82	329.79
DLPNO-MP2 $\varepsilon_{\mathrm{scale}} = 0$	10^{-8}	131.41	193.88	224.57	310.29	318.80	329.80

Table F.55: Errors (in Bohr^3) in the isotropic polarizabilities for the benchmark systems, calculated using different DLPNO-MP2 thresholds (set to zero unless noted), with respect to RI-MP2. The MO orthonormalization threhsold was set to 10^{-8}. No PNO level shift was applied, unless otherwise noted.

Settings	caffeine	penicillin	coronene	ATP^{4-}
$T_{\mathrm{CutPNO}} = 10^{-5}$ (valence)[a]	-1.110	-1.455	-4.275	-2.771
$T_{\mathrm{CutPNO}} = 10^{-6}$ (valence)[a]	-0.473	-0.711	-2.522	-0.575
$T_{\mathrm{CutPNO}} = 10^{-7}$ (valence)[a]	-0.173	-0.349	-0.893	-0.804
$T_{\mathrm{CutPNO}} = 10^{-8}$ (valence)[a]	-0.071	-0.153	-0.486	-0.269
$T_{\mathrm{CutPNO}} = 10^{-9}$ (valence)[a]	-0.034	-0.067	-0.219	-0.127
$T_{\mathrm{CutPNO}} = 10^{-10}$ (valence)[a]	-0.011	-0.027	-0.098	-0.219
$T_{\mathrm{CutPNO}} = 10^{-11}$ (valence)[a]	0.000	-0.014	-0.053	-0.016
$T_{\mathrm{CutPNO}} = 10^{-12}$ (valence)[a]	-0.001	-0.007	-0.147	-0.002
$T_{\mathrm{CutPNO}} = 10^{-7}$ (valence), $\varepsilon_{\mathrm{scale}} = 0.1$ [a]				-0.568
$T_{\mathrm{CutPNO}} = 10^{-10}$ (valence), $\varepsilon_{\mathrm{scale}} = 0.1$ [a]				-0.047
$T_{\mathrm{CutPNO}} = 10^{-12}$ (valence), $\varepsilon_{\mathrm{scale}} = 0.1$ [a]			-0.078	
$T_{\mathrm{CutPNO}} = 10^{-5}$ (core)[b]	-0.004	-0.008	-0.083	-0.175
$T_{\mathrm{CutPNO}} = 10^{-6}$ (core)[b]	-0.011	-0.025	-0.095	-0.243
$T_{\mathrm{CutPNO}} = 10^{-7}$ (core)[b]	-0.011	-0.041	-0.102	-0.235
$T_{\mathrm{CutPNO}} = 10^{-8}$ (core)[b]	-0.011	-0.027	-0.100	-0.227
$T_{\mathrm{CutPNO}} = 10^{-9}$ (core)[b]	-0.011	-0.028	-0.098	-0.221
$T_{\mathrm{CutPNO}} = 10^{-10}$ (core)[b]	-0.011	-0.028	-0.098	-0.220
$T_{\mathrm{CutPNO}} = 10^{-11}$ (core)[b]	-0.011	-0.028	-0.098	-0.219
$T_{\mathrm{CutPNO}} = 10^{-12}$ (core)[b]	-0.011	-0.027	-0.098	-0.219
$F_{\mathrm{Cut}} = 10^{-2}$ [c]	-0.027	-0.039	-0.104	0.526
$F_{\mathrm{Cut}} = 10^{-3}$ [c]	-0.012	-0.027	-0.146	-0.248
$F_{\mathrm{Cut}} = 10^{-4}$ [c]	-0.011	-0.029	-0.098	-0.220
$F_{\mathrm{Cut}} = 10^{-5}$ [c]	-0.011	-0.029	-0.098	-0.219
$F_{\mathrm{Cut}} = 10^{-6}$ [c]	-0.011	-0.029	-0.098	-0.219
$F_{\mathrm{Cut}} = 10^{-7}$ [c]	-0.011	-0.029	-0.098	-0.219
$F_{\mathrm{Cut}} = 10^{-8}$ [c]	-0.011	-0.027	-0.098	-0.219
$T_{\mathrm{CutDO}} = 0.100$, $T_{\mathrm{S}} = 10^{-5}$ [d]	-2.212	-2.816	-14.145	-6.184
$T_{\mathrm{CutDO}} = 0.060$, $T_{\mathrm{S}} = 10^{-5}$ [d]	-0.557	-1.597	-12.220	-2.130
$T_{\mathrm{CutDO}} = 0.030$, $T_{\mathrm{S}} = 10^{-5}$ [d]	-0.184	-0.517	-0.619	-0.831
$T_{\mathrm{CutDO}} = 0.020$, $T_{\mathrm{S}} = 10^{-5}$ [d]	-0.117	-0.368	-0.397	-0.682
$T_{\mathrm{CutDO}} = 0.010$, $T_{\mathrm{S}} = 10^{-5}$ [d]	-0.066	-0.268	-0.203	-0.423
$T_{\mathrm{CutDO}} = 0.006$, $T_{\mathrm{S}} = 10^{-5}$ [d]	-0.029	-0.191	-0.122	-0.269
$T_{\mathrm{CutDO}} = 0.003$, $T_{\mathrm{S}} = 10^{-5}$ [d]	-0.031	-0.126	-0.103	-0.212
$T_{\mathrm{CutDO}} = 0.002$, $T_{\mathrm{S}} = 10^{-5}$ [d]	-0.025	-0.101	-0.104	-0.237
$T_{\mathrm{CutDO}} = 0.001$, $T_{\mathrm{S}} = 10^{-5}$ [d]	-0.014	-0.065	-0.097	-0.172
$T_{\mathrm{CutDO}} = 0.100$, $T_{\mathrm{S}} = 10^{-8}$ [d]	-2.096	-2.393	-13.495	-5.836
$T_{\mathrm{CutDO}} = 0.060$, $T_{\mathrm{S}} = 10^{-8}$ [d]	-0.420	-1.261	-11.761	-1.815

Continued on next page

Continued from previous page

Settings	caffeine	penicillin	coronene	ATP^{4-}
$T_{\mathrm{CutDO}} = 0.030$, $T_{\mathrm{S}} = 10^{-8}$ [d]	-0.042	-0.268	-0.229	-0.578
$T_{\mathrm{CutDO}} = 0.020$, $T_{\mathrm{S}} = 10^{-8}$ [d]	-0.052	-0.203	2.036	-0.498
$T_{\mathrm{CutDO}} = 0.010$, $T_{\mathrm{S}} = 10^{-8}$ [d]	0.013	-0.137	124.915	-0.248
$T_{\mathrm{CutDO}} = 0.006$, $T_{\mathrm{S}} = 10^{-8}$ [d]	-0.011	-0.110	-18178.146	-0.284
$T_{\mathrm{CutDO}} = 0.003$, $T_{\mathrm{S}} = 10^{-8}$ [d]	-0.043	-0.048	618.034	-0.352
$T_{\mathrm{CutDO}} = 0.002$, $T_{\mathrm{S}} = 10^{-8}$ [d]	-0.006	-0.031	-1052.010	-0.236
$T_{\mathrm{CutDO}} = 0.001$, $T_{\mathrm{S}} = 10^{-8}$ [d]	-0.012	-0.032	-65.782	-0.269
$T_{\mathrm{CutPre}} = 10^{-2}$ [e]	-6.417	-9.497	-31.996	-21.716
$T_{\mathrm{CutPre}} = 10^{-3}$ [e]	-2.545	-4.084	-18.865	-8.638
$T_{\mathrm{CutPre}} = 10^{-4}$ [e]	-0.573	-1.099	-7.745	-2.484
$T_{\mathrm{CutPre}} = 10^{-5}$ [e]	-0.052	-0.169	-0.603	-0.588
$T_{\mathrm{CutPre}} = 10^{-6}$ [e]	-0.019	-0.075	-0.165	-0.210
$T_{\mathrm{CutPre}} = 10^{-7}$ [e]	-0.015	-0.067	-0.105	-0.177
$T_{\mathrm{CutPre}} = 10^{-8}$ [e]	-0.015	-0.065	-0.095	-0.173
$T_{\mathrm{CutPre}} = 10^{-2}$ $(+\Delta E_{\mathrm{Pre}})$[e]	-0.138	2.440	-9.773	11.753
$T_{\mathrm{CutPre}} = 10^{-3}$ $(+\Delta E_{\mathrm{Pre}})$[e]	-1.635	-2.365	-14.040	-4.509
$T_{\mathrm{CutPre}} = 10^{-4}$ $(+\Delta E_{\mathrm{Pre}})$[e]	-0.474	-0.837	-7.132	-1.915
$T_{\mathrm{CutPre}} = 10^{-5}$ $(+\Delta E_{\mathrm{Pre}})$[e]	-0.048	-0.150	-0.580	-0.509
$T_{\mathrm{CutPre}} = 10^{-6}$ $(+\Delta E_{\mathrm{Pre}})$[e]	-0.019	-0.074	-0.163	-0.204
$T_{\mathrm{CutPre}} = 10^{-7}$ $(+\Delta E_{\mathrm{Pre}})$[e]	-0.015	-0.066	-0.105	-0.177
$T_{\mathrm{CutPre}} = 10^{-8}$ $(+\Delta E_{\mathrm{Pre}})$[e]	-0.015	-0.065	-0.095	-0.173

[a] $T_{\mathrm{CutPNO}} = 10^{-12}$ (core), $F_{\mathrm{Cut}} = 10^{-8}$, $T_{\mathrm{S}} = 10^{-5}$
[b] $T_{\mathrm{CutPNO}} = 10^{-10}$ (valence), $F_{\mathrm{Cut}} = 10^{-8}$, $T_{\mathrm{S}} = 10^{-5}$
[c] $T_{\mathrm{CutPNO}} = 10^{-10}$ (valence), $T_{\mathrm{CutPNO}} = 10^{-12}$ (core), $T_{\mathrm{S}} = 10^{-8}$ (10^{-5} for coronene)
[d] $T_{\mathrm{CutPNO}} = 10^{-10}$ (valence), $T_{\mathrm{CutPNO}} = 10^{-12}$ (core), $F_{\mathrm{Cut}} = 10^{-5}$
[e] $T_{\mathrm{CutPNO}} = 10^{-10}$ (valence), $T_{\mathrm{CutPNO}} = 10^{-12}$ (core), $F_{\mathrm{Cut}} = 10^{-5}$, $T_{\mathrm{CutDO}} = 0.001$, $T_{\mathrm{S}} = 10^{-5}$

Table F.56: Errors (in Bohr^3) in the isotropic polarizabilities for the benchmark systems, calculated using different DLPNO-MP2 thresholds (set to zero unless noted), with respect to RI-MP2. The MO orthonormalization threhsold was set to 10^{-6}. No PNO level shift was applied.

Settings	caffeine	penicillin	coronene	ATP^{4-}
$T_{\mathrm{CutPNO}} = 10^{-5}$ (valence)[a]	-1.115	-1.460	-4.214	-2.724
$T_{\mathrm{CutPNO}} = 10^{-6}$ (valence)[a]	-0.477	-0.717	-2.461	-0.528
$T_{\mathrm{CutPNO}} = 10^{-7}$ (valence)[a]	-0.178	-0.355	-0.833	-0.757
$T_{\mathrm{CutPNO}} = 10^{-8}$ (valence)[a]	-0.075	-0.159	-0.426	-0.222
$T_{\mathrm{CutPNO}} = 10^{-9}$ (valence)[a]	-0.038	-0.073	-0.158	-0.080
$T_{\mathrm{CutPNO}} = 10^{-10}$ (valence)[a]	-0.015	-0.033	-0.037	-0.171
$T_{\mathrm{CutPNO}} = 10^{-11}$ (valence)[a]	-0.004	-0.020	0.007	0.031
$T_{\mathrm{CutPNO}} = 10^{-12}$ (valence)[a]	-0.005	-0.013	-0.086	0.045
$T_{\mathrm{CutPNO}} = 10^{-5}$ (core)[b]	-0.009	-0.014	-0.023	-0.128
$T_{\mathrm{CutPNO}} = 10^{-6}$ (core)[b]	-0.015	-0.031	-0.034	-0.196
$T_{\mathrm{CutPNO}} = 10^{-7}$ (core)[b]	-0.016	-0.047	-0.042	-0.187
$T_{\mathrm{CutPNO}} = 10^{-8}$ (core)[b]	-0.015	-0.033	-0.040	-0.180
$T_{\mathrm{CutPNO}} = 10^{-9}$ (core)[b]	-0.015	-0.034	-0.038	-0.173
$T_{\mathrm{CutPNO}} = 10^{-10}$ (core)[b]	-0.015	-0.034	-0.037	-0.173
$T_{\mathrm{CutPNO}} = 10^{-11}$ (core)[b]	-0.015	-0.033	-0.037	-0.172
$T_{\mathrm{CutPNO}} = 10^{-12}$ (core)[b]	-0.015	-0.033	-0.037	-0.171
$T_{\mathrm{CutDO}} = 0.100$, $T_{\mathrm{S}} = 10^{-8}$ [c]			-13.552	
$T_{\mathrm{CutDO}} = 0.030$, $T_{\mathrm{S}} = 10^{-8}$ [c]			-0.409	
$T_{\mathrm{CutDO}} = 0.020$, $T_{\mathrm{S}} = 10^{-8}$ [c]			-0.385	
$T_{\mathrm{CutDO}} = 0.010$, $T_{\mathrm{S}} = 10^{-8}$ [c]			-0.356	
$T_{\mathrm{CutDO}} = 0.006$, $T_{\mathrm{S}} = 10^{-8}$ [c]			0.013	
$T_{\mathrm{CutDO}} = 0.003$, $T_{\mathrm{S}} = 10^{-8}$ [c]			0.031	
$T_{\mathrm{CutDO}} = 0.002$, $T_{\mathrm{S}} = 10^{-8}$ [c]			0.057	
$T_{\mathrm{CutDO}} = 0.001$, $T_{\mathrm{S}} = 10^{-8}$ [c]			0.102	
$T_{\mathrm{CutDO}} = 0.100$, $T_{\mathrm{S}} = 10^{-5}$ [c]			-14.100	
$T_{\mathrm{CutDO}} = 0.030$, $T_{\mathrm{S}} = 10^{-5}$ [c]			-0.635	
$T_{\mathrm{CutDO}} = 0.020$, $T_{\mathrm{S}} = 10^{-5}$ [c]			-0.348	

Continued on next page

Continued from previous page

Settings	caffeine	penicillin	coronene	ATP^{4-}
$T_{\mathrm{CutDO}} = 0.010$, $T_{\mathrm{S}} = 10^{-5}$ [c]			-0.154	
$T_{\mathrm{CutDO}} = 0.006$, $T_{\mathrm{S}} = 10^{-5}$ [c]			-0.079	
$T_{\mathrm{CutDO}} = 0.003$, $T_{\mathrm{S}} = 10^{-5}$ [c]			-0.079	
$T_{\mathrm{CutDO}} = 0.002$, $T_{\mathrm{S}} = 10^{-5}$ [c]			-0.057	
$T_{\mathrm{CutDO}} = 0.001$, $T_{\mathrm{S}} = 10^{-5}$ [c]			-0.051	

[a] $T_{\mathrm{CutPNO}} = 10^{-12}$ (core), $F_{\mathrm{Cut}} = 10^{-8}$, $T_{\mathrm{S}} = 10^{-5}$
[b] $T_{\mathrm{CutPNO}} = 10^{-10}$ (valence), $F_{\mathrm{Cut}} = 10^{-8}$, $T_{\mathrm{S}} = 10^{-5}$
[c] $T_{\mathrm{CutPNO}} = 10^{-10}$ (valence), $T_{\mathrm{CutPNO}} = 10^{-12}$ (core), $F_{\mathrm{Cut}} = 10^{-5}$

Bibliography

[1] Günther, H. *NMR Spectroscopy: Basic Principles, Concepts and Applications in Chemistry*, 3rd ed.; Wiley-VCH Verlag GmbH & Co. KGaA: Weinheim, Germany, 2013.

[2] Ramsey, N. F. *Phys. Rev.* **1950**, *78*, 699–703.

[3] Tossell, J. A., Ed. *Nucl. Magn. Shield. Mol. Struct.*; Springer Netherlands: Dordrecht, 1993.

[4] Chesnut, D. *Annu. Reports NMR Spectrosc.*; Academic Press, 1994; Vol. 29; pp 71–122.

[5] Chesnut, D. B. In *Rev. Comput. Chem.*; Lipkowitz, K. B., Boyd, D. B., Eds.; John Wiley & Sons, Ltd, 1996; Vol. 8; pp 245–297.

[6] Jameson, C. J. *Annu. Rev. Phys. Chem.* **1996**, *47*, 135–169.

[7] de Dios, A. C. *Prog. Nucl. Magn. Reson. Spectrosc.* **1996**, *29*, 229–278.

[8] Fukui, H. *Prog. Nucl. Magn. Reson. Spectrosc.* **1997**, *31*, 317–342.

[9] Jameson, C. J. In *Nucl. Magn. Reson.*; Webb, G. A., Ed.; Royal Society of Chemistry, 1997; pp 46–87.

[10] Schreckenbach, G.; Ziegler, T. *Theor. Chem. Accounts Theory, Comput. Model. (Theoretica Chim. Acta)* **1998**, *99*, 71–82.

[11] Kaupp, M., Bühl, M., Malkin, V. G., Eds. *Calc. NMR EPR Parameters*; Wiley: Weinheim, FRG, 2004.

[12] Vaara, J. *Phys. Chem. Chem. Phys.* **2007**, *9*, 5399.

[13] Helgaker, T.; Jaszuński, M.; Ruud, K. *Chem. Rev.* **1999**, *99*, 293–352.

[14] Bühl, M.; van Mourik, T. *Wiley Interdiscip. Rev. Comput. Mol. Sci.* **2011**, *1*, 634–647.

[15] Lodewyk, M. W.; Siebert, M. R.; Tantillo, D. J. *Chem. Rev.* **2012**, *112*, 1839–1862.

[16] Gauss, J. In *Mod. Methods Algorithms Quantum Chem. Proceedings, Winterschool, 21-25 Febr. 2000 Forschungszentrum Jülich, Ger.*; Grotendorst, J., Ed.; John von Neumann Institute for Computing: Jülich, Germany, 2000; pp 541–592.

[17] Kutzelnigg, W. *J. Mol. Struct. THEOCHEM* **1989**, *202*, 11–61.

[18] Kutzelnigg, W. *Isr. J. Chem.* **1980**, *19*, 193–200.

[19] Schindler, M.; Kutzelnigg, W. *J. Chem. Phys.* **1982**, *76*, 1919–1933.

[20] Hansen, A. E.; Bouman, T. D. *J. Chem. Phys.* **1985**, *82*, 5035–5047.

[21] Bouman, T. D.; Hansen, A. E. *Chem. Phys. Lett.* **1990**, *175*, 292–299.

[22] Keith, T.; Bader, R. *Chem. Phys. Lett.* **1992**, *194*, 1–8.

[23] Keith, T. A.; Bader, R. F. *Chem. Phys. Lett.* **1993**, *210*, 223–231.

[24] Lazzeretti, P.; Malagoli, M.; Zanasi, R. *Chem. Phys. Lett.* **1994**, *220*, 299–304.

[25] Zanasi, R.; Lazzeretti, P.; Malagoli, M.; Piccinini, F. *J. Chem. Phys.* **1995**, *102*, 7150–7157.

[26] Lazzeretti, P.; Zanasi, R. *Int. J. Quantum Chem.* **1996**, *60*, 249–259.

[27] London, F. *J. Phys. Radium* **1937**, *8*, 397–409.

[28] Hameka, H. F. *Mol. Phys.* **1958**, *1*, 203–215.

[29] Ditchfield, R. *J. Chem. Phys.* **1972**, *56*, 5688–5691.

[30] Ditchfield, R. *Mol. Phys.* **1974**, *27*, 789–807.

[31] Wolinski, K.; Hinton, J. F.; Pulay, P. *J. Am. Chem. Soc.* **1990**, *112*, 8251–8260.

[32] Hall, G. G. *Int. J. Quantum Chem.* **1973**, *7*, 15–25.

[33] Helgaker, T.; Jørgensen, P. *J. Chem. Phys.* **1991**, *95*, 2595–2601.

[34] Gauss, J. *Chem. Phys. Lett.* **1992**, *191*, 614–620.

[35] Gauss, J. *J. Chem. Phys.* **1993**, *99*, 3629–3643.

[36] Gauss, J. *Chem. Phys. Lett.* **1994**, *229*, 198–203.

[37] Gauss, J.; Stanton, J. F. *J. Chem. Phys.* **1995**, *103*, 3561–3577.

[38] Gauss, J.; Stanton, J. F. *J. Chem. Phys.* **1995**, *102*, 251–253.

[39] Gauss, J.; Stanton, J. F. *J. Chem. Phys.* **1996**, *104*, 2574–2583.

[40] Gauss, J.; Stanton, J. F. *Phys. Chem. Chem. Phys.* **2000**, *2*, 2047–2060.

[41] Gauss, J. *J. Chem. Phys.* **2002**, *116*, 4773.

[42] Kállay, M.; Gauss, J. *J. Chem. Phys.* **2004**, *120*, 6841–6848.

[43] Auer, A. A.; Gauss, J.; Stanton, J. F. *J. Chem. Phys.* **2003**, *118*, 10407–10417.

[44] Harding, M. E.; Lenhart, M.; Auer, A. A.; Gauss, J. *J. Chem. Phys.* **2008**, *128*, 244111.

[45] Auer, A. A. *J. Chem. Phys.* **2009**, *131*, 024116.

[46] Prochnow, E.; Auer, A. A. *J. Chem. Phys.* **2010**, *132*, 064109.

[47] Flaig, D.; Maurer, M.; Hanni, M.; Braunger, K.; Kick, L.; Thubauville, M.; Ochsenfeld, C. *J. Chem. Theory Comput.* **2014**, *10*, 572–578.

[48] Kutzelnigg, W.; Wüllen, C.; Fleischer, U.; Franke, R.; Mourik, T. *Nucl. Magn. Shield. Mol. Struct.*; Springer Netherlands: Dordrecht, 1993; pp 141–161.

[49] van Wüllen, C.; Kutzelnigg, W. *Chem. Phys. Lett.* **1993**, *205*, 563–571.

[50] Ruud, K.; Helgaker, T.; Kobayashi, R.; Jo/rgensen, P.; Bak, K. L.; Jensen, H. J. A. *J. Chem. Phys.* **1994**, *100*, 8178–8185.

[51] Grimme, S. *J. Chem. Phys.* **2003**, *118*, 9095–9102.

[52] Fink, R. F. *J. Chem. Phys.* **2010**, *133*, 174113.

[53] Grimme, S.; Goerigk, L.; Fink, R. F. *Wiley Interdiscip. Rev. Comput. Mol. Sci.* **2012**, *2*, 886–906.

[54] Maurer, M.; Ochsenfeld, C. *J. Chem. Theory Comput.* **2015**, *11*, 37–44.

[55] Bühl, M.; Kaupp, M.; Malkina, O. L.; Malkin, V. G. *J. Comput. Chem.* **1999**, *20*, 91–105.

[56] Helgaker, T.; Wilson, P. J.; Amos, R. D.; Handy, N. C. *J. Chem. Phys.* **2000**, *113*, 2983–2989.

[57] Magyarfalvi, G.; Pulay, P. *J. Chem. Phys.* **2003**, *119*, 1350–1357.

[58] Lee, A. M.; Handy, N. C.; Colwell, S. M. *J. Chem. Phys.* **1995**, *103*, 10095–10109.

[59] Malkin, V.; Malkina, O.; Salahub, D. *Chem. Phys. Lett.* **1993**, *204*, 87–95.

[60] Malkin, V. G.; Malkina, O. L.; Casida, M. E.; Salahub, D. R. *J. Am. Chem. Soc.* **1994**, *116*, 5898–5908.

[61] Malkin, V. G.; Malkina, O. L.; Eriksson, L. A.; Salahub, D. R. *Theor. Comput. Chem.*; 1995; Vol. 2; pp 273–347.

[62] Reimann, S.; Ekström, U.; Stopkowicz, S.; Teale, A. M.; Borgoo, A.; Helgaker, T. *Phys. Chem. Chem. Phys.* **2015**, *17*, 18834–18842.

[63] Grayce, C. J.; Harris, R. A. *Phys. Rev. A* **1994**, *50*, 3089–3095.

[64] Vignale, G.; Rasolt, M. *Phys. Rev. Lett.* **1987**, *59*, 2360–2363.

[65] Vignale, G.; Rasolt, M. *Phys. Rev. B* **1988**, *37*, 10685–10696.

[66] Tellgren, E. I.; Kvaal, S.; Sagvolden, E.; Ekström, U.; Teale, A. M.; Helgaker, T. *Phys. Rev. A* **2012**, *86*, 062506.

[67] Becke, A. D. *J. Chem. Phys.* **2002**, *117*, 6935–6938.

[68] Maximoff, S. N.; Scuseria, G. E. *Chem. Phys. Lett.* **2004**, *390*, 408–412.

[69] Tao, J. *Phys. Rev. B* **2005**, *71*, 205107.

[70] Furness, J. W.; Verbeke, J.; Tellgren, E. I.; Stopkowicz, S.; Ekström, U.; Helgaker, T.; Teale, A. M. *J. Chem. Theory Comput.* **2015**, *11*, 4169–4181.

[71] Tellgren, E. I.; Teale, A. M.; Furness, J. W.; Lange, K. K.; Ekström, U.; Helgaker, T. *J. Chem. Phys.* **2014**, *140*, 034101.

[72] Schattenberg, C. J.; Kaupp, M. *J. Chem. Theory Comput.* **2021**, *17*, 1469–1479.

[73] Teale, A. M.; Lutnæs, O. B.; Helgaker, T.; Tozer, D. J.; Gauss, J. *J. Chem. Phys.* **2013**, *138*, 024111.

[74] Keal, T. W.; Tozer, D. J. *J. Chem. Phys.* **2003**, *119*, 3015–3024.

[75] Keal, T. W.; Tozer, D. J. *J. Chem. Phys.* **2004**, *121*, 5654–5660.

[76] Zhao, Y.; Truhlar, D. G. *J. Phys. Chem. A* **2008**, *112*, 6794–6799.

[77] Perdew, J. P.; Schmidt, K. Jacob's ladder of density functional approximations for the exchange-correlation energy. AIP Conf. Proc. 2001; pp 1–20.

[78] Grimme, S. *J. Chem. Phys.* **2006**, *124*, 034108.

[79] Goerigk, L.; Grimme, S. *Wiley Interdiscip. Rev. Comput. Mol. Sci.* **2014**, *4*, 576–600.

[80] Grimme, S. *J. Comput. Chem.* **2006**, *27*, 1787–1799.

[81] Grimme, S.; Antony, J.; Ehrlich, S.; Krieg, H. *J. Chem. Phys.* **2010**, *132*, 154104.

[82] Grimme, S.; Ehrlich, S.; Goerigk, L. *J. Comput. Chem.* **2011**, *32*, 1456–1465.

[83] Kozuch, S.; Gruzman, D.; Martin, J. M. L. *J. Phys. Chem. C* **2010**, *114*, 20801–20808.

[84] Kozuch, S.; Martin, J. M. L. *Phys. Chem. Chem. Phys.* **2011**, *13*, 20104.

[85] Kozuch, S.; Martin, J. M. L. *J. Comput. Chem.* **2013**, *34*, 2327–2344.

[86] Goerigk, L.; Grimme, S. *J. Chem. Theory Comput.* **2011**, *7*, 291–309.

[87] Goerigk, L.; Hansen, A.; Bauer, C.; Ehrlich, S.; Najibi, A.; Grimme, S. *Phys. Chem. Chem. Phys.* **2017**, *19*, 32184–32215.

[88] Mehta, N.; Casanova-Páez, M.; Goerigk, L. *Phys. Chem. Chem. Phys.* **2018**, *20*, 23175–23194.

[89] Santra, G.; Sylvetsky, N.; Martin, J. M. L. *J. Phys. Chem. A* **2019**, *123*, 5129–5143.

[90] Hait, D.; Head-Gordon, M. *J. Chem. Theory Comput.* **2018**, *14*, 1969–1981.

[91] Hait, D.; Head-Gordon, M. *Phys. Chem. Chem. Phys.* **2018**, *20*, 19800–19810.

[92] Neese, F.; Schwabe, T.; Grimme, S. *J. Chem. Phys.* **2007**, *126*, 124115.

[93] Kossmann, S.; Neese, F. *J. Chem. Theory Comput.* **2010**, *6*, 2325–2338.

[94] Koßmann, S. Efficient Novel Approaches for the Calculation of Molecular Response Properties : Second-Order Many-Body Perturbation and Double-Hybrid Density Functional Theory. Ph.D. Dissertation, Rheinischen Friedrich-Wilhelms-Universität Bonn, 2011.

[95] Gao, Q.; Yokojima, S.; Kohno, T.; Ishida, T.; Fedorov, D. G.; Kitaura, K.; Fujihira, M.; Nakamura, S. *Chem. Phys. Lett.* **2007**, *445*, 331–339.

[96] Cui, Q.; Karplus, M. *J. Phys. Chem. B* **2000**, *104*, 3721–3743.

[97] Sebastiani, D.; Rothlisberger, U. *J. Phys. Chem. B* **2004**, *108*, 2807–2815.

[98] Gao, Q.; Yokojima, S.; Fedorov, D. G.; Kitaura, K.; Sakurai, M.; Nakamura, S. *J. Chem. Theory Comput.* **2010**, *6*, 1428–1444.

[99] Zhu, T.; He, X.; Zhang, J. Z. H. *Phys. Chem. Chem. Phys.* **2012**, *14*, 7837–7845.

[100] Tan, H.-J.; Bettens, R. P. A. *Phys. Chem. Chem. Phys.* **2013**, *15*, 7541.

[101] Jose, K. V. J.; Raghavachari, K. *J. Chem. Theory Comput.* **2017**, *13*, 1147–1158.

[102] Steinmann, C.; Bratholm, L. A.; Olsen, J. M. H.; Kongsted, J. *J. Chem. Theory Comput.* **2017**, *13*, 525–536.

[103] Svensson, M.; Humbel, S.; Froese, R. D. J.; Matsubara, T.; Sieber, S.; Morokuma, K. *J. Phys. Chem.* **1996**, *100*, 19357–19363.

[104] Hall, K. F.; Vreven, T.; Frisch, M. J.; Bearpark, M. J. *J. Mol. Biol.* **2008**, *383*, 106–121.

[105] Beer, M.; Kussmann, J.; Ochsenfeld, C. *J. Chem. Phys.* **2011**, *134*, 074102.

[106] Kumar, C.; Kjærgaard, T.; Helgaker, T.; Fliegl, H. *J. Chem. Phys.* **2016**, *145*, 234108.

[107] Kussmann, J.; Beer, M.; Ochsenfeld, C. *Wiley Interdiscip. Rev. Comput. Mol. Sci.* **2013**, *3*, 614–636.

[108] Ochsenfeld, C.; Kussmann, J.; Koziol, F. *Angew. Chemie Int. Ed.* **2004**, *43*, 4485–4489.

[109] Kussmann, J.; Ochsenfeld, C. *J. Chem. Phys.* **2007**, *127*, 054103.

[110] Früchtl, H. A.; Kendall, R. A.; Harrison, R. J.; Dyall, K. G. *Int. J. Quantum Chem.* **1997**, *64*, 63–69.

[111] Weigend, F.; Köhn, A.; Hättig, C. *J. Chem. Phys.* **2002**, *116*, 3175–3183.

[112] Deglmann, P.; May, K.; Furche, F.; Ahlrichs, R. *Chem. Phys. Lett.* **2004**, *384*, 103–107.

[113] Neese, F.; Wennmohs, F.; Hansen, A.; Becker, U. *Chem. Phys.* **2009**, *356*, 98–109.

[114] Bykov, D.; Petrenko, T.; Izsák, R.; Kossmann, S.; Becker, U.; Valeev, E.; Neese, F. *Mol. Phys.* **2015**, *113*, 1961–1977.

[115] Weigend, F. *J. Comput. Chem.* **2008**, *29*, 167–175.

[116] Kossmann, S.; Neese, F. *Chem. Phys. Lett.* **2009**, *481*, 240–243.

[117] Loibl, S.; Manby, F. R.; Schutz, M. *Mol. Phys.* **2010**, *108*, 477–485.

[118] Friesner, R. A. *J. Chem. Phys.* **1987**, *86*, 3522–3531.

[119] Cao, Y.; Beachy, M. D.; Braden, D. A.; Morrill, L.; Ringnalda, M. N.; Friesner, R. A. *J. Chem. Phys.* **2005**, *122*.

[120] Kollwitz, M.; Gauss, J. *Chem. Phys. Lett.* **1996**, *260*, 639–646.

[121] Kollwitz, M.; Häser, M.; Gauss, J. *J. Chem. Phys.* **1998**, *108*, 8295–8301.

[122] Maurer, S. A.; Lambrecht, D. S.; Kussmann, J.; Ochsenfeld, C. *J. Chem. Phys.* **2013**, *138*, 014101.

[123] Friese, D. H.; Winter, N. O. C.; Balzerowski, P.; Schwan, R.; Hättig, C. *J. Chem. Phys.* **2012**, *136*, 174106.

[124] Pulay, P. *Chem. Phys. Lett.* **1983**, *100*, 151–154.

[125] Sæbø, S.; Pulay, P. *Chem. Phys. Lett.* **1985**, *113*, 13–18.

[126] Sæbø, S.; Pulay, P. *Annu. Rev. Phys. Chem.* **1993**, *44*, 213–236.

[127] Sinanoğlu, O. In *Adv. Chem. Phys.*; Prigogine, I., Ed.; wiley, 1964; Vol. 6; Chapter 7, pp 315–412.

[128] Nesbet, R. K. In *Adv. Chem. Phys.*; Prigogine, I., Ed.; John Wiley & Sons, Ltd, 1965; Vol. 9; Chapter 4, pp 321–363.

[129] Hampel, C.; Werner, H. *J. Chem. Phys.* **1996**, *104*, 6286–6297.

[130] Schütz, M.; Hetzer, G.; Werner, H.-J. *J. Chem. Phys.* **1999**, *111*, 5691–5705.

[131] Schütz, M.; Werner, H.-J. *Chem. Phys. Lett.* **2000**, *318*, 370–378.

[132] Schütz, M.; Werner, H.-J. *J. Chem. Phys.* **2001**, *114*, 661.

[133] Werner, H.-J.; Manby, F. R.; Knowles, P. J. *J. Chem. Phys.* **2003**, *118*, 8149–8160.

[134] Werner, H.-J.; Schütz, M. *J. Chem. Phys.* **2011**, *135*, 144116.

[135] Schwilk, M.; Usvyat, D.; Werner, H.-J. *J. Chem. Phys.* **2015**, *142*, 121102.

[136] Werner, H.-J. *J. Chem. Phys.* **2016**, *145*, 201101.

[137] Werner, H.-J.; Knizia, G.; Krause, C.; Schwilk, M.; Dornbach, M. *J. Chem. Theory Comput.* **2015**, *11*, 484–507.

[138] Schwilk, M.; Ma, Q.; Köppl, C.; Werner, H.-J. *J. Chem. Theory Comput.* **2017**, *13*, 3650–3675.

[139] Ma, Q.; Werner, H.-J. *J. Chem. Theory Comput.* **2018**, *14*, 198–215.

[140] Werner, H.-J.; Köppl, C.; Ma, Q.; Schwilk, M. In *Fragmentation*; Gordon, M. S., Ed.; John Wiley & Sons, Ltd: Chichester, UK, 2017; pp 1–79.

[141] Neese, F.; Hansen, A.; Liakos, D. G. *J. Chem. Phys.* **2009**, *131*, 064103.

[142] Neese, F.; Wennmohs, F.; Hansen, A. *J. Chem. Phys.* **2009**, *130*, 114108.

[143] Riplinger, C.; Neese, F. *J. Chem. Phys.* **2013**, *138*, 034106.

[144] Pinski, P.; Riplinger, C.; Valeev, E. F.; Neese, F. *J. Chem. Phys.* **2015**, *143*, 034108.

[145] Riplinger, C.; Pinski, P.; Becker, U.; Valeev, E. F.; Neese, F. *J. Chem. Phys.* **2016**, *144*, 024109.

[146] Saitow, M.; Becker, U.; Riplinger, C.; Valeev, E. F.; Neese, F. *J. Chem. Phys.* **2017**, *146*, 164105.

[147] Guo, Y.; Riplinger, C.; Becker, U.; Liakos, D. G.; Minenkov, Y.; Cavallo, L.; Neese, F. *J. Chem. Phys.* **2018**, *148*, 011101.

[148] Ayala, P. Y.; Scuseria, G. E. *J. Chem. Phys.* **1999**, *110*, 3660–3671.

[149] Scuseria, G. E.; Ayala, P. Y. *J. Chem. Phys.* **1999**, *111*, 8330–8343.

[150] Maurer, S. A.; Clin, L.; Ochsenfeld, C. *J. Chem. Phys.* **2014**, *140*, 224112.

[151] Yang, J.; Chan, G. K.-L.; Manby, F. R.; Schütz, M.; Werner, H.-J. *J. Chem. Phys.* **2012**, *136*, 144105.

[152] Kurashige, Y.; Yang, J.; Chan, G. K.-L.; Manby, F. R. *J. Chem. Phys.* **2012**, *136*, 124106.

[153] Schütz, M.; Yang, J.; Chan, G. K.-L.; Manby, F. R.; Werner, H.-J. *J. Chem. Phys.* **2013**, *138*, 054109.

[154] Schmitz, G.; Helmich, B.; Hättig, C. *Mol. Phys.* **2013**, *111*, 2463–2476.

[155] Schmitz, G.; Hättig, C.; Tew, D. P. *Phys. Chem. Chem. Phys.* **2014**, *16*, 22167–22178.

[156] Schmitz, G.; Hättig, C. *J. Chem. Phys.* **2016**, *145*, 234107.

[157] Schmitz, G.; Hättig, C. *J. Chem. Theory Comput.* **2017**, *13*, 2623–2633.

[158] Guo, Y.; Li, W.; Li, S. *J. Phys. Chem. A* **2014**, *118*, 8996–9004.

[159] Guo, Y.; Becker, U.; Neese, F. *J. Chem. Phys.* **2018**, *148*, 124117.

[160] Eriksen, J. J.; Baudin, P.; Ettenhuber, P.; Kristensen, K.; Kjærgaard, T.; Jørgensen, P. *J. Chem. Theory Comput.* **2015**, *11*, 2984–2993.

[161] Baudin, P.; Ettenhuber, P.; Reine, S.; Kristensen, K.; Kjærgaard, T. *J. Chem. Phys.* **2016**, *144*, 054102.

[162] Kjærgaard, T.; Baudin, P.; Bykov, D.; Kristensen, K.; Jørgensen, P. *WIREs Comput. Mol. Sci.* **2017**, *7*, e1319.

[163] Rolik, Z.; Szegedy, L.; Ladjánszki, I.; Ladóczki, B.; Kállay, M. *J. Chem. Phys.* **2013**, *139*, 094105.

[164] Nagy, P. R.; Samu, G.; Kállay, M. *J. Chem. Theory Comput.* **2016**, *12*, 4897–4914.

[165] Nagy, P. R.; Samu, G.; Kállay, M. *J. Chem. Theory Comput.* **2018**, *14*, 4193–4215.

[166] Raghavachari, K.; Trucks, G. W.; Pople, J. A.; Head-Gordon, M. *Chem. Phys. Lett.* **1989**, *157*, 479–483.

[167] Liakos, D. G.; Neese, F. *J. Chem. Theory Comput.* **2015**, *11*, 4054–4063.

[168] Liakos, D. G.; Guo, Y.; Neese, F. *J. Phys. Chem. A* **2020**, *124*, 90–100.

[169] El Azhary, A.; Rauhut, G.; Pulay, P.; Werner, H. J. *J. Chem. Phys.* **1998**, *108*, 5185–5193.

[170] Rauhut, G.; Werner, H. J. *Phys. Chem. Chem. Phys.* **2001**, *3*, 4853–4862.

[171] Schütz, M.; Werner, H.-J.; Lindh, R.; Manby, F. R. *J. Chem. Phys.* **2004**, *121*, 737–750.

[172] Ledermüller, K.; Kats, D.; Schütz, M. *J. Chem. Phys.* **2013**, *139*, 084111.

[173] Ledermüller, K.; Schütz, M. *J. Chem. Phys.* **2014**, *140*, 164113.

[174] Dornbach, M.; Werner, H.-J. *Mol. Phys.* **2019**, *117*, 1252–1263.

[175] Rauhut, G.; El Azhary, A.; Eckert, F.; Schumann, U.; Werner, H.-J. *Spectrochim. Acta Part A Mol. Biomol. Spectrosc.* **1999**, *55*, 647–658.

[176] Rauhut, G.; Werner, H.-J. *Phys. Chem. Chem. Phys.* **2003**, *5*, 2001.

[177] Hrenar, T.; Werner, H.-J.; Rauhut, G. *J. Chem. Phys.* **2007**, *126*, 134108.

[178] Gauss, J.; Werner, H.-J. *Phys. Chem. Chem. Phys.* **2000**, *2*, 2083–2090.

[179] Loibl, S.; Schütz, M. *J. Chem. Phys.* **2012**, *137*, 084107.

[180] Loibl, S.; Schütz, M. *J. Chem. Phys* **2014**, *141*, 24108.

[181] Korona, T.; Pflüger, K.; Werner, H.-J. *Phys. Chem. Chem. Phys.* **2004**, *6*, 2059–2065.

[182] Maurer, M.; Ochsenfeld, C. *J. Chem. Phys.* **2013**, *138*, 174104.

[183] Frank, M. S.; Schmitz, G.; Hättig, C. *Mol. Phys.* **2017**, *115*, 343–356.

[184] Zhou, R.; Liang, Q.; Yang, J. *J. Chem. Theory Comput.* **2020**, *16*, 196–210.

[185] Russ, N. J.; Crawford, T. D. *Phys. Chem. Chem. Phys.* **2008**, *10*, 3345.

[186] McAlexander, H. R.; Mach, T. J.; Crawford, T. D. *Phys. Chem. Chem. Phys.* **2012**, *14*, 7830.

[187] McAlexander, H. R.; Crawford, T. D. *J. Chem. Theory Comput.* **2016**, *12*, 209–222.

[188] D'Cunha, R.; Crawford, T. D. *J. Chem. Theory Comput.* **2021**, *17*, 290–301.

[189] Datta, D.; Kossmann, S.; Neese, F. *J. Chem. Phys.* **2016**, *145*, 114101.

[190] Saitow, M.; Neese, F. *J. Chem. Phys.* **2018**, *149*, 034104.

[191] Pinski, P.; Neese, F. *J. Chem. Phys.* **2018**, *148*, 031101.

[192] Pinski, P.; Neese, F. *J. Chem. Phys.* **2019**, *150*, 164102.

[193] Pinski, P. Domain-Based Local Pair Natural Orbital Second-Order Møller-Plesset Perturbation Theory , and the Development of its Analytical Gradient. Ph.D. thesis, Rheinische Friedrich-Wilhelms-Universität Bonn, 2020.

[194] Autschbach, J.; Ziegler, T. *Relativistic Computation of NMR Shieldings and Spin-spin Coupling Constants*; 2002; Vol. 9; pp 306–323.

[195] Autschbach, J. *Calc. NMR EPR Parameters*; Wiley-VCH Verlag GmbH & Co. KGaA: Weinheim, FRG, 2004; pp 227–247.

[196] Autschbach, J.; Zheng, S. *Chapter 1 Relativistic Computations of NMR Parameters from First Principles: Theory and Applications*; 2009; pp 1–95.

[197] Autschbach, J. *Philos. Trans. R. Soc. A Math. Phys. Eng. Sci.* **2014**, *372*, 20120489.

[198] Komorovský, S.; Repiský, M.; Malkina, O. L.; Malkin, V. G.; Malkin Ondík, I.; Kaupp, M. *J. Chem. Phys.* **2008**, *128*, 104101.

[199] Komorovský, S.; Repiský, M.; Malkina, O. L.; Malkin, V. G. *J. Chem. Phys.* **2010**, *132*, 154101.

[200] Xiao, Y.; Sun, Q.; Liu, W. *Theor. Chem. Acc.* **2012**, *131*, 1080.

[201] Wolff, S. K.; Ziegler, T.; Van Lenthe, E.; Baerends, E. J. *J. Chem. Phys.* **1999**, *110*, 7689–7698.

[202] Filatov, M.; Cremer, D. *J. Chem. Phys.* **2005**, *122*, 044104.

[203] Fukuda, R.; Hada, M.; Nakatsuji, H. *J. Chem. Phys.* **2003**, *118*, 1015–1026.

[204] Fukuda, R.; Hada, M.; Nakatsuji, H. *J. Chem. Phys.* **2003**, *118*, 1027–1035.

[205] Sun, Q.; Liu, W.; Xiao, Y.; Cheng, L. *J. Chem. Phys.* **2009**, *131*, 081101.

[206] Sun, Q.; Xiao, Y.; Liu, W. *J. Chem. Phys.* **2012**, *137*, 174105.

[207] Yoshizawa, T.; Hada, M. *J. Chem. Phys.* **2017**, *147*, 154104.

[208] Willoughby, P. H.; Jansma, M. J.; Hoye, T. R. *Nat. Protoc.* **2014**, *9*, 643–660.

[209] Grimme, S.; Bannwarth, C.; Dohm, S.; Hansen, A.; Pisarek, J.; Pracht, P.; Seibert, J.; Neese, F. *Angew. Chemie Int. Ed.* **2017**, *56*, 14763–14769.

[210] Searles, D. J.; Huber, H. *Calc. NMR EPR Parameters*; Wiley-VCH Verlag GmbH & Co. KGaA: Weinheim, FRG, 2004; pp 175–189.

[211] Ruden, T. A.; Ruud, K. *Calc. NMR EPR Parameters*; Wiley-VCH Verlag GmbH & Co. KGaA: Weinheim, FRG, 2004; pp 153–173.

[212] Ruud, K.; Åstrand, P.-O.; Taylor, P. R. *J. Chem. Phys.* **2000**, *112*, 2668–2683.

[213] Barone, V.; Crescenzi, O.; Improta, R. *Quant. Struct. Relationships* **2002**, *21*, 105–118.

[214] Ciofini, I. *Calc. NMR EPR Parameters*; Wiley-VCH Verlag GmbH & Co. KGaA: Weinheim, FRG, 2004; pp 191–208.

[215] Pfrommer, B. G.; Mauri, F.; Louie, S. G. *J. Am. Chem. Soc.* **2000**, *122*, 123–129.

[216] Mennucci, B.; Martínez, J. M.; Tomasi, J. *J. Phys. Chem. A* **2001**, *105*, 7287–7296.

[217] Mennucci, B. *J. Am. Chem. Soc.* **2002**, *124*, 1506–1515.

[218] Cossi, M.; Crescenzi, O. *Theor. Chem. Acc.* **2004**, *111*, 162–167.

[219] Neese, F. *Wiley Interdiscip. Rev. Comput. Mol. Sci.* **2012**, *2*, 73–78.

[220] Neese, F. *Wiley Interdiscip. Rev. Comput. Mol. Sci.* **2017**, e1327.

[221] Neese, F.; Wennmohs, F.; Becker, U.; Riplinger, C. *J. Chem. Phys.* **2020**, *152*, 224108.

[222] Kaup, L.; Kaup, B.; Barthel, G.; Bridgland, M. *Holomorphic Functions of Several Variables: An Introduction to the Fundamental Theory*; De Gruyter studies in mathematics; W. de Gruyter, 1983.

[223] Salter, E. A.; Trucks, G. W.; Fitzgerald, G. B.; Bartlett, R. J. *Chem. Phys. Lett.* **1987**, *141*, 61–70.

[224] Trucks, G. W.; Salter, E. A.; Sosa, C.; Bartlett, R. J. *Chem. Phys. Lett.* **1988**, *147*, 359–366.

[225] Salter, E. A.; Trucks, G. W.; Bartlett, R. J. *J. Chem. Phys.* **1989**, *90*, 1752–1766.

[226] Jørgensen, P.; Helgaker, T. *J. Chem. Phys.* **1988**, *89*, 1560–1570.

[227] Gauss, J.; Stanton, J. F.; Bartlett, R. J. *J. Chem. Phys.* **1991**, *95*, 2623–2638.

[228] Vahtras, O.; Almlöf, J.; Feyereisen, M. W. *Chem. Phys. Lett.* **1993**, *213*, 514–518.

[229] Neese, F. *J. Comput. Chem.* **2003**, *24*, 1740–1747.

[230] Weigend, F. *Phys. Chem. Chem. Phys.* **2002**, *4*, 4285–4291.

[231] Izsák, R.; Neese, F. *J. Chem. Phys.* **2011**, *135*, 144105.

[232] Hylleraas, E. A. *Zeitschrift für Phys.* **1930**, *65*, 209–225.

[233] Pulay, P.; Saebo, S.; Meyer, W. *J. Chem. Phys.* **1984**, *81*, 1901–1905.

[234] Pulay, P.; Sæbø, S. *Theor. Chim. Acta* **1986**, *69*, 357–368.

[235] Feyereisen, M.; Fitzgerald, G.; Komornicki, A. *Chem. Phys. Lett.* **1993**, *208*, 359–363.

[236] Weigend, F.; Häser, M.; Patzelt, H.; Ahlrichs, R. *Chem. Phys. Lett.* **1998**, *294*, 143–152.

[237] Weigend, F.; Häser, M. *Theor. Chem. Acc.* **1997**, *97*, 331–340.

[238] Lee, T. J.; Racine, S. C.; Rice, J. E.; Rendell, A. P. *Mol. Phys.* **1995**, *85*, 561–571.

[239] Handy, N. C.; Schaefer, H. F. *J. Chem. Phys.* **1984**, *81*, 5031–5033.

[240] Pople, J. A.; Krishnan, R.; Schlegel, H. B.; Binkley, J. S. *Int. J. Quantum Chem.* **1979**, *16*, 225–241.

[241] Lee, T. J.; Rendell, A. P. *J. Chem. Phys.* **1991**, *94*, 6229–6236.

[242] Pople, J. A.; Gill, P. M.; Johnson, B. G. *Chem. Phys. Lett.* **1992**, *199*, 557–560.

[243] Bates, J. E.; Furche, F. *J. Chem. Phys.* **2012**, *137*, 164105.

[244] Dobson, J. F. *J. Chem. Phys.* **1993**, *98*, 8870–8872.

[245] Cossi, M.; Rega, N.; Scalmani, G.; Barone, V. *J. Comput. Chem.* **2003**, *24*, 669–681.

[246] Garcia-Ratés, M.; Neese, F. *J. Comput. Chem.* **2020**, *41*, 922–939.

[247] Ángyán, J. G. *Chem. Phys. Lett.* **1995**, *241*, 51–56.

[248] Lantto, P.; Jackowski, K.; Makulski, W.; Olejniczak, M.; Jaszuński, M. *J. Phys. Chem. A* **2011**, *115*, 10617–10623.

[249] Raynes, W. T. In *Nucl. Magn. Reson. Vol. 7*; Abraham, R. J., Ed.; Royal Society of Chemistry: Cambridge, 1978; pp 1–25.

[250] Hindermann, D. K.; Cornwell, C. D. *J. Chem. Phys.* **1968**, *48*, 4148–4154.

[251] Hindman, J. C. *J. Chem. Phys.* **1966**, *44*, 4582–4592.

[252] Jameson, A.; Jameson, C. J. *Chem. Phys. Lett.* **1987**, *134*, 461–466.

[253] Sundholm, D.; Gauss, J.; Schäfer, A. *J. Chem. Phys.* **1996**, *105*, 11051–11059.

[254] Raymonda, J.; Klemperer, W. *J. Chem. Phys.* **1971**, *55*, 232–233.

[255] Jameson, C. J.; Jameson, A. K.; Oppusunggu, D.; Wille, S.; Burrell, P. M.; Mason, J. *J. Chem. Phys.* **1981**, *74*, 81–88.

[256] Makulski, W.; Jackowski, K. *J. Mol. Struct.* **2003**, *651-653*, 265–269.

[257] Jameson, C. J.; Jameson, A. K.; Burrell, P. M. *J. Chem. Phys.* **1980**, *73*, 6013–6020.

[258] Nebgen, J.; Rose, W.; Metz, F. *J. Mol. Spectrosc.* **1966**, *20*, 72–74.

[259] Jameson, C. J.; Jameson, A. K.; Honarbakhsh, J. *J. Chem. Phys.* **1984**, *81*, 5266–5267.

[260] Jameson, C. J.; De Dios, A.; Keith Jameson, A. *Chem. Phys. Lett.* **1990**, *167*, 575–582.

[261] Stoychev, G. L.; Auer, A. A.; Izsák, R.; Neese, F. *J. Chem. Theory Comput.* **2018**, *14*, 619–637.

[262] Jameson, C. J. *Encycl. Magn. Reson.*; John Wiley & Sons, Ltd: Chichester, UK, 2007.

[263] Scheiner, A. C.; Scuseria, G. E.; Rice, J. E.; Lee, T. J.; Schaefer, H. F. *J. Chem. Phys.* **1987**, *87*, 5361–5373.

[264] Scuseria, G. E. *J. Chem. Phys.* **1991**, *94*, 442–447.

[265] Woon, D. E.; Dunning, T. H. *J. Chem. Phys.* **1993**, *98*, 1358–1371.

[266] CFOUR, a quantum chemical program package written by J. F. Stanton, J. Gauss, M. E. Harding, and P. G. Szalay with contributions from A.A. Auer, R.J. Bartlett, U. Benedikt, C. Berger, D.E. Bernholdt, Y.J. Bomble, L. Cheng, O. Christiansen, F. Engel, R. Faber, M. Heckert, O. Heun, C. Huber, T.-C. Jagau, D. Jonsson, J. Jusélius, K. Klein, W.J. Lauderdale, F. Lipparini, D.A. Matthews, T. Metzroth, L.A. Mück, D.P. O'Neill, D.R. Price, E. Prochnow, C. Puzzarini, K. Ruud, F. Schiffmann, W. Schwalbach, C. Simmons, S. Stopkowicz, A. Tajti, J. Vázquez, F. Wang, J.D. Watts and the integral packages MOLECULE (J. Almlöf and P.R. Taylor), PROPS (P.R. Taylor), ABACUS (T. Helgaker, H.J. Aa. Jensen, P. Jørgensen, and J. Olsen), and ECP routines by A. V. Mitin and C. van Wüllen. For the current version, see http://www.cfour.de.

[267] Hunter, J. D. *Computing in Science & Engineering* **2007**, *9*, 90–95.

[268] Hanwell, M. D.; Curtis, D. E.; Lonie, D. C.; Vandermeersch, T.; Zurek, E.; Hutchison, G. R. *J. Cheminform.* **2012**, *4*, 17.

[269] Becke, A. D. *Phys. Rev. A* **1988**, *38*, 3098–3100.

[270] Lee, C.; Yang, W.; Parr, R. G. *Phys. Rev. B* **1988**, *37*, 785–789.

[271] Perdew, J.; Burke, K.; Wang, Y. *Phys. Rev. B* **1996**, *54*, 16533–16539.

[272] Stephens, P. J.; Devlin, F. J.; Chabalowski, C. F.; Frisch, M. J. *J. Phys. Chem.* **1994**, *98*, 11623–11627.

[273] Adamo, C.; Barone, V. *J. Chem. Phys.* **1999**, *110*, 6158–6170.

[274] Tao, J.; Perdew, J. P.; Staroverov, V. N.; Scuseria, G. E. *Phys. Rev. Lett.* **2003**, *91*, 146401.

[275] Zhao, Y.; Truhlar, D. G. *J. Chem. Phys.* **2006**, *125*, 194101.

[276] Furness, J. W.; Kaplan, A. D.; Ning, J.; Perdew, J. P.; Sun, J. *J. Phys. Chem. Lett.* **2020**, *11*, 8208–8215.

[277] Staroverov, V. N.; Scuseria, G. E.; Tao, J.; Perdew, J. P. *J. Chem. Phys.* **2003**, *119*, 12129–12137.

[278] Zhao, Y.; Truhlar, D. G. *Theor. Chem. Acc.* **2008**, *120*, 215–241.

[279] Mardirossian, N.; Head-Gordon, M. *Phys. Chem. Chem. Phys.* **2014**, *16*, 9904.

[280] Najibi, A.; Goerigk, L. *J. Chem. Theory Comput.* **2018**, *14*, 5725–5738.

[281] Karton, A.; Tarnopolsky, A.; Lamère, J.-F.; Schatz, G. C.; Martin, J. M. L. *J. Phys. Chem. A* **2008**, *112*, 12868–12886.

[282] Chai, J.-D.; Head-Gordon, M. *J. Chem. Phys.* **2009**, *131*, 174105.

[283] Lehtola, S.; Steigemann, C.; Oliveira, M. J.; Marques, M. A. *SoftwareX* **2018**, *7*, 1–5.

[284] Jensen, F. *J. Chem. Theory Comput.* **2015**, *11*, 132–138.

[285] Jensen, F. *J. Chem. Theory Comput.* **2008**, *4*, 719–727.

[286] Reid, D. M.; Kobayashi, R.; Collins, M. A. *J. Chem. Theory Comput.* **2014**, *10*, 146–152.

[287] Jensen, S. R.; Flå, T.; Jonsson, D.; Monstad, R. S.; Ruud, K.; Frediani, L. *Phys. Chem. Chem. Phys.* **2016**, *18*, 21145–21161.

[288] Weigend, F. *Phys. Chem. Chem. Phys.* **2006**, *8*, 1057–65.

[289] Stoychev, G. L.; Auer, A. A.; Neese, F. *J. Chem. Theory Comput.* **2017**, *13*, 554–562.

[290] Hättig, C. *Phys. Chem. Chem. Phys.* **2005**, *7*, 59–66.

[291] Peterson, K. A.; Dunning, T. H. *J. Chem. Phys.* **2002**, *117*, 10548–10560.

[292] Krack, M.; Köster, A. M. *J. Chem. Phys.* **1998**, *108*, 3226–3234.

[293] Gill, P. M.; Johnson, B. G.; Pople, J. A. *Chem. Phys. Lett.* **1993**, *209*, 506–512.

[294] Treutler, O.; Ahlrichs, R. *J. Chem. Phys.* **1995**, *102*, 346–354.

[295] Tarnopolsky, A.; Karton, A.; Sertchook, R.; Vuzman, D.; Martin, J. M. L. *J. Phys. Chem. A* **2008**, *112*, 3–8.

[296] Gauss, J.; Stanton, J. F. *Adv. Chem. Phys.*; John Wiley & Sons, Inc.: Hoboken, NJ, USA, 2002; Vol. 123; pp 355–422.

[297] Brown, S. P.; Schaller, T.; Seelbach, U. P.; Koziol, F.; Ochsenfeld, C.; Klärner, F.-G.; Spiess, H. W. *Angew. Chemie Int. Ed.* **2001**, *40*, 717–720.

[298] Jensen, F. *Introduction to Computational Chemistry*, 2nd ed.; John Wiley & Sons Ltd.: West Sussex, England, 2007.

[299] Foster, J. M.; Boys, S. F. *Rev. Mod. Phys.* **1960**, *32*, 300–302.

[300] Boys, S. F. In *Quantum Theory Atoms, Molecules and the Solid State: A Tribute to John C. Slater*; Löwdin, P.-O., Ed.; Academic Press: New York, 1966; pp 253–262.

[301] Hetzer, G.; Pulay, P.; Werner, H.-J. *Chem. Phys. Lett.* **1998**, *290*, 143–149.

[302] Bistoni, G.; Riplinger, C.; Minenkov, Y.; Cavallo, L.; Auer, A. A.; Neese, F. *J. Chem. Theory Comput.* **2017**, *13*, 3220–3227.

[303] Gerratt, J.; Mills, I. M. *J. Chem. Phys.* **1968**, *49*, 1730–1739.

[304] England, W. *Int. J. Quantum Chem.* **1971**, *5*, 683–697.

[305] Scheurer, P.; Schwarz, W. H. E. *Int. J. Quantum Chem.* **2000**, *76*, 428–433.

[306] Scheurer, P.; Schwarz, W. H. E. *Int. J. Quantum Chem.* **2000**, *76*, 420–427.

[307] Davis, H. B.; Einstein, F. W. B.; Glavina, P. G.; Jones, T.; Pomeroy, R. K.; Rushman, P. *Organometallics* **1989**, *8*, 1030–1039.

[308] Krause, C.; Werner, H.-J. *Phys. Chem. Chem. Phys.* **2012**, *14*, 7591.

[309] Hansen, A. S.; Baardsen, G.; Rebolini, E.; Maschio, L.; Pedersen, T. B. *Mol. Phys.* **2020**, *118*, e1733118.

[310] Hättig, C.; Schmitz, G.; Koßmann, J. *Phys. Chem. Chem. Phys.* **2012**, *14*, 6549.

[311] Weigend, F.; Ahlrichs, R. *Phys. Chem. Chem. Phys.* **2005**, *7*, 3297.

[312] Rappoport, D.; Furche, F. *J. Chem. Phys.* **2010**, *133*, 134105.

[313] Allouche, A.-R. *J. Comput. Chem.* **2011**, *32*, 174–182.

[314] Kendall, R. A.; Dunning, T. H.; Harrison, R. J. *J. Chem. Phys.* **1992**, *96*, 6796–6806.

[315] Dunning, T. H. *J. Chem. Phys.* **1989**, *90*, 1007–1023.

[316] Sparta, M.; Retegan, M.; Pinski, P.; Riplinger, C.; Becker, U.; Neese, F. *J. Chem. Theory Comput.* **2017**, *13*, 3198–3207.

[317] Stoychev, G. L.; Auer, A. A.; Gauss, J.; Neese, F. *J. Chem. Phys.* **2021**, *154*, 164110.